

University of St Andrews



Full metadata for this thesis is available in
St Andrews Research Repository
at:

<http://research-repository.st-andrews.ac.uk/>

This thesis is protected by original copyright

THEORY OF TRANSITION METAL IMPURITIES IN SEMICONDUCTORS

A Thesis

presented by

A.G. O'Neill B.Sc.

to the

University of St Andrews

in application for the

Degree of Doctor of Philosophy



14 9926

Declaration

I hereby certify that this thesis has been composed by me, and is a record of work done by me, and has not previously been presented for a higher degree.

The research was carried out in the Department of Physical Sciences of The University of St Andrews, under the supervision of Prof. J.W. Allen.

A.G. O'Neill

Certificate

I certify that A.G. O'Neill B.Sc. has spent nine terms at research work in the Department of Physical Sciences of The University of St Andrews under my direction, that he has fulfilled the conditions of the Resolution of the University Court, 1967, No.1, and that he is qualified to submit the accompanying thesis in application for the Degree of Doctor of Philosophy.

Research Supervisor

Acknowledgements

Firstly I thank the Science and Engineering Research Council for providing me with financial support.

I must thank Dr U. Lindefelt and Prof. A. Zunger for providing me with results from their QBCF calculations prior to publication. I would also like to thank Dr J.T. Henderson for his time spent with the MSXALPHA package program.

I gratefully acknowledge the encouragement of Prof. L.J. Challis, Dr C.A. Bates, Dr P.J. Gavin, and my parents during the earlier stages of my academic career.

Most of all I thank my supervisor, John Allen, for his expert help and advice throughout the project.

Finally I should like to thank my wife, Susan, for her patience and understanding, particularly during the writing of this thesis.

In the beginning was the Word, and the Word was with God, and the Word was God. He was with God in the beginning.

Through him all things were made; without him nothing was made that has been made. In him was life, and that life was the light of men. The light shines in the darkness, but the darkness has not understood it.

John 1: 1-6

Abstract

A new version of crystal field theory is presented in this thesis for transition metal impurities in tetrahedral or octahedral environments. Like the conventional theory it contains only three disposable parameters. Covalency effects have been accounted for by adjustable parameters which are defined by the modification of one-electron d-d electrostatic integrals rather than the modification of one-electron d-orbitals. These parameters may be determined empirically or from first principles theory, thus providing a vital link between theory and experiment.

In the construction of the new theory it is assumed that the d-orbitals of the transition metal impurity remain strongly localised, and only one-centre integrals on the impurity site are considered. The successful application of the theory to describe experimental data is evidence that these approximations are valid for transition metal impurities in II-VI and III-V compounds.

The new theory has been applied to a wide range of tetrahedral systems and the results are compared with previous studies. Several difficulties in the interpretation of experimental data encountered by the conventional crystal field theory have been resolved. A study of trends in the new parameters is also presented, following a discussion of errors in the construction and application of the theory.

A new method is introduced to calculate the valence electron contribution to the crystal field strength by using the pseudopotential method. The critical dependence of the crystal field splitting on the nature of the impurity radial function casts some doubt on the validity of many previous calculations.

CONTENTS

1	INTRODUCTION	1
2	DEEP LEVELS	4
2.1	-Introduction-	4
2.2	-Shallow and deep levels-	4
2.3	-Localised d-orbitals-	5
2.4	-Crystal field theory-	6
2.5	-One-electron theory-	7
2.5.1	-scattered wave method-	8
2.5.2	-quasiband crystal field Green's function method-	9
2.6	-Experimental observations-	11
2.7	-Selection rules-	11
2.7.1	-spin selection rule-	12
2.7.2	-parity selection rule-	12
2.7.3	-symmetry selection rule-	13
2.8	-Line broadening-	13
2.9	-Summary-	14
3	CRYSTAL FIELD THEORY	15
3.1	-Introduction-	15
3.2	-One-electron orbitals-	16
3.3	-The crystal field-	17
3.4	-The secular determinant-	20

3.5	-Crystal field matrix elements-	20
3.6	-Electrostatic matrix elements-	21
3.6.1	-partial diagonalisation of the secular determinant-	22
3.6.2	-starting wavefunctions-	23
3.6.3	-the general electrostatic matrix elements-	25
3.7	-The general crystal field theory-	26
3.8	-The free ion-	27
3.9	-The B Δ version of crystal field theory-	30
3.10	-A new version of crystal field theory-	31
3.10.1	-the energy matrices-	36
3.10.2	-electrons and holes-	37
3.10.3	-comparison with other covalency models-	38
3.10.4	-comparison with one-electron theory-	40
3.11	-Energy level diagrams-	41
3.12	-Smaller perturbations-	43
3.12.1	-spin orbit coupling-	43
3.12.2	-Jahn-Teller Effect-	46
3.12.3	-Racah-Trees and seniority corrections-	47
3.12.4	-Trigonal distortion-	47
3.13	-Summary-	48
4	APPLICATIONS OF CRYSTAL FIELD THEORY I: IMPURITIES IN II-VI COMPOUNDS	50
4.1	-Introduction-	50
4.2	-Cobalt in II-VI semiconductors-	53

4.2.1	-ZnS:Co, an example-	56
4.2.2	-ZnO:Co-	58
4.2.3	-ZnSe:Co-	60
4.2.4	-ZnTe:Co-	63
4.2.5	-CdS:Co-	63
4.2.6	-CdSe:Co-	65
4.2.7	-CdTe:Co-	66
4.2.8	-Summary-	66
4.3	-Nickel in II-VI semiconductors-	68
4.3.1	-ZnO:Ni-	70
4.3.2	-ZnS:Ni-	72
4.3.3	-ZnSe:Ni-	73
4.3.4	-CdS:Ni-	77
4.3.5	-CdSe:Ni-	78
4.3.6	-Summary-	78
4.4	-3d ⁿ transition metal ions in ZnS-	79
4.4.1	-ZnS:Ti(d ²)-	80
4.4.2	-ZnS:V(d ³)-	82
4.4.3	-ZnS:Cr(d ⁴)-	83
4.4.4	-ZnS:Mn(d ⁵)-	85
4.4.5	-ZnS:Fe(d ⁶)-	88
4.4.6	-ZnS:Co(d ⁷) and ZnS:Ni(d ⁸)-	89
4.4.7	-Summary-	89
4.5	-Summary-	90

5	ERRORS IN THE CRYSTAL FIELD THEORY	92
5.1	-Introduction-	92
5.2	-Errors in the construction of the theory-	93
5.2.1	-modified free ion wavefunction-	94
5.2.2	-first principles wavefunction-	99
5.2.3	-relative error in the construction of the theory	102
5.3	-Errors in the Analysis-	104
5.4	-The error bars-	106
5.5	-Summary-	107
6	TRENDS IN THE CRYSTAL FIELD PARAMETERS	110
6.1	-Introduction-	110
6.2	-General comments on the parameters-	111
6.3	-Covalent radius correlation-	113
6.4	-The crystal field parameter Δ_p -	115
6.5	-The absorption edge in $Cd_{1-x}Mn_xTe$ -	123
6.6	-Comparison with esr data-	126
6.7	-Summary-	129
7	APPLICATIONS OF CRYSTAL FIELD THEORY II: IMPURITIES IN III-V COMPOUNDS	133
7.1	-Introduction-	133
7.2	-GaAs:Co-	135
7.3	-GaP:Co-	136
7.4	-Discussion-	136
7.5	-Summary-	138

8	THE CRYSTAL FIELD STRENGTH139
8.1	-Introduction-139
8.2	-Pseudopotential method-141
8.3	-The pseudocharge density-144
8.4	-Calculation of the crystal field contributions-147
8.4.1	-valence electron perturbing potential-148
8.4.2	-ion core perturbing potential-149
8.4.3	-crystal field splitting-150
8.5	-Summary-155
9	SUMMARY156

APPENDIX

The energy matrices

Atomic spectral parameters

Energy level diagrams

REFERENCES

CHAPTER ONE

INTRODUCTION

1 INTRODUCTION

The study of transition metal impurities in semiconductors is currently an active and rapidly developing field. These impurities are of great interest in their own right and because of their technological usefulness. There are frequent additions to the quantity of experimental data available and useful advances in the first principles theory of deep levels continue to be made. Despite this progress, it is not possible to compare directly experimental data with first principles theory in the study of the excited states of a transition metal impurity. This thesis describes research into a semiempirical theory through which experiment and first principles theory may be compared.

The semiempirical theory, which is a new version of crystal field theory, allows the experimentalist to describe large quantities of data in terms of three disposable parameters. These same parameters may be calculated from first principles theory. Thus theory and experiment may be compared by their estimates of the crystal field parameters. Previously experimental data has been described in terms of the conventional crystal field theory using three disposable parameters whose theoretical interpretation is difficult [1]. At the same time first principles theory has been frequently used to calculate quantities, such as the degree of localisation of d-orbitals [2,3], which can not be found directly from experimental data on excited states. There is therefore a need for a theoretical framework, intermediate between experiment and first principles theory, which is of use to both theorists and experimentalists.

The new version of crystal field theory is developed in chapters

two and three for transition metal impurities in tetrahedral semiconductors. Some theoretical considerations of deep levels relevant to crystal field theory are given in chapter two together with some mention of the experimental observation of excited states. In chapter three sufficient details of the crystal field theory are given so that the derivation of the energy matrices for the new theory given in the appendix can be understood. A general form of crystal field theory and that version frequently used by experimentalists are also described.

In chapter four it is demonstrated that the new version of crystal field theory is capable of describing the broad details of the optical absorption data arising from the excited states of transition metal impurities in II-VI compounds, using physically reasonable values for the disposable parameters. The results are compared with previous descriptions of the spectra. The choice of systems investigated enables a study of trends in the disposable parameters. It is important to know whether the approximations made in the crystal field theory are satisfactory for transition metals in the III-V compounds. The work presented in chapter seven shows that the crystal field theory may be used to describe these more covalent systems.

Errors in the construction and application of the crystal field theory are discussed in chapter five. Also contained in this chapter is an estimate of crystal field parameters from a first principles calculation. The estimation of errors in the empirically determined parameters allows an investigation of trends in these parameters in chapter six. The significance of these trends is discussed, and several useful applications of the trends are demonstrated.

The magnitude of the crystal field strength is the subject of chapter eight. A new method is introduced to calculate the valence

electron contribution to the crystal field by using the pseudopotential method. The critical dependence of the crystal field splitting on the nature of the impurity radial function casts some doubt on the validity of many previous calculations.

It is the objective of the final chapter to show what the present research has added to the field of transition metal impurities in semiconductors and to consider those areas in which further research would be useful.

CHAPTER TWO

DEEP LEVELS

2 DEEP LEVELS

2.1 -Introduction-

In this chapter I aim to provide a concise summary of those aspects of deep levels relevant to the crystal field theory. In the first four sections, I indicate the essential role of crystal field theory in the study of deep levels. The rest of the chapter is concerned with the experimental observation of the excited states.

In the course of my work on crystal field theory I have found the texts of Griffith [4], Ballhausen [5], Theissing and Caplan [6], and Allen and Pearson [7] invaluable. Throughout the thesis I have tried to provide references to more detailed work, when my discussion of a subject is brief.

2.2 -Shallow and deep levels-

The presence of substitutional impurities in a tetrahedral semiconductor may give rise to localised energy levels. It is useful to identify shallow and deep levels. A shallow impurity wavefunction is described by a linear combination of the pure crystal wavefunctions taken from the nearest band. The corresponding energy levels lie typically within 1000cm^{-1} (around 0.1eV) of either the valence or conduction band. Transition metal impurities produce deep levels. Too many lattice wavefunctions would be required to describe the wavefunctions of deep levels, and so an alternative theoretical

description is necessary. These levels may lie deeper than 1000cm^{-1} in the gap.

Compared to the shallow impurity level, the high ionisation energy of the deep level means that the electron is more tightly bound, which suggests that the wavefunction is more localised. In view of the localised nature of the deep levels, a reasonable and useful approach is to regard the impurity levels as atomic like, but modified by the crystal environment. In this way, excited states of the deep level are described as internal transitions within the incomplete d-shell of the $3d^n$ transition metal impurity. Different charge states of the impurity correspond to different occupancies of the $3d^n$ shell.

2.3 -Localised d-orbitals-

In this section, the evidence for and against the localised nature of transition metal deep levels is examined. There exists a conflict between those experimental data which indicate that the d-orbitals are mainly localised, and some one-electron theories which predict delocalisation of the d-orbitals.

Fig.2.1 shows the optical absorption spectra of substitutional nickel in a number of host crystals [8,9,10]. It is seen that the general features are retained in different hosts, that is nickel keeps something of its atomic identity.

Clark and Dean [11] have reported luminescence spectra of $\text{Fe}(d^6)$, $\text{Co}(d^7)$, and $\text{Ni}(d^8)$ in GaP. In each case strong coupling to a localised (gap) phonon is observed, which suggests a strong localisation of the d-orbitals.

One-electron calculations by Hemstreet [2] and by Il'in and Masterov [3] find that the degree of delocalisation of the d-orbitals

in the gap increases with increasing n for the $3d^n$ transition metal impurities in GaAs. Unfortunately there is no detailed agreement between the two sets of calculations, or with experimental data. The lack of agreement with experimental data suggests that these one-electron calculations are neglecting some fundamental interactions.

Experimental evidence suggests that the deep levels are strongly localised d-orbitals. In view of the uncertainty in the one-electron wavefunction calculations, comparison with experiment by a semiempirical method such as the crystal field theory is more useful than a complete first principles calculation.

2.4 -Crystal field theory-

In chapter three crystal field theory is dealt with extensively and so here the discussion is kept brief. The aim is to give an overview of the method.

The deep levels produced by a transition metal impurity are taken to be atomic like, but modified by the crystal environment. The effects of the crystal are two-fold. The point group symmetry of the tetrahedral crystal splits the d-orbitals into two groups, e and t_2 . This leads to a splitting of the free ion energy levels. The other effect is to reduce the electrostatic interaction within the d-shell. The reduction is different for e and t_2 -orbitals. Because the degree of delocalisation of the d-orbitals is assumed to be small, then only one-centre electrostatic interaction integrals on the impurity site are significant. Two centre integrals and other one-centre integrals are ignored.

The electrostatic integrals involving one-electron wavefunctions, together with the "crystal field splitting" of the e and t_2 -orbitals, are taken to be experimentally determinable quantities. Empirical values for the integrals can be compared with those integrals calculated using the one-electron wavefunctions found from first principles. The one-electron theories also estimate the crystal field splitting.

The crystal field theory provides a convenient way of comparing theory with experiment. But it assumes that the degree of delocalisation of the d-orbitals is small. However, if good agreement is reached with experiment using reasonable values of the adjustable parameters, then this gives further support to the model where d-orbitals are strongly localised for a transition metal impurity.

2.5 -One-electron theory-

One-electron wavefunctions from first principles calculations can be used to calculate electrostatic integrals. These integrals can be compared to those determined empirically. In this way, first principles theory can be compared with experimental data. A variety of theoretical methods have been proposed for the calculation of one-electron wavefunctions for transition metal impurities [3,12,13]. In this section, two of these methods are described.

2.5.1 -scattered wave method-

The scattered wave method [12] describes the crystal by a small cluster of atoms with some boundary condition to simulate the rest of the crystal. The atom potentials are taken in the muffin tin approximation, and the cluster is surrounded by a Watson sphere [14]. The one-electron Schrodinger equation is solved within the atomic spheres and outside the Watson sphere. In the interatomic region of the cluster, the wavefunction is written in terms of waves "incident" and "scattered" from each atomic potential and the cluster boundary. By satisfying boundary conditions and equating the incident wave on one atom with the scattered waves from all of the other spheres a set of molecular orbitals can be calculated.

This is the starting point for a self consistent calculation. The molecular orbitals can be used to generate a new potential from which new molecular orbitals can be computed. The numerical procedure is repeated until self consistency of the potentials and charge densities is reached.

The method has been used for transition metal impurity calculations by several workers [15,16,17]. The main differences lie in the choice of the boundary conditions. Hemstreet and Dimmock [15] use hydrogen atoms to saturate the dangling bonds, whilst Fazzio and Leite [17] transfer electrons filling the dangling bonds at the cluster surface to the Watson sphere.

2.5.2 quasiband crystal field Green's function method

The basic idea in any Green's function technique [18] is that the impurity site is a break in the translational symmetry of the crystal. This is characterised by a defect potential $U(\underline{r})$ which tends to zero moving away from the disturbance. The system can be described by the one-electron Schrodinger equation

$$\{H_0 + U(\underline{r})\} \psi_i(\underline{r}) = E \psi_i(\underline{r}) \quad 2.1$$

where H_0 is the Hamiltonian for the perfect crystal. The eigenfunctions for the perfect crystal $\phi_j(\underline{r}, \underline{k})$ are solutions of the equation

$$H_0 \phi_j(\underline{r}, \underline{k}) = E_j(\underline{k}) \phi_j(\underline{r}, \underline{k}). \quad 2.2$$

A useful representation of the Green's function for the perfect crystal is

$$G(\underline{r}, \underline{r}', E) = \sum_j \sum_{\underline{k}} \frac{\phi_j(\underline{r}, \underline{k}) \phi_j(\underline{r}', \underline{k})}{E - E_j(\underline{k})} \quad 2.3$$

Using this Green's function, the Schrodinger equation, eq.2.1, can be rewritten as an integral equation:

$$\psi_i(\underline{r}) = \int G(\underline{r}, \underline{r}', E) U(\underline{r}') \psi_i(\underline{r}') d^3 \underline{r}' \quad 2.4$$

Usually the eigenfunctions chosen for the perfect crystal $\phi_j(\underline{r}, \underline{k})$ are the Bloch functions. In the quasiband crystal field (QBCF) method [13] the basis set chosen is $\phi_j^{QB}(\underline{r}, \underline{k})$ so that the impurity wavefunction is

$$\psi_i(\underline{r}) = \sum_j \sum_{\underline{k}} A_{ij}^{QB}(\underline{k}) \phi_j^{QB}(\underline{r}, \underline{k}) \quad 2.5$$

where \sum_j is a small summation, and $\sum_{\underline{k}}$ is a sum over all \underline{k} points in the Brilluoin Zone. The quasiband basis function $\phi_j^{QB}(\underline{r}, \underline{k})$ is written as a sum of both band structure orbitals $\phi_j^{BS}(\underline{r}, \underline{k})$ and localised orbitals $\chi_{j,,}(\underline{r}, \underline{k})$:

$$\phi_j^{QB}(\underline{r}, \underline{k}) = \sum_j b_{jj}(\underline{k}) \phi_j^{BS}(\underline{r}, \underline{k}) + \sum_{j'} a_{jj'}(\underline{k}) \chi_{j'}(\underline{r}, \underline{k}) \quad 2.6$$

The impurity wavefunction can be conveniently written as an expansion of localised orbitals centred at the impurity:

$$\theta(r - R_c) \psi_i^{\alpha\lambda}(\underline{r}) = \sum_{l=0}^{l_{\max}} G_{il}^{\alpha}(|\underline{r}|) K_l^{\alpha\lambda}(\hat{\underline{r}}) \quad 2.7$$

Here $\psi_i^{\alpha\lambda}$ denotes the wavefunction transforming as the λ th partner in the α th irreducible representation. The step function $\theta(r - R_c)$ is zero for $r > R_c$, where R_c is the boundary of the defect potential region. The localised orbitals are written as a product of the radial part $G_{il}^{\alpha}(|\underline{r}|)$ and the angular part $K_l^{\alpha\lambda}(\hat{\underline{r}})$ which are Kubic harmonics of order l . The sum $\sum_{l=0}^{l_{\max}}$ runs typically up to $l_{\max} = 4$. The complementary quasiband representation of the impurity wavefunction is

$$\psi_i^{\alpha\lambda} = \sum_j \sum_k A_{ij}^{\alpha\lambda}(\underline{k}) \phi_j^{QB}(\underline{r}, \underline{k}) \quad 2.8$$

where the coefficients $A_{ij}^{\alpha\lambda}(\underline{k})$ are related to the radial functions $G_{il}^{\alpha}(|\underline{r}|)$.

The QBCF method has an advantage over previous Green's function methods in that the particular choice of basis set $\phi_j^{QB}(\underline{r}, \underline{k})$ incorporates the physical characteristics of the impurity wavefunction so that the summation \sum_j in eq.2.5 is small. The method has been used to study transition metal impurities in Si [19] and more recently for transition metal impurities in GaP [20].

2.6 -Experimental observations-

The excited states of deep impurities are most usually studied by optical absorption spectroscopy [21]. Transitions from the ground state to excited states lead to the absorption of incident light at particular frequencies. Thus the intensity of transmitted light measures the excited states.

In excitation spectra [22] the intensity of a radiative transition from a low lying excited state to the ground state is measured. Incident light causes transitions from the ground state to high energy excited states which are followed by relaxation to the low lying excited state.

2.7 -Selection rules-

The optical absorption spectra observed experimentally are the result of internal transitions between the many-electron energy levels of the d-shell. These transitions are governed by certain selection rules. The probability of a transition from the ground state ψ_i to an excited state ψ_e is

$$\frac{2\pi}{\hbar^2} | \langle \psi_i | \tilde{O} | \psi_e \rangle |^2 \quad 2.9$$

The operator \tilde{O} depends on the nature of the transition. For electric dipole transitions, the operator \tilde{O} is ez . The selection rules can be divided into three sections, these being the spin, parity, and symmetry selection rules.

2.7.1 -spin selection rule-

The electric dipole operator e_z does not give rise to any changes in spin. Therefore, if the spin of the initial state differs from the spin of the final state, the transition probability is zero because of spin orthogonality. Transitions from the high spin ground state to excited states with lower spin are observed experimentally. The reason for this is that spin-orbit coupling mixes states with different spin. Thus the low spin states have some high spin character, so that transitions are allowed. However, these transitions are weaker than the transitions between high spin states. The spin selection rule means that transitions to high spin states may be distinguished from transitions to low spin states.

2.7.2 -parity selection rule-

For the transition probability, eq.2.9, to be non zero, the integrand must have even parity. The electric dipole operator e_z has odd parity, and so electric dipole transitions are only allowed between states of opposite parity. This is known as the Laporte rule [23]. For a free transition metal, the d-d electric dipole transitions are parity forbidden, because the d-states have even parity, and so the weaker magnetic dipole transitions are the most intense [6].

For the impurity ion, the electric dipole transitions are allowed. The tetrahedral field may be expanded in terms of spherical harmonics. In this expansion, the lack of inversion symmetry in the T_d point group means that there is a non zero third order term in the

expansion [5]. This term causes mixing of the t_2 -orbitals with p-orbitals leading to states with some odd character. Transitions between states of mixed parity are not forbidden by the parity selection rule, and so electric dipole transitions within the d-shell are observed in the impurity ion. The parity selection rule does not give rise to any preferred transitions and so no identification of the excited states may be inferred from this selection rule.

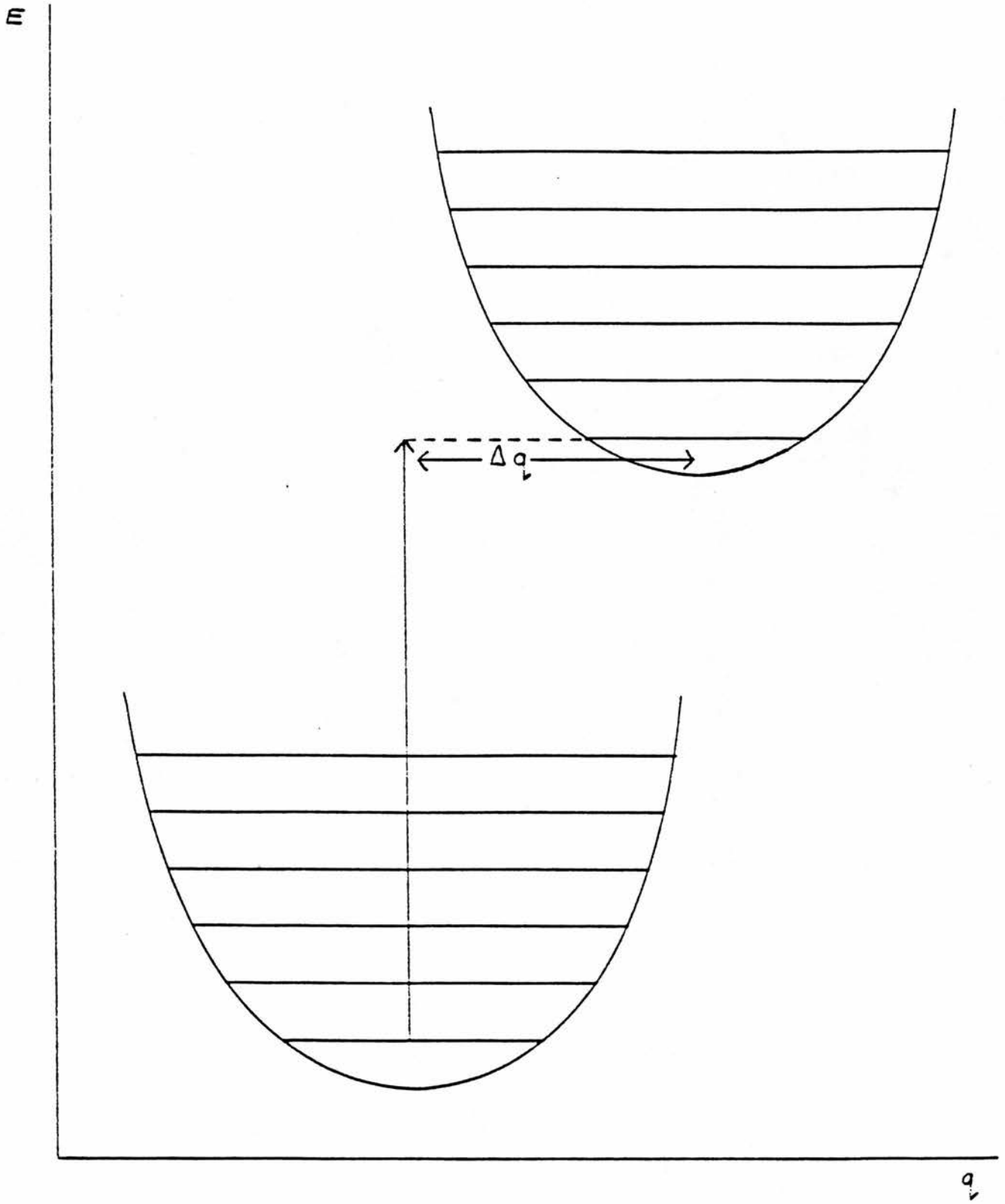
2.7.3 -symmetry selection rule-

The transition matrix element, eq.2.9, must contain the representation A_1 [24]. The electric dipole operator ez has T_2 symmetry, and so the symmetry (or fundamental) selection rule requires that $\Gamma_i \times \Gamma_e$ contains T_2 , where Γ_i is the symmetry of the ground state and Γ_e is the symmetry of the excited state. The intensity of transitions to excited states is governed by this selection rule, and so it may be used in the identification of energy levels.

2.8 -Line broadening-

Crystal field theory predicts a series of sharp transitions, whereas the experimentally observed transitions are broad. This line broadening is brought about by the electronic states coupling to the lattice. The ground state and the first excited state for some transition metal impurity are shown with their vibrational levels in fig.2.2, which is called a configuration coordinate diagram. The ground state and the excited state are displaced with respect to one

Fig.2.2
Configuration coordinate diagram.



another. This is because the electron-phonon coupling differs for two states having different electron configurations.

Optical absorption from the ground state is fast and appears vertically on the configuration coordinate diagram. Transitions between the two vibrational ground states must be accompanied by a displacement Δq of the ions. This displacement means that the transition (called the zero phonon line or zpl) does not correspond to the level calculated in the static crystal field model. Transitions to a number of the vibrational electronic levels are possible and this produces a broad absorption band. The mean of this absorption band, or the barycentre, corresponds to a vertical line with no displacement of the ions in fig.2.2, and it is this energy which should be compared with the static crystal field energy level [25].

2.9 -Summary-

Substitutional transition metal impurities give rise to localised energy levels deep in the forbidden gap. Experimental evidence suggests that these levels are strongly localised d-orbitals. Crystal field theory describes the excited states of deep levels semiempirically, and assumes that the d-orbitals are atomic like but modified by the crystal environment: one-electron d-orbitals are split into two groups, e and t_2 , and the electrostatic interactions within the d-shell are reduced by covalency. Crystal field theory provides a way of comparing experimental data with first principles theory.

The excited states are observed experimentally by optical absorption spectroscopy. Selection rules mean that only certain transitions are observed. The line broadening of crystal field electronic transitions is a consequence of electron-phonon coupling.

CHAPTER THREE
CRYSTAL FIELD THEORY

3 CRYSTAL FIELD THEORY

3.1 -Introduction-

Two important points emerge from the discussion of deep levels in the previous chapter. First, one-electron theories are not at the stage where they can accurately explain experimental data. Therefore to compare first principles theory with experiment, some intermediate semiempirical theory is required. Second, experimental evidence suggests that the deep levels are strongly localised d-orbitals. This fact points to the crystal field theory as an ideal choice for the intermediate theory.

A semiempirical theory is of great use to the experimentalist. It provides a framework for the organisation of large quantities of data. In itself, crystal field theory is not a complete description of experimental results, but it provides a necessary clarification of data so that finer interactions can be considered.

The crystal field theory was first treated in detail by Bethe [26], and applied to electronic optical absorption spectra by Van Vleck [27]. Further theoretical work has been carried out notably by Orgel [28] and by Tanabe and Sugano [1]. A useful review of the applications of crystal field theory is given by McClure [29].

It is my intention in this chapter to treat crystal field theory to a sufficient depth that the complete derivation of the energy matrices for the new theory given in the appendix can be understood. In this way the crystal field method, together with the approximations therein, may become clear. The original contribution to this chapter,

that is the new version of crystal field theory, is contained within sections 3.10 and 3.11. I conclude the chapter with a discussion of the smaller interactions which may be included in a more detailed description of the impurity levels.

3.2 -One-electron orbitals-

For the many-electron calculation of excited states, one-electron orbitals are required for use as basis functions. Such basis functions may be obtained as eigenfunctions of the central field problem. Here, each electron is assumed to move in a spherically averaged potential, $U(r_i)$, arising from the nucleus and all of the other electrons. The one-electron Schrodinger equation is:

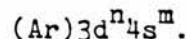
$$[(-\hbar^2/2m) \nabla_i^2 + U(r_i)] \phi(i) = E_i \phi(i) \quad 3.1$$

The solution of this equation is separable:

$$\phi(i) = R_{nl}(r_i) Y_{lm_l}(\theta_i, \phi_i) \quad 3.2$$

where $R_{nl}(r_i)$ is the radial part and $Y_{l,m_l}(\theta_i, \phi_i)$ is a spherical harmonic. In addition, the electron has a spin characterised by the spin quantum number $m_s = \pm 1/2$. Thus each orbital can be characterised by the four quantum numbers (n, l, m_l, m_s) .

The electronic configuration of the iron group transition metals is:



The eighteen inner electrons making up the Argon core are in tightly bound filled shells, and so are of no interest here. Instead, interest is concentrated on the $3d^n$ electrons. For one-electron orbitals in the 3d shell, $n=3$ and $l=2$. Therefore these orbitals are characterised by m_l and m_s alone.

There are five possible d-orbitals, each with two spin states.

These may be written as:

$$(-2^+), (-2^-), (-1^+), (-1^-), (0^+), (0^-), (1^+), (1^-), (2^+), (2^-). \quad 3.3$$

where, for example, (-2^+) represents a wavefunction where $m_l = -2$ and $m_s = +1/2$. Linear combinations of these orbitals are used as basis functions in the calculation of excited states presented in this thesis. Specifically, these are:

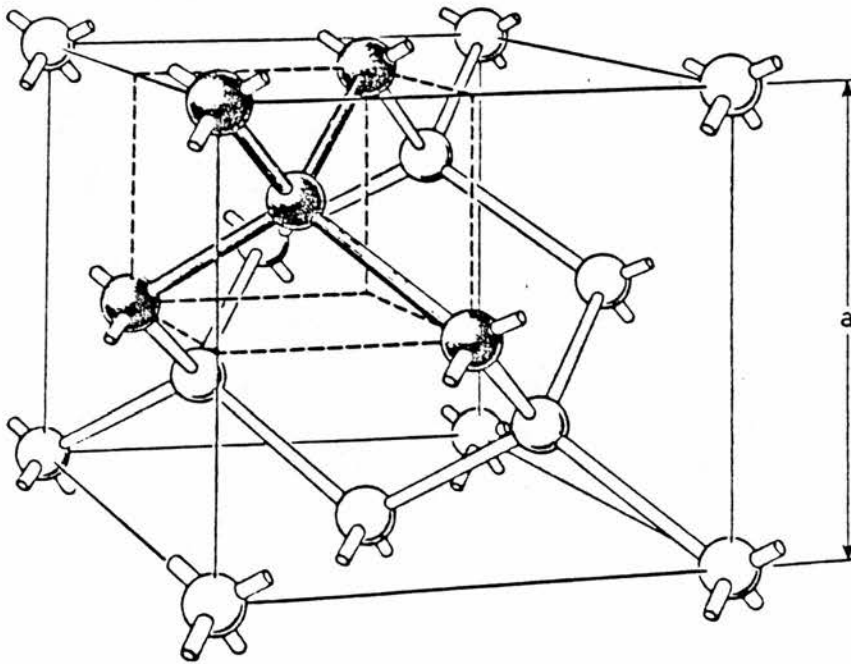
$$\begin{aligned} \xi &= (i/\sqrt{2}) [1 + (-1)]; \quad \eta = (-1/\sqrt{2}) [1 - (-1)]; \quad \zeta = (1/i\sqrt{2}) [2 - (-2)] \\ \theta &= 0; \quad \epsilon = (i/\sqrt{2}) [2 + (-2)] \end{aligned} \quad 3.4$$

where each orbital has two possible spin states. This set of states is called the strong field configuration, whilst the set of states in eq.3.3 is known as the weak field configuration. For the general case a different radial function is associated with each basis function. There is no real distinction between using either eq.3.3 or eq.3.4 as a basis set. The resulting energy levels will be the same.

3.3 -The crystal field-

The excited states, within the $3d^n$ configuration of a transition metal impurity, are described in crystal field theory. In this thesis, the transition metal is taken to be substitutional on a cation site in a tetrahedral semiconductor. With the exception of CdO, for example, in each of the II-VI compounds the impurity is surrounded by four nearest neighbours lying at the vertices of a perfect or slightly distorted tetrahedron. Thus the crystal field theory developed here is generally applicable to $3d^n$ transition metal impurities in II-VI compounds. A ball and spoke model of such a tetrahedral crystal is given in fig.3.1. The impurity site has point group symmetry T_d

Fig.3.1
Ball and spoke diagram of a tetrahedral crystal.



(Schoenflies) or $\bar{4}3m$ (international), and is surrounded by a tetrahedron of four anions.

It is assumed that for a transition metal impurity in a tetrahedral crystal, there are electrons which can be identified as originating from a d-shell. The five d-orbitals that these electrons may occupy belong to a reducible representation which has irreducible components e (doubly degenerate) and t_2 (triply degenerate). The impurity d-orbitals are labelled according to the basis functions of the irreducible representations. Thus ξ , η , and ζ are the one-electron t_2 -orbitals, whilst θ and ϵ are the one-electron e-orbitals.

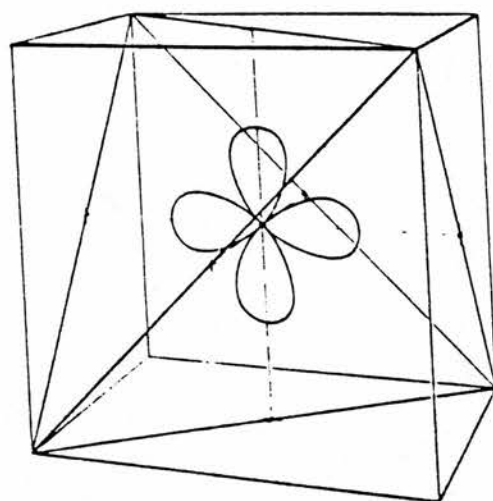
In physical terms, the reduction of the d representation into irreducible components e and t_2 means that a single d-electron in a tetrahedral environment can have two possible energy levels, one being two fold degenerate (e), and the other three fold degenerate (t_2). The separation of these one-electron energy levels is called Δ :

$$\Delta = E(t_2) - E(e) \quad 3.5$$

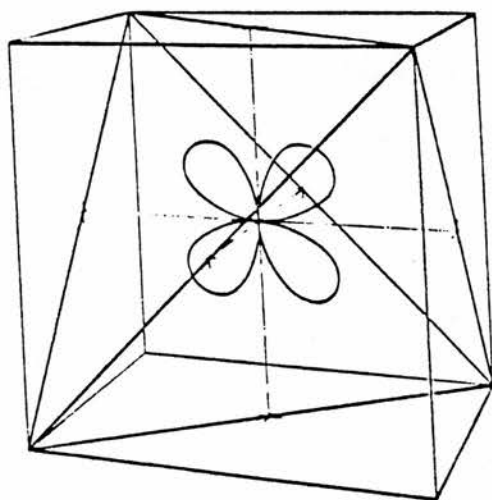
for tetrahedral symmetry.

The nature of the crystal field splitting can be illustrated by a simple example [29]. Consider a single electron in a d-orbital surrounded by four negative point charges in tetrahedral coordination (fig.3.2). For a free atom, the electron may occupy any of the five d-orbitals with equal energy. In the tetrahedral field, an electron in one orbital is repelled from the point charges by an amount which depends on the spatial distribution of that orbital. The particular orientation of the three t_2 -orbitals means that they are repelled more by the point charges than the two e-orbitals. As a result the five d-orbitals are no longer degenerate. They split into a lower group of two e-orbitals and an upper group of three t_2 -orbitals.

Fig.3.2
One-electron d-orbitals in T_d symmetry.



e-orbital



t_2 -orbital

Similarly, the T_d point symmetry of the impurity site gives rise to a separation, Δ , of the e - and t_2 -orbitals. The physical origin of the splitting for a transition metal impurity is the crystal field, $\sum_i U(r_i) + V_c(r_i)$, where the sum runs over all of the electrons. Here $U(r_i)$ is the spherically averaged electrostatic potential at the impurity neglecting many-electron effects. This attractive potential is almost balanced by the repulsive potential from the spherically symmetric part of the d-d electrostatic interaction (see section 6.4). The term $V_c(r_i)$ is taken to be the fourth order spherical harmonic contribution to the electrostatic potential due to the whole crystal which interacts with the partially filled $3d^n$ shell. The crystal field at the impurity site has T_d point group symmetry and so splits the d-orbitals. Contributions to $V_c(r_i)$ may come from the crystal valence electrons, as well as from the lattice of ion cores. An attempt has been made to estimate the contribution to $V_c(r_i)$ from the crystal valence electrons from pseudopotential calculations for a pure T_d semiconductor. The results of this calculation are presented in a later chapter. The crystal field strength is taken to be an experimentally determinable parameter, and so its origin is unimportant. The important factor is the point symmetry of the crystal field at the impurity site.

3.4 -The secular determinant-

So far, one-electron wavefunctions have been found which are solutions of the central field problem, eq.3.1. However, the Hamiltonian for the impurity ion is:

$$H = \sum_{i=1}^n \left[\left(-\frac{\hbar^2}{2m} \right) \nabla_i^2 - \frac{Ze^2}{r_i} + eV_c(r_i) + \sum_{j>i}^n \frac{e^2}{r_{ij}} \right]$$

$$= H_o + H_e + H_c \quad 3.6$$

where H_o is the Hamiltonian of the central field problem, H_e is the electrostatic interaction within the d-shell, and H_c is the crystal field part. The contributions H_c and H_e are included by perturbation theory, taking antisymmetric products of the one-electron orbitals as basis functions and solving the secular determinant:

$$| H_{ij} - E \delta_{ij} | = 0 \quad 3.7$$

where $H_{ij} = \langle \psi_i | H_e + H_c | \psi_j \rangle$ are the matrix elements, E is the eigenvalue, and ψ_i, ψ_j are the antisymmetric products of one-electron orbitals. The construction of the matrix elements is illustrated in the following sections.

3.5 -Crystal field matrix elements-

It has previously been shown that the tetrahedral environment splits the d-orbitals into two groups, e and t_2 . For an impurity ion with two d-electrons, then t_2^2 , et_2 , and e^2 are the three possible strong field configurations. The crystal field is diagonal within the strong field configuration bases, and so only diagonal crystal field matrix elements are non-zero.

It was stated in eq.3.5 that the energy difference between a

t_2 -orbital and an e-orbital is Δ . Therefore if the zero of energy is chosen as the $e t_2$ configuration, then the t_2^2 configuration has energy Δ and the e^2 configuration has energy $-\Delta$. Thus the terms Δ , 0, and $-\Delta$ would appear in the secular determinant as the crystal field matrix elements for the configurations t_2^2 , $e t_2$, and e^2 respectively. The choice of the zero of energy is arbitrary, because the relative separation of the levels is of interest here. Conventionally, the orbital energy of a state in the strong field configuration $t_2^m e^l$ is

$$1/5 \cdot \Delta \cdot (2m - 3l) \quad 3.8$$

Thus for a d^2 configuration, the orbital energies are $4/5 \Delta$, $-1/5 \Delta$, and $-6/5 \Delta$ for the configurations t_2^2 , $e t_2$, and e^2 respectively. In the hole formalism, the sign of the matrix elements is reversed, because the holes have positive, rather than negative, charge.

3.6 -Electrostatic matrix elements-

In this section, the matrix elements of the electrostatic operator $\sum_{i>j} e^2/r_{ij}$ are sought. The central part of the electrostatic d-d interaction is large and it may appear questionable whether the perturbation method can be applied with confidence. But the central part of the repulsive d-d interaction is almost equal and opposite to an attractive central field term $U(r_i)$. As a result the actual perturbation of the levels is small [6].

A particular choice of the starting wavefunctions leads to a partial diagonalisation of the secular determinant, and this point is discussed first.

3.6.1 -partial diagonalisation of the secular determinant-

For the $3d^2$ electrons, the three possible strong field electron configurations are t_2^2 , et_2 , and e^2 . The (strong field) terms belonging to each of these configurations can be found by taking the direct product of the constituent orbitals:

$$\begin{aligned}
 t_2^2 \text{ configuration} \quad t_2 \times t_2 &= {}^1A_1 + {}^1E + {}^3T_1 + {}^1T_2 \\
 et_2 \text{ configuration} \quad t_2 \times e &= {}^1T_1 + {}^3T_1 + {}^1T_2 + {}^3T_2 \\
 e^2 \text{ configuration} \quad e \times e &= {}^1A_1 + {}^1E + {}^3A_2.
 \end{aligned}
 \tag{3.9}$$

The multiplication table for the orbital representations in T_d symmetry is given in table 3.1. The assignment of triplet and singlet states requires further discussion. The total configuration wavefunctions need to be antisymmetric in order to satisfy the exclusion principle. The wavefunctions are constructed from a spin part and an orbital part. Ballhausen [5] shows that A_1 , E , and T_2 are symmetric representations whilst T_1 is antisymmetric. For the total wavefunction to be antisymmetric, then the spin function must be symmetric for T_1 (i.e. a triplet), whilst it must be antisymmetric (i.e. a singlet) for the others [30]. This result, together with those for the other configurations are summarised in Table A25 of Griffith [4].

The starting wavefunctions are written indicating both their configuration and term symmetry as

$$\begin{aligned}
 &t_2^2({}^1A_1); t_2^2({}^1E); t_2^2({}^3T_1); t_2^2({}^1T_2); e^2({}^1A_1); e^2({}^3A_2); e^2({}^1E); \\
 &et_2({}^1T_1); et_2({}^1T_2); et_2({}^3T_1); et_2({}^3T_2).
 \end{aligned}
 \tag{3.10}$$

For the d^2 configuration, an 11×11 secular determinant is necessary for the calculation of excited states, corresponding to the eleven starting wavefunctions listed above.

The choice of the starting wavefunctions is such that many of

Table 3.1
 Multiplication table for representations in T_d .

T_d	A_1	A_2	E	T_1	T_2
A_1	A_1	A_2	E	T_1	T_2
A_2		A_2	E	T_1	T_2
E			$A_1 + A_2 + E$	$T_1 + T_2$	$T_1 + T_2$
T_1				$A_1 + E + T_1 + T_2$	$A_2 + E + T_1 + T_2$
T_2					$A_1 + E + T_1 + T_2$

the electrostatic matrix elements are zero. This can be explained as follows. The matrix elements are of the form:

$$H_{ij} = \langle \psi_i | H_e | \psi_j \rangle \quad 3.11$$

where ψ_i and ψ_j are starting wavefunctions from eq.3.10. The matrix element is a scalar and so must have spherical symmetry A_1 . Since the operator also has symmetry A_1 , then $\Gamma_i \times \Gamma_j$ must contain A_1 , where Γ_i , Γ_j are the symmetries of ψ_i , ψ_j . In other words, for H_{ij} to be non-zero, the starting wavefunctions ψ_i and ψ_j must have the same symmetry. Thus, a matrix element of the form $\langle t^2(1A_1) | H_e | e^2(1A_1) \rangle$ is non-zero, whilst $\langle t^2(1A_1) | H_e | e^2(1E) \rangle$ is zero. This leads to a partial diagonalisation of the secular determinant as shown in fig.3.3. In the figure, matrix elements within the shaded region are non zero, whilst those outside are zero. This means that the secular determinant can be split up into a number of smaller and more manageable sub-determinants, often referred to as the energy matrices here.

3.6.2 -starting wavefunctions-

It has been shown that the secular determinant can be partially diagonalised into a series of sub-determinants which considerably simplifies the calculation of excited states. The number of matrix elements to be calculated is drastically reduced. I now go on to express these matrix elements in terms of integrals between the basis functions of eq.3.4.

It is necessary, first, to find expressions for the starting wavefunctions of eq.3.10 in terms of the bases ξ , η , ζ , θ , ϵ . The construction of the starting wavefunctions is illustrated here, by the

example of a d^5 starting wavefunction with symmetry 4T_2 and electron configuration $t_2^4 e$. This starting wavefunction can be conveniently written as

$$t_2^4 e({}^4T_2) = |t_2^4({}^3T_1) e({}^2E) {}^4T_2 \zeta \rangle \quad 3.12$$

of which the general form is

$$| \Gamma' \Gamma'' \Gamma M_\Gamma \rangle \quad 3.13$$

where Γ' is the symmetry of the t_2 part, Γ'' is the symmetry of the e part, Γ is the symmetry of the whole term, and M_Γ is a quantum number associated with Γ .

The starting wavefunction can be made up from a linear combination of products of the t_2 part and the e part, using Wigner's formula:

$$| \Gamma' \Gamma'' M_\Gamma \rangle = \sum | \Gamma' M_{\Gamma'} \rangle | \Gamma'' M_{\Gamma''} \rangle \langle \Gamma' M_{\Gamma'} \Gamma'' M_{\Gamma''} | \Gamma' \Gamma'' M_\Gamma, M_\Gamma \rangle \quad 3.14$$

The components $| \Gamma' M_{\Gamma'} \rangle$, $| \Gamma'' M_{\Gamma''} \rangle$ have been calculated previously and are tabulated in table A24 of Griffith [4]. The Wigner, or Clebsch-Gordan, coefficients $\langle \Gamma' M_{\Gamma'} \Gamma'' M_{\Gamma''} | \Gamma' \Gamma'' M_\Gamma, M_\Gamma \rangle$ can be found in table A20 of Griffith. For the example of $|t_2^4({}^3T_1) e({}^2E) {}^4T_2 \zeta \rangle$, it can be seen from table A20 that for the total wavefunction to have only T_2 orbital symmetry, then $M_{\Gamma'} = z$, $M_{\Gamma''} = \theta$ or ϵ . The sum has one term only, so that

$$\begin{aligned} |t_2^4({}^3T_1) e({}^2E) {}^4T_2 \zeta \rangle &= |t_2^4({}^3T_1) 1z, e({}^2E) \epsilon {}^4T_2 \zeta \rangle \\ &= |t_2^4({}^3T_1) 1z \rangle |e({}^2E) \epsilon \rangle \end{aligned} \quad 3.15$$

From table A24

$$\begin{aligned} |t_2^4({}^3T_1) 1z \rangle &= | \xi^+ \eta^+ \zeta^+ \zeta^- \rangle \\ |e({}^2E) \epsilon \rangle &= | \epsilon^+ \rangle \end{aligned} \quad 3.16$$

so that

$$|t_2^4({}^3T_1) e({}^2E) {}^4T_2 \zeta \rangle = | \xi^+ \eta^+ \zeta^+ \zeta^- \epsilon^+ \rangle \quad 3.17$$

which is the required wavefunction. The spin part has been included by

inspection: ζ^+ and ζ^- must have opposite spin to satisfy the exclusion principle, and the total spin of the wavefunction is $s=3/2$ so that the other functions must be ξ^+ , η^+ , and ϵ^+ .

In this way, all of the starting wavefunctions may be found, by using tables A20 and A24 of Griffith [4]. The starting wavefunction must be antisymmetric, so that $|\xi^+ \eta^+ \zeta^+ \zeta^- \epsilon^+ \rangle$ is not just a simple product but a Slater determinant:

$$(1/5!) \begin{vmatrix} \xi^+(1) & \xi^+(2) & \xi^+(3) & \xi^+(4) & \xi^+(5) \\ \eta^+(1) & \eta^+(2) & \eta^+(3) & \eta^+(4) & \eta^+(5) \\ \zeta^+(1) & \zeta^+(2) & \zeta^+(3) & \zeta^+(4) & \zeta^+(5) \\ \zeta^-(1) & \zeta^-(2) & \zeta^-(3) & \zeta^-(4) & \zeta^-(5) \\ \epsilon^+(1) & \epsilon^+(2) & \epsilon^+(3) & \epsilon^+(4) & \epsilon^+(5) \end{vmatrix} \quad 3.18$$

Thus for a d^5 configuration, the starting wavefunctions are 5×5 Slater determinants whose one-electron functions are ξ , η , ζ , θ , ϵ . For any configuration d^n , the starting wavefunctions are $n \times n$ Slater determinants.

3.6.3 -the general electrostatic matrix elements-

Having found suitable starting wavefunctions, and having partially diagonalised the secular determinant, it remains to find the electrostatic matrix elements.

A typical matrix element between starting wavefunctions of the d^5 configuration may be written as a sum of elements such as

$$\int \phi_1(1) \phi_2(2) \phi_3(3) \phi_4(4) \phi_5(5) \frac{e^2}{r_{12}} \phi_6(1) \phi_7(2) \phi_8(3) \phi_9(4) \phi_{10}(5) \cdot d\tau_1 d\tau_2 d\tau_3 d\tau_4 d\tau_5 \quad 3.19$$

$$= \int \phi_1(1) \phi_2(2) \frac{e^2}{r_{12}} \phi_6(1) \phi_7(2) d\tau_1 d\tau_2 \int \phi_3(3) \phi_4(4) \phi_5(5) \phi_8(3) \phi_9(4) \phi_{10}(5) d\tau_3 d\tau_4 d\tau_5 \quad 3.20$$

If the two one-electron-orbital-products in eq.3.19 differ by more than two constituent orbitals, then the second term in eq.3.20 is zero; otherwise it is unity and the element becomes simply

$$\int \phi_1(1) \phi_2(2) \frac{e^2}{r_{12}} \phi_6(1) \phi_7(2) d\tau_1 d\tau_2 \quad 3.21$$

Thus the electrostatic matrix elements are made up of sums of two-electron integrals with the general form of eq.3.21. Each of the general one-electron functions ϕ can be ξ , η , ζ , θ or ϵ . Griffith [4] has shown that there are just ten independent two-electron integrals of this form for the d^n configurations. The ten integrals are tabulated in table 3.2.

The only assumption made so far is that there are orbitals in the crystal which are identified as being the impurity d-orbitals. From this, the electrostatic interactions within the d^n configuration can be described in terms of ten independent parameters.

3.7 -The general crystal field theory-

The excited states of the d^n configuration may be described by a secular determinant containing ten independent electrostatic parameters, and one crystal field parameter, Δ . Accurate one-electron wavefunctions, corresponding to those in the electrostatic integrals, have not yet been found for transition metal impurities in II-VI or III-V compounds. Instead, the electrostatic integrals, and the crystal field parameter, must be determined by a comparison of theory

Table 3.2
The ten independent electrostatic integrals

General parameter	Electrostatic integral
a	$\langle \xi\xi H_e \xi\xi \rangle$
b	$\langle \xi\eta H_e \xi\eta \rangle$
c	$\langle \theta\xi H_e \epsilon\xi \rangle$
d	$\langle \epsilon\xi H_e \epsilon\xi \rangle$
e	$\langle \theta\theta H_e \theta\theta \rangle$
f	$\langle \theta\theta H_e \epsilon\epsilon \rangle$
g	$\langle \theta\theta H_e \eta\eta \rangle$
h	$\langle \theta\epsilon H_e \eta\eta \rangle$
i	$\langle \theta\eta H_e \xi\zeta \rangle$
j	$\langle \xi\xi H_e \eta\eta \rangle$

with experiment.

A problem is immediately obvious. The secular determinant contains eleven adjustable parameters. Comparison with experimental data would involve varying eleven parameters until "satisfactory" agreement is reached between the theoretical lines from the energy matrices and the observed absorption barycentres. For such a study to be meaningful, far more experimental data would be required than is possibly available. Thus the excessively large number of variable parameters present in the general crystal field theory means that it is of no practical use to the experimentalist in the interpretation of data.

To proceed, some simplification of this general form of the theory is necessary. Approximations in the theory are presented in this thesis, which reduce the number of adjustable parameters to three. Comparison between theory and experiment is then possible. The new version of the theory assumes that the d-orbitals of the impurity retain their atomic character to a large extent. For this reason, the energy levels for a free transition metal are calculated in the following section.

3.8 -The free ion-

The $3d^n$ energy levels for a free ion can be calculated from a modified crystal field theory secular determinant. For a free ion, the five d-orbitals are degenerate, so that the parameter Δ , and so the separation of the e and t_2 -orbitals, is zero. The excited states are then described just in terms of the electrostatic integrals.

A considerable simplification of the integrals occurs for the

free ion because the one-electron wavefunctions are separable:

$$\phi(i) = R_{nl}(r_i) Y_{lm_l}(\theta_i, \phi_i) \quad 3.22$$

where $Y_{l,m_l}(\theta, \phi)$ is a second order spherical harmonic for the d-orbitals, and the radial part $R_{n,l}(r)$ is the same for all of the orbitals. A typical two-electron integral is

$$\int \phi_i(1) \phi_j(2) \frac{e^2}{r_{12}} \phi_m(1) \phi_t(2) d\tau_1 d\tau_2 \quad 3.23$$

The operator, e^2/r_{12} , can be separated into radial and angular parts [4]:

$$\frac{e^2}{r_{12}} = \frac{e^2}{r_>} \sum_{k=0}^{\infty} \frac{r_<^k}{r_>^k} P_k(\cos\omega) \quad 3.24$$

where $r_>$, $r_<$ are the greater and lesser of r_1 , r_2 respectively, and $P_k(\cos\omega)$ is a Legendre polynomial.

The two-electron integral can be rewritten:

$$\begin{aligned} & \sum_{k=0}^{\infty} \int R_{n_i l_i}(r_1) R_{n_j l_j}(r_2) \frac{e^2 r_<^k}{r_>^{k+1}} R_{n_m l_m}(r_1) R_{n_t l_t}(r_2) r_1^2 r_2^2 dr_1 dr_2 \\ & \cdot \int Y_{l_i m_i}(\theta_1, \phi_1) Y_{l_j m_j}(\theta_2, \phi_2) P_k(\cos\omega) Y_{l_m m_m}(\theta_1, \phi_1) Y_{l_t m_t}(\theta_2, \phi_2) d\theta_1 d\theta_2 d\phi_1 d\phi_2 \\ & \cdot \delta(s^i s^m) \delta(s^j s^t) \end{aligned} \quad 3.25$$

The radial part of this expression defines the Slater-Condon parameters F^k for 3d (equivalent) electrons. The angular part, A_k , can be evaluated exactly and tabulated once and for all. The delta function $\delta(s^i s^m)$ is zero unless $s^i = s^m$, and a similar result holds for $\delta(s^j s^t)$. Therefore, the matrix elements for a free ion can be written in terms of one-electron integrals:

$$\begin{aligned} & \int \phi_i(1) \phi_j(2) \frac{e^2}{r_{12}} \phi_m(1) \phi_t(2) d\tau_1 d\tau_2 \\ & = \sum_{k=0}^{\infty} F^k A_k \end{aligned} \quad 3.26$$

The adjustable parameters of the theory are now the Slater-Condon parameters F^k . Since the ϕ belong to the $l=2$ representation, D^2 , and the electrostatic matrix element is a scalar, then the product $D^2 \times D^2 \times D^k$ must contain A_1 . This is equivalent to saying that D^k must be contained in

$$D^2 \times D^2 = D^4 + D^3 + D^2 + D^1 + D^0. \quad 3.27$$

Therefore, the maximum value of k is four [24], and the energy matrices contain three non zero parameters F^0 , F^2 , and F^4 . These are usually rewritten as

$$\begin{aligned} F_0 &= F^0 \\ F_2 &= 1/49 F^2 \\ F_4 &= 1/441 F^4 \end{aligned} \quad 3.28$$

for clarity. An alternative notation, which is widely used, is that due to Racah [31]:

$$\begin{aligned} A &= F_0 - 49 F_4 \\ B &= F_2 - 5 F_4 \\ C &= 35 F_4. \end{aligned} \quad 3.29$$

Evaluation of the energy matrices in terms of the three Racah parameters A , B , and C shows that terms involving A occur identically on each diagonal matrix element. In the calculation of excited states, only the relative separation of the levels is important, and so terms involving A can be omitted.

The parameters B and C are adjusted to give the best agreement between theory and experiment. These "free ion" Racah parameters have been tabulated by Griffith [4] and also appear in the appendix of this thesis. The particular combinations of the Slater-Condon Parameters F^k chosen by Racah in his parameterisation are such that transitions between high spin states only involve the parameter B .

In summary, for the free ion, the secular determinant describing the excited states within the $3d^n$ configuration can be simplified so that it contains just two adjustable parameters. Comparison between free ion data and the determinant leads to the free ion values of the Racah parameters, which have been tabulated.

3.9 -The BCA version of crystal field theory-

For a free ion, the absorption spectrum can be described by two independent parameters. For an impurity ion, the traditional method of describing the spectrum, using a secular determinant with a manageable number of parameters, involves the same electrostatic matrix elements. However, the crystal field parameter, Δ , is no longer zero. Comparison between theory and experiment involves the use of three adjustable parameters B, C, and Δ [1]. For this reason, it is referred to as the BCA crystal field theory in this thesis.

Agreement between theory and experiment is good in many cases. But there are problems, for example in the interpretation and explanation of some data, and in the predictions of low spin states by the theory in some systems [32].

Within the BCA theory there are inconsistencies. The most serious one is this: the parameter Δ exists because there is a difference between the e and t_2 -orbitals, but the simplification of the electrostatic matrix elements to leave just two adjustable parameters relies on the fact that the d-orbitals are identical.

Another problem with the BCA theory is in the interpretation of the electrostatic parameters B and C. There is no physical reason for the ratio of C/B to change between that found in the free ion and that

found for the impurity ion. However, large differences in the ratio are sometimes necessary in order to give good agreement with observed data [33]. The parameters B and C found for an impurity ion are in general reduced from the free ion value. This reduction is believed to be a consequence of covalency effects. The physical interpretation is difficult here, because the radial functions of the e and t_2 -orbitals are the same, in the BCA model, and so the degree of covalent mixing is also the same. But the t_2 -orbitals are allowed by symmetry to mix with the ligand orbitals whilst the e-orbitals are forbidden, suggesting that the degree of covalent mixing should be different.

The BCA theory is a simplified version of the general crystal field theory. But the simplifications lead to inconsistencies in the theory, and the interpretation of the parameters found by comparison of theory and experiment is difficult.

3.10 -A new version of crystal field theory-

The foregoing discussion illustrates the problems encountered in the interpretation of experimental data from internal transitions within a $3d^n$ configuration. In a most general theory eleven parameters are required to describe the energy levels, and so this theory is of no practical use to the experimentalist in the interpretation of data. On the other hand, the simplifications in the BCA theory lead to inconsistencies in the theory, and the interpretation of the parameters is difficult. There is therefore a need for a new intermediate version of crystal field theory, where simplifications made to the general theory lead to a small number of

adjustable parameters, but where the physical significance of those parameters is not lost. Such a theory is outlined here.

When a transition metal impurity is substitutional on a cation site in a compound semiconductor with T_d point group symmetry, the d representation is reduced into irreducible components e and t_2 . In physical terms, the e and t_2 -orbitals are modified, to different extents, by the crystalline environment. Several effects may contribute to the modification of the impurity d -orbitals, and two examples are given here.

First, the d -orbitals are partially screened from the impurity core by the other electrons in the crystal. Therefore, the radial functions of the impurity d -orbitals might be more extended than in the free ion. Second, the valence electrons of the four nearest neighbours, tetrahedrally coordinated about the impurity ion, have T_2 symmetry. Consequently the t_2 -orbitals are allowed by symmetry to mix with the ligand orbitals, leading to delocalisation. The e -orbitals are forbidden to mix, and so delocalise to a lesser extent.

Thus it seems reasonable to expect that the impurity e and t_2 -orbitals are modified from their free ion states to different extents. The d -orbitals delocalise, and so the electrostatic interaction between them is reduced. It is assumed that the modifications are small, so that the one-electron functions of the impurity ion are still separable into radial and angular parts, and that the angular function is unchanged from that in the free ion, i.e. it is still a second order spherical harmonic. Then, analogous to the free ion case, the electrostatic integrals will have the form:

$$\sum_{k=0}^{\infty} \int R_{n_i l_i}(r_1) R_{n_j l_j}(r_2) e^2 \frac{r_1^k}{r_2^{k+1}} R_{n_m l_m}(r_1) R_{n_t l_t}(r_2) r_1^2 r_2^2 dr_1 dr_2$$

$$\cdot \int Y_{l_i m_i}(\theta_1, \phi_1) Y_{l_j m_j}(\theta_2, \phi_2) P_k(\cos \omega) Y_{l_m m_m}(\theta_1, \phi_1) Y_{l_t m_t}(\theta_2, \phi_2) d\theta_1 d\theta_2 d\phi_1 d\phi_2$$

$$\cdot \delta(s^i s^m) \delta(s^j s^t)$$

This equation and eq.3.25 are identical, except that here there is an impurity radial integral, whereas in eq.3.25 there is a free ion radial integral. The angular and spin parts are the same in both equations, and have the same numerical solution. For the free ion, all the radial functions are identical. For the impurity, the t_2 radial functions differ from the e radial functions.

The impurity radial integrals of eq.3.30 may be related to the free ion radial integrals. A parameter ϵ is defined such that the radial electrostatic integral between e-orbitals is related to the free ion radial integral by:

$$\int_{\frac{r_<}{r_>}} R_e R_e e^2 r_<^k R_e R_e r_1^2 r_2^2 dr_1 dr_2 = \epsilon^4 \int_{\frac{r_<}{r_>}} R_o R_o e^2 r_<^k R_o R_o r_1^2 r_2^2 dr_1 dr_2 \quad 3.31$$

Another parameter τ is defined, relating the t_2 radial integral to the free ion radial integral:

$$\int_{\frac{r_<}{r_>}} R_t R_t e^2 r_<^k R_t R_t r_1^2 r_2^2 dr_1 dr_2 = \tau^4 \int_{\frac{r_<}{r_>}} R_o R_o e^2 r_<^k R_o R_o r_1^2 r_2^2 dr_1 dr_2 \quad 3.32$$

From these definitions, half of the general electrostatic integrals from table 3.2 can be rewritten in terms of ϵ , τ , and the free ion Racah parameters A, B, and C:

$$\begin{aligned} a &= \langle \xi \xi | H_e | \xi \xi \rangle = \tau^4 (A + 4B + 3C) \\ b &= \langle \xi \eta | H_e | \xi \eta \rangle = \tau^4 (A - 2B + C) \\ e &= \langle \theta \theta | H_e | \theta \theta \rangle = \epsilon^4 (A + 4B + 2C) \\ f &= \langle \theta \theta | H_e | \epsilon \epsilon \rangle = \epsilon^4 (4B + C) \\ j &= \langle \xi \xi | H_e | \eta \eta \rangle = \tau^4 (3B + C) \end{aligned} \quad 3.33$$

It is assumed that the ratio of the impurity and free ion electrostatic integrals involving both e and t_2 orbitals can be simply related to ϵ and τ . Thus, to a good approximation, the other impurity

radial integrals can be related to free ion radial integrals by the relations

$$\begin{aligned}
 \int R_e R_t e^{\frac{2}{r_{<}^{k+1}}} R_e R_t r_1^2 r_2^2 dr_1 dr_2 &= \epsilon^2 \tau^2 \int R_o R_o e^{\frac{2}{r_{>}^{k+1}}} R_o R_o r_1^2 r_2^2 dr_1 dr_2 \\
 \int R_e R_e e^{\frac{2}{r_{>}^{k+1}}} R_t R_t r_1^2 r_2^2 dr_1 dr_2 &= \epsilon^2 \tau^2 \int R_o R_o e^{\frac{2}{r_{>}^{k+1}}} R_o R_o r_1^2 r_2^2 dr_1 dr_2 \\
 \int R_e R_t e^{\frac{2}{r_{>}^{k+1}}} R_t R_t r_1^2 r_2^2 dr_1 dr_2 &= \epsilon \tau^3 \int R_o R_o e^{\frac{2}{r_{>}^{k+1}}} R_o R_o r_1^2 r_2^2 dr_1 dr_2
 \end{aligned} \quad 3.34$$

The accuracy of this approximation is discussed further in Chapter 5.

The remaining general electrostatic integrals may be rewritten as

$$\begin{aligned}
 c &= \langle \theta \xi | H_e | \epsilon \xi \rangle = \epsilon^2 \tau^2 (2\sqrt{3}B) \\
 d &= \langle \epsilon \xi | H_e | \epsilon \xi \rangle = \epsilon^2 \tau^2 (A - 2B + C) \\
 g &= \langle \theta \theta | H_e | \eta \eta \rangle = \epsilon^2 \tau^2 (B + C) \\
 h &= \langle \theta \epsilon | H_e | \eta \eta \rangle = \epsilon^2 \tau^2 (\sqrt{3}B) \\
 i &= \langle \theta \eta | H_e | \xi \eta \rangle = \epsilon \tau^3 (\sqrt{3}B)
 \end{aligned} \quad 3.35$$

In this way, all of the electrostatic matrix elements can be written in terms of the free ion Racah parameters A, B, C, together with the new adjustable parameters of the theory, ϵ and τ , which are defined by the ratio of the impurity radial integrals to the free ion radial integral. Values for B and C, found by fitting the free ion energy matrices to atomic data, have been tabulated by Griffith [4] for the $3d^n$ transition metals, and the table is reproduced in the appendix. Thus the parameters B and C are not adjustable, but fixed by previous studies of atomic data.

The electrostatic integrals between impurity d-orbitals are reduced significantly from their free ion values. This reduction is measured by the reduction of ϵ and τ from their free ion values of unity. The reduction of the electrostatic interaction between the d electrons is a covalency effect, and so it is appropriate to refer to the parameters ϵ and τ as covalency parameters.

When ϵ and τ are both equal to one, the electrostatic integrals are at their free ion limit. This corresponds to no covalency effect. Conversely when ϵ and τ are zero, the electrostatic integrals are zero meaning that there are no orbitals present. Suppose that the degree of delocalisation is small. Then typical values for ϵ and τ may be in the region of 0.8 or 0.9 for the localised part. Simple calculations show that this leads to a reduction in the magnitude of the electrostatic interaction of around 50%. So the multiplet splitting of the transition metal impurity is significantly reduced with respect to the free ion.

In this version of the crystal field theory, the approximation is made that only one-centre integrals on the impurity site are significant. The electrostatic interactions between d-orbitals outside the impurity, together with d-orbital-ligand and ligand-ligand interactions, have been neglected. This is not a new idea, but has been used by many workers [34,35,36,15]. Because this approximation is made, then the new theory is only valid provided the degree of delocalisation of the d-orbitals is small. For a strong delocalisation of either t_2 or e-orbitals, then the d-d interaction integrals from outside the impurity become significant and must be included within the secular determinant. Such an inclusion would necessarily increase the number of adjustable parameters and so render the method intractable.

The application of the theory is a test of the assumption that the d-orbitals only delocalise by a small amount. If agreement between theory and experiment is good, when the values of the parameters ϵ and τ are physically reasonable, i.e. close to unity, then this is strong evidence to support the crystal field picture of a substitutional transition metal impurity.

3.10.1 -the energy matrices-

The new secular determinant now contains matrix elements in terms of the free ion Racah parameters A, B, C, the covalency parameters ϵ and τ , and the crystal field parameter Δ . In this form the new theory involves four adjustable parameters ϵ , τ , Δ , A. Terms involving A appeared identically on the diagonal of the free ion secular determinant, so that A can not be found from atomic data. For the impurity ion, terms involving A still only appear on the diagonal of the secular determinant, and so they can be combined with Δ to produce a single, new disposable parameter called Δ_p . The new parameter contains both one-electron and two-electron components. Now in the application of the new version of the theory, only three disposable parameters ϵ , τ , and Δ_p , appear in the energy matrices.

A problem arises by reducing the number of adjustable parameters from four to three. The new parameter Δ_p is determined from experiment and is therefore taken to be constant for each system. This means that the difference in energy between the configurations $t^m e^l$ and $t^{m+1} e^{l-1}$ arising from terms in A should also be constant for all values of m and l. Unfortunately this is not the case and so some error is introduced into the theory by combining terms in A and Δ to make a single parameter. This error is not large, and is discussed in chapter six. Because comparison with experiment, using the new version of crystal field theory, involves the use of the adjustable parameters ϵ , τ , and Δ_p , it is called the $\epsilon\tau\Delta_p$ theory in this thesis. The energy matrices for d^2 , d^3 , d^4 , and d^5 have been calculated and are presented in the appendix.

3.10.2 -electrons and holes-

Griffith [4] shows that there is a general relationship between electrostatic interaction matrix elements for the electron configuration d^n and the hole configuration d^{10-n} or d^{nh} . The energy matrices for d^n are the same as for d^{10-n} , except for an additional contribution to the diagonal matrix elements. This diagonal contribution, in terms of the parameters of the $\epsilon\tau\Delta_p$ theory, is:

$$t_2^{6-m} e^{4-1} = t_2^m e^1 + \tau^4 (3-m)(5A - 10B + 5C) + \epsilon^2 \tau^2 (2m + 31 - 12) \cdot (-2A + 2B - C) + \epsilon^4 (2-1)(3A - 8B + 4C) \quad 3.36$$

where $t_2^{6-m} e^{4-1}$ and $t_2^m e^1$ in this case are the diagonal matrix elements of the respective configurations. This contribution to the diagonal is constant between the configurations $t^m e^1$ and $t^{m+1} e^{1-1}$ for all m and l , and can be included within Δ_p .

Therefore it is only necessary to calculate the secular determinants for d^n , where $n < 5$. For $n > 5$, the d^{10-n} secular determinant is the same as the d^n determinant, except that the sign of Δ_p is reversed. This makes the conversion between d^n and d^{10-n} energy matrices very similar to the conversion in the $BC\Delta$ theory, where only the sign of Δ is reversed. However it should be remembered that Δ_p has both one-electron and two-electron contributions. In the electron configuration matrices, it has contributions arising from terms in A, whilst in the hole formalism there are terms in B and C too.

3.10.3 -comparison with other covalency models-

Several attempts have been made previously to include covalency effects within crystal field theory. The new theory outlined in the previous sections is more general than these.

Koide and Pryce [34], treating $Mn(d^5)$ in octahedral compounds, introduced new electron orbitals which were a linear combination of the e-orbitals and ligand orbitals:

$$\text{Cos}\theta |3d e\rangle + \text{Sin}\theta |\sigma\rangle \quad 3.37$$

where $|\sigma\rangle$ is some appropriate linear combination of ligand σ orbitals. The t_2 -orbitals are unaffected by covalency. The degree of delocalisation is not large, so that $\text{Cos}\theta$ is close to unity and $\text{Sin}\theta$ is close to zero. Thus in the evaluation of the electrostatic matrix elements, the second term in eq.3.37 is neglected. The energy matrices which they calculated are analytically equivalent to the $\epsilon\tau\Delta_p$ energy matrices if ϵ is set equal to $\text{Cos}\theta$ and τ is unity.

Curie et al [37], when studying $Mn(d^5)$ in a series of compounds, introduced "normalisation parameters" as multiplicative factors for the d-orbitals, N_t and N_e . Improvements to the model were made by including the ligand orbitals, so that the impurity e and t_2 -orbitals become

$$\psi_e = N_e (\phi_e - \lambda_e \chi_\sigma); \quad \psi_t = N_t (\phi_t - \lambda_t \chi_\pi) \quad 3.38$$

As a result, several new parameters are introduced into the secular determinant.

Previously, Lohr treated the $Mn(d^5)$ energy levels in some detail using an LCAO model [35]. He assumes a mostly 3d molecular orbital of the form

$$\psi = C_d \phi_d + C_l \phi_l; \quad C_d > C_l \quad 3.39$$

where ϕ_d is the one-electron d-orbital and ϕ_l is a ligand symmetry

orbital. Electrostatic matrix elements are then reduced from the free ion value by a multiplicative constant f_d^2 , where

$$f_d = c_d^2 + c_d c_1 S_{dl}$$

and S_{dl} is an overlap integral. The covalency parameters ϵ and τ correspond with $(f_d)^{1/2}$. Terms involving metal-ligand integrals are ignored. This is a reasonable approximation if the degree of delocalisation, and therefore c_1 , is small. The term c_1 appears to the fourth power, making the integrals very small. In later work [38], the previously neglected terms were included in the calculation of excited states. These extra terms appear mainly on the diagonal matrix elements.

Biernacki and Schulz [36,39] include covalency effects by modifying free ion Radial Slater functions. It is reasonable to expect that the 3d wavefunctions of the impurity in the crystal are extended in comparison to the free ion wavefunctions, and so the orbital exponent is modified:

$$R(r) = [(2ky/6!)^7]^{1/2} r^2 \exp(-ykr)$$

where k characterises the extent of the free ion and y is less than unity. These radial functions are then used to construct and solve a secular determinant.

In each of these previous attempts at including covalency effects in crystal field theory, the one-electron wavefunctions are modified in a specific way. Then matrix elements are constructed using these modified wavefunctions. Therefore the adjustable parameters contained in the secular determinant define the particular choice of modification imposed on the one-electron function.

In the $\epsilon\tau\Delta_p$ theory, it is recognised that the one-electron functions are modified from their free ion state, and that this will affect the electrostatic matrix elements of the secular determinant.

But instead of modifying the one-electron functions, the adjustable parameters of the theory are defined in terms of the modifications of the electrostatic integrals themselves. The parameter ϵ is defined by reduction of the electrostatic interaction between e-orbitals, whilst τ is defined by the reduced interaction between the t_2 -orbitals. The $\epsilon\tau\Delta_p$ theory is therefore more general in its approach to the inclusion of covalency in a practical crystal field fitting scheme.

3.10.4 -comparison with one-electron theory-

Crystal field theory provides a way of comparing experimental data with first principles theory. This comparison is made through the adjustable parameters of the $\epsilon\tau\Delta_p$ theory.

The parameters can be found from experiment: they are varied until the best agreement is found between the absorption barycentres and the crystal field energy levels. The parameters can also be found from theory: the one-electron functions can be calculated from a variety of approximate methods [13,15]. These functions may then be used to construct the radial integrals of eq.3.31 and eq.3.32, from which ϵ and τ can be found. One-electron theories also provide an estimate of Δ , which is contained within Δ_p . More importantly, theoretical calculations may be used to check the validity of the assumptions in eqs.3.34, which are crucial to the $\epsilon\tau\Delta_p$ theory. A test of these assumptions has been made in chapter five, where, first, modified free ion Slater wavefunctions, and then radial functions from the quasiband crystal field method [13] have both been used.

Hemstreet and Dimmock [15] have reported $X\alpha$ scattered wave calculations for transition metals in GaAs. To compare the results

with experiment, they constructed a secular determinant which is analytically the same as the $\epsilon\tau\Delta_p$ determinant if ϵ^2 is taken to be the fraction of d-like charge associated with the e-orbital contained within the impurity sphere, called R_{ee} , and τ^2 is the fraction of charge associated with the t_2 -orbital, called R_{tt} . This interpretation of the covalency parameters differs from the one presented in this thesis, where they are taken to define the reduction of the d-d electrostatic interaction in the crystal. The parameters R_{ee} and R_{tt} were found from the scattered wave calculations and then used to find the roots of the secular determinant, which they compared to the experimentally observed energy levels.

3.11 -Energy level diagrams-

It is helpful to have diagrams showing the variation of energy levels for each configuration, as a function of the adjustable parameters of the theory. Such diagrams have been made for the energy levels of the $BC\Delta$ theory, and are useful in the interpretation of the absorption data. Tanabe and Sugano [1] show the excited states of the $3d^n$ configurations as a function of Δ/B , whilst Orgel [28] plots energy levels against Δ . In both cases, the ratio C/B is fixed, usually at the free ion value.

The energy levels calculated by the $\epsilon\tau\Delta_p$ theory must be shown both as a function of Δ_p and of ϵ or τ . Each of the electrostatic matrix elements contain a multiplicative product $\tau^m \epsilon^l$, where $l+m=4$. This product can be written as

$$\tau^4 (\epsilon/\tau)^l$$

If the electrostatic matrix elements are all written in this way then

it is clear that the $(\epsilon/\tau)^1$ term governs the relative separation of the levels, whilst τ^4 just scales the separation of all levels. In other words, it is the ratio of ϵ/τ which governs the energy level relative separations, which are of interest here.

Thus, in the $\epsilon\tau\Delta_p$ energy level diagrams, ϵ is fixed at unity whilst τ is varied. This is equivalent to varying the ratio ϵ/τ , which governs the relative separation of the levels. When ϵ and τ are equal, the analytic form of the $\epsilon\tau\Delta_p$ secular determinant is the same as the $BC\Delta$ determinant. For the latter, it has been seen that the variation of Δ has a considerable impact on the separation of the levels. In the same way, Δ_p will have a significant effect on the energy levels found from the $\epsilon\tau\Delta_p$ theory.

Ideally, therefore, a 3-dimensional plot of Energy versus τ and versus Δ_p is necessary to display the range of possible energy levels. In view of the large number of energy levels, such a graph would be unintelligible. As an alternative, "slices" through the 3-dimensional graph can be presented quite clearly. Such a graph is shown in fig.3.4 for the d^7 configuration. Three graphs (the slices), of the d^7 energy levels as a function of τ , for $\Delta_p=0$, $\Delta_p=B/2$ and $\Delta_p=B$ are shown. Of course, the slices may be taken at any values of Δ_p . With several slices shown together, the variation of the levels as a function of Δ_p can be seen. An alternative would be to compare graphs of energy levels as a function of τ , for different values of Δ_p , in the same way. In the application of the theory to experimental data, I have used both of these styles of energy level diagram. Energy level diagrams for the other d^n configurations in tetrahedral symmetry are given in the appendix.

3.12 -Smaller perturbations-

Crystal field theory provides the experimentalist with a method of describing a large quantity of optical absorption data using only three parameters. It describes the main features of the spectrum, but does not explain why the observed crystal field transitions are broad, often with fine structure. This is because perturbations which are small in comparison to the crystal field splittings have been ignored. Their inclusion leads to a considerable complication of the analysis, by introducing additional adjustable parameters which confuse the picture.

In this section, some of these small perturbations and their impact on the observed spectra are discussed.

3.12.1 -spin orbit coupling-

The interaction between the electron spin magnetic moment, s , and the internal magnetic field of an atom is called the spin orbit interaction. For a one-electron atom, using Dirac's relativistic equation for a central field, the interaction is

$$H_{SO} = \frac{-e}{2m^2 c^2 r} \frac{dU(r)}{dr} \underline{l} \cdot \underline{s} = \xi(r) \underline{l} \cdot \underline{s} \quad 3.40$$

where $U(r)$ is the electrostatic central field [4]. For a many-electron atom, the equation is generalised by retaining the one-electron operator and summing over the electrons:

$$H_{SO} = \sum_k^n \xi(r_k) \underline{l}_k \cdot \underline{s}_k \quad 3.41$$

It may be recalled from sec 3.6.2 that the starting wavefunctions of the crystal field secular determinant are taken to be

$n \times n$ Slater determinants, typically

$$\psi_i = |\phi_1^i(1), \phi_2^i(2), \dots, \phi_n^i(n)\rangle \quad 3.42$$

The spin orbit interaction matrix element between two such starting wavefunctions ψ_i and ψ_j is

$$\langle \psi_i | H_{SO} | \psi_j \rangle = \sum_k^n \langle \phi_k^i(k) | \xi(r_k) \frac{1}{k} \cdot \frac{s_k}{k} | \phi_k^j(k) \rangle \quad 3.43$$

If the one-electron functions are separable into radial, angular, and spin parts as before, then the angular and spin parts may be evaluated once and for all leaving the radial integrals

$$\int R_i(r) \xi(r) R_j(r) r^2 dr \quad 3.44$$

For a free ion values for this integral, found by a comparison with atomic data, vary between 50cm^{-1} and 650cm^{-1} for the transition metals studied in this thesis. For an impurity ion, there are three possible radial integrals, because of the two radial functions R_e and R_t :

$$\begin{aligned} \zeta &= \int R_t \xi R_t r^2 dr \\ \zeta' &= \int R_t \xi R_e r^2 dr \\ \zeta'' &= \int R_e \xi R_e r^2 dr \end{aligned} \quad 3.45$$

The parameters ζ , ζ' , and ζ'' are called the spin orbit coupling constants. But the matrix elements between two e-orbitals are zero [40] which leaves just two coupling parameters ζ and ζ' .

The spin orbit matrix elements must be spherically symmetric, and the operator H_{SO} has A_1 symmetry. Therefore, spin orbit matrix elements are only non zero between two starting wavefunctions of the same double group symmetry. The symmetry is found by taking the direct product of the spin and orbital symmetries of the crystal field levels. As an example, for the 3T_1 level the double group symmetry is

$$T_1 \times T_1 = A_1 + T_1 + E + T_2.$$

In table 3.3, the double group symmetry for all of the d^2 configuration crystal field levels is given. The table shows that the crystal field levels 1T_2 , 3T_1 , 3A_2 and 3T_2 each contain the double

Table 3.3
 Double group representations for the d^2 configuration in T_d .

Crystal Field Term	Double Group Representation
1A_1	A_1
1E	E
1T_1	T_1
1T_2	T_2
3A_2	T_2
3T_1	$A_1 + E + T_1 + T_2$
3T_2	$A_2 + E + T_1 + T_2$

group symmetry T_2 . The T_2 "sublevels" couple by the spin orbit interaction, because they have the same double group symmetry. Thus each T_2 sublevel will be shifted in energy by the spin orbit interaction.

In this way, each sublevel will couple to other sublevels of the same double group symmetry, resulting in an energy shift. In the 3T_1 crystal field level, each of the four sublevels couple via different spin orbit matrices, so that each level shifts by a different amount as a result of the spin orbit interaction. In other words the crystal field level 3T_1 is split into four sub-levels by the spin orbit interaction.

The spin orbit levels appear as sharp fine structure in the crystal field absorption bands. Covalency effects reduce the spin orbit coupling constants from the free ion value. The parameter ζ is expected to be less than ζ' because the t_2 -orbitals delocalise to a greater extent than the e-orbitals. Spin orbit coupling introduces two new adjustable parameters into the theory.

The mixing of crystal field levels by spin orbit coupling means that previously forbidden transitions may be allowed. For this reason, spin orbit coupling has been included in some calculations, usually with ζ and ζ' fixed at a value reduced from the free ion value.

3.12.2 -Jahn-Teller Effect-

The Jahn-Teller theorem states that a degenerate electronic state of an impurity is unstable against a distortion that will remove the degeneracy and split the level [41]. Consider a transition metal with a degenerate ground state in a cubic crystal, when a strain, or distortion, is applied. There is an increase of the lattice energy quadratically with strain, whilst the electronic ground state will be split by the induced electric field, thus lowering the electronic energy linearly with strain. At small strains, the total (lattice + electronic) energy decreases, but for larger strains it increases. The total energy therefore passes through a minimum at a non-zero value of strain.

The degenerate electronic level may couple to more than one lattice vibration mode. As a rule, for an electronic state of symmetry Γ_i to couple to a mode of symmetry Γ_j then Γ_j must be contained within the symmetric square of Γ_i , $[\Gamma_i]^2$ [42]. The calculation of vibrational electronic (vibronic) energy levels is complicated, particularly when several lattice modes are active [42]. Calculations using the Jahn-Teller model are made (see for example ref [43]) but the modifications to the spectrum are small compared to the crystal field effects.

If Jahn-Teller coupling is weak then a strong zpl appears together with small phonon replicas. For strong coupling, the zpl intensity is reduced, and the intensity of the side bands is increased.

3.12.3 -Racah-Trees and seniority corrections-

Agreement between the free ion energy matrices and atomic data may be improved by including the terms

$$\alpha L(L+1) + \beta q \quad 3.46$$

to the diagonal matrix elements. The parameters α and β are adjustable, whilst L and q are defined in references [44,45]. The first term is called the Racah-Trees correction, and the second is the seniority correction.

Curie et al [37] have included these corrections in a study of $Mn(d^5)$ using $\alpha = 65\text{cm}^{-1}$ and $\beta = -131\text{cm}^{-1}$. The effect on the energy levels is small compared with the crystal field splittings and so the corrections are ignored in this thesis.

3.12.4 -Trigonal distortion-

In some of the II-VI semiconductors studied in this thesis, the crystal structure is not purely cubic T_d , but has a small trigonal distortion. For these systems, the crystal field is written as a sum of the tetrahedral part and the trigonal part. The trigonal field gives rise to a further small splitting of the crystal field levels, thus adding fine structure to the absorption bands. The tetrahedral part is parameterised by Δ in the crystal field theory, whilst the trigonal part is ignored in this thesis. Macfarlane [46] has constructed matrix elements for the trigonal field. They contain two adjustable parameters v and v' . For the absorption spectrum of $ZnO:Co$, Koidl [47] finds the values of v and v' to be 120cm^{-1} and 320cm^{-1} respectively, by comparing Macfarlane's matrices with

experimental data.

3.13 -Summary-

In this chapter a description of crystal field theory has been given in sufficient detail to show how the secular determinants given in the appendix have been derived. The starting wavefunctions are constructed from a strong-field basis set which are obtained as eigenfunctions of the central field problem. The choice of starting wavefunctions leads to a partial diagonalisation of the secular determinant into smaller sub-determinants or energy matrices. The crystal field matrix elements are written in terms of Δ , the separation of the one-electron e and t_2 -orbitals. The electrostatic matrix elements are written in terms of ten independent two-electron integrals.

A general version of crystal field theory involves eleven adjustable parameters which means it is of no practical use. The BCA theory is a simplified version of the theory where the free ion electrostatic matrix elements are used. But the simplification leads to inconsistencies in the theory and the interpretation of the adjustable parameters is difficult.

A new version of crystal field theory is proposed in this chapter. The electrostatic interactions within the d-shell are reduced from their free ion values by covalency effects. The reduction of the interactions between e-orbitals and between t_2 -orbitals are defined by the adjustable parameters ϵ and τ respectively. A third adjustable parameter Δ_p , corresponding to Δ in the BCA theory, contains both one-electron and two-electron

contributions. The approximation is used that only one-centre integrals on the impurity site are significant. For a strong delocalisation of the d-orbitals, the other one-centre integrals and the two-centre integrals become significant, which introduces many more parameters and renders the method intractable.

The new theory involves the use of three adjustable parameters, ϵ , τ , and Δ_p . It is as easy to use as the BCA theory and agreement between theory and experiment is often better (see chapter four). In addition the comparison between first principles theory and the new adjustable parameters is more meaningful.

Several attempts have been made previously to include covalency effects in the crystal field theory. The $\epsilon\tau\Delta_p$ theory is more general than these, because it defines its adjustable parameters in terms of the modification of the electrostatic interaction rather than the one-electron orbitals.

CHAPTER FOUR
APPLICATIONS OF CRYSTAL FIELD THEORY I:
IMPURITIES IN II-VI COMPOUNDS

4 APPLICATIONS OF CRYSTAL FIELD THEORY I: IMPURITIES IN II-VI COMPOUNDS

4.1 -Introduction-

This chapter reports the successful application of the $\epsilon\tau\Delta_p$ theory to a wide range of transition metal impurities in II-VI compounds. The optical absorption spectrum of $\text{Co}(d^7)$ in seven different crystals and $\text{Ni}(d^8)$ in five crystals have been investigated using the $\epsilon\tau\Delta_p$ theory. These spectra have been considered previously in terms of the BCA theory, and a comparison between the two methods of analysis is made here. A similar treatment is given to the spectra of a range of impurities from $\text{Ti}(d^2)$ through to $\text{Ni}(d^8)$ in ZnS .

It was of interest to study the variation of the parameters ϵ , τ and Δ_p for a specific host crystal as the impurity ion was varied, as well as to study specific impurity ions as the host was varied. These objectives determined my choice of systems to be investigated.

This chapter concentrates on the analysis of the spectra in terms of the $\epsilon\tau\Delta_p$ theory, and compares the results with the BCA analysis. The work is concerned mainly with a description of the broad details of the spectra, and an interpretation of the fine structure is not usually included. Before trends in the parameters can be discussed, errors in the construction of the theory and its application must be considered, so that genuine trends and random fluctuations resulting from inaccuracies in the theory can be separated. The estimation of errors in the theory, and a discussion of trends observed in the parameters will be dealt with in later chapters.

It is an advantage in the application of a semiempirical theory such as the $\epsilon\tau\Delta_p$ theory to have a lot of experimental data. In this way some of the data can be compared with specific theoretical energy levels and the empirical parameters calculated. The predicted levels can then be compared with the other observed structure and refinements to the parameters can be made where necessary.

For a transition metal impurity with a d^n configuration, the position of the impurity level with respect to the conduction band may be defined as the energy required to take an electron from the configuration and place it at the bottom of the conduction band far from the impurity. Griffith [4] has shown that for free ions, ignoring electrostatic interactions within the d-shell and crystal field effects, the ionisation potential varies approximately linearly with atomic number. If it is assumed that for ions in crystals the same approximation holds, then the position of the impurity levels within the energy gap varies as shown in fig.4.1a [7]. Consequently it will be easiest to populate those levels whose configurations contain most d-electrons. To fill the levels d^2 or d^3 a high concentration of donors is required so as to push the Fermi level closer to the conduction band. In addition, impurity to band transitions will hide more of the d^n spectrum when n is low. When electrostatic and crystal field effects are included, deviations from the linear variation with atomic number occur. These deviations are typically as shown in fig.4.1b [48,49]. Thus more experimental data are available for $\text{Co}(d^7)$ and $\text{Ni}(d^8)$ than for the other transition metal impurities, and so these systems are well suited to the application of the $\epsilon\tau\Delta_p$ theory.

Table 4.1 lists those tetrahedral II-VI compounds containing transition metal impurities neutral with respect to the lattice which

Fig 4.1a
 Energy levels of $3d^n$ impurities in a semiconductor, ignoring electrostatic and crystal field interactions.

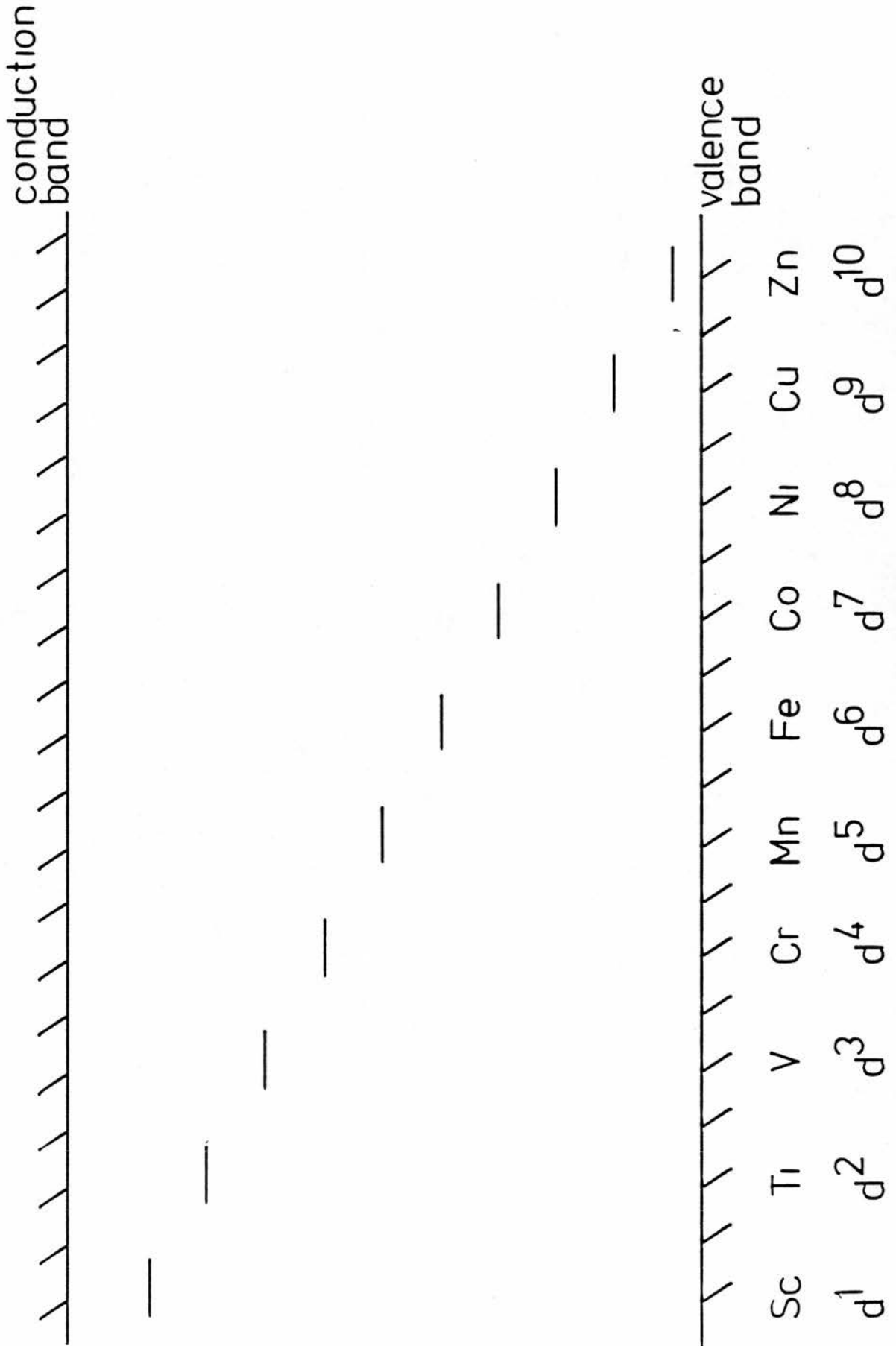
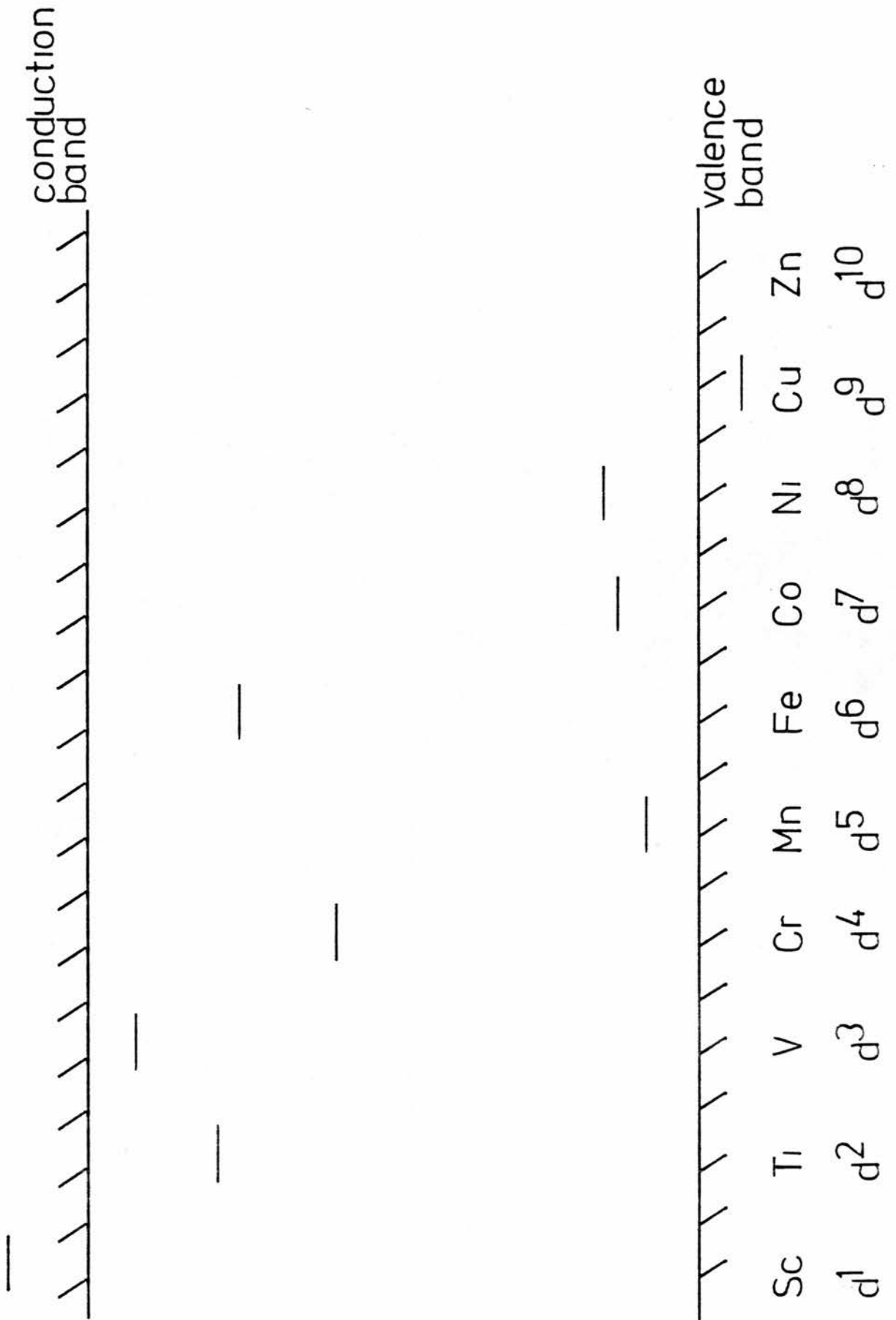
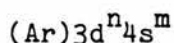


Fig 4.1b
 Energy levels of $3d^n$ impurities in a semiconductor (eg GaAs), including electrostatic and crystal field interactions



have been studied by an optical method or by spin resonance. Optical studies of $\text{Co}(d^7)$ have been carried out in all seven of the semiconductors tabulated, making it a good choice for studying the variation of parameters for a specific impurity in a range of hosts. Optical studies of $\text{Ni}(d^8)$ have been made in five hosts and so it too is used to study the same parameter trends. Zinc Sulphide is chosen to study the parameters for a specific host containing different impurities. The large band gap of ZnS (3.6eV) means that fewer d-d transitions are hidden by band to band and impurity to band transitions [48]. Table 4.1 shows that optical studies have been made for ZnS with a wide range of impurities.

The transition metals in the period Sc to Cu have the atomic configuration:



When one of the II-VI compounds is doped with such a metal, there are several possible sites that the impurity ion might occupy. The impurity ion can replace a cation on a lattice site, or become an interstitial.

Ludwig and Woodbury [50] have obtained esr data for several tetrahedrally bonded materials, and propose the following model to explain their results. If an impurity has a free atom configuration $(\text{Ar})3d^n4s^2$, and if it is substituted for the group II element in a II-VI compound then the resulting impurity will have a $3d^n$ configuration and is neutral with respect to the lattice. Different charge states correspond to an increase or decrease in the number of electrons in the d shell. If an impurity occupies an interstitial site, the s electrons collapse into the d shell. Thus an impurity with a free atom configuration $(\text{Ar})3d^n4s^2$ would have the configuration $3d^{n+2}$ as a neutral interstitial. The interpretation of experimental

Table 4.1
 Observed $3d^n$ configurations in II-VI systems

	ZnO	ZnS	ZnSe	ZnTe	CdS	CdSe	CdTe
Sc(d^1)							
Ti(d^2)		O R	O		O R	O	O R
V(d^3)		O?	O		O	O	
Cr(d^4)		O R	O R	O R	O R	O	O R
Mn(d^5)	R	O R	O R	R	R	R	R
Fe(d^6)		O	O	O	O	O	O
Co(d^7)	O	O R	O R	O R	O R	O	O R
Ni(d^8)	O	O	O		O	O	
Cu(d^9)	O R	O		O			

O indicates study by an optical method

R indicates study by spin resonance

results presented in this thesis are consistent with the above model for an impurity.

4.2 -Cobalt in II-VI semiconductors-

Measurements from esr have been reported for cobalt impurities in ZnS, ZnSe, ZnTe, CdS and CdTe [50,95]. In each case the results suggest that cobalt is substitutional for a group II atom, neutral with respect to the host, and with a d^7 configuration. There are similarities between the optical absorption spectra for these systems and the spectra of cobalt impurities in ZnO and CdSe. Each spectrum can be described in terms of transitions within the $3d^7$ shell of the cobalt impurity. The two sets of results suggest that cobalt occurs as substitutional $3d^7$ for all of the systems studied here.

Weakliem [8] has published optical data on ZnO:Co, ZnS:Co, and CdS:Co, fitting the data to a BCA crystal field level scheme and Baranowski, Allen and Pearson [51] have done the same for ZnSe:Co, ZnTe:Co, and CdTe:Co. Langer and Baranowski [9] have studied CdSe:Co and additional data on the various spectra provided by other workers [52,10,47,32,53] have all been examined in the present investigation.

The crystal field ground state for $Co(d^7)$ is 4A_2 and so the strongest transitions are to the other quartet states ${}^4T_1(P)$, ${}^4T_1(F)$ and 4T_2 . The spectra display several similarities. A strong, broad band is observed in the region of 12000cm^{-1} to 15000cm^{-1} due to the ${}^4A_2 - {}^4T_1(P)$ transition showing structure due to spin orbit splitting and mixing with nearby doublets. Another, narrower, band is found around 6000cm^{-1} due to the ${}^4A_2 - {}^4T_1(F)$ transition, and a third, much weaker, absorption due to the symmetry forbidden ${}^4A_2 - {}^4T_2(F)$

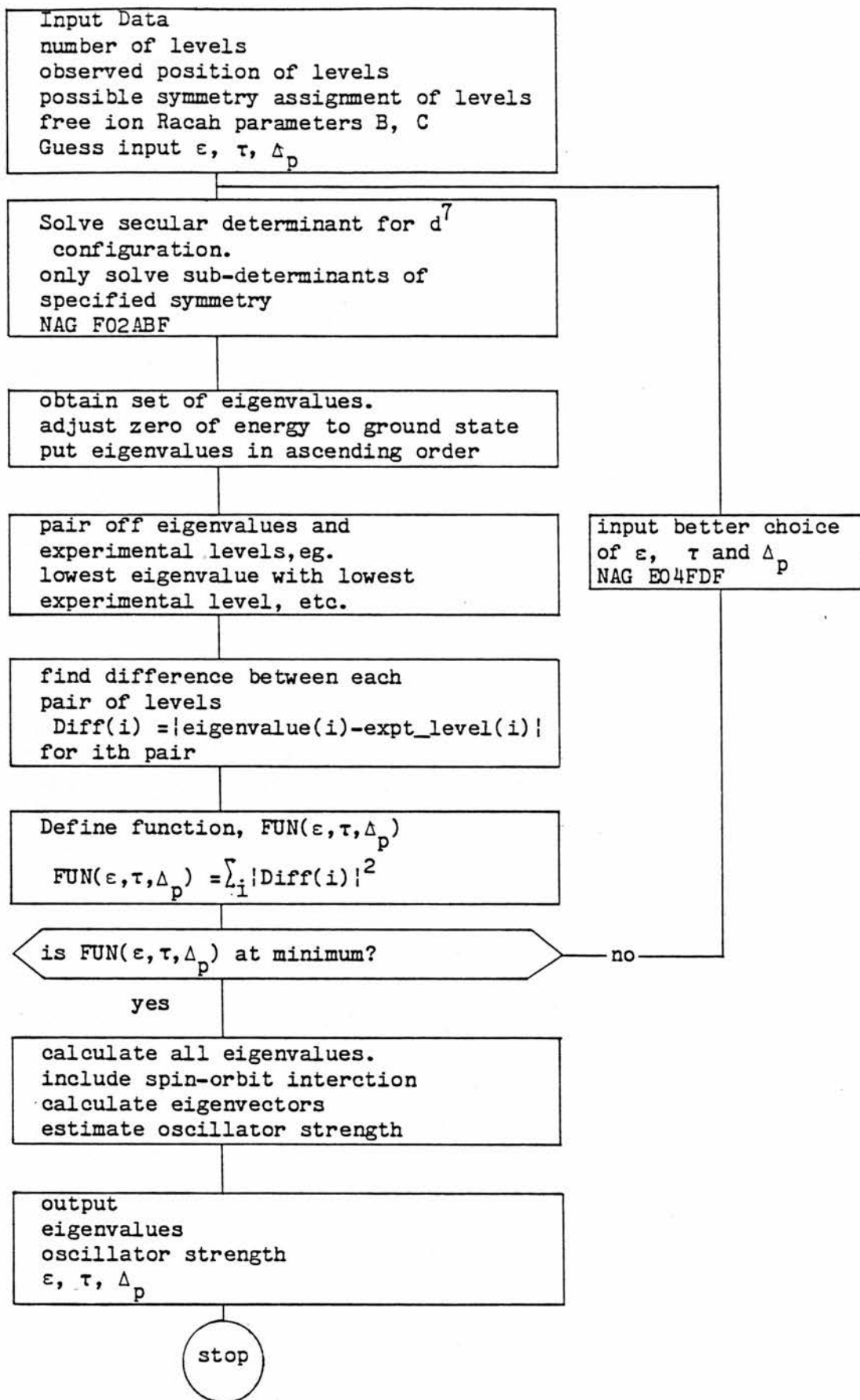
transition around 3500cm^{-1} is found only in some of the spectra. The transition ${}^4A_2 - {}^4T_1(P)$ might be expected to be broader than the other quartet transitions as it involves a transition between the hole configurations $t_2^3 \rightarrow e^2t_2$, compared with $t_2^3 \rightarrow et_2^2$ for the other two.

Using a reasonable choice of parameters with either the $\epsilon\tau\Delta_p$ theory or the original BCA theory, agreement with experiment for the position of the quartet-quartet transitions is good. However the assignment of transitions corresponding to the weaker structure in the spectra, as well as the extra structure predicted by the theories, is quite often different.

The $\epsilon\tau\Delta_p$ theory is applied by varying three disposable parameters ϵ , τ and Δ_p so as to obtain crystal field energy levels in closest agreement with the many electron energy levels observed experimentally. To begin with a provisional assignment of parameters is made by fitting to just the three quartet levels. The resulting "best fit" will predict some quartet-doublet structure. This predicted structure can be compared with the weaker structure experimentally observed and from this comparison an assignment of the weaker structure to specific transitions is possible. Thus a second assignment of parameters is attempted fitting not only to the quartet levels but also to some of the doublet levels. For those spectra where only two quartet levels have been observed then doublet levels have to be included throughout the analysis. Calculations of the best values of disposable parameters for each spectrum and the corresponding eigenvalues have been carried out using a Digital Vax-11/780 computer. A flow chart describing the programs used is shown in fig.4.2.

Having obtained a best set of parameters, spin orbit coupling is

Fig.4.2

Flow chart describing programs used in the application of the $\epsilon\tau\Delta_p$ theory

included in the d^7 configuration energy matrices approximately by setting the spin orbit coupling parameters ζ and ζ' equal to -400cm^{-1} . Evaluation of these energy matrices gives the final set of theoretical energy levels. Electric dipole transitions from the crystal field ground state 4A_2 are only symmetry allowed to 4T_1 levels. When spin orbit coupling is included then electric dipole transitions from the ground state (with double group symmetry representation Γ_8) are allowed to levels with representation Γ_6 , Γ_7 or Γ_8 . Thus spin orbit coupling is necessary to explain all of the experimental detail. It was not included until the final stages of my calculations because it would have led to an unnecessary complication of the calculations earlier. Other interactions, in particular Jahn-Teller coupling, have also been neglected to simplify the analysis, since this work is primarily concerned with a description of the broad details of the spectra investigated.

The optical absorption spectra for seven of the II-VI compounds containing $\text{Co}(d^7)$ as an impurity have been analysed in this way. A description of the analysis in terms of the $\epsilon\tau\Delta_p$ theory for each of the systems, together with a comparison with previous work using the $\text{BC}\Delta$ model is presented in the following sections. A concise summary of the results is presented in table 4.2. The top section of the table summarises the initial assignment of parameters by fitting the crystal field levels mainly to quartet levels. For each level considered in the analysis, the experimentally observed barycentre is given followed by the theoretically determined barycentre and the representation assignment for that level. Below the levels are given the corresponding assignment of parameters ϵ , τ and Δ_p , from which the theoretical levels were determined. In the lower section of the table, details of the final assignment are provided. The format is

Table 4.2
Summary of results for $\text{Co}(d^7)$ in II-VI compounds.

		ZnO	ZnS	ZnSe	ZnTe	CdS	CdSe	CdTe

First Assignment								
Level 1	energy	expt 4070	3700	3500	text	6000	3200	5430
		theory 4070	3700	3605	3448	6000	3305	5430
	symmetry	$4T_2$	$4T_2$	$4T_2$	$4T_2$	$4T_2$	$4T_2$	$4T_1$
Level 2	energy	expt 6800	6200	6300	text	14000	5800	11000
		theory 6800	6200	6234	5893	14000	5735	11000
	symmetry	$4T_1$	$4T_1$	$4T_1$	$4T_1$	$4T_1$	$4T_1$	$4T_1$
Level 3	energy	expt 16460	14200	13500	text		13000	11930
		theory 16400	14200	13500	12500		13000	11930
	symmetry	$4T_1$	$4T_1$	$4T_1$	$4T_1$		$4T_1$	$2T_1$
parameters	ϵ	0.860	0.960	0.884	0.900	0.959	0.878	0.828
	τ	0.935	0.821	0.837	0.800	0.820	0.837	0.788
	Δ_p	2760	5560	4510	4660	5440	3864	3614

Final Assignment								
Level 1	energy	expt 4070	3700	3500	5800	6000	text	5430
		theory 4119	3748	3674	5778	6000	text	5388
	symmetry	$4T_2$	$4T_2$	$4T_2$	$4T_1$	$4T_1$		$4T_1$
Level 2	energy	expt 6800	6200	6300	11070	14400	text	11000
		theory 6826	6179	6186	11182	14400	text	11124
	symmetry	$4T_1$	$4T_1$	$4T_1$	$4T_1$	$4T_1$		$4T_1$
Level 3	energy	expt 15200	14200	13500	11785	16400	text	11930
		theory 15190	14613	13720	11737	16400	text	11882
	symmetry	$2E$	$4T_1$	$4T_1$	$2T_1$	$2T_2$		$2T_1$
Level 4	energy	expt 16460	20526	19100	12250		text	12320
		theory 16274	20225	18944	12213		text	12273
	symmetry	$4T_1$	$2T_1$	$2T_1$	$2T_2$			$2T_2$
BEST PARAMETERS								
	ϵ	0.849	0.981	0.945	0.854	0.947	0.935	0.859
	τ	0.934	0.823	0.813	0.770	0.842	0.813	0.780
	Δ_p	2650	5900	5370	4290	5000	4700	4020

All energies are given in cm^{-1}

similar to the first assignment. The set of parameters obtained in the final assignment are considered the best parameters to describe the particular system.

4.2.1 -ZnS:Co, an example-

As an illustration of the procedure outlined above, the $\epsilon\tau\Delta_p$ theory is applied to the problem of ZnS:Co(d^7). The absorption spectrum has been studied in detail by Weakliem [8] who has observed the three quartet-quartet transitions with barycentres around 3700cm^{-1} , 6200cm^{-1} , and 14200cm^{-1} . More recently Noras, Szawelska and Allen [32] have observed a series of sharp peaks at higher energies in absorption which they believed were due to three zero phonon lines (zpl) and vibronic sidebands associated with excited states of the Co(d^7) impurity. That part of the spectrum between 18000cm^{-1} and 20400cm^{-1} was found to be flat and featureless.

The closest agreement of crystal field energy levels with the three quartet states is found with the choice of disposable parameters:

$$\epsilon = 0.960 \qquad \tau = 0.821 \qquad \Delta_p = 5560\text{cm}^{-1}$$

Table 4.3a lists the eigenvalues for the d^7 configuration using these parameters and with the spin orbit coupling parameters ζ and ζ' equal to -400cm^{-1} . The list shows that a gap occurs in the eigenvalues between 16500cm^{-1} and 19600cm^{-1} . It is reasonable to suppose that this corresponds with the experimentally observed gap in levels between 18000cm^{-1} and 20400cm^{-1} . A similar gap in absorption detail has been observed with ZnSe:Co, and its interpretation has been the subject of some debate [32,54,55]. This matter is discussed at

Table 4.3a
 First assignment of parameters for ZnS:Co

$\epsilon=0.960$

$\tau=0.821$

$\Delta_p=5560\text{cm}^{-1}$

Energy(cm^{-1})	Assignment	
22074	Γ_6	$2T_1$
21446	Γ_8	$2T_1$
19901	Γ_8	$2T_1$
19586	Γ_6	$2T_1$
16511	Γ_7	$2T_2$
16424	Γ_8	$2T_2$
15678	Γ_8	$2E$
15480	Γ_6	$2T_1$
15204	Γ_8	$2T_1$
14492	Γ_6	$4T_1$
14138	Γ_8	$4T_1$
14130	Γ_7	$4T_1$
14054	Γ_7	$4T_1$
12692	Γ_8	$2T_2$
12445	Γ_7	$2T_2$
12240	Γ_6	$2A_1$
9771	Γ_8	$2T_1$
9522	Γ_6	$2T_1$
9092	Γ_8	$2E$
6661	Γ_8	$4T_1$
6575	Γ_7	$4T_1$
6125	Γ_8	$4T_1$
5768	Γ_6	$4T_1$
3931	Γ_7	$4T_2$
3839	Γ_8	$4T_2$
3646	Γ_6	$4T_2$
3529	Γ_8	$4T_2$
0	Γ_8	$4A_2$

greater length in sec.4.2.3. I assigned the structure with a barycentre around 20500cm^{-1} to a transition from the ground state to the doublet at the top of the theoretical gap in eigenvalues. The best fit of the doublet and the three quartets with the experimental data is found with:

$$\epsilon = 0.981 \qquad \tau = 0.823 \qquad \Delta_p = 5900\text{cm}^{-1}$$

Using these parameters and with ζ and ζ' set equal to -400cm^{-1} the eigenvalues have been evaluated and are given in table 4.3b. An estimate of the intensity of the calculated levels can be made by finding the fraction of quartet T_1 character in each level (assuming that this is directly proportional to the line intensity.) The levels are plotted as a function of intensity together with the experimentally observed absorption spectrum in fig.4.4a. Using the parameters derived by Weakliem [8], a plot of energy levels as a function of intensity, found by applying the $BC\Delta$ theory, together with the observed spectrum is given in fig.4.4b

There are two principal differences between the results. Using the $BC\Delta$ theory there are doublet levels predicted in the region from 18000cm^{-1} to 20000cm^{-1} which have not been observed experimentally. In the $\epsilon\tau\Delta_p$ model a 2T_2 level has been pushed down and a 2T_1 level pushed up in energy giving a gap in the energy levels in this region. Secondly, some weak doublet structure is predicted using the $\epsilon\tau\Delta_p$ theory in the region between 9000cm^{-1} and 10000cm^{-1} which is not expected in the $BC\Delta$ theory. No search has previously reported any structure in this region of the spectrum. However the levels may not be observed because they are strongly forbidden, being far from any quartet states. The oscillator strengths of the doublet levels in the region of 20000cm^{-1} are believed to be enhanced by the mixing of these states with conduction band states, giving them greater quartet

Table 4.3b
 Final assignment of parameters for ZnS:Co

$\epsilon=0.981$

$\tau=0.823$

$\Delta_p=5900\text{cm}^{-1}$

Energy(cm-1)	Assignment	
23046	Γ_6	$2T_1$
22423	Γ_8	$2T_1$
20495	Γ_8	$2T_1$
20180	Γ_6	$2T_1$
17183	Γ_7	$2T_2$
17082	Γ_8	$2T_2$
15957	Γ_8	$2E$
15827	Γ_6	$2T_1$
15559	Γ_8	$2T_1$
14898	Γ_6	$4T_1$
14538	Γ_7	$4T_1$
14530	Γ_8	$4T_1$
14460	Γ_8	$4T_1$
12851	Γ_8	$2T_2$
12583	Γ_7	$2T_2$
12419	Γ_6	$2A_1$
9854	Γ_8	$2T_1$
9613	Γ_6	$2T_1$
9161	Γ_8	$2E$
6643	Γ_8	$4T_1$
6557	Γ_7	$4T_1$
6106	Γ_8	$4T_1$
5746	Γ_6	$4T_1$
3978	Γ_7	$4T_2$
3885	Γ_8	$4T_2$
3692	Γ_6	$4T_2$
3573	Γ_8	$4T_2$
0	Γ_8	$4A_2$

Fig 4.4a
Absorption spectrum of ZnS:Co(d⁷) compared with
energy levels calculated by the $\epsilon\tau\Delta_p$ theory

ZnS:Co

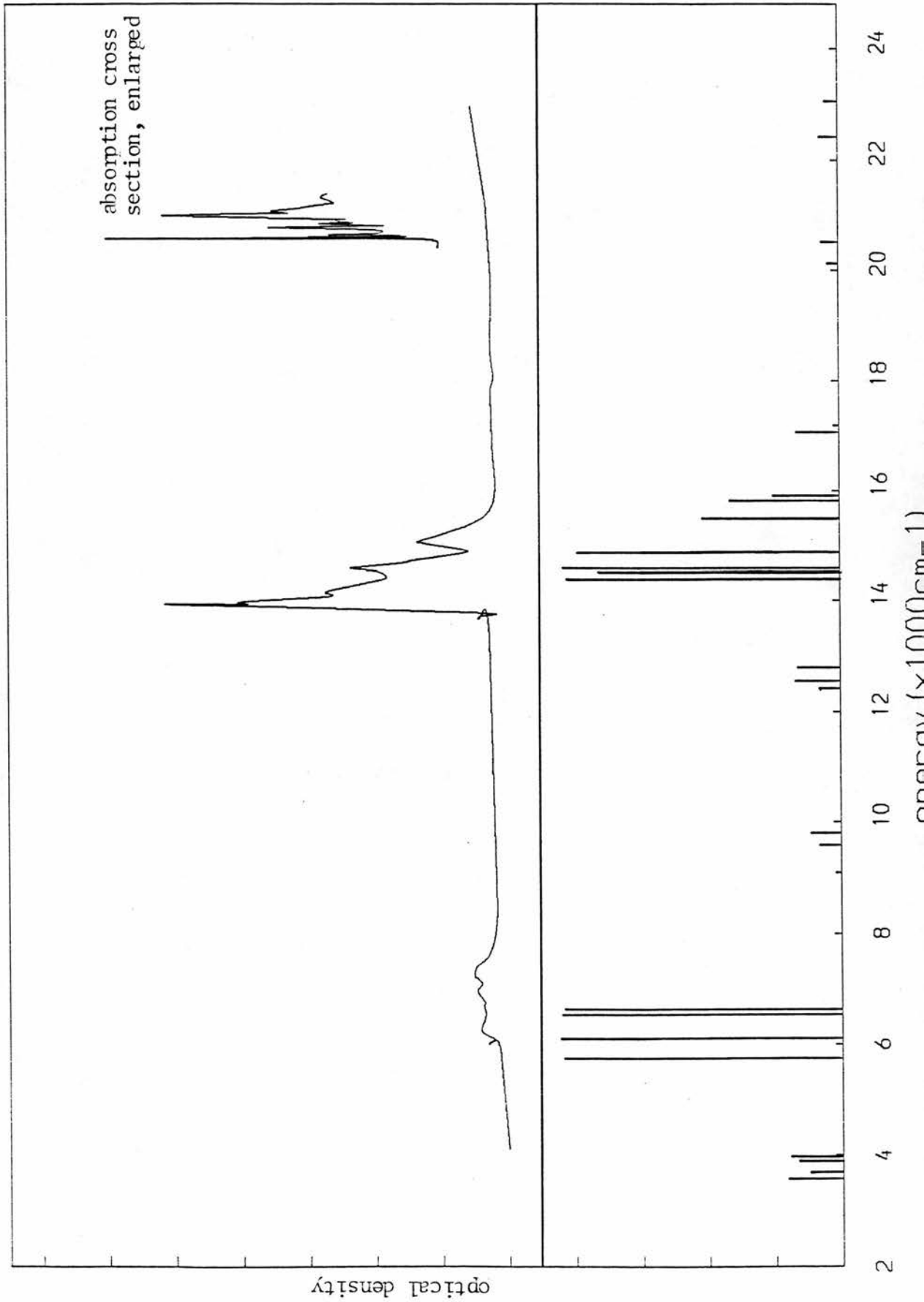
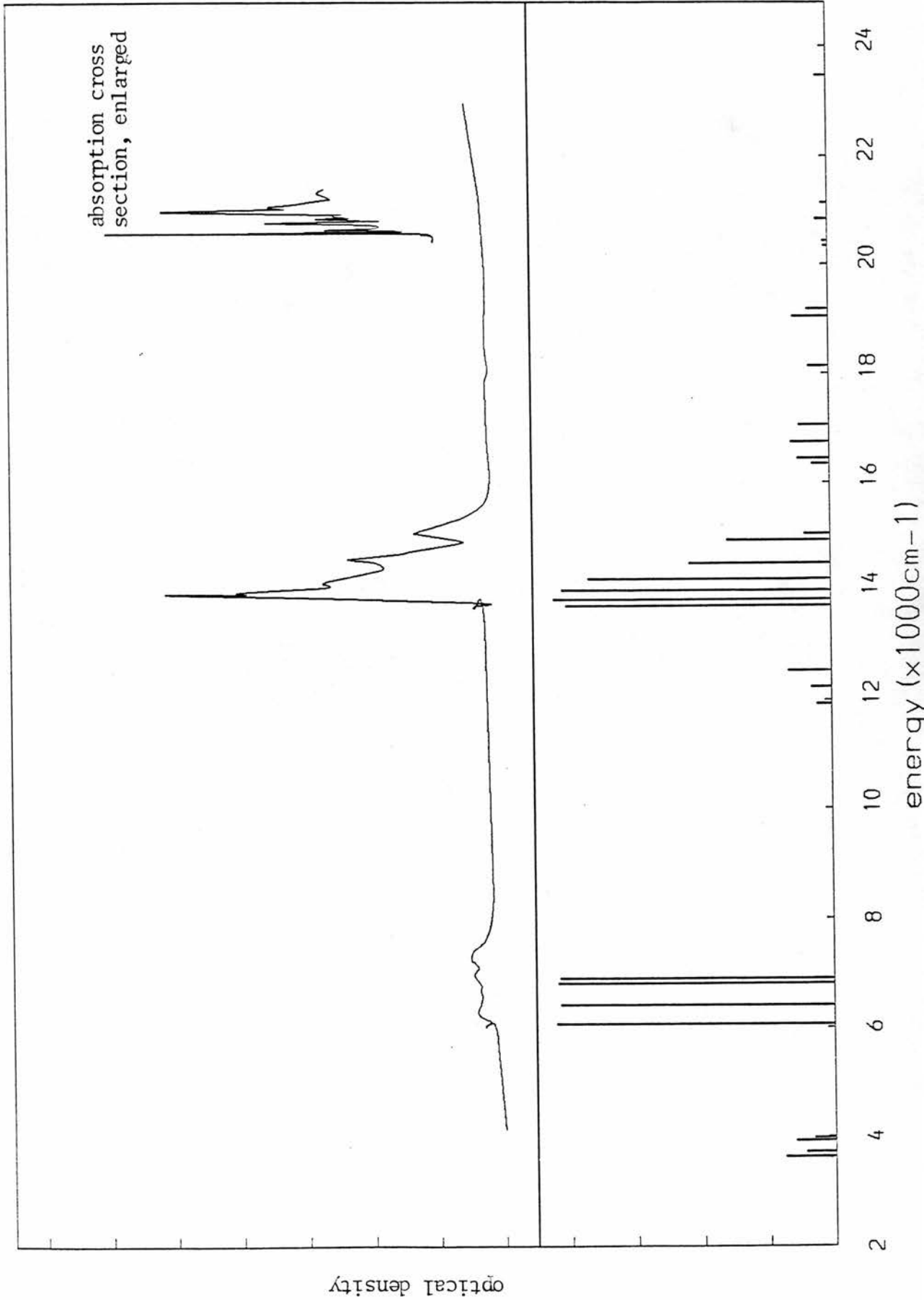


Fig 4.4b
Absorption spectrum of ZnS:Co(d⁷) compared with
energy levels calculated by the BCA theory

ZnS:Co



character [32].

4.2.2 -ZnO:Co-

The absorption spectrum of ZnO:Co is shown in figs 4.3a and 4.3b together with the theoretically determined energy levels (tabulated in tables 4.4a and 4.4b) and their approximate oscillator strengths [8]. There is a good agreement between the assignment of the levels ${}^4T_1(F)$ and ${}^4T_2(F)$ with experiment using either the $\epsilon\tau\Delta_p$ theory or the BC Δ theory. The weaker structure observed around 20200cm^{-1} is also predicted by both theories. Some doublet structure at energies just below 20000cm^{-1} is predicted by the $\epsilon\tau\Delta_p$ theory which has not been observed experimentally. The small oscillator strength of these doublets suggests that they may be too weak to observe.

Weakliem [8] using the BC Δ theory assigned the following values to his disposable parameters:

$$B = 775\text{cm}^{-1} \quad C = 3490\text{cm}^{-1} \quad \Delta = 3900\text{cm}^{-1}$$

The band observed from 15000cm^{-1} to 18000cm^{-1} is much broader than the corresponding absorption band in ZnS:Co or ZnSe:Co. Weakliem described the width as being due to the strong mixing of nearby doublets with the quartet ${}^4T_1(P)$. For ZnS:Co and ZnSe:Co these doublets are too far away from the quartet to gain oscillator strength and so appear as weak absorptions. The anisotropy of the broad band for the two polarisations $E \perp c$ and $E \parallel c$ is a consequence of the trigonal distortion in ZnO:Co, and Weakliem gives a qualitative account of this. The distortion (C_{3v}) leads to a splitting of the crystal field energy levels. The correlation between the representations in T_d and C_{3v} is summarised in table 4.5. In

Fig 4.3a
Absorption spectrum of ZnO:Co(d⁷) compared with
energy levels calculated by the $\epsilon\tau\Delta_p$ theory

ZnO:Co

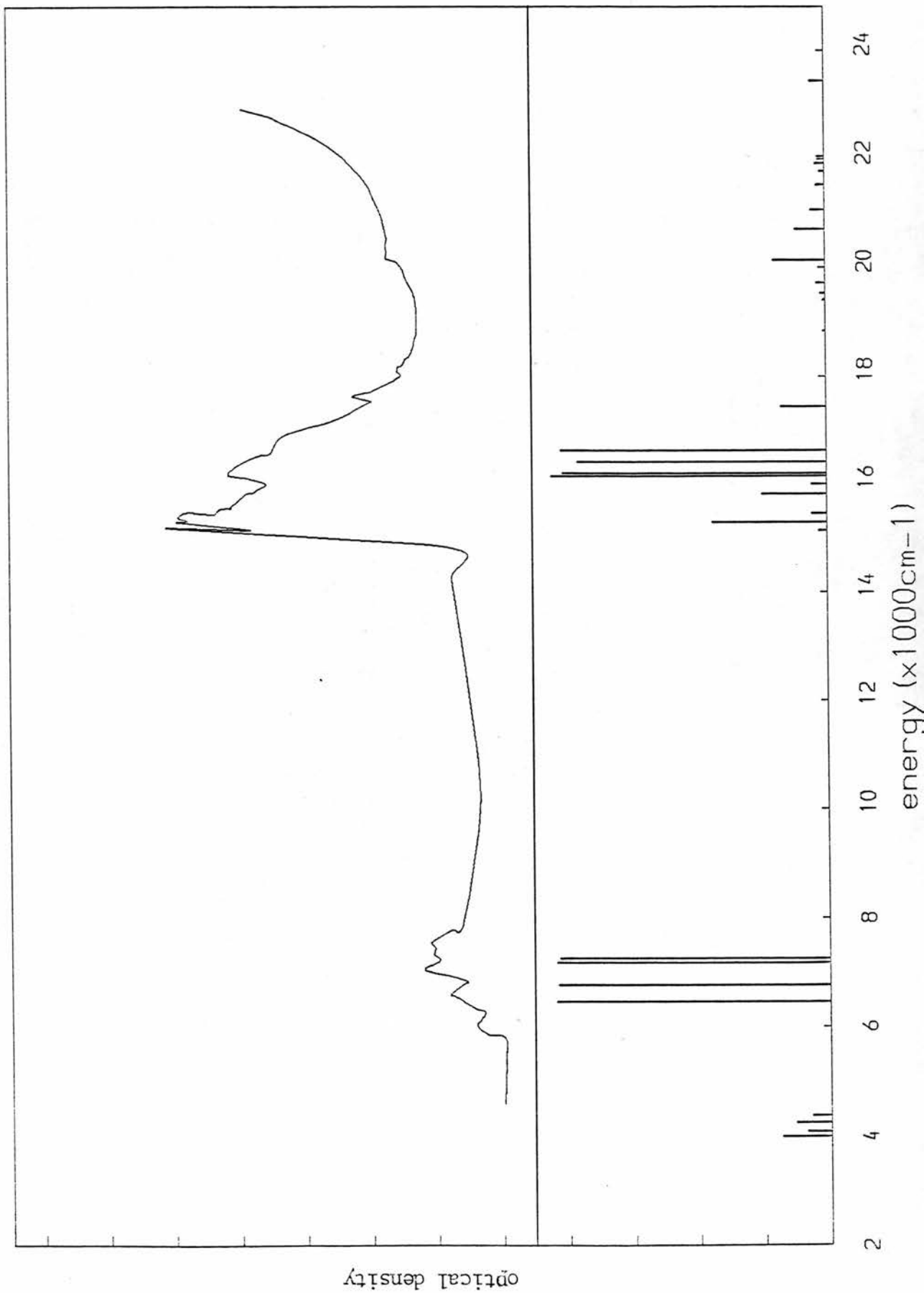


Fig 4.3b
Absorption spectrum of ZnO:Co(d^7) compared with
energy levels calculated by the $BC\Delta$ theory

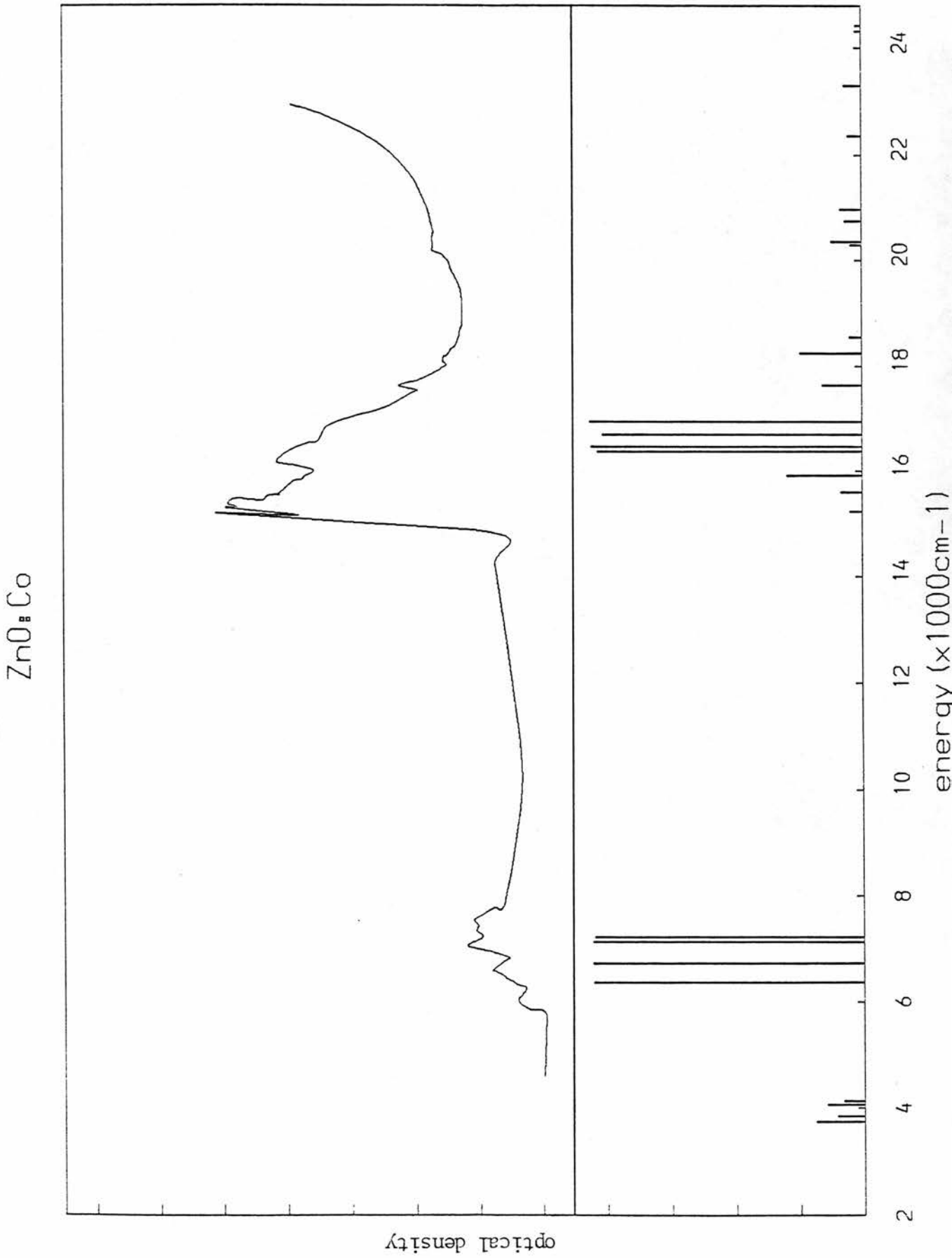


Table 4.4

Comparison of energy levels calculated for ZnO:Co

a) $\epsilon\tau\Delta_p$ theory		b) BC Δ theory	
$\epsilon=0.849$		$B=775\text{cm}^{-1}$	
$\tau=0.934$		$C=3490\text{cm}^{-1}$	
$\Delta_p=2650\text{cm}^{-1}$		$\Delta=3900\text{cm}^{-1}$	
3975	Γ_8	3762	Γ_8
4066	Γ_6	3851	Γ_6
4249	Γ_8	4042	Γ_8
4339	Γ_7	4125	Γ_7
6434	Γ_6	6359	Γ_6
6756	Γ_8	6692	Γ_8
7173	Γ_7	7130	Γ_7
7249	Γ_8	7202	Γ_8
15137	Γ_8	15226	Γ_8
15364	Γ_8	15605	Γ_6
15436	Γ_6	15944	Γ_8
18544	Γ_8	16378	Γ_8
15983	Γ_7	16442	Γ_7
16165	Γ_7	16683	Γ_8
16251	Γ_8	16907	Γ_6
16425	Γ_8	17653	Γ_6
16577	Γ_6	18268	Γ_8
17356	Γ_6	18541	Γ_7
18858	Γ_8		
19405	Γ_7		
19513	Γ_6	20321	Γ_7
19716	Γ_8	20377	Γ_8
20156	Γ_8	20709	Γ_8
20708	Γ_6	20976	Γ_6

all energies are measured in cm^{-1}

Table 4.5

Correlation between the symmetry representations in T_d and C_{3v}

T_d	Correlated representation in C_{3v}
A_1	A_1
A_2	A_2
E	E
T_1	$A_2 + E$
T_2	$A_1 + E$

particular, for the doublets at the low energy side of the band:

$${}^2T_1 \text{ ---> } A_2 + E$$

and ${}^2E \text{ ---> } E$

Under the point group symmetry C_{3v} the orbital selection rules for electric dipole transitions from the ground state A_2 become:

$$A_2 \text{ ---> } A_2 \quad \text{for } E \parallel c$$

$$A_2 \text{ ---> } E \quad \text{for } E \perp c$$

Consequently more transitions will be observed for the $E \perp c$ spectrum than the $E \parallel c$ spectrum.

Anderson [56] has studied in more detail the broad band. He reported Zeeman effect experiments, carried out by Weakliem, which identified transitions between the ground state and the 2E level. Both levels have been split by spin orbit coupling and by the trigonal distortion.

Koidl [47] tried to find suitable parameters to describe the fine structure observed using the energy matrices of Macfarlane [46] which include the effects of a C_{3v} distortion in a $BC\Delta$ model. He uses slightly different disposable parameters to Weakliem,

$$B = 760\text{cm}^{-1} \quad C = 3500\text{cm}^{-1} \quad \Delta = 4000\text{cm}^{-1}$$

and finds

$$v = 120\text{cm}^{-1} \quad v' = 320\text{cm}^{-1} \quad \zeta = -430\text{cm}^{-1}$$

Here v and v' are the trigonal field crystal field parameters. In my analysis of ZnO:Co the effect of the trigonal distortion has been ignored since Koidl has shown that it is a small perturbation of about the same order of magnitude as spin orbit coupling. Its inclusion would have led to a significant complication of the calculation.

The main difference found when using the $\epsilon\tau\Delta_p$ theory is that a 2T_2 level is predicted at the low energy side of the broad band in addition to the doublets 2T_1 and 2E (see fig.4.3.) The $\epsilon\tau\Delta_p$ theory

goes further than the $BC\Delta$ theory to account for the large amount of structure between 15000cm^{-1} and 16000cm^{-1} . A greater anisotropy of the polarised spectra would also be expected because the C_{3v} distortion splits the doublet:

$$T_2 \longrightarrow E + A_1$$

The disposable parameters found in the $\epsilon\tau\Delta_p$ analysis are

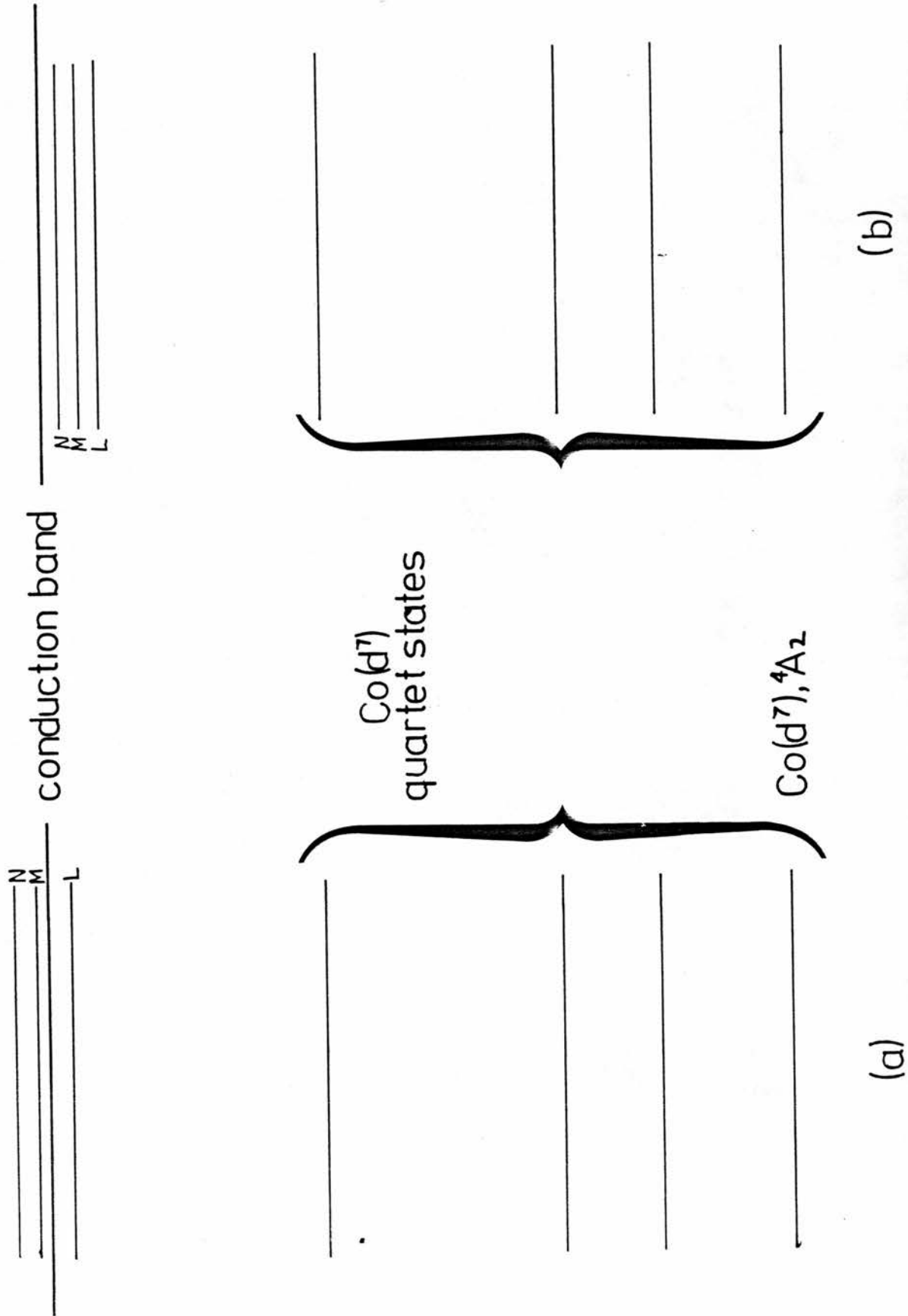
$$\epsilon = 0.849 \qquad \tau = 0.934 \qquad \Delta_p = 2650\text{cm}^{-1}$$

The most striking feature about these parameters is that τ is greater than ϵ . For a $3d^n$ impurity in a II-VI compound with point group symmetry T_d , only the t_2 electrons are allowed by symmetry to mix with the ligand orbitals (also of t_2 symmetry) so that ϵ should be greater than τ . In ZnO:Co the point group symmetry is reduced to C_{3v} and so the t_2 representation reduces to $a_1 + e$. The e representation is irreducible in C_{3v} . Thus the ligand orbitals have symmetry $a_1 + e$ so that both e and t_2 (i.e. $a_1 + e$) orbitals are allowed by symmetry to mix with the ligands, giving the result here that τ is greater than ϵ .

4.2.3 -ZnSe:Co-

The absorption spectrum of ZnSe:Co [51,10,32] displays similarities to the ZnS:Co spectrum. In particular, there is a gap in energy levels in the range 15000cm^{-1} to 19000cm^{-1} followed by some structure around 20000cm^{-1} . Luminescence arising from transitions from the lowest of these levels to quartet states has been seen [54,55]. Two models have been suggested to account for the high energy peaks around 20000cm^{-1} . In the first [32], the peaks are ascribed to transitions from the 4A_2 ground state to excited doublet

Fig 4.5
 Two models proposed to account for absorption data around 2000cm^{-1}
 in ZnSe:Co.



states near or in the conduction band (fig.4.5a). In the second [54,55] the peaks are ascribed to states in which an electron is excited from a d-orbital of the $\text{Co}(d^7)$ configuration into a localised orbital split off from some conduction band minimum under the influence of the resultant cobalt impurity potential. The electron remains weakly bound to the impurity (fig.4.5b).

There are difficulties with both of these models. In the second, at least the two higher states M and N would be expected to be describable to a good approximation by effective mass theory but this is not so. Also the line widths and photoionisation data [32] strongly suggest that the levels M and N (and possibly L) are degenerate with the conduction band, which is inconsistent with the model. For the first model, the BCA method can be used to find B and Δ from the spin-allowed transitions from the ground state. Then, with values of C/B between 3 and 5 the positions of the doublet states can be predicted. The parameters of Baranowski, Allen and Pearson [51] were used to find the energy levels and intensities given in table 4.6 and fig.4.6. There are doublet states in the required energy range but there are also doublet states predicted in the energy range between 15000cm^{-1} and 19000cm^{-1} where the observed absorption spectrum is flat and featureless [32]. To resolve this problem it was suggested that the doublets L, M and N in the vicinity of 20000cm^{-1} admix strongly with conduction band levels giving them greater quartet character and hence greater oscillator strengths than the doublet levels at lower energy. As a result, only doublets in the vicinity of 20000cm^{-1} have sufficient oscillator strength to be observed. An objection to this model, raised by Robbins et al [55], is that the numerous doublet levels predicted by the BCA theory should provide an efficient non-radiative ladder for loss of excitation energy.

Fig 4.6a
Absorption spectrum of ZnSe:Co(d⁷) compared with
energy levels calculated by the $\epsilon\tau\Delta_p$ theory

ZnSe:Co

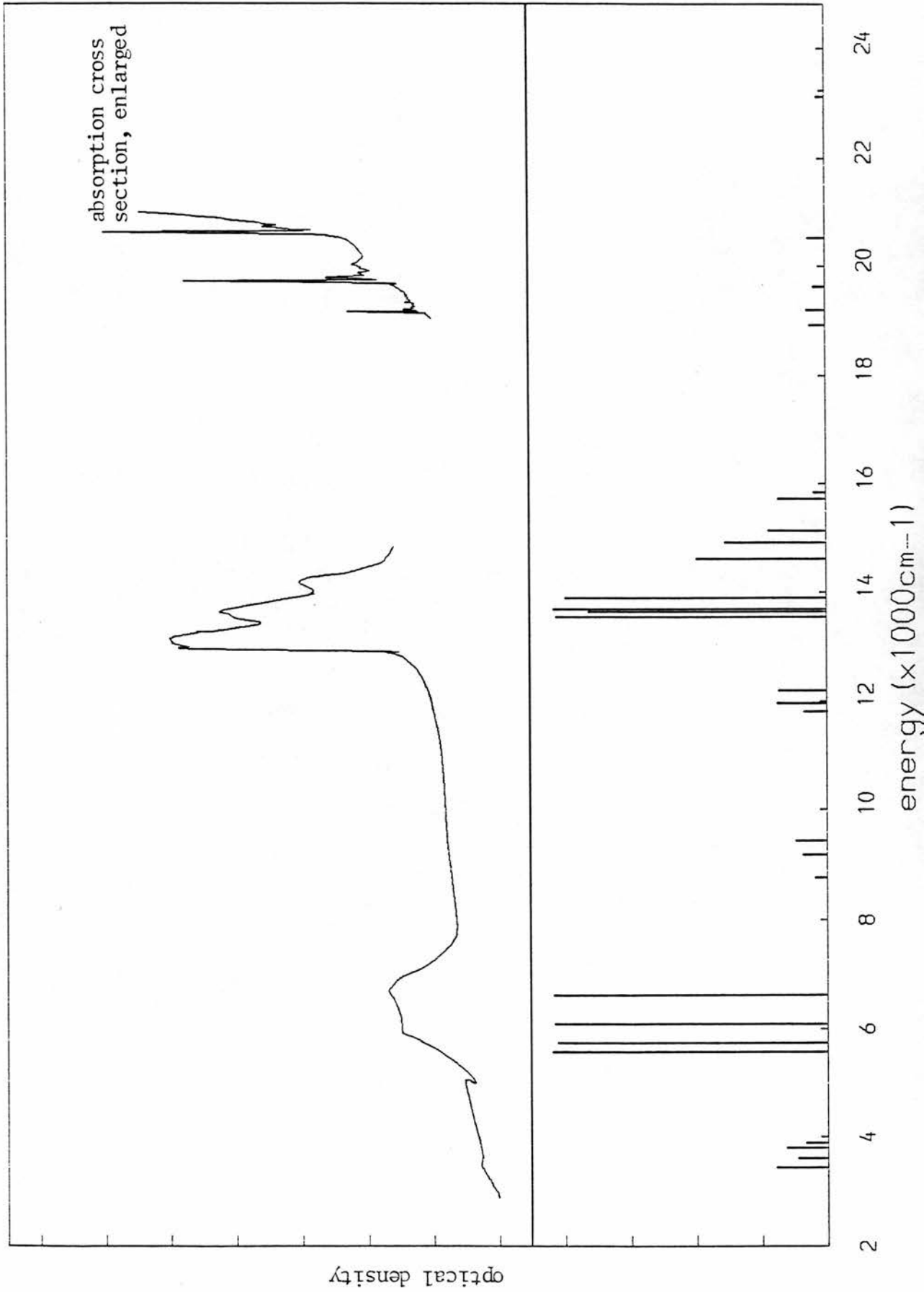


Fig 4.6b
Absorption spectrum of ZnSe:Co(d⁷) compared with
energy levels calculated by the BC Δ theory

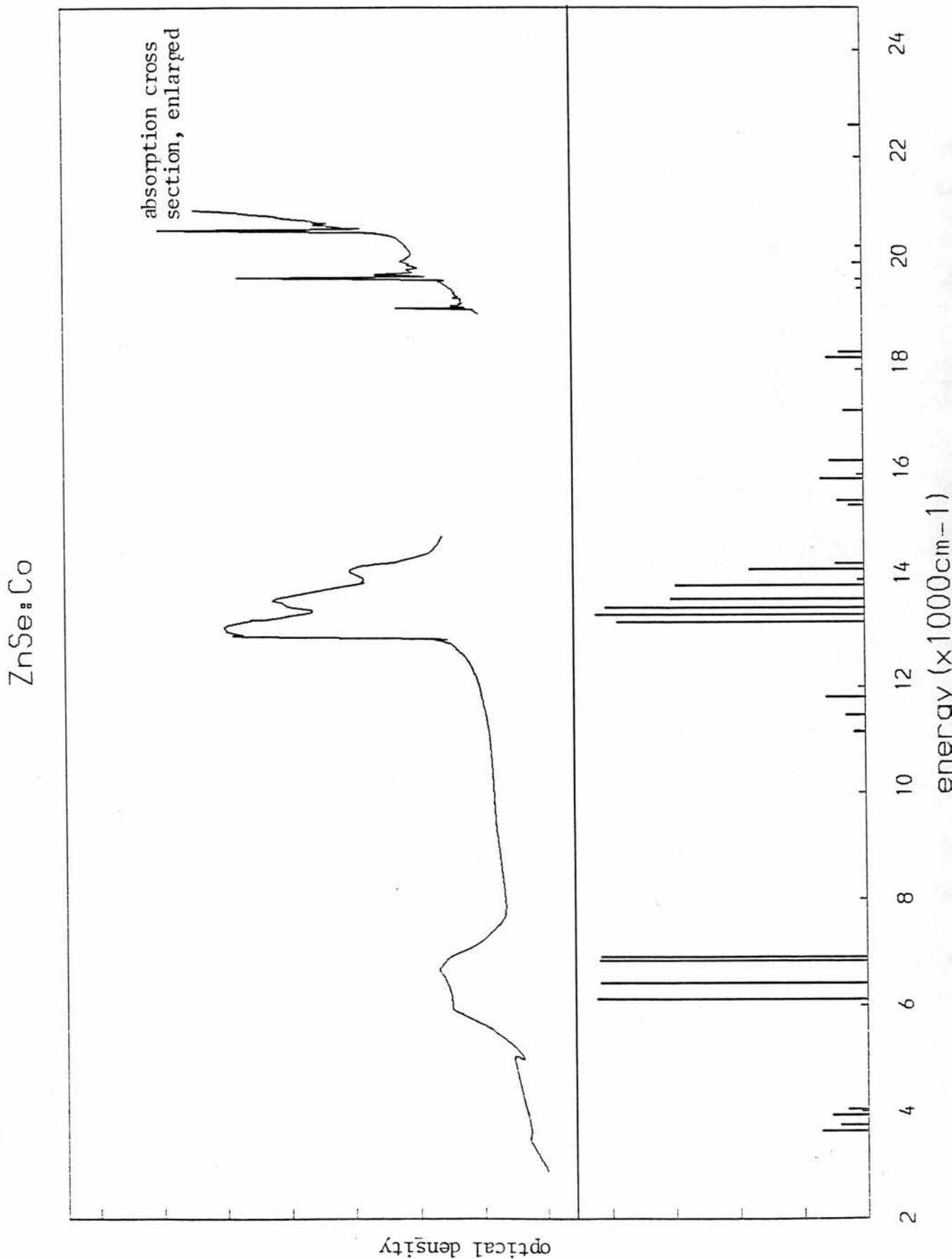


Table 4.6

Comparison of energy levels calculated for ZnSe:Co

a) $\epsilon\tau\Delta_p$ theory		b) BCA theory	
$\epsilon=0.945$		$B=570\text{cm}^{-1}$	
$\tau=0.813$		$C=2500\text{cm}^{-1}$	
$\Delta_p=5370\text{cm}^{-1}$		$\Delta=3800\text{cm}^{-1}$	
3487	Γ_8	3651	Γ_8
3606	Γ_6	3751	Γ_6
3800	Γ_8	3940	Γ_8
3892	Γ_7	4029	Γ_7
5729	Γ_6	6095	Γ_6
6085	Γ_8	6422	Γ_8
6534	Γ_7	6837	Γ_7
6621	Γ_8	6917	Γ_8
8746	Γ_8	11160	Γ_8
9155	Γ_6	11476	Γ_6
9402	Γ_8	11800	Γ_8
11853	Γ_6	13210	Γ_8
11974	Γ_7	13352	Γ_7
12215	Γ_8	13490	Γ_8
13549	Γ_8	13665	Γ_6
13625	Γ_8	13907	Γ_6
13627	Γ_7	14255	Γ_8
13982	Γ_6	14318	Γ_7
14665	Γ_8	15464	Γ_7
14937	Γ_6	15592	Γ_8
15138	Γ_8	15900	Γ_8
15755	Γ_8	16262	Γ_6
15831	Γ_7	17240	Γ_8
18871	Γ_6	18201	Γ_8
19185	Γ_8	18343	Γ_6
20538	Γ_8	19574	Γ_8
21165	Γ_6	19692	Γ_6

all energies are measured in cm^{-1}

Luminescence from L is weak with a fast decay so non-radiative decay is occurring, but not at so great a rate that it makes luminescence unobservable.

The parameters obtained using the $\epsilon\tau\Delta_p$ theory give a good fit between the observed and calculated quartet levels.

$$\epsilon = 0.945 \qquad \tau = 0.813 \qquad \Delta_p = 5370\text{cm}^{-1}$$

A new feature is that a gap opens in the doublet energies where the BC Δ theory predicts a ladder of states. The gap occurs between 15800cm^{-1} and 18900cm^{-1} with the values of parameters quoted above, and a similar gap occurs for a wide range of physically reasonable parameters ϵ and τ . Thus the objection to the doublet model of states L, M and N is removed. The gap in levels below them reduces the non-radiative decay rate and permits luminescence to be seen. The oscillator strength of the absorptions is still enhanced by mixing of the doublet states with conduction band states, but with the $\epsilon\tau\Delta_p$ theory there is no necessity for such strong mixing as there was previously, because the problem of accounting for missing transitions to lower energy doublets no longer arises. Zeeman effect and uniaxial stress measurements [55] have shown that the lines at 19040cm^{-1} and 19060cm^{-1} are due to transitions from a Γ_8 ground state to final energy levels of symmetry representation Γ_6 and Γ_8 . This is consistent with the findings of this thesis where the energy levels near 19050cm^{-1} have crystal field symmetry 2T_1 , so their spin orbit double group symmetry representation is $\Gamma_6 \times T_1 = \Gamma_6 + \Gamma_8$.

4.2.4 -ZnTe:Co-

Absorption data for ZnTe:Co was reported and analysed in terms of the BC Δ method by Baranowski, Allen and Pearson [51]. Using their parameters:

$$B = 460\text{cm}^{-1} \quad C = 2020\text{cm}^{-1} \quad \Delta = 3450\text{cm}^{-1}$$

most details of the experimental spectrum are accounted for (see fig.4.7). Exceptions are the structure around 7000cm^{-1} and at around 12500cm^{-1} .

Because only two quartets have been observed in absorption for ZnTe:Co, the first assignment of parameters in the $\epsilon\tau\Delta_p$ analysis was made by choosing values similar to those previously found for ZnS:Co and ZnSe:Co. The final fit, with two quartets and two doublets yields the parameters:

$$\epsilon = 0.854 \quad \tau = 0.770 \quad \Delta_p = 4290\text{cm}^{-1}$$

As with the BC Δ analysis, agreement between experiment and the $\epsilon\tau\Delta_p$ energy levels is good (see fig.4.7). Two doublets, 2E and 2T_1 , account for the structure around 7000cm^{-1} .

4.2.5 -CdS:Co-

Details of the absorption spectrum of CdS:Co have been reported by Pappalardo and Dietz [52] and by Weakliem [8]. Both analysed their results in terms of the BC Δ method and obtained similar parameters:

Weakliem,

$$B = 610\text{cm}^{-1} \quad C = 2680\text{cm}^{-1} \quad \Delta = 3300\text{cm}^{-1}$$

Pappalardo and Dietz,

$$B = 664\text{cm}^{-1} \quad C = 2990\text{cm}^{-1} \quad \Delta = 3160\text{cm}^{-1}$$

Fig 4.7a
Absorption spectrum of ZnTe:Co(d^7) compared with
energy levels calculated by the $\epsilon\tau\Delta_p$ theory

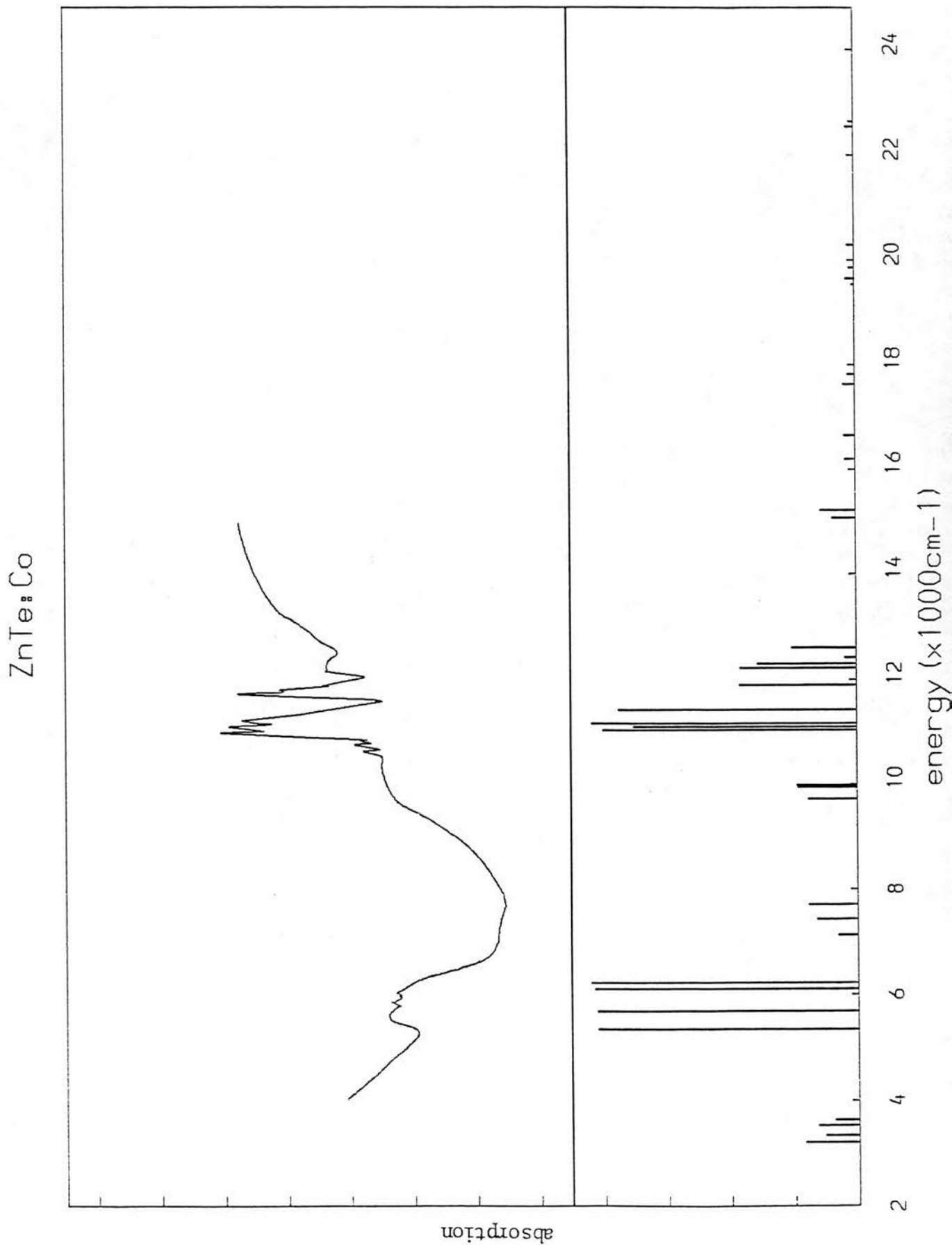


Fig 4.7b
Absorption spectrum of ZnTe:Co(d⁷) compared with
energy levels calculated by the BCΔ theory

ZnTe:Co

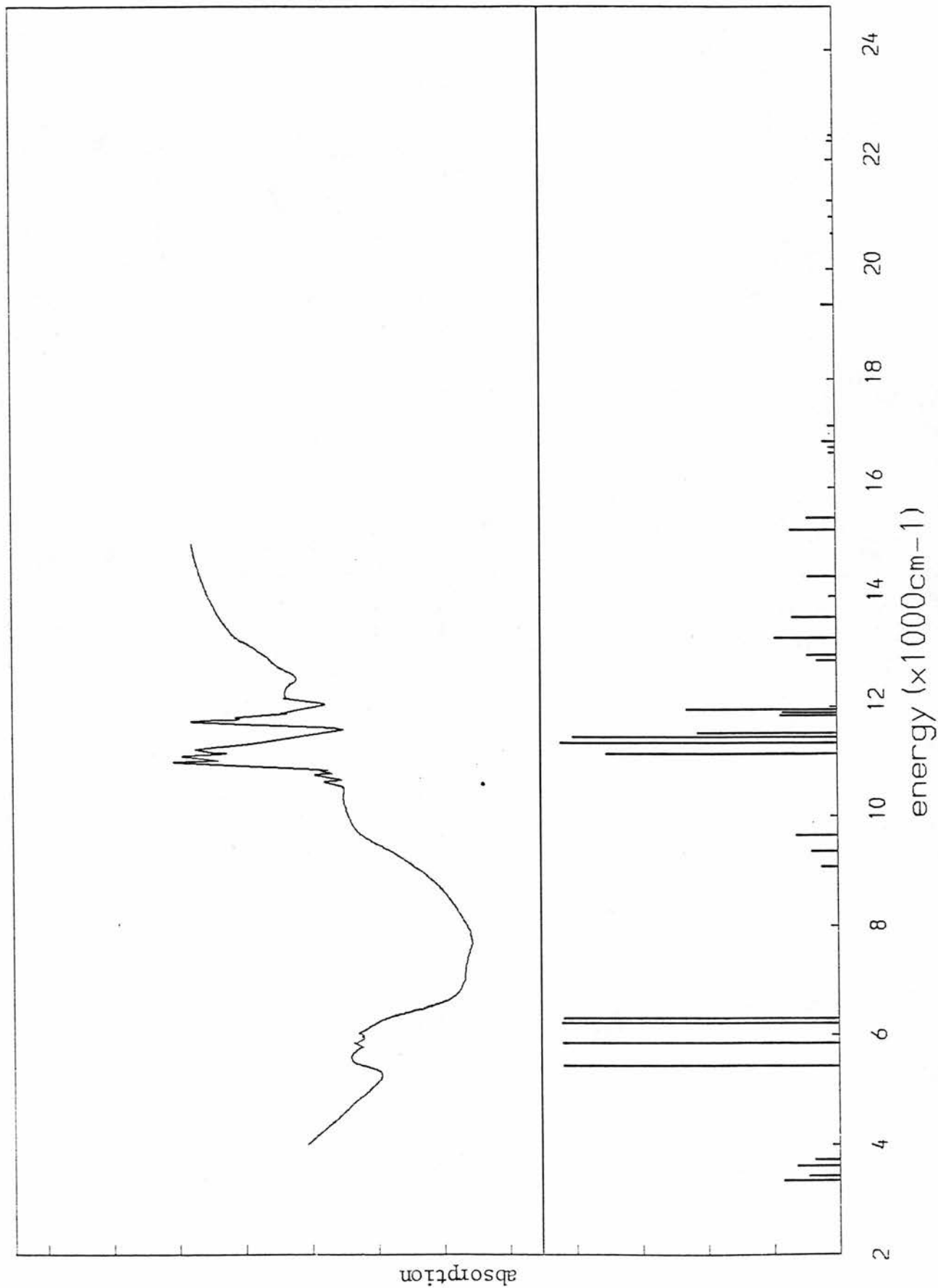


Table 4.7
 Comparison of the energy levels calculated for ZnTe:Co

a) $\epsilon\tau\Delta_p$ theory		BCA theory	
$\epsilon=0.854$		$B=460\text{cm}^{-1}$	
$\tau=0.770$		$C=2020\text{cm}^{-1}$	
$\Delta_p=4290\text{cm}^{-1}$		$\Delta=3450\text{cm}^{-1}$	
3203	Γ_8	3290	Γ_8
3334	Γ_6	3404	Γ_6
3530	Γ_8	3594	Γ_8
3625	Γ_7	3686	Γ_7
5349	Γ_6	5460	Γ_6
5695	Γ_8	5785	Γ_8
6122	Γ_7	6180	Γ_7
6225	Γ_8	6273	Γ_8
7142	Γ_8	9059	Γ_8
7444	Γ_6	9313	Γ_6
7695	Γ_8	9622	Γ_8
9771	Γ_7	11102	Γ_8
9948	Γ_8	11310	Γ_7
9950	Γ_6	11396	Γ_8
11030	Γ_8	11487	Γ_6
11077	Γ_8	11791	Γ_6
11128	Γ_7	11859	Γ_7
11429	Γ_6	11935	Γ_8
11956	Γ_8	12837	Γ_7
12262	Γ_6	12916	Γ_8
12310	Γ_8	13250	Γ_8
12395	Γ_7	13593	Γ_6

All energies are measured in cm^{-1}

Spin orbit coupling was taken into account by Pappalardo and Dietz using the free ion value of $\zeta = -540\text{cm}^{-1}$ which gives an upper limit to the predicted splittings, whereas Weakliem treated spin orbit coupling to first order using $\lambda = -195\text{cm}^{-1}$ (compared with the free ion value of $\lambda = -178\text{cm}^{-1}$.) The spin orbit coupling parameters ζ and λ are related by $\lambda = \zeta/2S$, where the configuration ground state is $2S+1L$. Thus for $\text{Co}(d^7)$, $\zeta = 2\lambda$. Using Weakliem's parameters B, C and Δ , and treating spin orbit coupling to second order with $\zeta = -400\text{cm}^{-1}$ a set of levels can be calculated and are compared with the observed spectrum in fig.4.8b. The levels appear to be lower than Weakliem claims for the broad absorption between 13500cm^{-1} and 15000cm^{-1} , which may be due to a mistake in his table of parameters.

The parameters obtained with the $\epsilon\tau\Delta_p$ fitting are:

$$\epsilon = 0.947 \qquad \tau = 0.842 \qquad \Delta_p = 5000\text{cm}^{-1}$$

and the energy levels together with the observed spectrum are given in fig.4.8a.

Agreement with experiment is quite good but may be improved if the effect of the trigonal distortion in CdS is included. A difference between the two results is found in the explanation of detail in the broad absorption band between 13500cm^{-1} and 15000cm^{-1} . In the $\epsilon\tau\Delta_p$ theory the low energy structure is assigned to doublet transitions, whose oscillator strength has been enhanced by coupling to nearby quartets, similar to ZnO:Co . Using the BCA method, this structure is assigned to transitions to quartet states.

Fig 4.8a
Absorption spectrum of CdS:Co(d⁷) compared with
energy levels calculated by the $\epsilon\tau\Delta_p$ theory

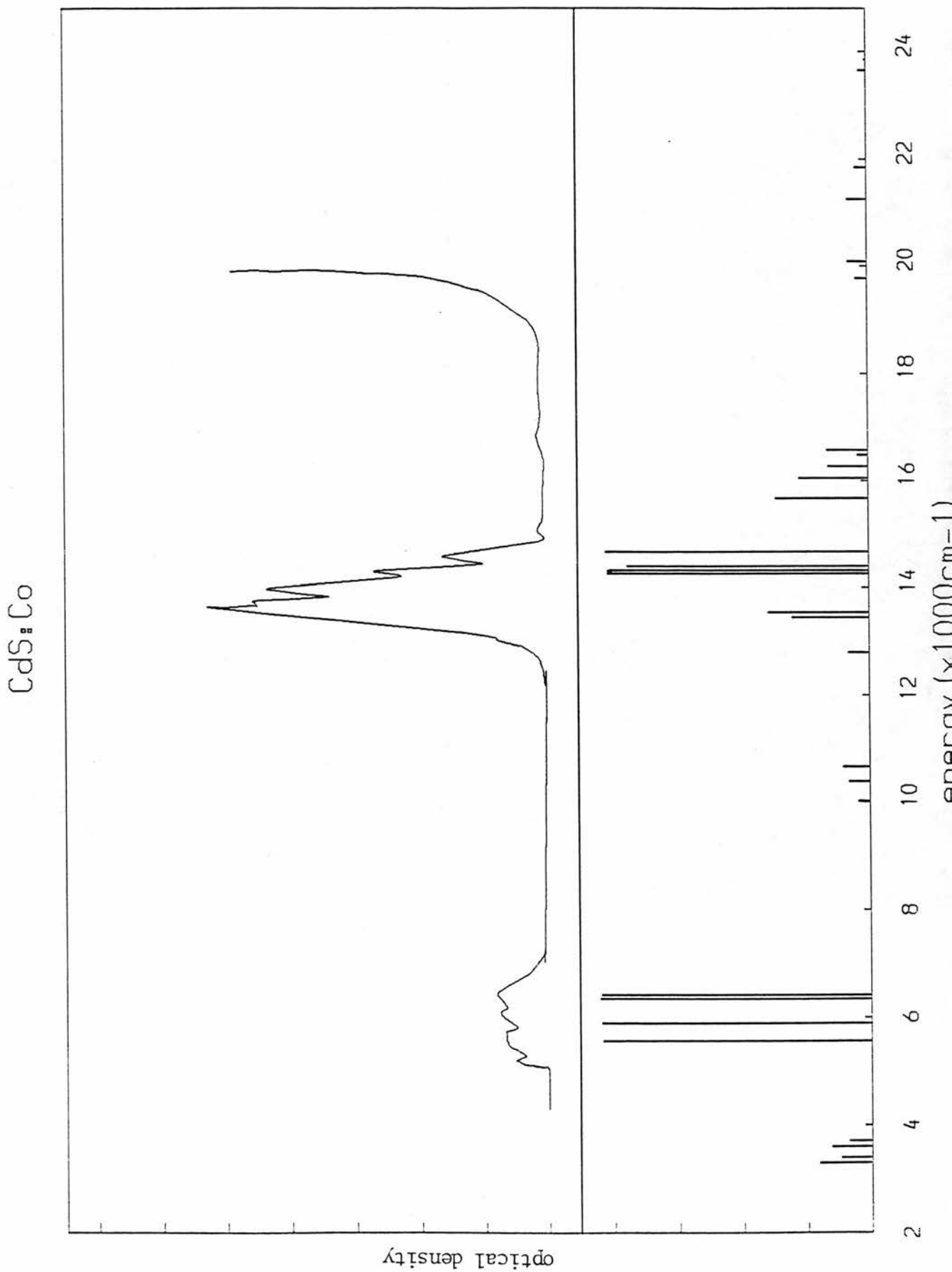


Fig 4.8b
Absorption spectrum of CdS:Co(d⁷) compared with
energy levels calculated by the BCΔ theory

CdS:Co

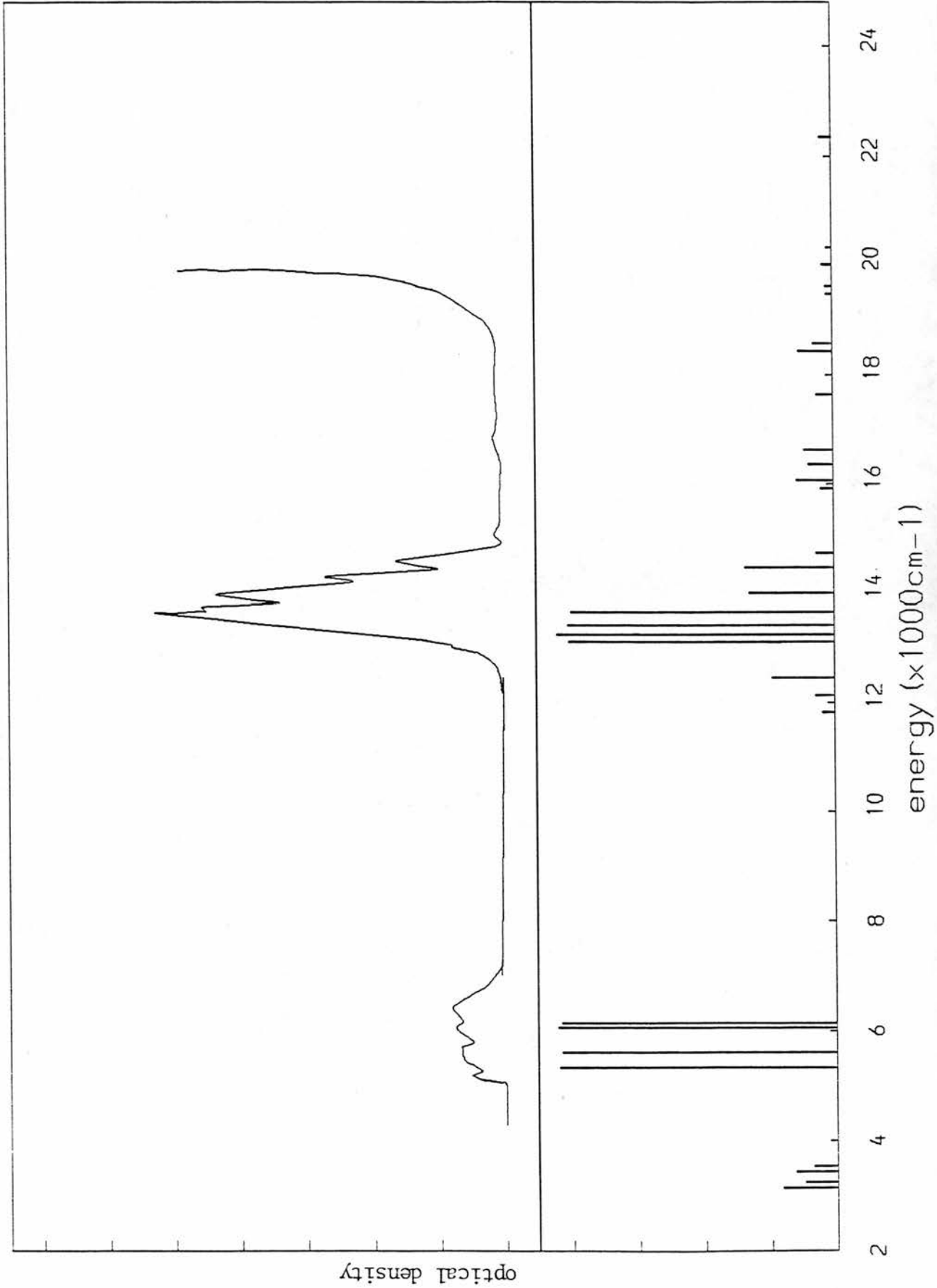


Table 4.8

Comparison of energy levels calculated for CdS:Co

a) $\epsilon\tau\Delta_p$ theory		b) BC Δ theory	
$\epsilon = 0.947$		$B = 610 \text{ cm}^{-1}$	
$\tau = 0.842$		$C = 2680 \text{ cm}^{-1}$	
$\Delta_p = 5000 \text{ cm}^{-1}$		$\Delta = 3300 \text{ cm}^{-1}$	
3356	Γ_8	3154	Γ_8
3466	Γ_6	3258	Γ_6
3662	Γ_8	3454	Γ_8
3749	Γ_7	3536	Γ_7
5595	Γ_6	5314	Γ_6
5948	Γ_8	5653	Γ_8
6395	Γ_7	6078	Γ_7
6479	Γ_8	6162	Γ_8
10019	Γ_8	11834	Γ_8
10442	Γ_6	12126	Γ_6
10727	Γ_8		
12821	Γ_6	12477	Γ_8
13497	Γ_7	13142	Γ_8
13636	Γ_8	13241	Γ_7
14304	Γ_8	13428	Γ_8
14364	Γ_7	13670	Γ_6
14462	Γ_8	14030	Γ_6
14731	Γ_6	14478	Γ_8
15747	Γ_8	14691	Γ_7
16085	Γ_6	15961	Γ_7
16372	Γ_8	16060	Γ_8
16570	Γ_7	16355	Γ_8
16609	Γ_8	16658	Γ_6
19797	Γ_6	17656	Γ_8

all energies are measured in cm^{-1}

4.2.6 -CdSe:Co-

The absorption spectrum of CdSe:Co was reported by Langer and Baranowski [4.6], who used the $BC\Delta$ method and first order spin orbit coupling to account for the observed data. Their values of B, C and Δ are used in fig.4.9b, but spin orbit effects have been included to second order, with $\zeta = -400\text{cm}^{-1}$. Buhman, Schulz and Thiede [4.11] considered the fine structure of the spectrum in more detail.

The parameters obtained using the $\epsilon\tau\Delta_p$ method to fit to the quartet transitions were compared with the fit to quartet transitions for ZnSe:Co - ϵ and τ are similar for both. No data for the doublets are available for CdSe:Co, but their inclusion in the analysis of ZnSe:Co leads to a final assignment with new values of the disposable parameters. The parameters for ZnSe:Co and CdSe:Co are expected to be similar since for both systems the impurity is surrounded by four selenide ions. Therefore in the final assignment for CdSe:Co, the three parameters were increased/decreased by the same fraction as they had been increased/decreased between first and final assignments in the analysis of ZnSe:Co. This gives the parameters:

$$\epsilon = 0.935 \qquad \tau = 0.813 \qquad \Delta_p = 4700\text{cm}^{-1}$$

The corresponding energy levels agree satisfactorily with the available experimental detail (see fig.4.9a).

Fig 4.9a
Absorption spectrum of CdSe:Co(d^7) compared with
energy levels calculated by the $\epsilon\tau\Delta_p$ theory

CdSe:Co

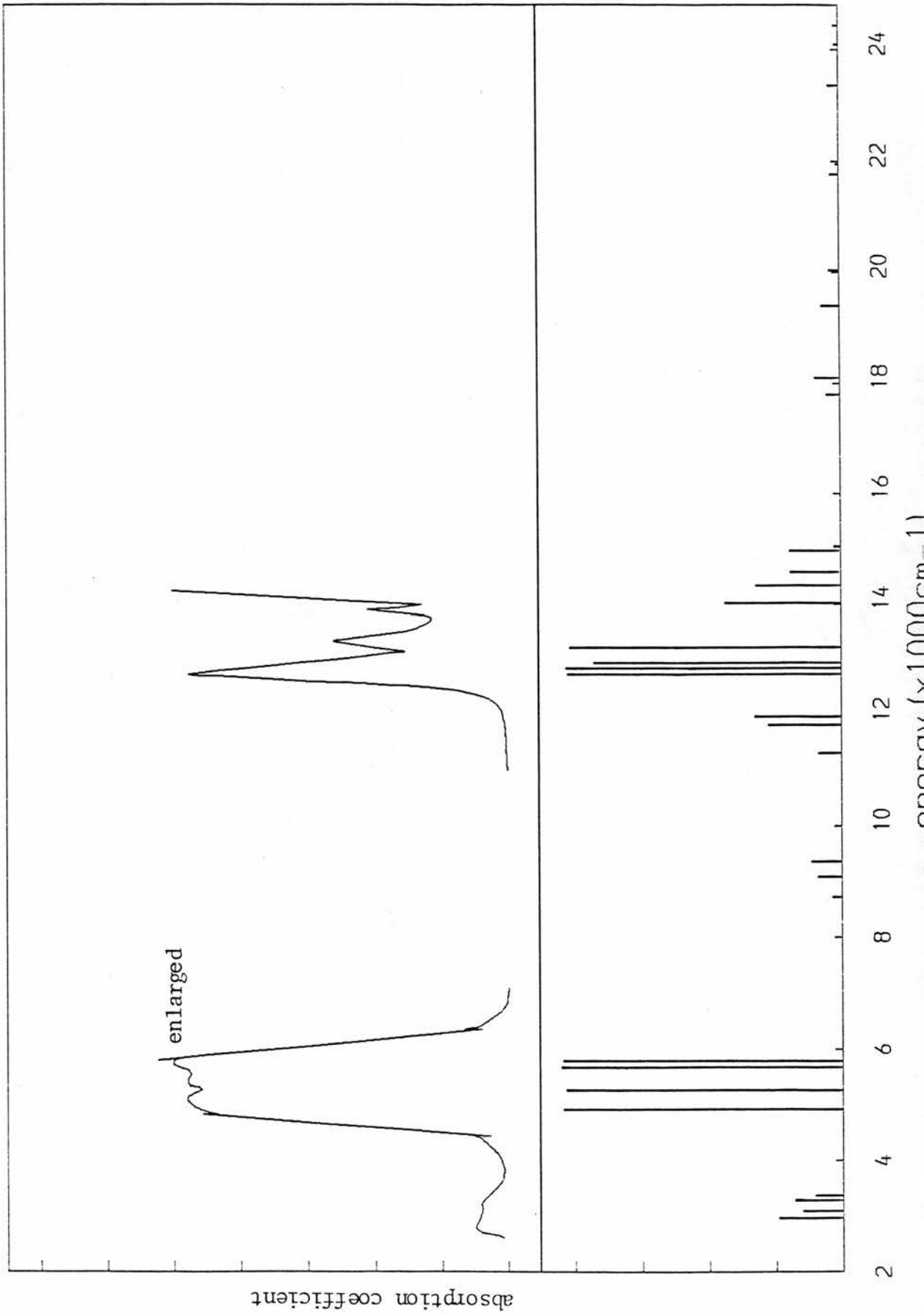


Fig 4.9b
Absorption spectrum of CdSe:Co(d^7) compared with
energy levels calculated by the $BC\Delta$ theory

CdSe:Co

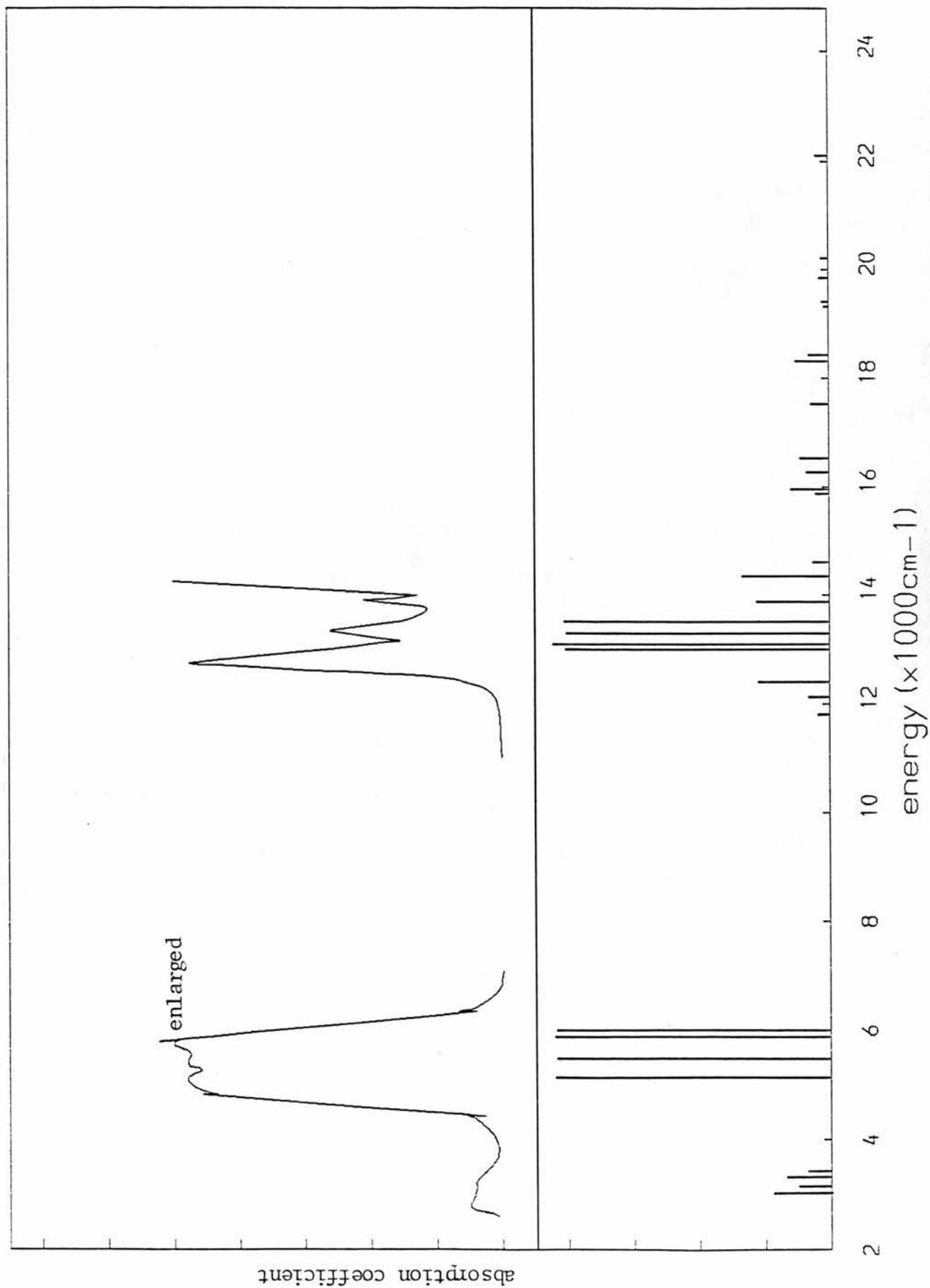


Table 4.9

Comparison of energy levels calculated for CdSe:Co

a) $\epsilon\tau\Delta_p$ theory	b) BCA theory
$\epsilon = 0.935$	$B = 610 \text{ cm}^{-1}$
$\tau = 0.813$	$C = 2684 \text{ cm}^{-1}$
$\Delta_p = 4700 \text{ cm}^{-1}$	$\Delta = 3200 \text{ cm}^{-1}$
2960 Γ_8	3054 Γ_8
3084 Γ_6	3160 Γ_6
3284 Γ_8	3357 Γ_8
3371 Γ_7	3438 Γ_7
4876 Γ_6	5151 Γ_6
5239 Γ_8	5493 Γ_8
5680 Γ_7	5918 Γ_7
5774 Γ_8	6004 Γ_8
8706 Γ_8	11818 Γ_8
9079 Γ_6	12102 Γ_6
9355 Γ_8	12455 Γ_8
11320 Γ_6	13012 Γ_8
11789 Γ_7	13107 Γ_7
11983 Γ_8	13301 Γ_8
12775 Γ_8	13544 Γ_6
12852 Γ_7	13931 Γ_6
12900 Γ_8	14375 Γ_8
13209 Γ_6	14602 Γ_7
14022 Γ_8	15892 Γ_7
14332 Γ_6	
14558 Γ_8	
14955 Γ_8	
15028 Γ_7	
17775 Γ_6	

All energies are measured in cm^{-1}

4.2.7 -CdTe:Co-

The spectrum was interpreted using the B Δ method by Baranowski, Allen and Pearson [4.5], and their parameters are used in fig.4.10b.

Although the 4T_2 level has not been involved in the $\epsilon\tau\Delta_p$ analysis of the spectrum, the predicted position of the level agrees well with the observed absorption at around 3300cm^{-1} (see fig.4.10a). Thus for ZnTe:Co where the 4T_2 transition is obscured, the result for CdTe:Co means that the predicted position of the 4T_2 level is likely to coincide with the actual position of that level.

4.2.8 -Summary-

The spectra of $\text{Co}(d^7)$ in seven II-VI compounds have been analysed in terms of the $\epsilon\tau\Delta_p$ theory. Similarities between each of these spectra have been noted. Typically four absorption bands were used in the calculation of the parameters. The parameters were varied so as to obtain crystal field levels in closest agreement with the observed levels. One doublet and three quartet crystal field levels were used in the analysis when possible. In some of the spectra the ${}^4A_2 - {}^4T_2$ transition is not observed and so an extra doublet was included in the analysis. A summary of the results is given in table 4.2.

Agreement between theory and experiment is good and the positions of the quartet levels agree with those predicted by the B Δ theory. However the positions of the doublet levels predicted by the two theories is often quite different. In the cases of ZnS:Co and ZnSe:Co this has helped to resolve the problem of the assignment of observed structure around 20000cm^{-1} [4.12-4.14].

Fig 4.10a
Absorption spectrum of CdTe:Co(d⁷) compared with
energy levels calculated by the $\epsilon\tau\Delta_p$ theory

CdTe:Co

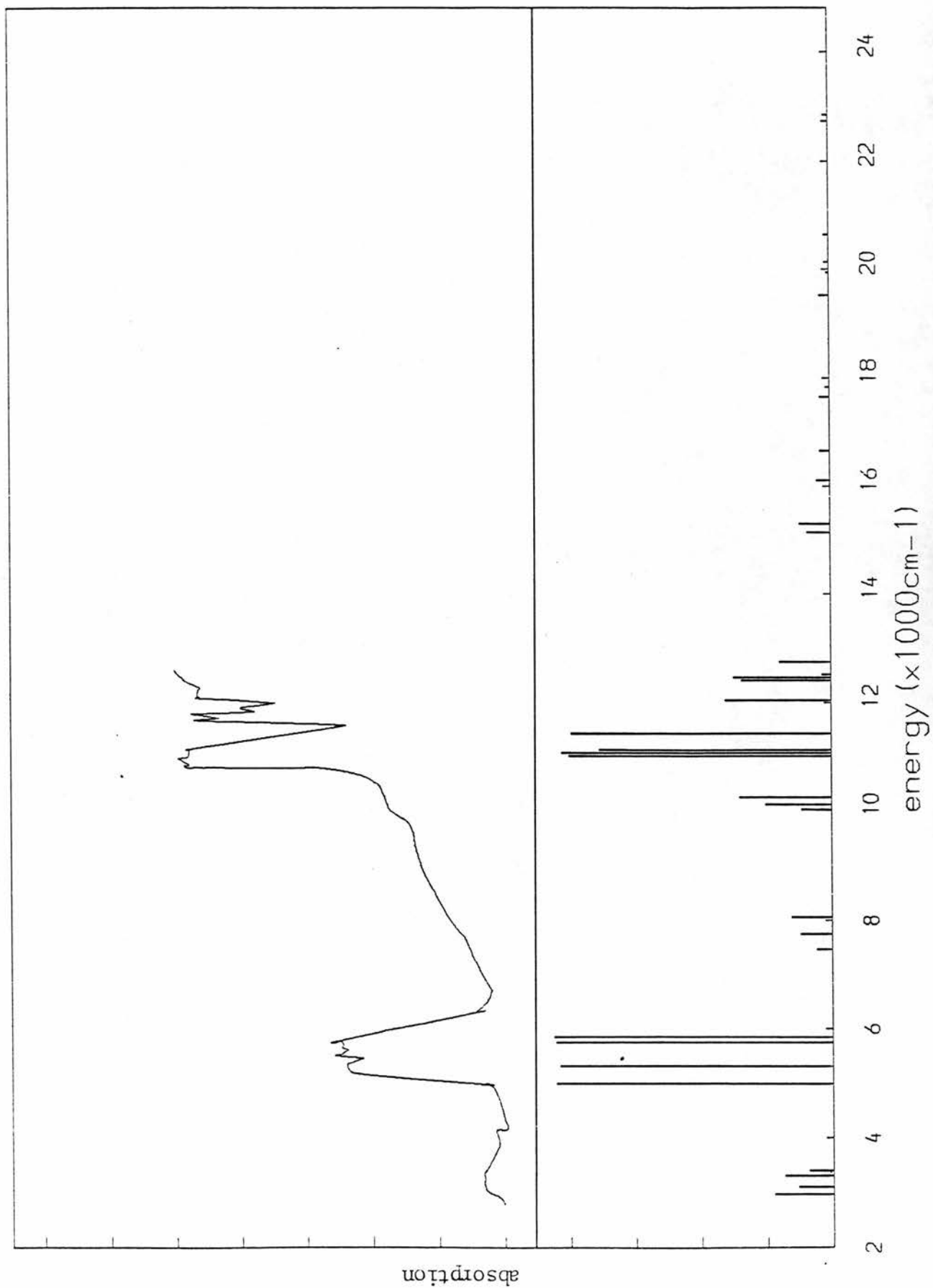


Fig 4.10b
Absorption spectrum of CdTe:Co(d^7) compared with
energy levels calculated by the BCA theory

CdTe:Co

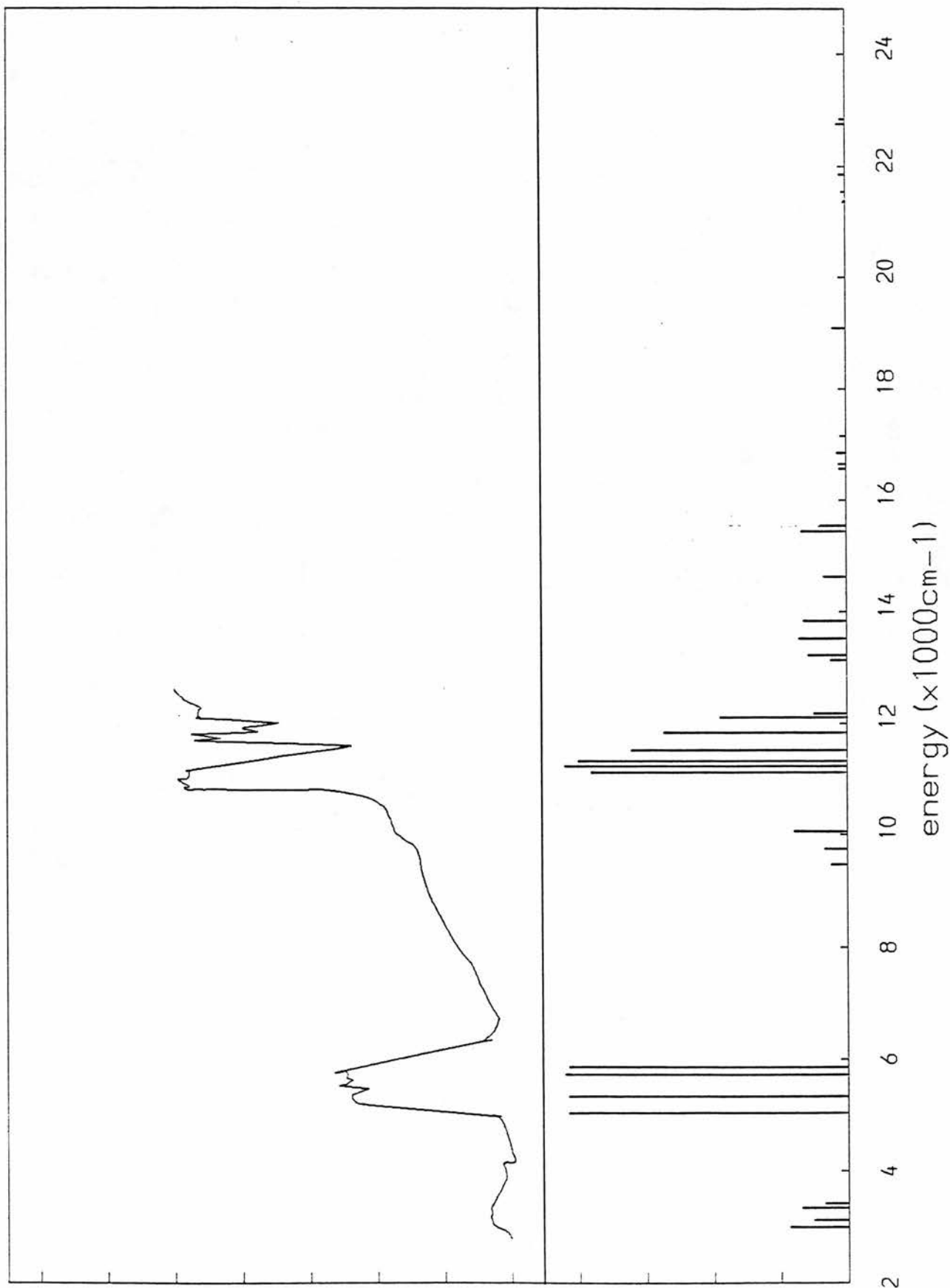


Table 4.10

Comparison of energy levels calculated for CdTe:Co

a) $\epsilon\tau\Delta_p$ theory	b) BC Δ theory
$\epsilon=0.859$	$B=485\text{cm}^{-1}$
$\tau=0.780$	$C=2130\text{cm}^{-1}$
$\Delta_p=4020\text{cm}^{-1}$	$\Delta=3150\text{cm}^{-1}$
2964 Γ_8	2994 Γ_8
3094 Γ_6	3109 Γ_6
3292 Γ_8	3304 Γ_8
3383 Γ_7	3391 Γ_7
4973 Γ_6	5008 Γ_6
5327 Γ_8	5345 Γ_8
5754 Γ_7	5751 Γ_7
5853 Γ_8	5844 Γ_8
7469 Γ_8	9488 Γ_8
7766 Γ_6	9733 Γ_6
8036 Γ_8	10064 Γ_8
10027 Γ_6	11092 Γ_8
10120 Γ_7	11242 Γ_7
10245 Γ_8	11365 Γ_8
11001 Γ_8	11570 Γ_6
11085 Γ_7	11808 Γ_6
11110 Γ_8	12093 Γ_8
11413 Γ_6	12170 Γ_7
12055 Γ_8	13107 Γ_7
12394 Γ_6	
12394 Γ_8	
12460 Γ_7	
12768 Γ_8	
15111 Γ_6	

All energies are measured in cm^{-1}

In the spectrum of ZnO:Co, the parameter τ is greater than ϵ . Usually for impurities in tetrahedral compounds only the t_2 electrons are allowed by symmetry to mix with the ligand electrons, so that ϵ should be greater than τ . But the result can be explained by the trigonal distortion in ZnO. The $\epsilon\tau\Delta_p$ theory also goes further than the $BC\Delta$ theory in explaining the anisotropy of the ZnO:Co spectrum [8].

In some of the spectra the ${}^4A_2 - {}^4T_2$ absorption is not observed. For the spectrum of CdTe:Co the 4T_2 level was omitted from the analysis, but the predicted position of this level agrees well with the observed level. Luminescence data due to transitions from the lowest spin orbit level of 4T_2 to the ground state 4A_2 has been reported by Radlinski [57] for $Co(d^7)$ in five of the II-VI hosts studied here. If it is assumed that the degree of phonon coupling is approximately equal in absorption and luminescence then some estimate of the ${}^4A_2 - {}^4T_2$ absorption energy can be established from these data. In table 4.11 the absorption band for the lowest spin orbit level of 4T_2 is estimated from the luminescence data. This is compared with the position of the level predicted by the $\epsilon\tau\Delta_p$ theory. The agreement between the two results is quite satisfactory. This suggests that for those spectra where the 4T_2 level is obscured the predicted level is likely to coincide with the real absorption barycentre.

Table 4.11
 Comparison of calculated ${}^4A_2-{}^4T_2$ level
 for $\text{Co}(d^7)$ with modified luminescence data

system	zpl	separation of fine structure	absorption band	level from $\epsilon\tau\Delta_p$ theory
ZnS:Co	3514	622	3500-->4200	3600
ZnSe:Co	3291	229	3300-->3500	3500
ZnTe:Co	3119	215	3100-->3300	3200
CdS:Co	3050	305	3050-->3350	3350
CdTe:Co	2853	133	2850-->3000	2960

all energies are measured in cm^{-1}

4.3 -Nickel in II-VI semiconductors-

The method of analysis for the $\text{Ni}(d^8)$ spectra is in principle the same as the method for $\text{Co}(d^7)$, and a fit to four or five observed absorption bands is possible in each case. For ZnSe:Ni spin orbit effects have been considered in some detail, and so a comparison can be made between the resulting parameters ϵ , τ and Δ_p with and without the inclusion of spin orbit coupling in the analysis.

Atomic nickel has the electronic configuration $(\text{Ar})3d^84s^2$, and so would be expected to have a d^8 configuration when it occurs as a substitutional impurity neutral with respect to the lattice in the II-VI semiconductors. Optical data on $\text{Ni}(d^8)$ in ZnO and ZnS have been reported by Weakliem [8], Kaufmann and Koidl [43], and Kaufmann, Koidl and Schirmer [58]. Pappalardo, Wood and Linares [59] also reported work on ZnO:Ni , and Roussos and Schulz [60] further work on ZnS:Ni . Karipidou, Nelkowski and Roussos [61], Wray and Allen [10], and Noras [21], have studied ZnSe:Ni , whilst Weakliem [8] and Pappalardo and Dietz [52] have studied CdS:Ni . Langer and Baranowski [9] have reported the absorption spectrum for CdSe:Ni .

In each spectrum, either four or five absorption peaks can be identified, and similarities between line shapes and between the relative intensity of lines are apparent. The absorptions are believed to correspond to electronic transitions from the crystal field ground state in $\text{Ni}(d^8)$, ${}^3T_1(F)$, to excited states of the d^8 configuration. Good agreement between experiment and both the $BC\Delta$ and the $\epsilon\tau\Delta_p$ versions of crystal field theory support this view. The crystal field ground state splits into four sub-levels when spin orbit coupling is considered. The lowest of these levels has the double group symmetry representation A_1 . Thus electric dipole transitions

are allowed to other levels with double group symmetry representation $A_1 \times T_2 = T_2$. These levels are included in the crystal field levels 3T_1 , 1T_2 , 3A_2 , 3T_1 , and 1T_2 . Therefore a description of the observed spectra will involve just transitions to these crystal field levels.

The appearance of the $Ni(d^8)$ spectra can be described in terms of crystal field theory as follows. The lowest energy level, between 4000cm^{-1} and 5000cm^{-1} , corresponds to the 3T_2 level. The two peaks above this, in the range 8000cm^{-1} to 10000cm^{-1} , are assigned to transitions to the levels 1T_2 and 3A_2 . The strongest absorption, found between 11500cm^{-1} and 13000cm^{-1} (15600cm^{-1} in $ZnO:Ni$), is due to the ${}^3T_1(F) - {}^3T_1(P)$ transition. In some of the spectra a smaller peak is observed at higher energies which is believed to be due to a transition to the 1T_2 level.

A strong absorption band, like the one found at 11500cm^{-1} in $ZnSe:Ni$, is clearly identifiable in each of the spectra. For each spectrum it can immediately be assigned to the same crystal field transition. However, although two levels similar to those at 7900cm^{-1} and 8800cm^{-1} in $ZnSe:Ni$ always occur in each of the spectra, their relative intensity and shapes are usually different, making individual assignments for each level difficult from these considerations alone. This difference in line characteristics is in part a consequence of their difference in energy separation, which in turn will alter the degree of spin orbit coupling between the levels. When the two levels are very close together, spin orbit coupling will mix them to such an extent that identification of the levels as distinct crystal field levels would not be appropriate.

The method of analysis of the $Ni(d^8)$ spectra in terms of the $\epsilon\tau\Delta_p$ theory is similar to that for $Co(d^7)$ and is summarised by the flow chart in fig.4.2. The three disposable parameters ϵ , τ and Δ_p

Fig 4.11
Absorption spectra of Ni(d⁸) compared with levels
calculated by the $\epsilon\tau\Delta_p$ theory.

ZnO:Ni

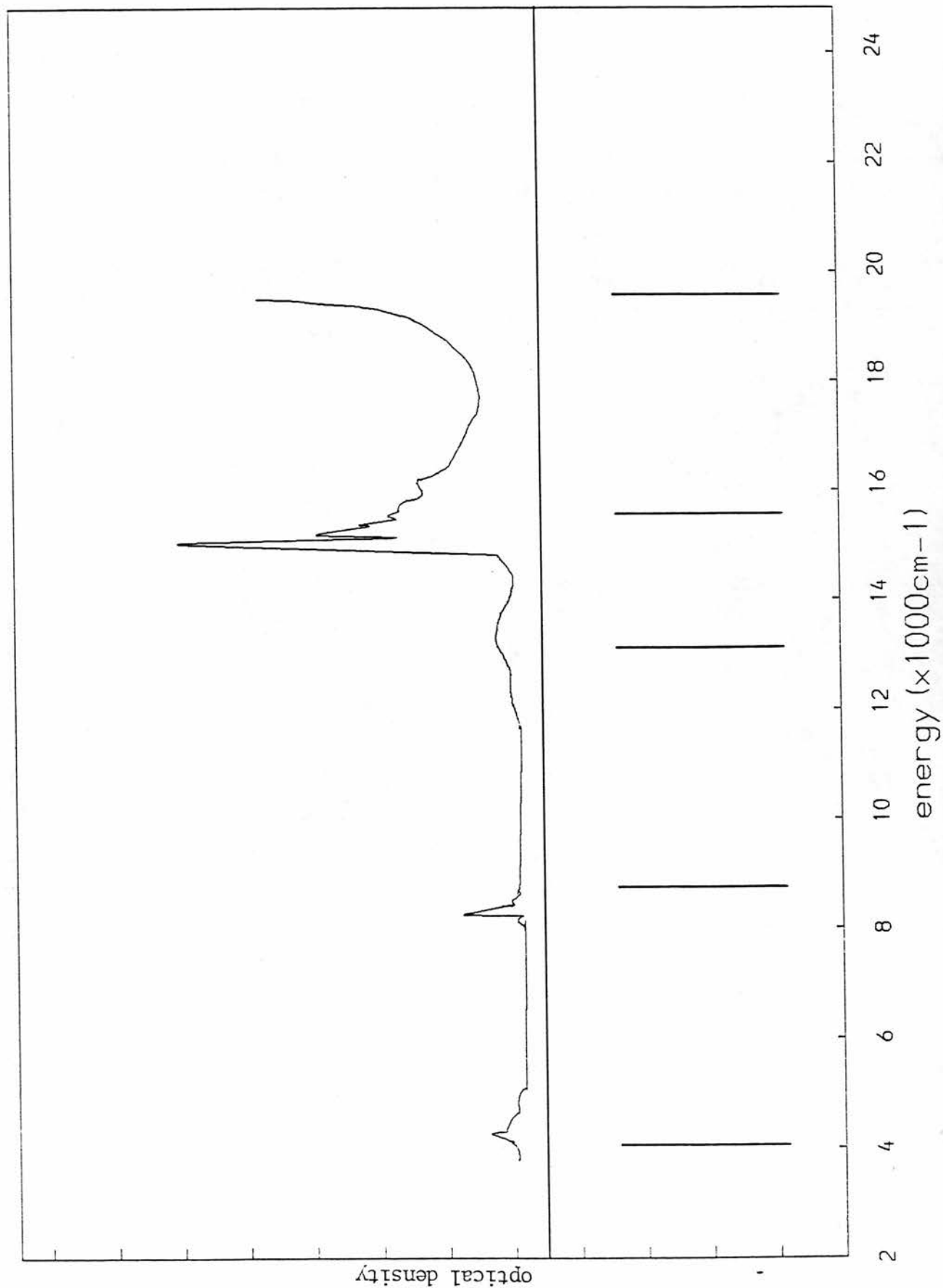


Fig 4.11
Absorption spectra of Ni(d⁸) compared with levels
calculated by the $\epsilon\tau\Delta_p$ theory.

ZnS:Ni

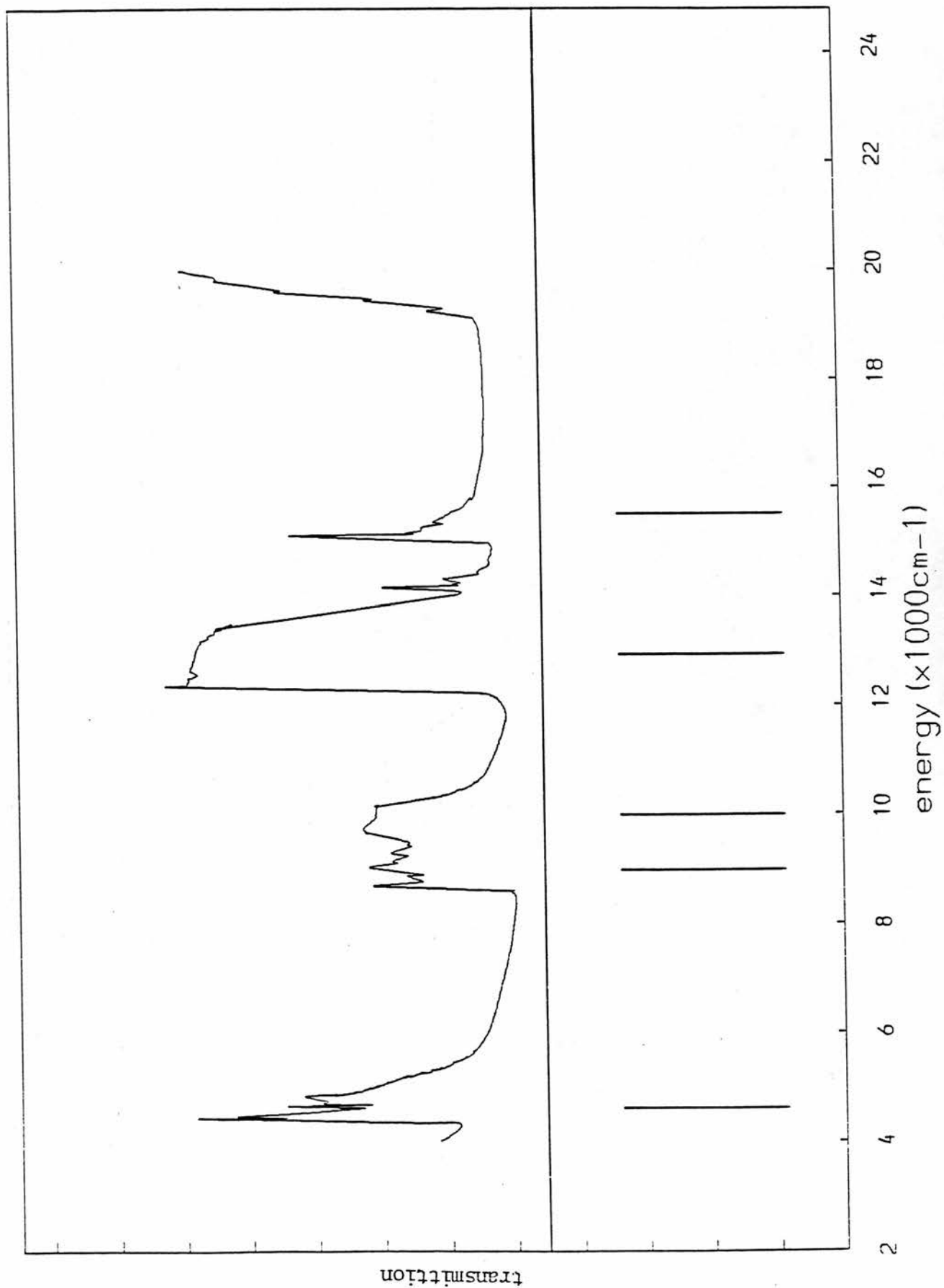


Fig 4.11
Absorption spectra of Ni(d⁸) compared with levels
calculated by the $\epsilon\tau\Delta_p$ theory.

ZnSe:Ni

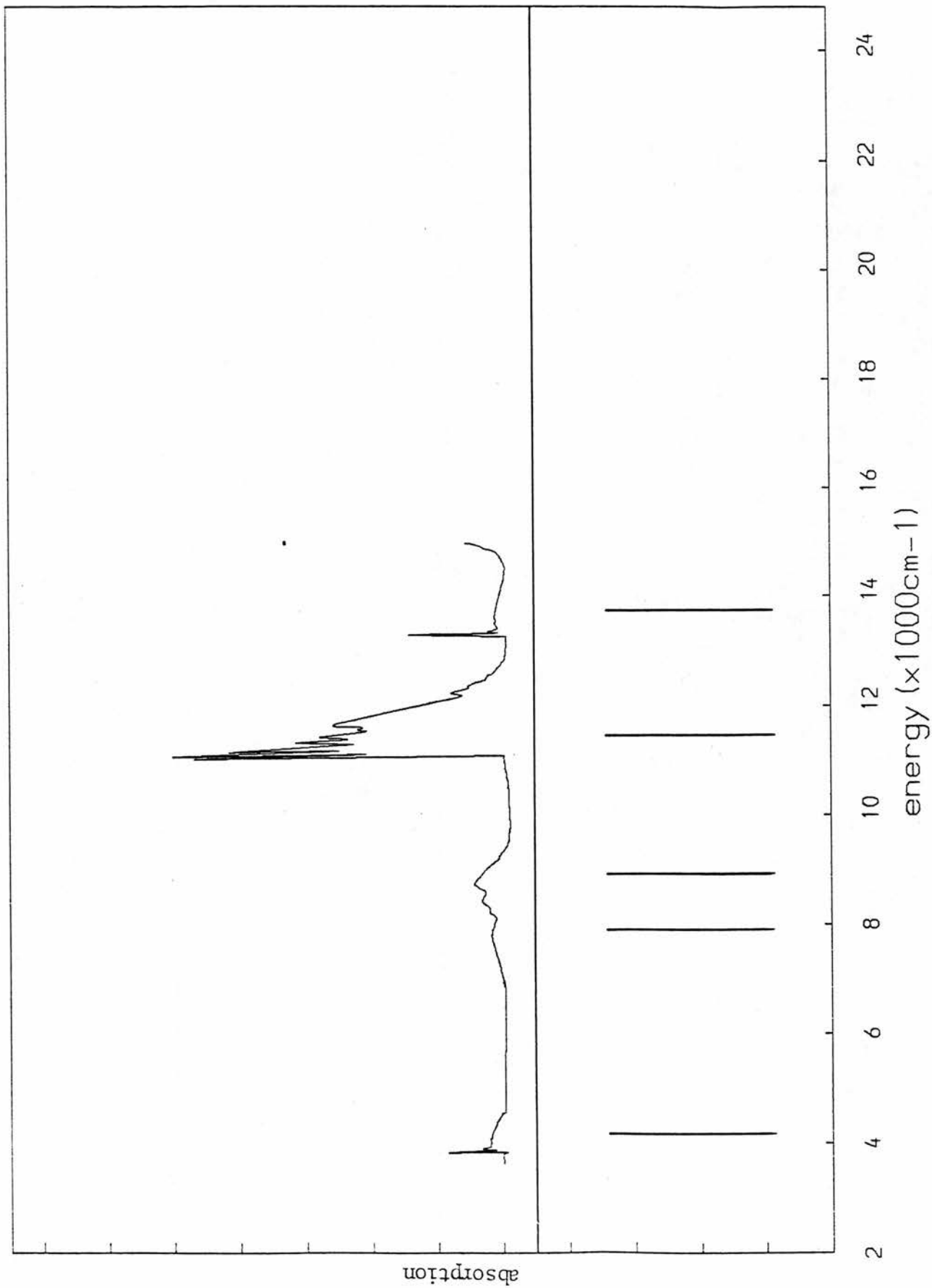


Fig 4.11
 Absorption spectra of Ni(d⁸) compared with levels
 calculated by the $\epsilon\tau\Delta_p$ theory.

CdS₈Ni

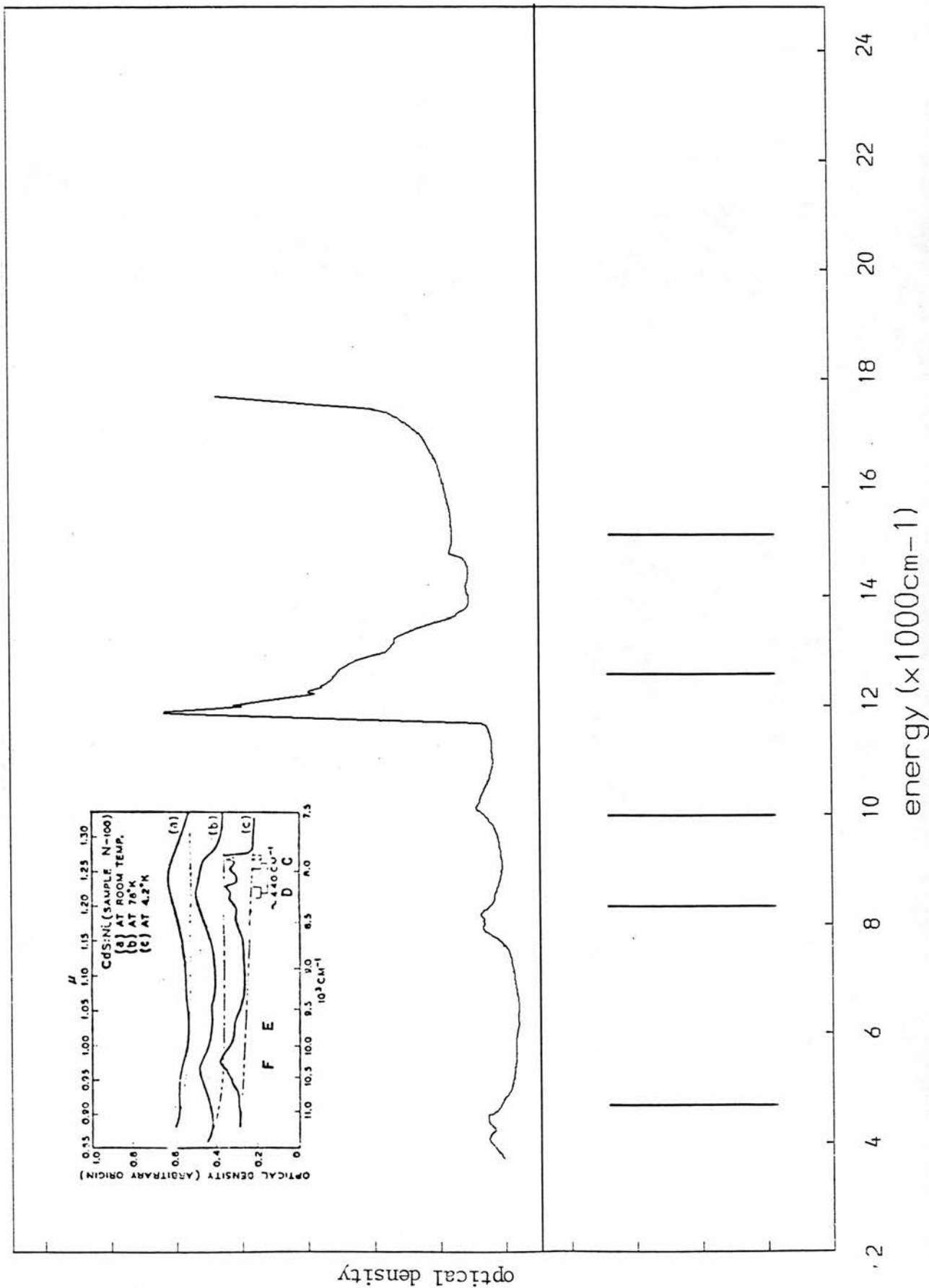
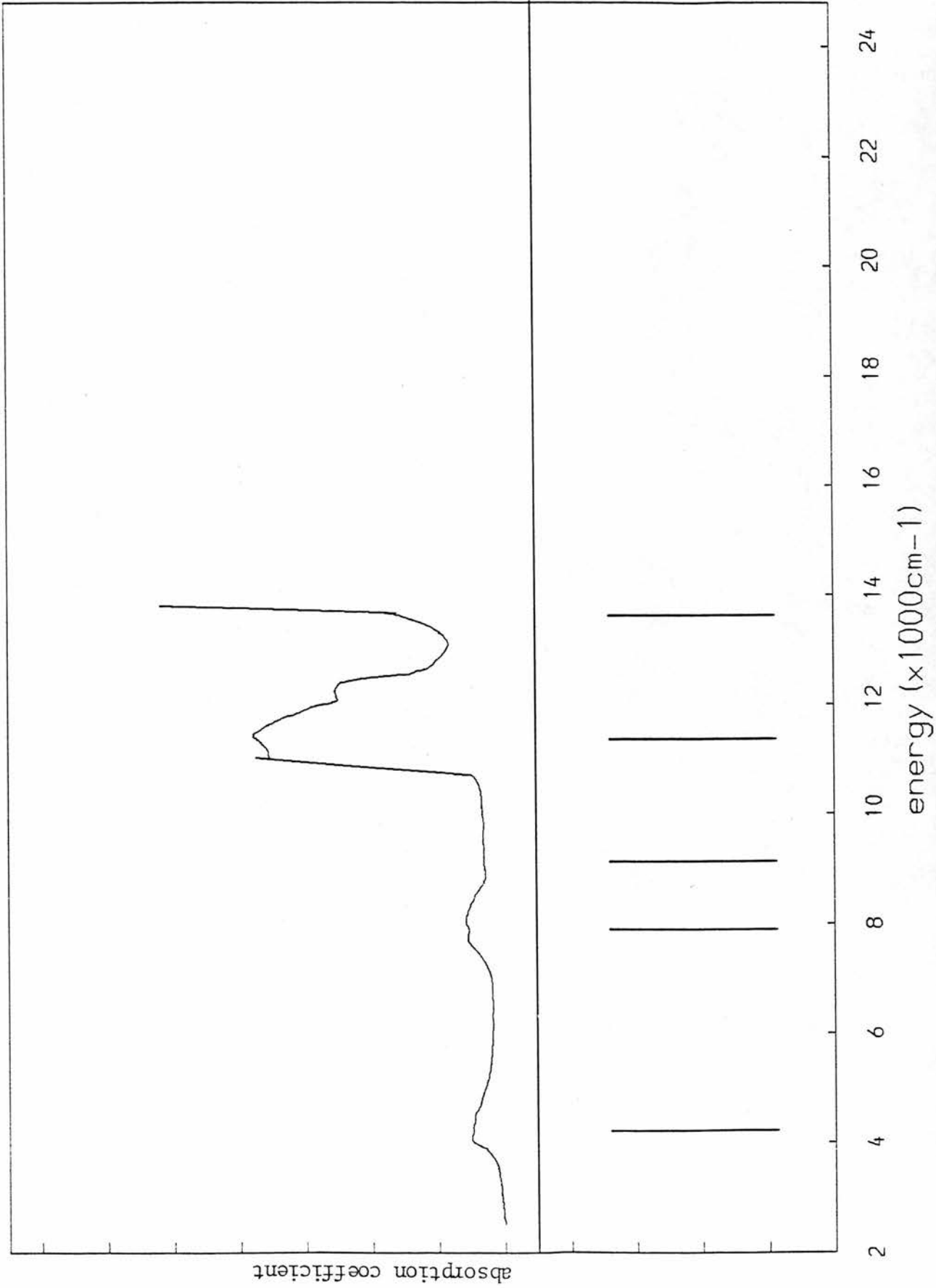


Fig 4.11
Absorption spectra of Ni(d^8) compared with levels
calculated by the $\epsilon\tau\Delta_p$ theory.

CdSe:Ni



are varied so as to obtain crystal field energy levels in closest agreement to those levels observed experimentally. For some spectra only four levels can be seen. Consequently a "best fit" was made just to four levels for each spectrum, and in addition a fit to all five levels when this was possible. I did this as a check on the error being introduced by fitting just to four levels instead of five. Spin orbit interaction has been considered in some detail for the spectrum of ZnSe:Ni where I found that its inclusion does not significantly alter the values of the parameters ϵ , τ and Δ_p . For the other spectra spin orbit coupling and other effects of comparable magnitude (e.g. Jahn-Teller coupling) have been ignored as they just complicate the analysis without significantly affecting the results of interest, namely the variation of the parameters ϵ , τ and Δ_p as the host is changed. A description of the analysis in terms of the $\epsilon\tau\Delta_p$ theory for each system, together with a comparison with previous work using the $BC\Delta$ model, is presented in the following sections. A summary of the results is given in table 4.12. In fig.4.11 the comparison between experimental data and the symmetry allowed transitions predicted by the $\epsilon\tau\Delta_p$ theory is shown.

4.3.1 -ZnO:Ni-

The absorption spectrum of ZnO:Ni was first reported by Pappalardo, Wood and Linares [59]. They account for the broad details of the spectrum in terms of a $BC\Delta$ model with:

$$B = 795\text{cm}^{-1} \quad C = 3470\text{cm}^{-1} \quad \Delta = 4050\text{cm}^{-1}$$

They compared spectra taken at 78 K and 4.2 K and an attempt was made to describe the fine structure in terms of first order spin orbit

splitting. Discrepancies in the interpretation of the fine structure were believed to be due to vibrational coupling and low symmetry effects. A similar treatment was carried out by Weakliem [8] using polarised spectra to investigate the anisotropy of the $E_{\perp c}$ and $E_{\parallel c}$ spectra due to the trigonal distortion in ZnO. His values for the disposable parameters were comparable to those of Pappalardo, Wood and Linares. More recently, Kaufmann and Koidl [43], and Kaufmann, Koidl and Schirmer [58] attempted to account for the fine structure of the 3T_2 and ${}^3T_1(P)$ crystal field levels in terms of the Jahn-Teller effect.

A fit to the four observed peaks using the $\epsilon\tau\Delta_p$ method gives the parameters:

$$\epsilon = 0.910 \qquad \tau = 0.949 \qquad \Delta_p = 4230 \text{ cm}^{-1}$$

The value of τ is greater than the corresponding value of ϵ . This was found to be the case in ZnO:Co, and the same explanation of the result holds. The trigonal distortion in ZnO reduces the t_2 representation to $a_1 + e$, but the e representation is irreducible in C_{3v} . Thus e and t_2 (i.e. $a_1 + e$) orbitals of the impurity d^8 configuration are both allowed by symmetry to mix with the ligand orbitals (which now have symmetry $a_1 + e$). The assignment of the levels is the same as that predicted by the $BC\Delta$ theory.

4.3.2 -ZnS:Ni-

Weakliem has observed the ZnS:Ni spectrum and described his results in terms of the $BC\Delta$ model including first order spin orbit coupling to explain the fine structure. His choice of disposable parameters was:

$$B = 560\text{cm}^{-1} \quad C = 2520\text{cm}^{-1} \quad \Delta = 4750\text{cm}^{-1}$$

Kaufmann and Koidl [43], and Kaufmann, Koidl and Schirmer [58] have studied the fine structure of the 3T_2 and ${}^3T_1(P)$ levels in more detail. The spectrum given by Roussos and Schulz [59] differs from the other reported spectra in that a zpl is present at around 14200cm^{-1} which the authors claim corresponds to a 1T_2 crystal field level. However, since this level has not been reported in any other high resolution studies of ZnS:Ni in the same region of the spectrum [21,8], I have ignored it in the present investigation, believing that it may be due to a stray impurity.

The $\epsilon\tau\Delta_p$ theory has been used neglecting spin orbit coupling and an assignment to the five observable crystal field levels gives the parameters:

$$\epsilon = 0.874 \quad \tau = 0.855 \quad \Delta_p = 5490\text{cm}^{-1}$$

By comparison a fit to just four levels, omitting the level at around 15500cm^{-1} , gives the parameters:

$$\epsilon = 0.878 \quad \tau = 0.855 \quad \Delta_p = 5540\text{cm}^{-1}$$

These parameters predict the 1T_2 crystal field level at 15660cm^{-1} . Agreement between these two sets of results is close.

In a pure crystal field scheme the assignment of the levels 3A_2 and 1T_2 , corresponding to the observed peaks at 9000cm^{-1} and 9800cm^{-1} respectively in the $BC\Delta$ model, is reversed for the $\epsilon\tau\Delta_p$ analysis. Because the two observed peaks lie close in energy, spin orbit

coupling will make each a mixture of the two crystal field levels. The shape of the 1T_2 level at 15500cm^{-1} most closely resembles the lower absorption, which supports the claim of the $\epsilon\tau\Delta_p$ theory that the lower level has the greater 1T_2 character. A third crystal field level, 1E , is predicted at an energy in between the 3A_2 and 1T_2 levels, which may explain some of the additional structure in that part of the spectrum.

4.3.3 -ZnSe:Ni-

The absorption spectrum of ZnSe:Ni was reported by Wray and Allen [10] who calculated values for B and Δ by fitting to the three high spin crystal field levels:

$$B = 530\text{cm}^{-1} \quad \Delta = 4400\text{cm}^{-1}$$

Noras [21] reported the absorption spectrum in more detail, and calculated the positions of the low spin states taking the ratio of C/B to lie between 3.7 and 4. Spin orbit coupling was taken into account by setting the parameter $\zeta = -500\text{cm}^{-1}$. This was the value used by Weakliem in the analysis of $\text{Ni}(d^8)$ in ZnO, ZnS, and CdS. The other fine structure in the spectrum was discussed in terms of Jahn-Teller coupling.

Photoluminescence data was reported for the transitions ${}^3T_1(P) - {}^3T_1(F)$ [61,62] and ${}^3T_2 - {}^3T_1(F)$ [61] and for both a coincidence of the zpl in luminescence and absorption was observed. For the transition ${}^3T_2 - {}^3T_1(F)$ in ZnS:Ni a coincidence of the zpl in absorption and emission has also been reported. Electric dipole transitions from the spin orbit ground state A_1 are symmetry allowed only to T_2 levels. Thus the coincidence of the zpl in absorption and

emission means that the T_2 sublevel must be the lowest of the four spin orbit levels originating from the 3T_2 and ${}^3T_1(P)$ crystal field levels, as shown in fig.4.12a. Using the $BC\Delta$ method this is found to be the case for the ${}^3T_1(P)$ level but not for the 3T_2 level.

Two models have been proposed to explain the coincidence of the zpl in absorption and luminescence for the 3T_2 level in $Ni(d^8)$. The models were originally proposed for Ni in GaP, but it has since been shown that $Ni(d^9)$ was responsible for that experimental data [63]. Clark and Dean [11] suggested that Jahn-Teller quenching of the first order spin orbit coupling may force the T_2 level to be the lowest level originating from the 3T_2 crystal field level. However no quantitative treatment of this idea has been presented. Noras and Allen [64], using the $BC\Delta$ theory, proposed that if the crystal field Δ was large enough then triplet-singlet mixing between the 3T_2 and 1T_2 crystal field levels may result in the T_2 spin orbit level originating from the 1T_2 level being the lowest level. Then absorption and emission transitions would be observed between the ${}^3T_1(A_1)$ and ${}^1T_2(T_2)$ levels. Such a model is inappropriate for ZnSe:Ni, because the two levels 3T_2 and 1T_2 are believed to be far apart (see fig.4.13).

Applying the $\epsilon\tau\Delta_p$ theory to the spectrum of ZnSe:Ni, and initially ignoring spin orbit coupling, two sets of parameters were obtained, by fitting first to four crystal field levels and then to five:

$$\begin{array}{lll} \epsilon = 0.851 & \tau = 0.827 & \Delta_p = 4960\text{cm}^{-1} \\ \epsilon = 0.844 & \tau = 0.828 & \Delta_p = 4940\text{cm}^{-1} \end{array}$$

The difference between the two sets of parameters is small, and agreement with experimental data is good for both cases. When spin orbit coupling was included, with ζ equal to -500cm^{-1} , then the lowest spin orbit level of the 3T_2 crystal field level is T_1 . But the

Fig 4.12a
Theoretical model to account for data in ZnSe:Ni

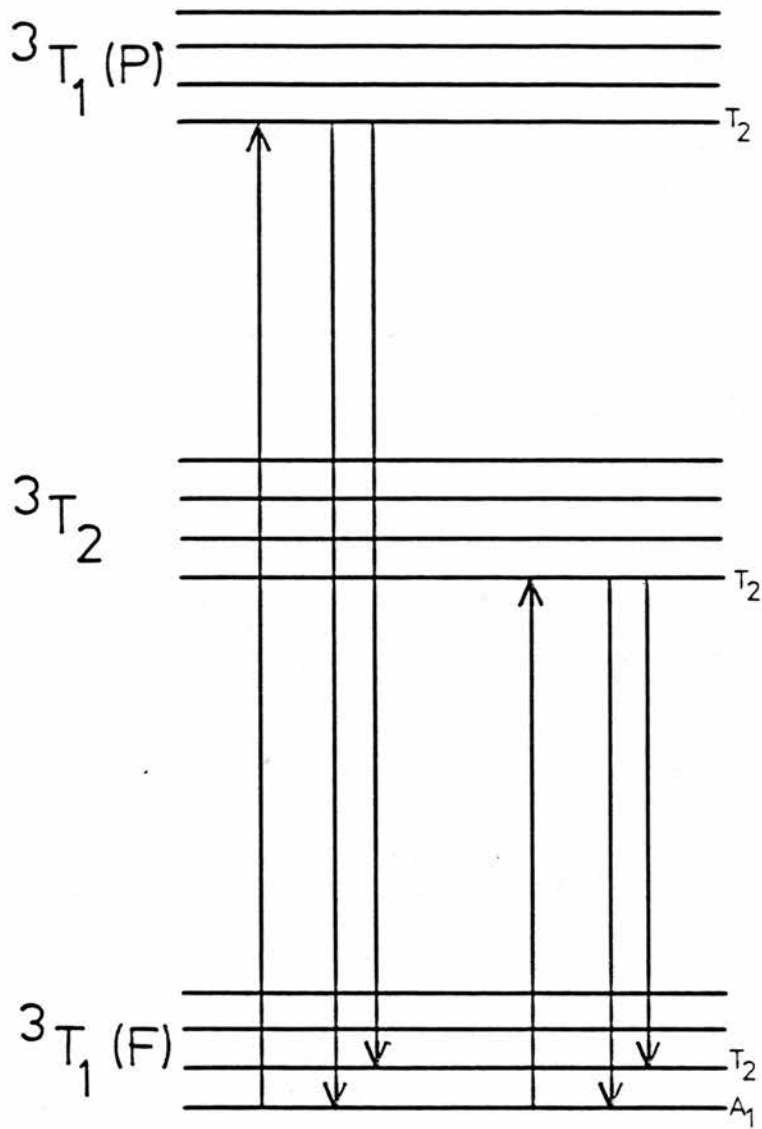


Fig 4.12b
Observed coincidence of absorption and luminescence in ZnSe:Ni

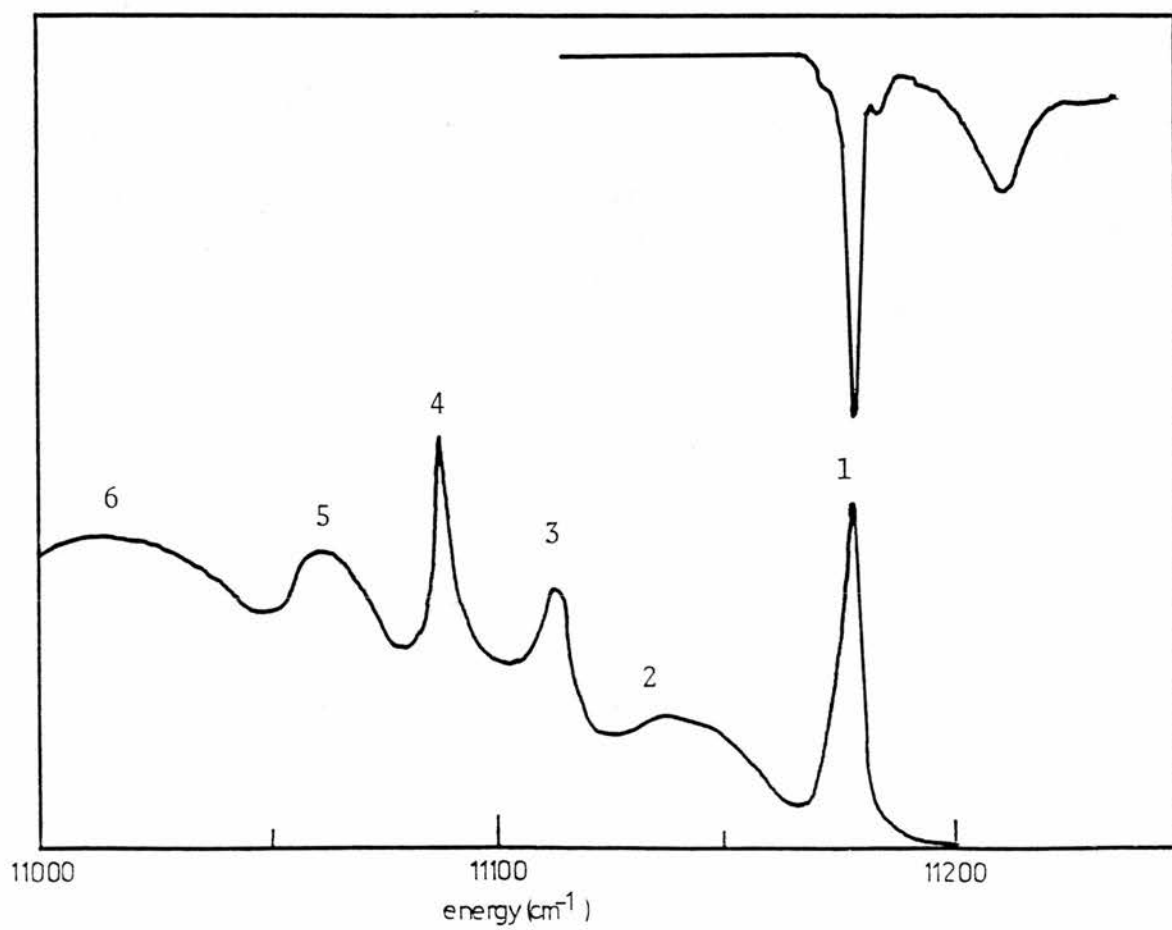
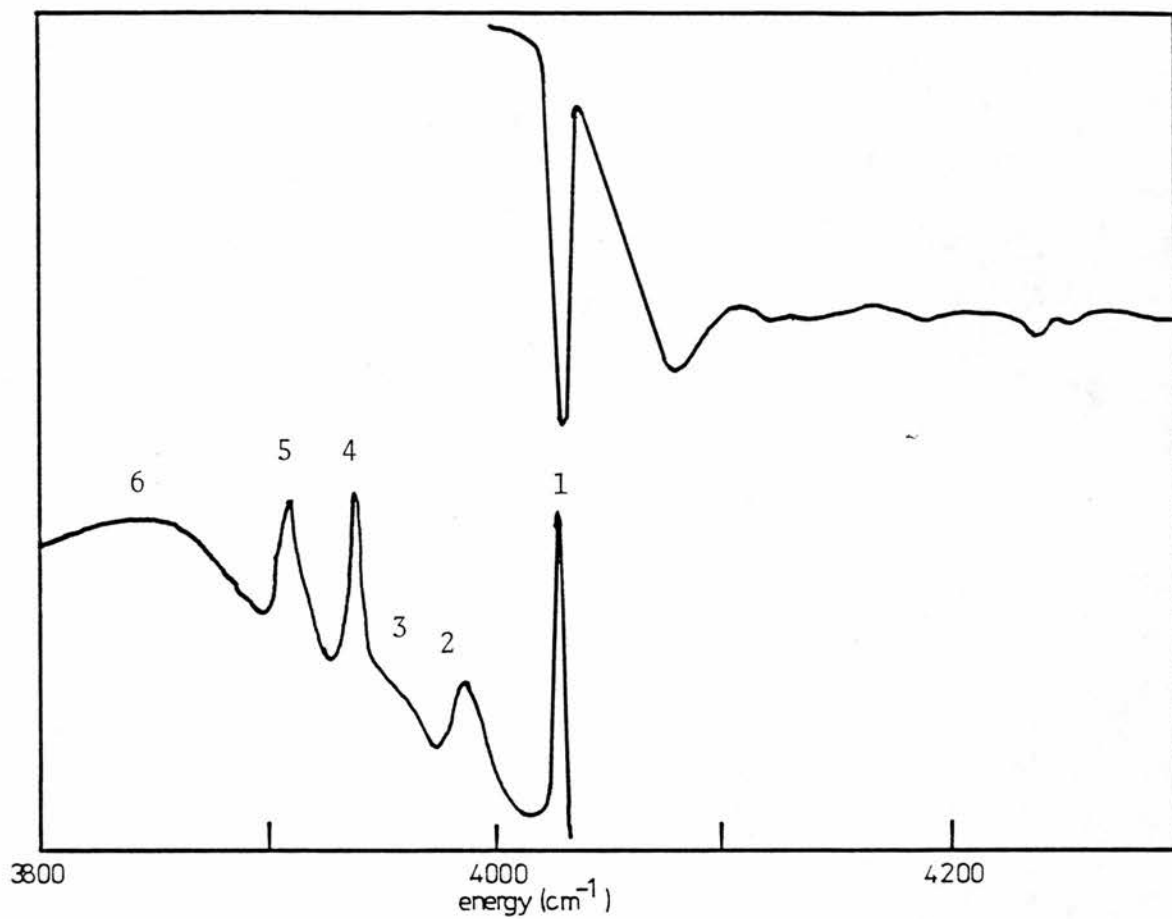
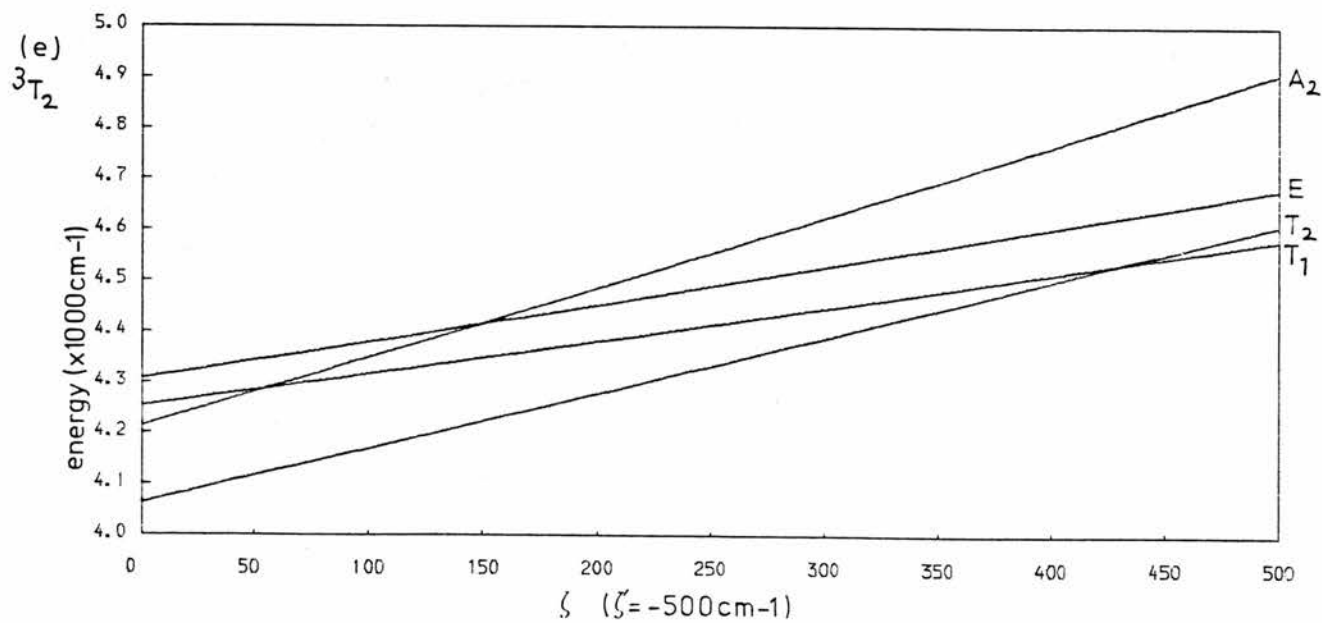
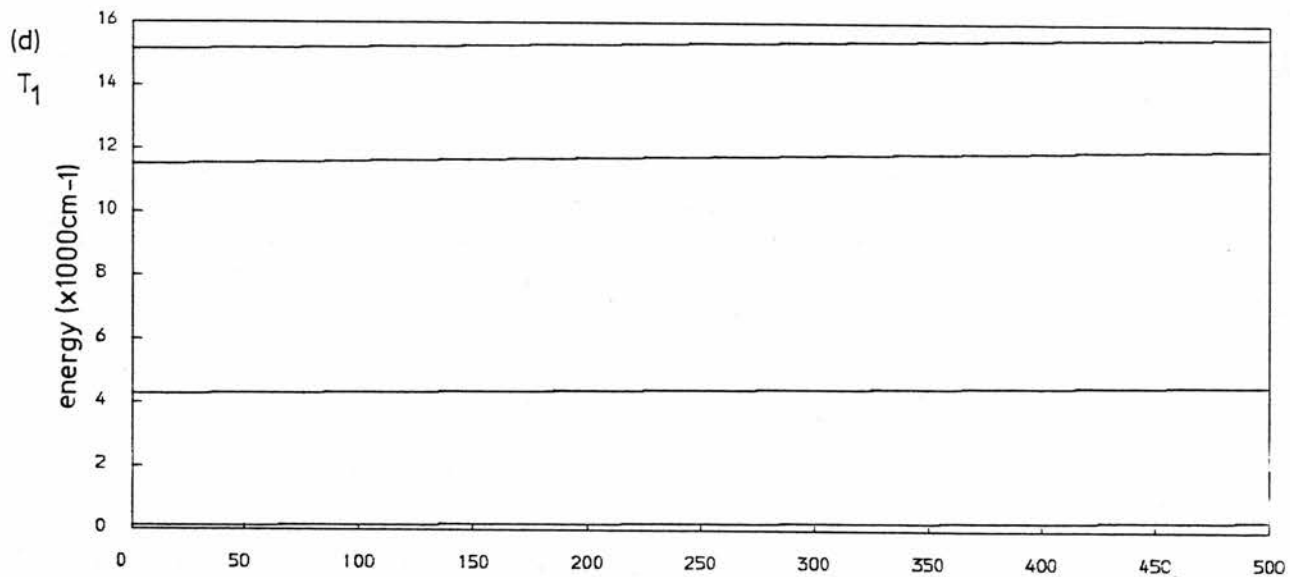
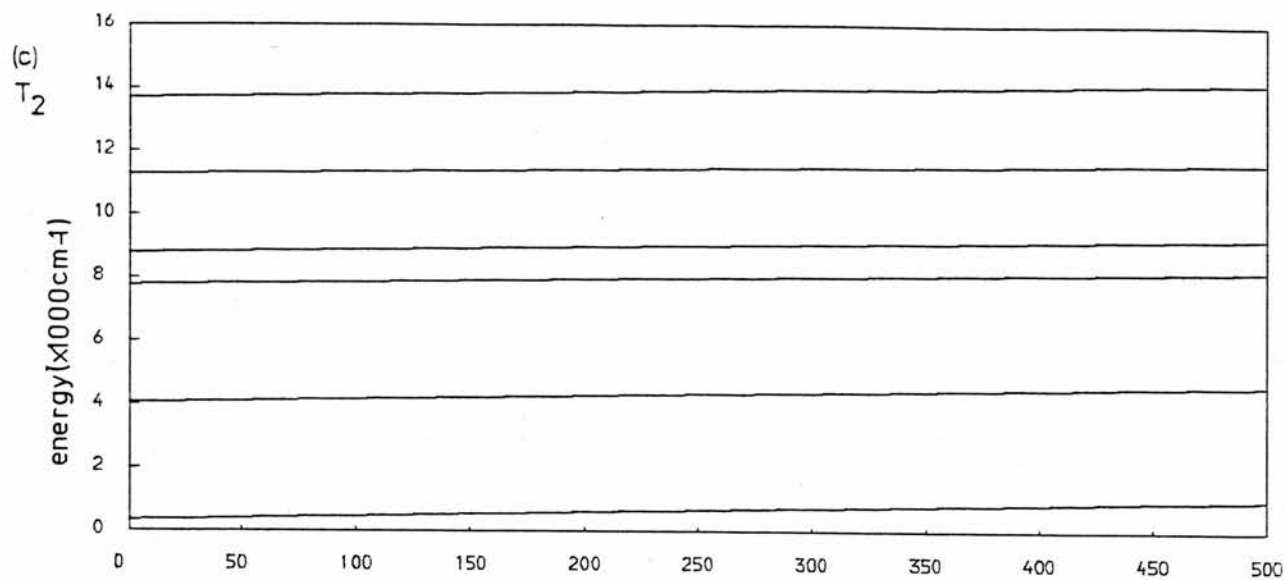


Fig 4.12 Spin orbit levels in ZnSe:Ni. c) T_2 symmetry, d) T_1 symmetry, e) levels originating from triplet T_2 .



observed coincidence of the zpl in absorption and luminescence suggests that for ZnSe:Ni the T_2 level should be lowest in energy (fig.4.12a).

In the $\epsilon\tau\Delta_p$ model, two spin orbit coupling parameters, ζ and ζ' , are appropriate. Both of the parameters are less than the corresponding free ion parameter as a result of the delocalisation of the d-orbitals. Since the degree of delocalisation of the t_2 orbitals is greater than that of the e orbitals, and since

$$\zeta = \langle R_t | H_{so} | R_t \rangle$$

$$\zeta' = \langle R_t | H_{so} | R_e \rangle$$

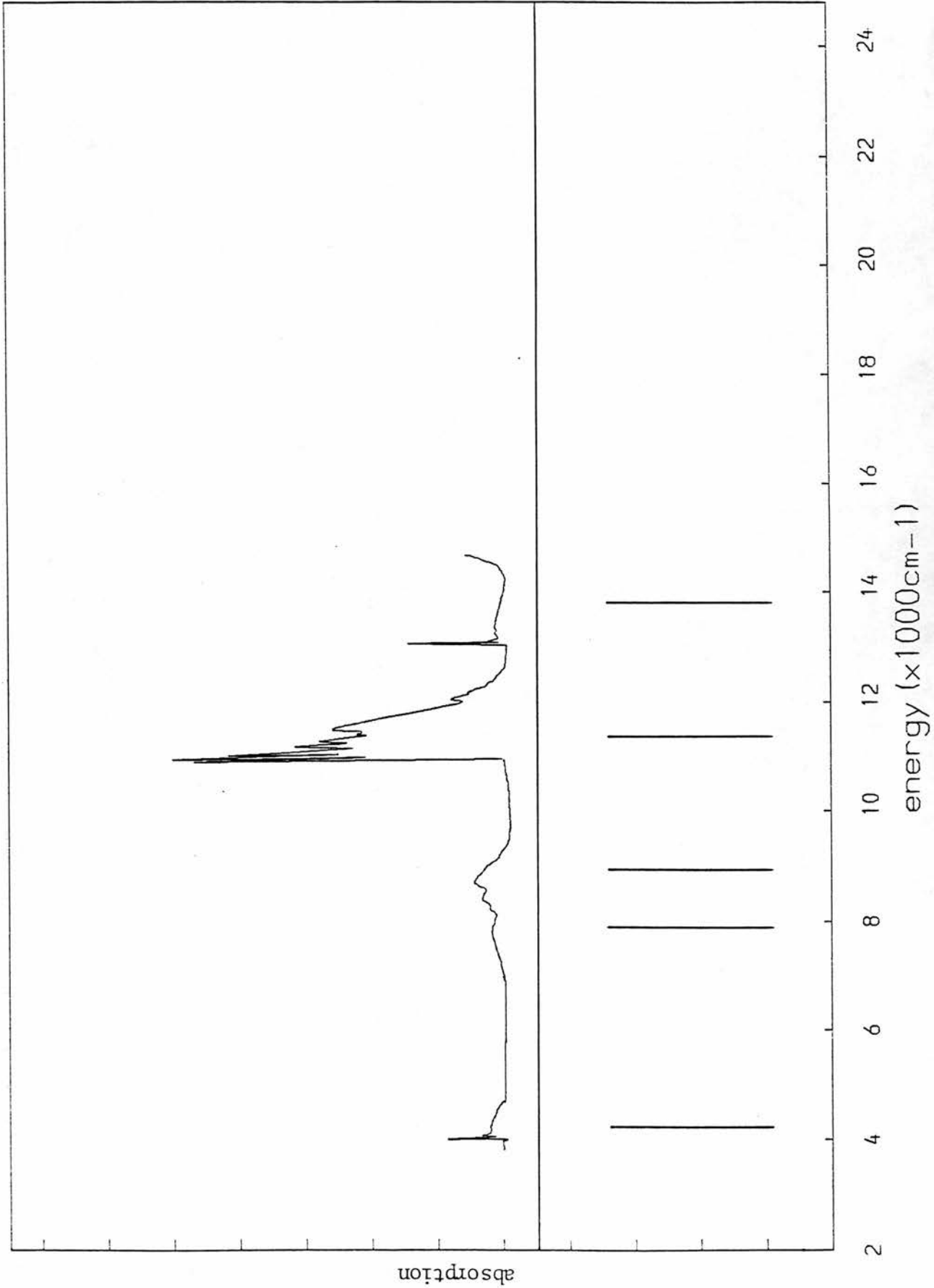
it follows that the magnitude of ζ must be less than ζ' . A precise numerical relationship between ζ and ζ' has not yet been established.

A graph of the spin orbit levels as a function of ζ with ζ' held at 500cm^{-1} is given in fig.4.12c for levels of T_2 symmetry representation, and in fig.4.12d for levels of T_1 symmetry representation. In each graph the levels decrease as ζ increases from -500cm^{-1} , but the rate of decrease is greater for the T_2 levels than for the T_1 levels. The four spin orbit levels originating from the 3T_1 crystal field level are shown in fig.4.12e. Only the level A_2 decreases more rapidly with increasing ζ than the T_2 level. But the A_2 level lies about 500cm^{-1} higher in energy when $\zeta = -500\text{cm}^{-1}$, and when $\zeta = 0\text{cm}^{-1}$ it is still some 150cm^{-1} above the T_2 level. The levels T_1 and T_2 cross over for values of ζ close to -420cm^{-1} . Thus T_2 becomes the lowest level originating from the 3T_2 crystal field level provided that ζ is greater than -430cm^{-1} when $\zeta' = -500\text{cm}^{-1}$. This result agrees with the experimentally observed coincidence of the zpl in absorption and emission, and with the theoretical conclusion that the magnitude of ζ should be less than ζ' . For higher values of ζ' the cross over of the T_1 and T_2 levels occurs at lower values of ζ . In the limit

Fig 4.13

Best fit to absorption spectrum of ZnSe:Ni with spin orbit coupling included.

ZnSe:Ni



when ζ' is at the free ion value for Ni, -649cm^{-1} , then the T_2 level is lowest in energy for all values of ζ between 0 and -649cm^{-1} .

Karipidou et al [61] have suggested that the separations observed between two strong peaks (line 1 and line 4 in fig.4.12b) in the ${}^3T_1(P) - {}^3T_1(F)$ and ${}^3T_2 - {}^3T_1(F)$ luminescence bands correspond with the splitting of the ${}^3T_1(F)$ ground state. This experimentally observed separation of 91cm^{-1} can be compared with the separation of 158cm^{-1} predicted by the $\epsilon\tau\Delta_p$ model. The comparison suggests that the spin orbit splitting of the ground state has been reduced, possibly by Jahn-Teller coupling. Alternatively the reduction of the spin orbit coupling parameters by covalency effects has been underestimated.

By a comparison of the broad details of the experimental data with the theoretically determined spin orbit symmetry allowed transitions shown in fig.4.13, the empirical parameters were calculated:

$$\begin{array}{lll} \epsilon = 0.849 & \tau = 0.817 & \Delta_p = 4790\text{cm}^{-1} \\ \zeta = -150\text{cm}^{-1} & \zeta' = -500\text{cm}^{-1} & \end{array}$$

These parameters differ by less than 4% from those obtained in the analysis where spin orbit coupling was ignored. For the other $\text{Ni}(d^8)$ spectra the difference has been assumed to be small, and so spin orbit coupling has not been included since it unnecessarily complicates the analysis.

4.3.4 -CdS:Ni-

The spectrum was reported and described in terms of the BCA model by Pappalardo and Dietz [52]. They included the spin orbit interaction to first order with $\zeta = -630\text{cm}^{-1}$ and obtained the crystal field parameters:

$$B = 615\text{cm}^{-1} \quad C = 2700\text{cm}^{-1} \quad \Delta = 4150\text{cm}^{-1}$$

Agreement with the data is adequate, but there is no satisfactory interpretation of the complex structure around 8000cm^{-1} where the BCA theory predicts a single crystal field level 3A_2 (see fig.4.11). Weakliem [8] has studied CdS:Ni using polarised spectra. His choice of parameters is close to that of Pappalardo and Dietz.

When the $\epsilon\tau\Delta_p$ theory is applied to this spectrum the assignment of the levels at around 8000cm^{-1} and 10000cm^{-1} is reversed. In addition a 1E level is predicted just above the 1T_2 level. These two levels more adequately explain the complex structure of the absorption around 8000cm^{-1} .

There is a good agreement between the two sets of parameters obtained when assignments are made first to four crystal field levels and then to five. The parameters for the latter fit are:

$$\epsilon = 0.873 \quad \tau = 0.838 \quad \Delta_p = 5700\text{cm}^{-1}$$

4.3.5 -CdSe:Ni-

Langer and Baranowski [9] reported the spectrum of CdSe:Ni and obtained the parameters:

$$B = 530\text{cm}^{-1} \quad C = 2460\text{cm}^{-1} \quad \Delta = 3850\text{cm}^{-1}$$

Applying the $\epsilon\tau\Delta_p$ theory to the four observable absorptions leads to the adjustable parameters:

$$\epsilon = 0.835 \quad \tau = 0.828 \quad \Delta_p = 4950\text{cm}^{-1}$$

The change in the assignment of levels around 8000cm^{-1} from 3A_2 to 1T_2 and 1E helps to describe the complex structure of that absorption, which was also the case for CdS:Ni. This then leads to the as yet unresolved problem of explaining the reduced oscillator strength of the spin allowed transition ${}^3T_1(F) - {}^3A_2$ predicted around 9200cm^{-1} . There is good reason to suppose that the predicted position of the 1T_2 level at 13650cm^{-1} is an accurate assignment, as has been the case with the other Ni(d^8) spectra.

4.3.6 -Summary-

The spectrum of Ni(d^8) has been studied in five different II-VI compounds and good agreement between theory and experiment has been found. Similarities were noted between the spectra. The analysis involved fitting to four absorption levels and also, when possible, to five levels. There is only a small difference between the two possible sets of parameters for each system.

The assignment of levels with the $BC\Delta$ theory is the same as with the $\epsilon\tau\Delta_p$ theory, except that occasionally the levels 3A_2 and 1T_2 are reversed. These two levels lie close together in energy, so that spin

orbit coupling will make each observed peak a mixture of the two crystal field levels.

The effect of spin orbit coupling on the spectrum of ZnSe:Ni was considered in some detail. Using the $\epsilon\tau\Delta_p$ theory, and for a wide range of physically reasonable values of ζ and ζ' , the observed coincidence of a zpl in absorption and luminescence for the transitions ${}^3T_1(P) - {}^3T_1(F)$ and ${}^3T_2 - {}^3T_1(F)$ is predicted [61,62]. Calculations have shown that the omission of spin orbit coupling does not significantly change ϵ , τ and Δ_p for ZnSe:Ni. The free ion value of ζ is larger for Ni(d^8) than for any other $3d^n$ transition metal ion studied in this thesis, and so it has been assumed that the neglect of spin orbit coupling does not distort the values of calculated parameters for any other system.

For the spectrum of ZnO:Ni the parameter τ is greater than ϵ . This result is a consequence of the trigonal distortion in ZnO and was also found to be the case with ZnO:Co.

4.4 $3d^n$ transition metal ions in ZnS-

For the analysis of each of the spectra reported in this section, electrostatic interactions within a different d^n electron configuration have had to be considered. In the previous two sections the spectra contained common features, such as the strong ${}^3T_1(F) - {}^3T_1(P)$ absorption in each of the Ni(d^8) spectra, which were used to establish the assignment of data to a specific configuration. This method of assignment is not possible with some of the spectra studied in this section, because of a lack of data for similar systems with which to make a comparison. In other systems the impurity ground

Table 4.13
 Summary of results for $3d^n$ impurities in ZnS

system	ϵ	τ	Δ_p
ZnS:Ti(d^2)	0.881	0.864	2960cm^{-1}
ZnS:V(d^3)	0.985	0.783	2220cm^{-1}
ZnS:Cr(d^4)	0.945	0.900	4790cm^{-1}
ZnS:Mn(d^5)	1.034	0.910	7140cm^{-1}
ZnS:Fe(d^6)	0.915	0.913	3310cm^{-1}
ZnS:Co(d^7)	0.981	0.823	5900cm^{-1}
ZnS:Ni(d^8)	0.874	0.855	5490cm^{-1}

state is close to the conduction band edge so that only a small number of crystal field transitions can be observed. At least three crystal field levels must be observed if the $\epsilon\tau\Delta_p$ theory is to be applied.

Spin orbit coupling has been omitted from the analysis of the spectra in this section. The parameter ζ is largest for $\text{Ni}(d^8)$, and so spin orbit coupling should have its greatest impact on the spectra of $\text{Ni}(d^8)$. It was observed in the previous section that its inclusion does not lead to a significant change of parameters. Therefore I believe that in the present section the omission of spin orbit coupling should not lead to any distortion of the resulting crystal field parameters.

The results presented in this section should be read with these considerations in mind. A summary of results is presented in table 4.13.

4.4.1 -ZnS:Ti(d²)-

Data from esr showing that Ti occurs as a substitutional impurity, neutral with respect to the lattice, in ZnS was presented by Schneider and Rauber [65]. The absorption spectrum was reported by Noras [21] and is shown in fig.4.14. He discussed the evidence for supposing that the data corresponds to transitions within a d^2 configuration in terms of a $BC\Delta$ model and arrived at the parameters:

$$B = 350\text{cm}^{-1} \quad C = 1580\text{cm}^{-1} \quad \Delta = 3660\text{cm}^{-1}$$

The spectrum consists of two wide absorption peaks. From the shape and width of the absorption band around 6000cm^{-1} I decided to assign two crystal field levels centred at 5250cm^{-1} and 6300cm^{-1} to the observed structure. The barycentre of the third crystal field level

Fig.4.14
Absorption spectrum of ZnS:Ti(d²) compared with
energy levels calculated by the $\epsilon\tau\Delta_p$ theory

ZnS:Ti

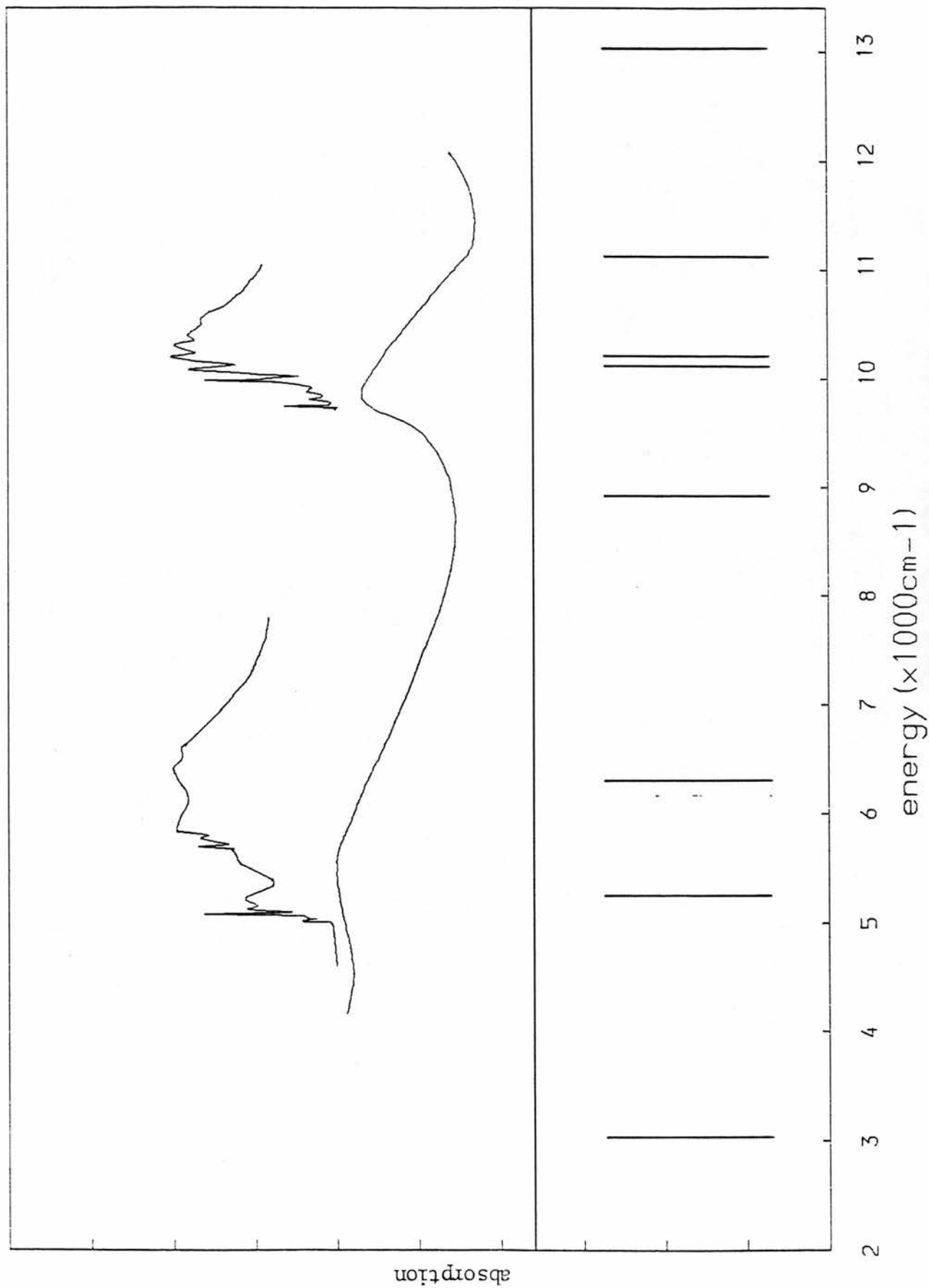


Table 4.14

Comparison of energy levels calculated for ZnS:Ti

a) $\epsilon\tau\Delta_p$ theory		b) BC Δ theory	
$\epsilon=0.881$		$B=350\text{cm}^{-1}$	
$\tau=0.864$		$C=1580\text{cm}^{-1}$	
$\Delta_p=2960\text{cm}^{-1}$		$\Delta=3660\text{cm}^{-1}$	
3086	3T_2	3660	3T_2
5250	3T_1	5763	1E
6300	1E	6000	3T_2
8933	1T_2	9271	1T_2
10108	1A_1	9344	1A_1
10200	3T_1	10230	3T_1
11127	1T_1	11010	1T_1
13030	1E	13807	1E
13236	1T_2	13958	1T_2

All energies are measured in cm^{-1}

considered was chosen to be 10200cm^{-1} . For an indication of which crystal field levels were responsible for the observed absorptions, the energy levels calculated from the d^2 energy matrices were plotted as a function of Δ_p for different values of ϵ and τ between 0.75 and 1.0. In addition to the two symmetry allowed transitions from the ground state 3A_2 to the states 3T_1 , a third transition to the level 1E is observed. This transition gains in oscillator strength as a result of spin orbit coupling with the nearby triplet level. Two physically reasonable sets of parameters were found by fitting to these three levels with the $\epsilon\tau\Delta_p$ method:

3T_1 higher than 1E

$$\epsilon = 0.838$$

$$\tau = 0.808$$

$$\Delta_p = 3680\text{cm}^{-1}$$

3T_1 lower than 1E

$$\epsilon = 0.881$$

$$\tau = 0.864$$

$$\Delta_p = 2960\text{cm}^{-1}$$

The two assignments differ in their ordering of the lower two crystal field levels 1E and 3T_1 at 5250cm^{-1} and 6300cm^{-1} . Because the structure around 10200cm^{-1} looks more like the structure at 5250cm^{-1} than that at 6300cm^{-1} I believe that the second set of parameters, which assigns the structure at 5250cm^{-1} to the $^3A_2 - ^3T_1$ transition to be the more likely. The crystal field levels corresponding to the second set of parameters appear in table 4.14.

4.4.2 ZnS:V(d³)-

The main interest in this section is the optical absorption spectrum for ZnS:V(d³), rather than ZnS:V(d²) which has also been reported in the literature. It is likely that both V(d²) and V(d³) exist together in ZnS for that system studied in absorption in this section [66]. This point is discussed before details of a fit to the absorption spectrum of V(d³) are given.

Holten et al [67] interpret their esr data in terms of a V(d²) configuration, and Allen [68] has been able to describe the excitation spectrum of Meijer and Avinor [69,70] in terms of V(d²) using the BCA theory. An absorption spectrum for ZnS:V, which differs from the V(d²) excitation spectrum, has been reported by Hoang and Baranowski [66]. This data is described by internal transitions within V(d³), but they also report luminescence and excitation data which display similarities to those data reported by Meijer and Avinor, suggesting that a d² configuration may also be present. Some ambiguity remains concerning the configuration assignment for the excitation spectrum of Hoang and Baranowski which contains a strong band around 10000cm⁻¹, similar to the d² excitation spectrum, but also similar to the d³ absorption spectrum. Meijer and Avinor report structure around 14500cm⁻¹ in their d² excitation spectrum, whilst Hoang and Baranowski do not report on this region of the excitation spectrum.

It seems a reasonable conclusion that the ZnS:V system studied here contains a mixture of d² and d³ configurations [71]. This accounts for the luminescence and excitation spectra which are d² like, and the absorption spectrum which is d³ like. It is assumed that the system contains mainly V(d³) so that contributions from V(d²) in absorption can be ignored.

Fig.4.15
Absorption spectrum of ZnS:V(d³) compared with
energy levels calculated by the $\epsilon\tau\Delta_p$ theory

ZnS:V

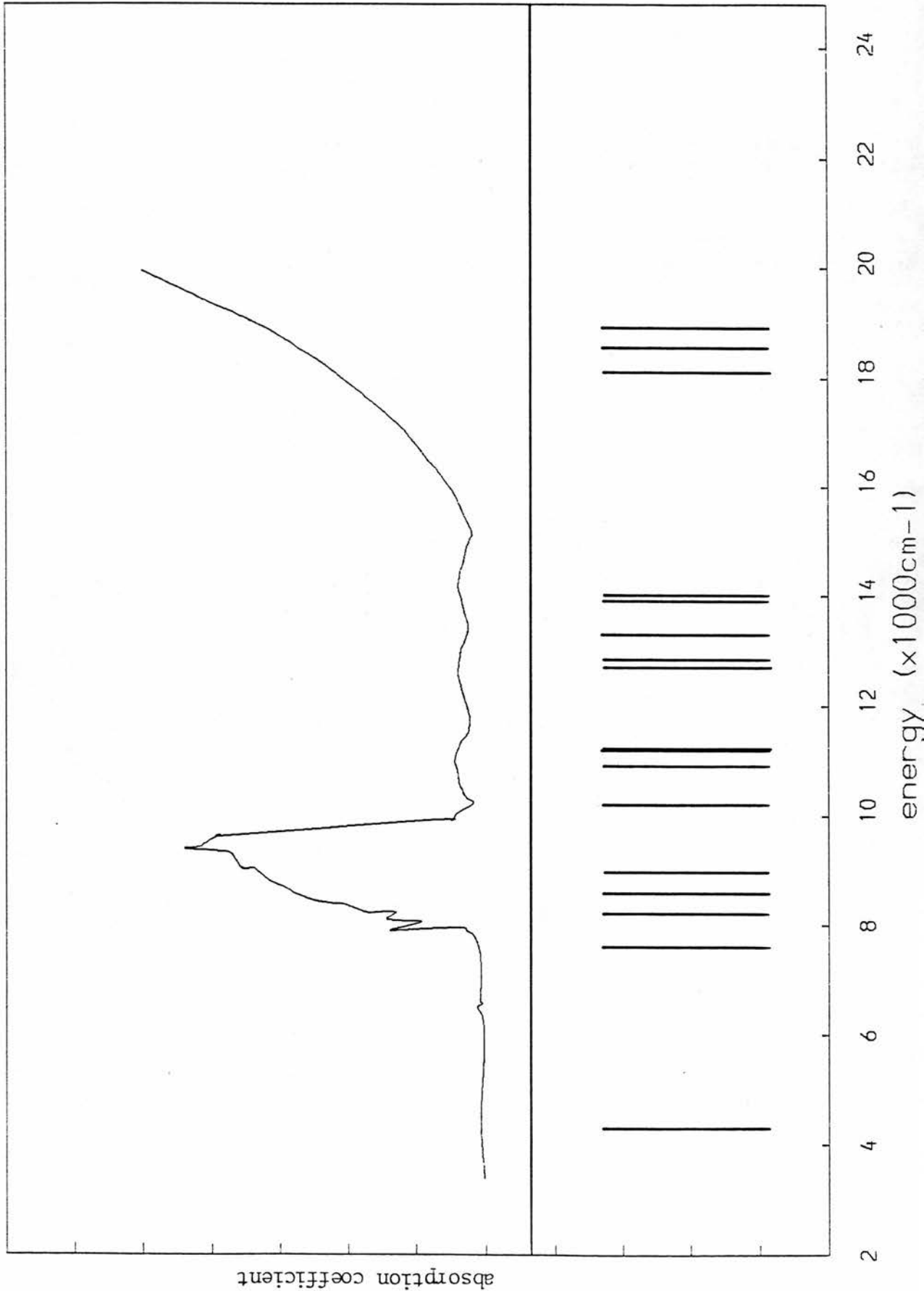


Table 4.15
Comparison of energy levels for ZnS:V

a) $\epsilon\tau\Delta_p$ theory

$$\begin{aligned}\epsilon &= 0.985 \\ \tau &= 0.783 \\ \Delta_p &= 2220 \text{ cm}^{-1}\end{aligned}$$

4300	$4T_2$
7610	$2T_1$
8550	$2E$
8200	$4A_2$
8960	$2A_1$
10300	$4T_1$
10900	$2T_1$
11200	$2E$
11200	$2T_2$
12700	$2T_1$
12800	$2T_2$
13300	$2E$
13900	$2T_1$
14000	$2T_2$
18100	$2A_2$
18600	$2T_2$
18900	$2T_1$
24600	$2E$

b) BCA theory

$$\begin{aligned}B &= 500 \text{ cm}^{-1} \\ C &= 2290 \text{ cm}^{-1} \\ \Delta &= 5000 \text{ cm}^{-1}\end{aligned}$$

4370	$4T_2$
5560	$2E$
9370	$4A_2$
9500	$2T_1$
9730	$2T_2$
11200	$4T_1$
12100	$2T_1$
13200	$2A_1$
14500	$2T_2$
15100	$2T_1$
16300	$2E$
17900	$2T_2$
18600	$2T_1$
19300	$2E$
21700	$2T_2$
23200	$2A_2$
23300	$2T_1$
34300	$2E$

all energies are measured in cm^{-1}

The optical absorption spectrum for ZnS:V is shown in fig.4.15 [66]. Using the BCΔ theory Hoang and Baranowski described the absorption spectrum as $V(d^3)$ with the parameters

$$B = 500\text{cm}^{-1} \qquad \Delta = 5000\text{cm}^{-1}.$$

A better agreement between theory and experiment is obtained using the $\epsilon\tau\Delta_p$ theory. The best fit was made by assigning two high spin transitions to the broad absorption band between 8000cm^{-1} and 10000cm^{-1} . Improvements in the assignment of levels were made by including some doublet transitions within the broad band. The final assignment is

$$\epsilon = 0.985 \qquad \tau = 0.783 \qquad \Delta_p = 2220\text{cm}^{-1}.$$

More experimental work on this system is needed to determine what proportion of the V has a d^3 configuration. It may be that the d^2 configuration electrons make a significant contribution to the absorption spectrum, in which case a re-examination of the data in terms of crystal field theory would be necessary.

4.4.3 ZnS:Cr(d^4)

Chromium ions in ZnS have been studied in absorption by Kelley and Williams [72] and Vallin et al [73] and in emission by Nelkowski and Grebe [74]. They have reported a strong absorption around 5800cm^{-1} and assigned it to the ${}^5T_2 - {}^5E$ transition of $\text{Cr}(d^4)$. A calculation of the crystal field parameters B and C was not possible as no other crystal field levels were observed. Detailed calculations on the observed fine structure were attempted by including the effects, on the ground state and the excited state, of spin orbit coupling [72,73], a deformation of the lattice at the impurity site by

Fig.4.16
Absorption spectrum of ZnS:Cr(d⁴) compared with
energy levels calculated by the $\epsilon\tau\Delta_p$ theory

ZnS:Cr

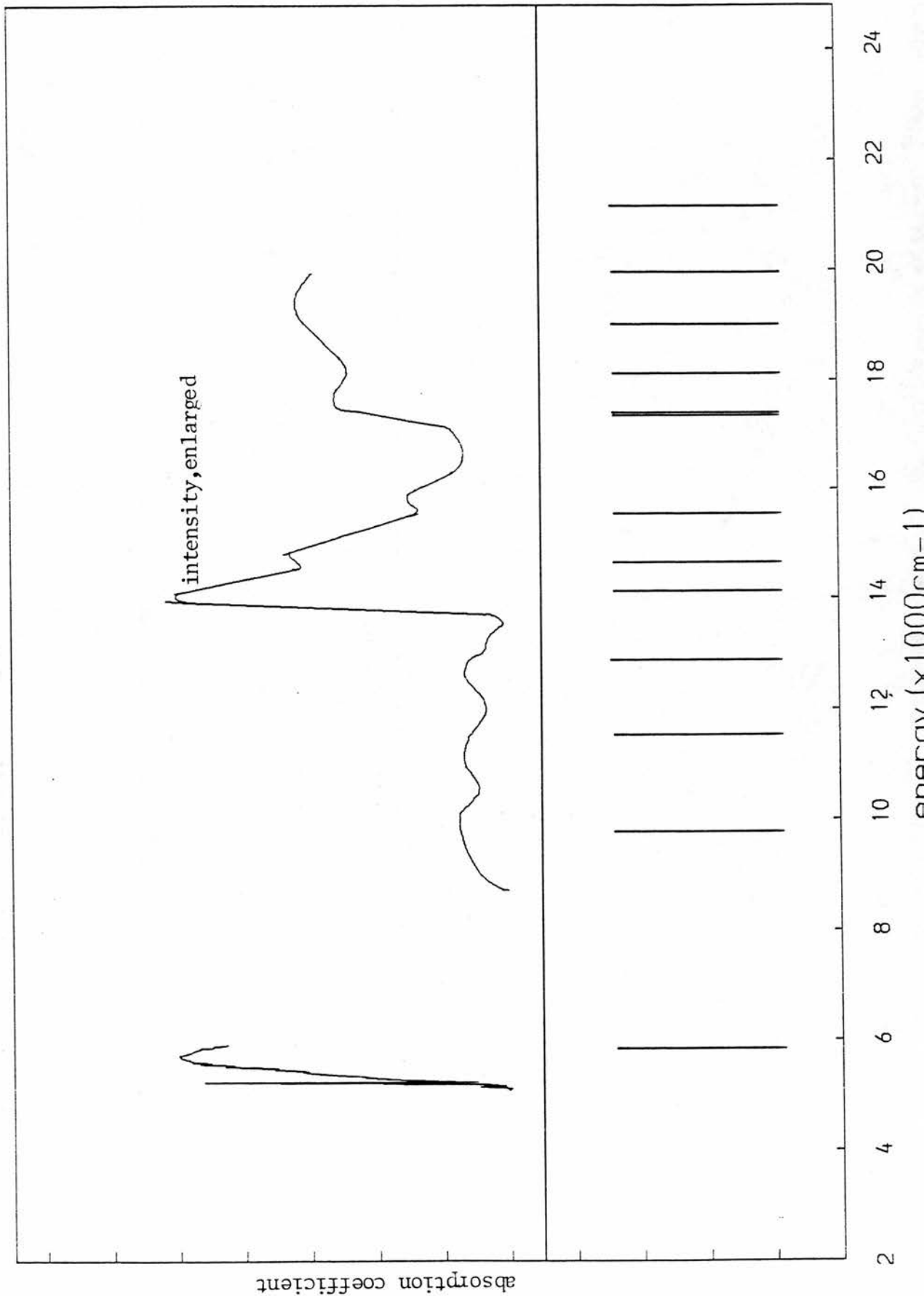


Table 4.16

Comparison of energy levels calculated for ZnS:Cr

a) $\epsilon\tau\Delta_p$ theory	b) ECA theory
$\epsilon=0.945$	$B=500\text{cm}^{-1}$
$\tau=0.900$	$C=2850\text{cm}^{-1}$
$\Delta_p=4790\text{cm}^{-1}$	$\Delta=5100\text{cm}^{-1}$
5852 5E	5100 5E
9771 3T_1	10037 3T_1
11543 3T_2	11856 3T_2
12924 3T_1	?
14160 3E	14062 3T_1
14675 3T_2	14862 3T_2
15543 3T_1	15595 3E
17362 3T_2	16082 3T_1
17366 3A_2	17987 3T_2
18124 3T_1	19413 3A_2
19007 3E	19491 3E
19971 3A_1	19528 3T_1
21168 3T_2	21000 3A_1

All energies are in units cm^{-1}

the Jahn-Teller effect [73], and by considering phonon assisted absorptions [72,73].

The excitation spectrum was reported by Grebe and Schulz [22]. Here several crystal field levels can be identified and a calculation of the crystal field parameters using the B Δ method gave the result:

$$B = 500\text{cm}^{-1} \quad C = 2850\text{cm}^{-1} \quad \Delta = 5100\text{cm}^{-1}$$

The difference between the ratio of C/B for ZnS:Cr (5.7) compared with the free ion ratio (4.1) has not been satisfactorily explained. In addition there is no crystal field level corresponding to the peak observed at 11000cm^{-1} , and agreement between experiment and theory in other places is unsatisfactory, see table 4.16. More recently [75] a new assignment of parameters was made by ignoring data in the region of 10000cm^{-1} , as it is sensitive to pretreatment and therefore unreliable. The parameters B and C remain almost constant whilst Δ is reduced by 1000cm^{-1} . Whereas the agreement between experiment and some of the triplets has been improved, there exists a discrepancy of more than 1000cm^{-1} between the observed ${}^5\text{E}$ level and theory, and the large ratio of C/B remains unexplained.

Ten "absorption" barycentres have been reported for the excitation spectrum of ZnS:Cr [22]. This structure must correspond to transitions from the ${}^5\text{T}_2$ ground state to triplet levels, since transitions to singlet levels are more strongly forbidden, and the absorption around 5800cm^{-1} corresponds to the ${}^5\text{T}_2 - {}^5\text{E}$ transition. Electric dipole transitions are allowed from the ground state to levels of symmetry $\text{T}_2 \times \text{T}_2 = \text{A}_1 + \text{E} + \text{T}_1 + \text{T}_2$. Assignment of the observed structure to crystal field triplet levels with these orbital symmetries was attempted using the $\epsilon\tau\Delta_p$ theory. Initially, a fit was made just between the lower energy levels and corresponding theoretical levels. I found that the structure observed at higher

energies (i.e. above 17000cm^{-1}) could only be described by assigning two crystal field levels to some of the observed barycentres. In this way fitting to all of the observed structure the values of parameters found to give the best agreement with data are:

$$\epsilon = 0.945 \qquad \tau = 0.900 \qquad \Delta_p = 4790\text{cm}^{-1}$$

The observed barycentres and corresponding theoretical levels are given in table 4.16. For each observed barycentre there corresponds a crystal field level when the $\epsilon\tau\Delta_p$ theory is used. Discrepancies between two corresponding energy levels is typically between 100cm^{-1} and 500cm^{-1} . Previous studies of ZnS:Cr [73] have shown that the Jahn-Teller effect strongly distorts the ground state. The combined effect of this distortion, together with spin orbit splitting, may account for the discrepancies in the present study.

Although optical absorption is involved, additional selection rules need to be considered when studying the intensities of the lines observed in the excitation spectrum. For this reason the intensity of the observed spectrum has not been discussed in detail.

In view of the complicated nature of the system, the accuracy of the spectrum analysis in terms of the $\epsilon\tau\Delta_p$ theory is as good as can be expected.

4.4.4 -ZnS:Mn(d⁵)-

McClure [76] reported the spectrum of ZnS:Mn shown in fig.4.17. Langer and Ibuki [77] looked in more detail at each of the absorption peaks. They reported five zpl's which were used by Euwema to calculate the crystal field parameters using the $BC\Delta$ model. A discussion of the widths of the absorption bands in terms of phonon

Fig.4.17
Absorption spectrum of ZnS:Mn(d⁵) compared with
energy levels calculated by the $\epsilon\tau\Delta_p$ theory

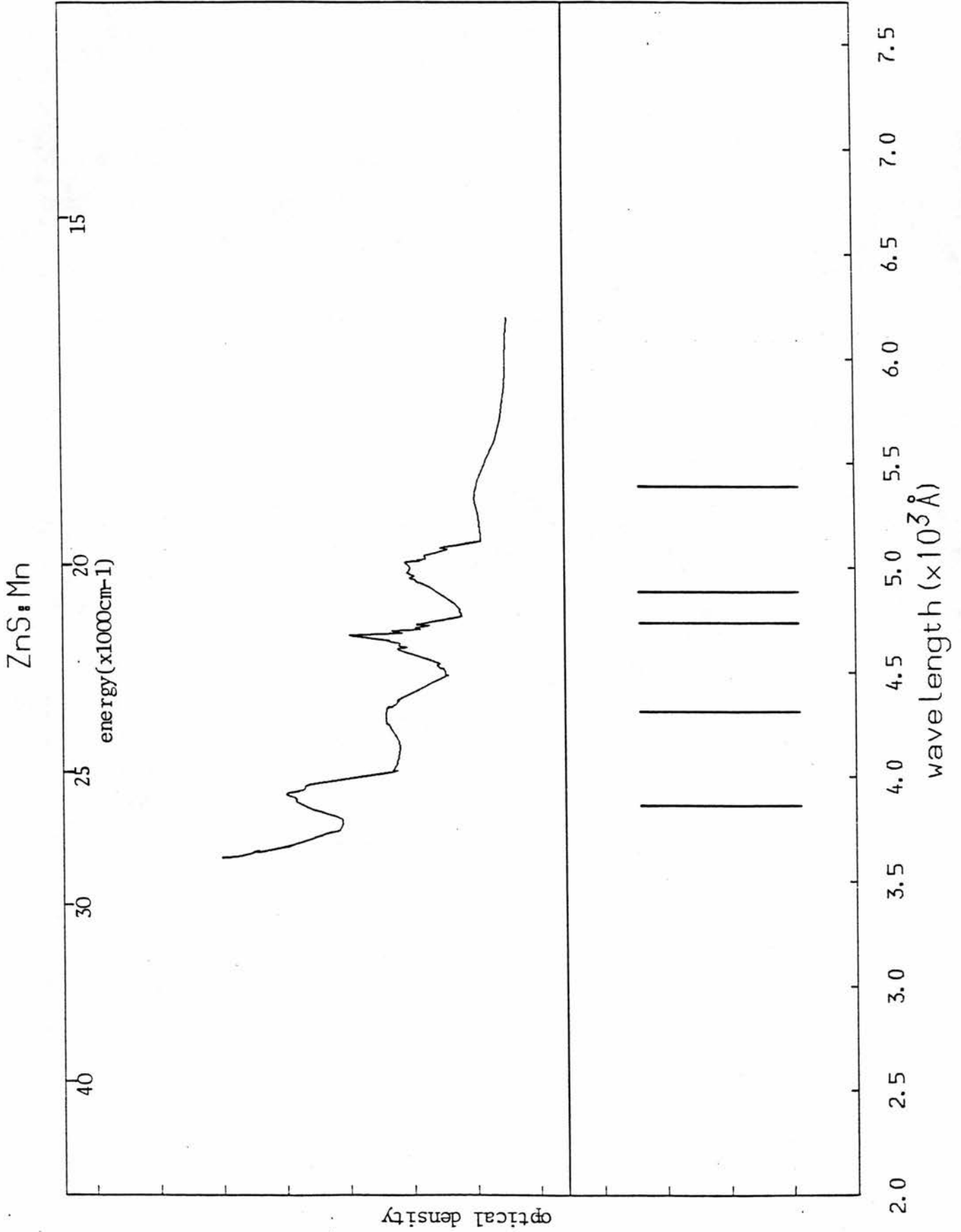


Table 4.17
 comparison of energy levels for ZnS:Mn

a) $\epsilon\tau\Delta_p$ theory	b) BCA theory
$\epsilon = 1.034$	$B = 459 \text{ cm}^{-1}$
$\tau = 0.910$	$C = 3425 \text{ cm}^{-1}$
$\Delta_p = 7140 \text{ cm}^{-1}$	$\Delta = 5290 \text{ cm}^{-1}$
18562 (4T_1)	18427 (4T_1)
20539 (4T_2)	20514 (4T_2)
21110 (4E)	21720 (${}^4E, {}^4A_1$)
23221 (4A_1)	23912 (4T_2)
25984 (4T_2)	24935 (4E)

All energies are in units cm^{-1}

coupling was presented. Mehra [78] agrees with the assignment of the first three levels but attempted to assign new levels to the higher peaks. He included a Racah-Trees correction and obtained a new set of parameters B , C , and Δ . His results suggest that two crystal field levels are responsible for the structure around 25700cm^{-1} . The analysis of the spectrum by Curie, Barthou and Canny [37] includes the effects of covalency by the use of normalising coefficients N_t and N_e . They find that they are unable to place the ${}^4T_1(P)$ level and the 4A_1 level appears to have been ignored.

In the $BC\Delta$ version of crystal field theory, the levels 4E and 4A_1 are degenerate. Koide and Pryce, working on Mn^{2+} ions in octahedral systems, showed that this degeneracy is removed when covalency effects are considered [34]. In octahedral systems the ligand orbitals have e symmetry representation. Thus, in the $\epsilon\tau\Delta_p$ formalism, ϵ will be less than τ , corresponding to a greater degree of mixing of the e orbitals with the ligand orbitals. In fig.4.18a the positions of the levels 4E and 4A_1 are plotted as functions of the parameter ϵ ($\tau=1.0$). The graph shows that the separation of the two levels is small in the case of octahedral systems, in agreement with the work of Koide and Pryce [34] and with Stout for MnF_2 [79].

Fig.4.18b shows the effect of covalency on the positions of the levels 4E and 4A_1 for tetrahedral systems. The levels are plotted against decreasing τ with ϵ held at 1.0. The separation of the levels is now quite appreciable for physically reasonable differences in ϵ and τ . As a consequence of this, when the $\epsilon\tau\Delta_p$ theory is applied to the ZnS:Mn spectrum, the 4E and 4A_1 levels might be expected to correspond to separate absorption peaks, rather than to a single absorption peak as would be expected with the $BC\Delta$ model or with Mn in octahedral coordination.

Fig.4.18a
Energy levels 4E and 4A_1 in octahedral environment

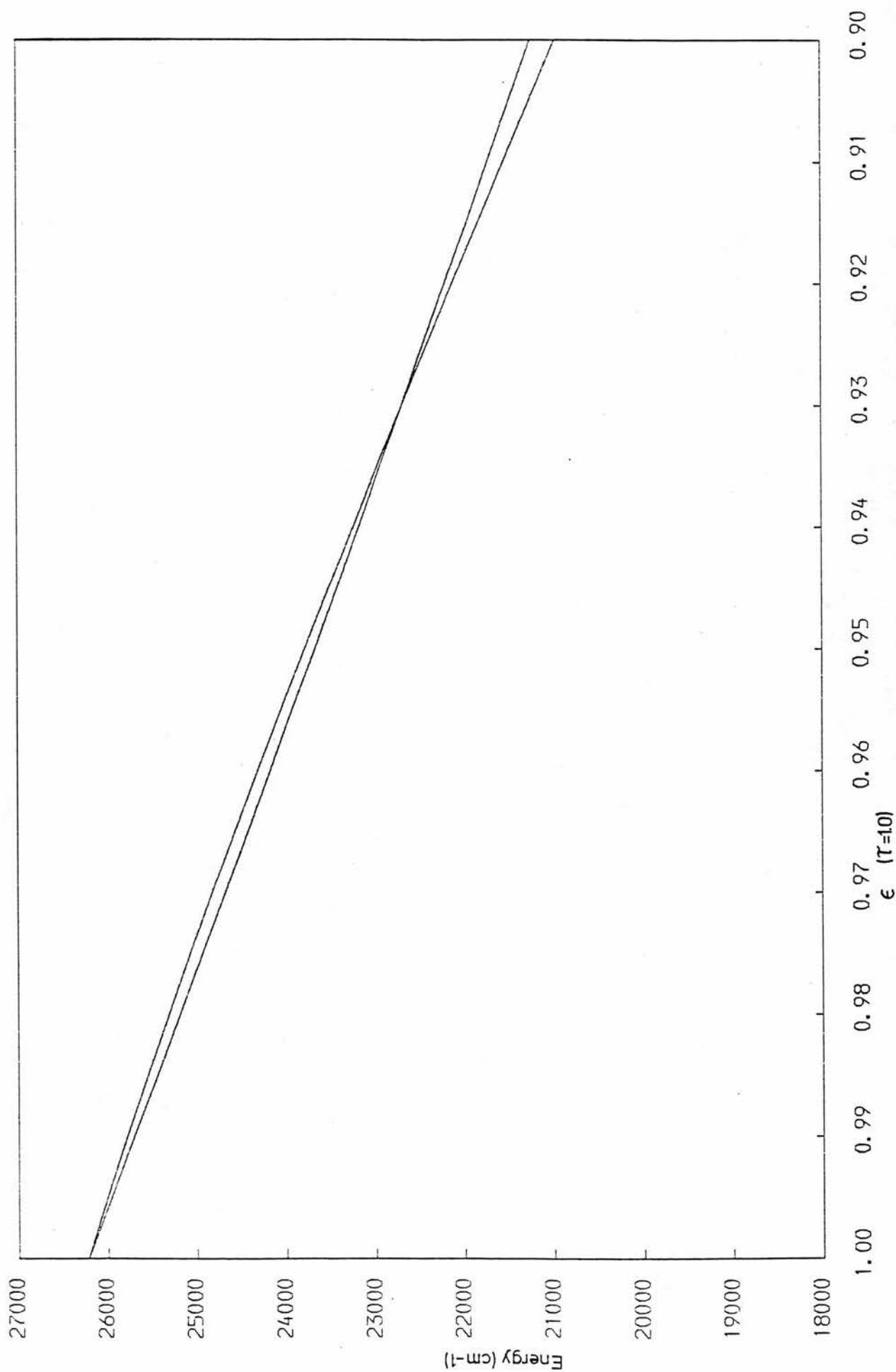
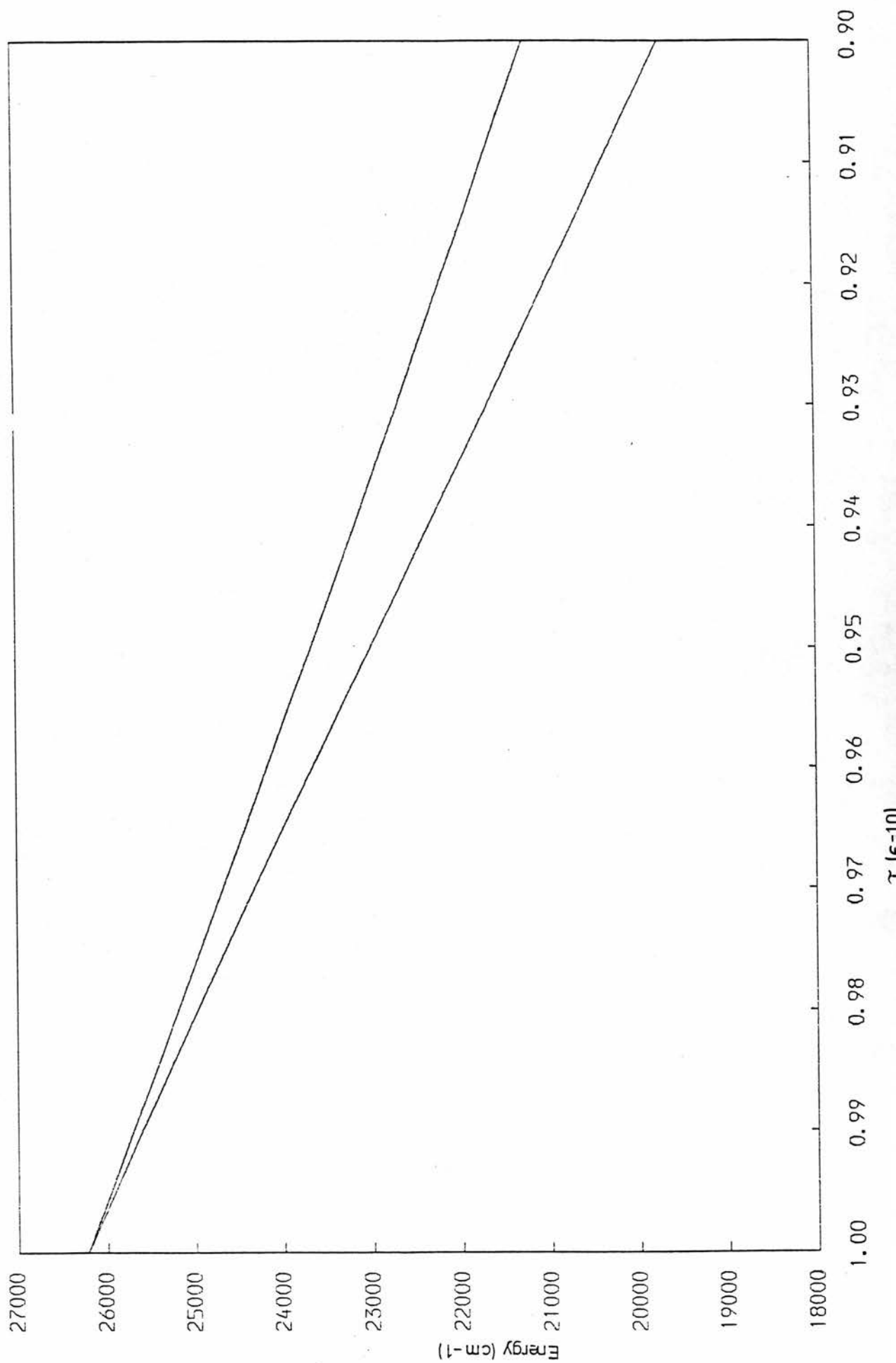


Fig.4.18b
Energy levels 4E and 4A_1 in tetrahedral environment



In the initial calculation of parameters using the $\epsilon\tau\Delta_p$ theory I considered just the three lower absorption peaks. Using the resulting set of parameters I was able to compare predicted crystal field levels with the observed structure at higher energies. The final assignment of parameters involved all five peaks and gives a better agreement with the data:

$$\epsilon = 1.034 \qquad \tau = 0.910 \qquad \Delta_p = 7140\text{cm}^{-1}$$

The crystal field energy levels derived from these parameters are listed in table 4.17 and plotted with the observed spectrum in fig.4.17. A comparison of the assignments of crystal field levels shows that for each, the level at 18850cm^{-1} is assigned to 4T_1 , 20100cm^{-1} to 4T_2 , and 21550cm^{-1} to 4E . However, the level at 23300cm^{-1} has been assigned to 2T_2 [77], 4T_1 [78], 4T_2 [37] and 4A_1 in the present work, whilst the level at 25700cm^{-1} has been assigned to 4T_2 [77], 4T_2 and 4E [78], 4E [37], and 4T_2 in the present work. Since zpl's have been reported [77] for the absorptions around 23300cm^{-1} and 25700cm^{-1} it should be possible to carry out Zeeman effect experiments to establish the crystal field assignment of these observed levels.

Recently Busse et al [33] have observed six sharp lines within the broad absorption band around 23300cm^{-1} . These data are something of a surprise because the $\epsilon\tau\Delta_p$ theory predicts no doublet levels nearby which may otherwise have gained oscillator strength by mixing with the quartet level and so explain the additional structure.

The assignment of parameters using the $\epsilon\tau\Delta_p$ theory requires some further discussion. There exists a precise interrelation between ϵ , τ and Δ_p and it is necessary to use these three related parameters accurate to three significant figures if crystal field levels close to the observed levels are to be obtained when the energy matrices are

evaluated. The absolute accuracy of each parameter is around 4% (see sec.5.3). Although the assignment of $\epsilon=1.034$ looks at first sight physically unreasonable, a range of values for ϵ less than unity exist within the limits of accuracy of ϵ .

4.4.5 -ZnS:Fe(d⁶)-

The only spin allowed transition from the Fe(d⁶) ground state ⁵E is to the level ⁵T₂. This transition was observed around 3500cm⁻¹ in absorption by Slack, Ham and Chrenko [80] who made a detailed study of the fine structure. Their analysis included spin orbit and Jahn-Teller splitting. Marfunin, Platonov and Fedorov [81] reported the weaker transitions to the spin forbidden triplet levels found between 10000cm⁻¹ and 25000cm⁻¹. The BCΔ theory was used to assign crystal field levels to the observed structure. Skowronski and Liro [82] also reported the spin forbidden transitions but with more of the fine structure detail observable. They calculated the parameters:

$$B = 670\text{cm}^{-1} \quad C = 2870\text{cm}^{-1} \quad \Delta = 3500\text{cm}^{-1}$$

and included spin orbit interaction with $\zeta=-335\text{cm}^{-1}$. Their absorption spectrum is shown in fig.4.19.

The values of parameters chosen in the $\epsilon\tau\Delta_p$ analysis were:

$$\epsilon = 0.915 \quad \tau = 0.913 \quad \Delta_p = 3310\text{cm}^{-1}$$

Since ϵ and τ are almost equal, then the two electron contributions to Δ_p cancel out, so that it is just equivalent to Δ in the BCΔ theory. Further, the free ion Racah parameters are reduced by the same amount in each matrix element, because $\tau^4 = \epsilon\tau^3 = \epsilon^2\tau^2 = \epsilon^4$. Thus, the $\epsilon\tau\Delta_p$ theory is just equivalent to the BCΔ theory where C/B is held at its free ion value. This choice of parameters corresponds to

Fig.4.19
Absorption spectrum of $\text{ZnS:Fe}(d^6)$ compared with
energy levels calculated by the $\epsilon\tau\Delta_p$ theory

ZnS:Fe

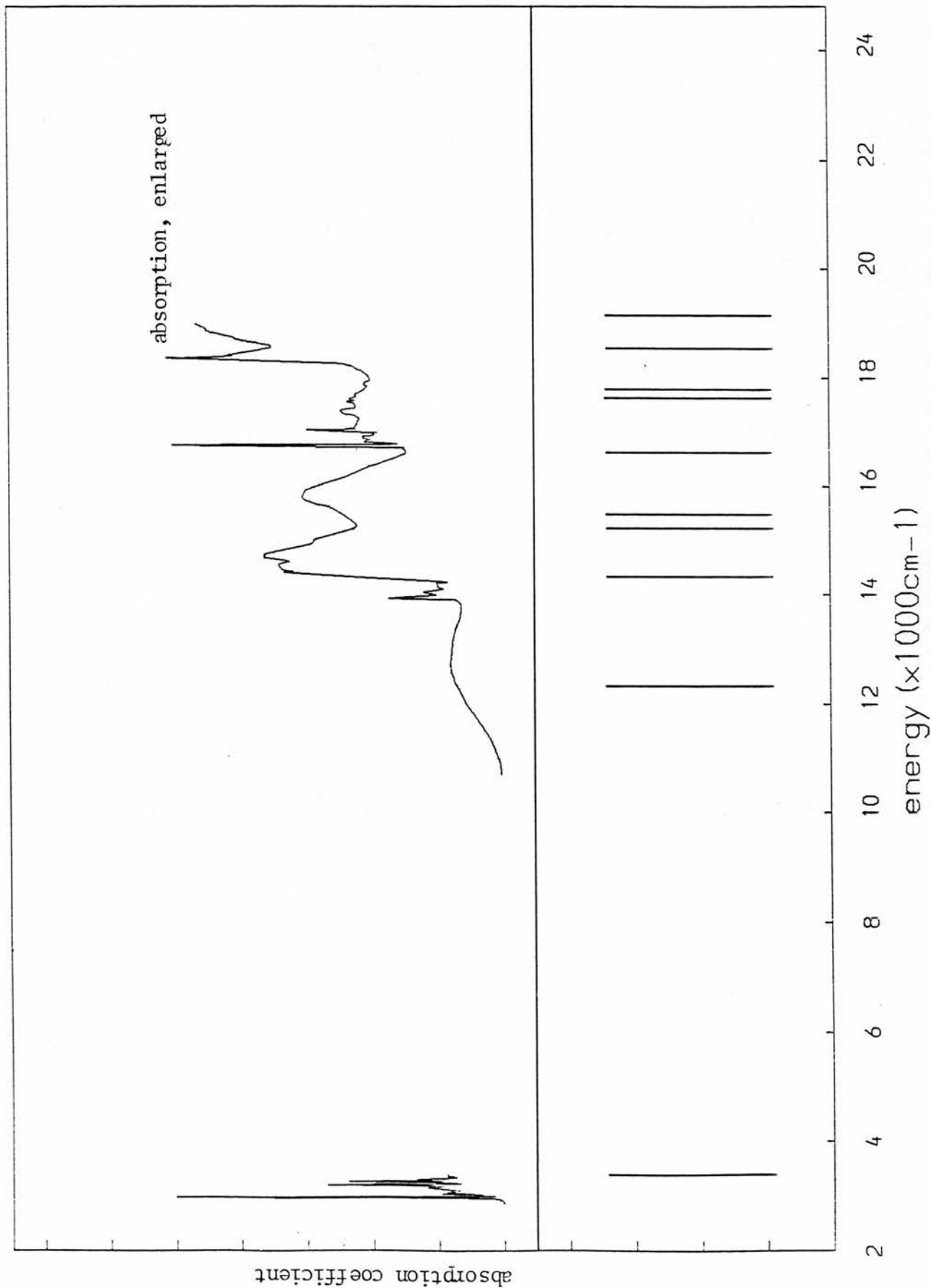


Table 4.18

Comparison of energy levels calculated for ZnS:Fe

a) $\epsilon\tau\Delta_p$ theory		b) BCD theory	
$\epsilon = 0.915$		$B = 670 \text{ cm}^{-1}$	
$\tau = 0.913$		$C = 2870 \text{ cm}^{-1}$	
$\Delta_p = 3310 \text{ cm}^{-1}$		$\Delta = 3500 \text{ cm}^{-1}$	
3371	5T_2	3500	5T_2
12314	3T_1	12455	3T_1
14307	3E	14562	3E
15230	3T_1	15539	3T_1
15450	3T_2	15718	3T_2
16633	3A_2	16867	3A_2
17633	3A_1	17510	3A_1
17765	3T_1	18168	3T_1
18509	3T_2	18897	3T_2
19123	3E	19043	3E

All energies are measured in units cm^{-1}

$$B = 725\text{cm}^{-1} \quad C = 2680\text{cm}^{-1} \quad \Delta = 3310\text{cm}^{-1}$$

using the $BC\Delta$ theory. The position and assignment of levels is almost identical to that of Skowronski and Liro, and is given in table 4.18.

4.4.6 ZnS:Co(d^7) and ZnS:Ni(d^8)-

The spectrum of ZnS:Co(d^7) was discussed in section 4.2.1, whilst the spectrum of ZnS:Ni(d^8) was discussed in section 4.3.2. For completeness, the results for these two systems have also been included in the summary presented in table 4.13.

4.4.7 -Summary-

In this section the optical absorption spectra of impurities from Ti(d^2) to Ni(d^8) in the wide gap semiconductor ZnS have been studied in terms of the $\epsilon\tau\Delta_p$ theory and the results compared with the $BC\Delta$ theory. For the spectrum of Ti(d^2), very little data is available and two possible parameter assignments have been proposed. The absorption spectrum of ZnS:V can be explained in terms of V(d^3), but it is believed that V(d^2) is also present in the sample studied which accounts for details in the luminescence and excitation spectra. The complicated nature of the Cr(d^4) and Fe(d^6) spectra means that errors may arise in the assignment of crystal field levels to specific absorptions. A new assignment of levels is proposed for the spectrum of Mn(d^5) and it is noted that the $\epsilon\tau\Delta_p$ theory lifts the degeneracy of the levels 4E and 4A_2 . The separation of these levels is much larger for tetrahedral crystals than for octahedral crystals. The

parameters obtained from each of the calculations are physically reasonable but the higher degree of error involved in some of the analyses means that trends in the parameters may be obscured.

4.5 -Summary-

In this chapter, the $\epsilon\tau\Delta_p$ theory has been used to describe successfully the spectra of a wide range of transition metal impurities in II-VI semiconductors. The interpretation of the results is consistent with the model of Ludwig and Woodbury for a substitutional transition metal impurity [50]. The method of application of the theory has been explained and illustrated by the example of ZnS:Co(d^7). Similarities between each of the Ni(d^8) spectra, and each of the Co(d^7) spectra, helped in the assignment of crystal field transitions to specific absorption details. The agreement between theory and experiment is very good for Ni(d^8) and Co(d^7), but not quite so good for some of the spectra of the other impurities in ZnS. The parameters ϵ and τ obtained have values between 0.75 and 1.0 corresponding to a small delocalisation of the d-electrons from the impurity ion site.

New assignments, particularly for low spin states using the $\epsilon\tau\Delta_p$ theory, have resolved some of the problems previously encountered using the BCA theory. Examples are the high energy peaks around 20000cm^{-1} in ZnS:Co and ZnSe:Co, and the coincidence of absorption and luminescence for the ${}^3T_2 - {}^3T_1(F)$ transition in ZnSe:Ni. Other new assignments, such as the 4A_2 level at 23300cm^{-1} in ZnS:Mn may lead to further experiments being carried out so as to test the theory.

Spin orbit coupling was dealt with only approximately in some of the spectra and ignored altogether in others. Calculations with ZnSe:Ni showed that the inclusion of spin orbit coupling did not significantly affect the values of ϵ , τ and Δ_p . Jahn-Teller coupling and the effects of fields of low symmetry were likewise ignored in the calculations as their inclusion would have unnecessarily complicated the analysis.

In conclusion, the work in this chapter has shown that the $\epsilon\tau\Delta_p$ theory as a method of describing absorption data is preferable to the $BC\Delta$ method. The $\epsilon\tau\Delta_p$ theory predicts low spin crystal field energy levels which are in better agreement with experimental data. In addition the physical interpretation of the adjustable parameters found from the theory is more meaningful. The method of application of the theory is quite similar to the $BC\Delta$ method and so the experimentalist should have little difficulty in adjusting to the new method of analysis.

CHAPTER FIVE

ERRORS IN THE CRYSTAL FIELD THEORY

5 ERRORS IN THE CRYSTAL FIELD THEORY

5.1 -Introduction-

In the previous chapter, the $\epsilon\tau\Delta_p$ theory was used to describe the absorption spectra of a number of transition metal impurities in II-VI hosts. Before trends in these parameters can be discussed, a consideration of the errors associated with the calculated parameters is necessary. In this way random fluctuations and genuine trends can be separated and identified.

The discussion of errors falls naturally into two distinct sections. In the first section I consider the validity of the assumptions that

$$\begin{aligned}\langle R_t R_t | H_e | R_e R_e \rangle &= \epsilon^2 \tau^2 \langle R_0 R_0 | H_e | R_0 R_0 \rangle \\ \langle R_t R_e | H_e | R_t R_e \rangle &= \epsilon^2 \tau^2 \langle R_0 R_0 | H_e | R_0 R_0 \rangle \\ \langle R_t R_t | H_e | R_t R_e \rangle &= \epsilon \tau^3 \langle R_0 R_0 | H_e | R_0 R_0 \rangle\end{aligned}$$

given that

$$\begin{aligned}\langle R_t R_t | H_e | R_t R_t \rangle &= \tau^4 \langle R_0 R_0 | H_e | R_0 R_0 \rangle \\ \langle R_e R_e | H_e | R_e R_e \rangle &= \epsilon^4 \langle R_0 R_0 | H_e | R_0 R_0 \rangle.\end{aligned}\tag{5.1}$$

To simplify these equations, as elsewhere in this chapter, the argument of the functions has been omitted, and H_e is the d-d electrostatic interaction Hamiltonian, as defined in chapter three. In the second section errors in the application of the theory are illustrated by looking, as an example, at the analysis of the spectrum of ZnSe:Co.

The relative errors, arising as a consequence of each of these sources of error, have been calculated for the parameters ϵ , τ and

Δ_p , and are presented in this chapter. The total error associated with each parameter is taken to be the square root of the sum of the square of the relative errors:

$$\text{Total error} = [(\delta a/a)^2 + (\delta b/b)^2]^{1/2} \quad 5.2$$

where $\delta a/a$ is the relative error due to the assumptions in the theory, and $\delta b/b$ is the relative error in the application of the theory.

In the next chapter, where trends in the parameters are discussed, the variation of ϵ , τ and Δ_p as a function of the different systems is shown graphically. Each parameter is plotted with an associated error bar which is taken to be \pm (total error) as calculated in this chapter. The inclusion of the error bars when plotting the parameters means that real trends can be identified. If the fluctuation of a parameter for a series of similar systems is smaller than the error bar width, then such a fluctuation may be due to errors in the theory, rather than a consequence of physical changes in the system. However, if the variation of parameters is larger than the error bars, one can be more certain that this variation is correlated to specific differences between the systems. The errors associated with the theory mean that this method of investigation is "blind" to small variations in the parameters.

5.2 -Errors in the construction of the theory-

The errors introduced as a consequence of the assumptions included within the $\epsilon\tau\Delta_p$ crystal field theory (see eq.5.1) can be quantified in terms of a relative error, typically:

$$\frac{|\langle R_t R_t | H_e | R_e R_e \rangle - \epsilon^2 \tau^2 \langle R_0 R_0 | H_e | R_0 R_0 \rangle|}{\langle R_t R_t | H_e | R_e R_e \rangle} \quad 5.3$$

and so on.

To construct and then calculate the integrals in the above expression, one-electron radial wavefunctions for the e and t_2 orbitals must be found. In the absence of any reliable radial function calculations, I had to select an approximate method of calculating the radial functions from the range of approaches available. In the past, a variety of theoretical studies [2,3,13,16] and analytical "modification" methods [34,36] for estimating the radial functions for a transition metal impurity in a semiconductor have been attempted, and it would be beyond the scope of this thesis to develop and apply a completely new method.

An attempt has been made to calculate the relative error in the construction of the theory using two different approaches to calculate the radial integrals. In the first, modified free ion radial wavefunctions were used. In the second, the radial functions used were obtained from first principles theory.

5.2.1 -modified free ion wavefunction-

A simple analytical form for radial wavefunctions in a spherically symmetric environment was proposed by Slater:

$$R(r) = [(2\alpha)^7/6!]^{1/2} r^2 e^{-\alpha r} \quad 5.4$$

where the orbital exponent, α , is determined by the set of rules outlined in his original paper [83]. Hartree-Fock calculations by Watson [84] for $3d^n$ transition metal atoms have shown that these functions are too extended spatially. However, linear combinations of the analytical radial functions can give good agreement with Hartree-Fock calculations [85 and references therein].

When a transition metal substitutes for a cation in a tetrahedral crystal, there is a modification of the one-electron d-wavefunctions. The radial function is affected for example by a decrease in magnitude of the d-wavefunction at the impurity core region, caused by mixing with the ligands, and a spatial extension of the d-orbitals, caused in part by ligand mixing and by partial screening of the impurity core by the host electrons. Some combination of these effects is believed to account for the change from the free-ion d-orbitals to those in the crystal. The modifications are different for e and t_2 orbitals. It is assumed that on the impurity the angular function is unchanged from that in the free ion, i.e. it may still be described in terms of a linear combination of second order spherical harmonics.

The decrease in magnitude in the impurity core region of the wavefunction can be accounted for by introducing into the Slater function the multiplicative constant θ_t , if the function is to describe a t_2 orbital, or θ_e if it is an e orbital. The value of θ_e (less than unity) is larger than θ_t because the degree of delocalisation of the e orbital is less for an impurity in tetrahedral symmetry. The coefficient θ_e corresponds with $\text{Cos}\theta$ in the formalism of Koide and Pryce [34] where θ_t is set at unity.

The extension of the radial function can be included by modifying the orbital exponent α to $\alpha\alpha_e$ or $\alpha\alpha_t$. The greater delocalisation of the t_2 orbitals suggests that they should be more extended than the e orbitals, from which it follows that $\alpha_t < \alpha_e$. Biernacki and Schulz [36] also introduced adjustable parameters into the orbital exponent to describe the extension of the radial function for an impurity ion in a crystal. In their notation $\alpha_e = y$ (< 1.0) and $\alpha_t = xy$ where $x > 1.0$. Contrary to the model proposed in this thesis,

they suggest that the greater delocalisation of the t_2 orbitals corresponds to a lesser extension of that radial function. This may have been introduced for mathematical convenience. Making these modifications, the impurity ion 3d one-electron radial wavefunctions become linear combinations of:

$$R_t(r) = \theta_t [(2\alpha_t)^7/6!]^{1/2} r^2 e^{-\alpha_t r}$$

$$R_e(r) = \theta_e [(2\alpha_e)^7/6!]^{1/2} r^2 e^{-\alpha_e r} \quad 5.5$$

For clarity in the error analysis, just these single functions will be used to represent the impurity ion radial function.

A general form for the electrostatic radial integral is:

$$F^k(1,2,3,4) = \langle R_1 R_2 | H_e | R_3 R_4 \rangle$$

$$= \iint R_1(r_1) R_2(r_2) H_e R_3(r_1) R_4(r_2) r_1^2 r_2^2 dr_1 dr_2. \quad 5.6$$

For electrostatic interactions within the d-shell of a transition metal ion in a T_d crystal, each of the four radial functions contained in the integral may be an e radial function or a t_2 radial function. An analytical expression for this integral may be found by using the modified Slater functions of eq.5.5:

$$F^k(1,2,3,4) = \theta_1 \theta_2 \theta_3 \theta_4 (\alpha_1 \alpha_2 \alpha_3 \alpha_4)^{7/2} \alpha (2^7/6)^2$$

$$\cdot \left[\frac{(6+k)! (5-k)!}{(\alpha_1 + \alpha_3)^{7+k} (\alpha_2 + \alpha_4)^{6-k}} \right.$$

$$+ \sum_{n=0}^{5-k} \frac{(5-k)! (6+k+n)!}{n! (\alpha_1 + \alpha_3)^{6-k-n} (\alpha_1 + \alpha_2 + \alpha_3 + \alpha_4)^{7+k+n}}$$

$$\left. - \sum_{m=0}^{6+k} \frac{(6+k)! (5-k+m)!}{m! (\alpha_1 + \alpha_3)^{7+k-m} (\alpha_1 + \alpha_2 + \alpha_3 + \alpha_4)^{6-k+m}} \right] \quad 5.7$$

where I have made use of the standard integral:

$$\int_a^b x^n e^{-ux} dx = \sum_{i=0}^n \frac{n!}{i! u^{n+1-i}} (a^i e^{-ua} - b^i e^{-ub}) \quad 5.8$$

The two modifications of the radial wavefunction can be treated separately. To begin with, I considered the effects of a decrease in magnitude of the function at the impurity site and ignored the extension modification. In this case, the definitions of ϵ and τ in eq.5.1 can be compared with

$$\begin{aligned} \iint R_t(r_1)R_t(r_2) H_e R_t(r_1)R_t(r_2)r_1^2r_2^2dr_1dr_2 \\ = \theta_t^4 \iint R_0(r_1)R_0(r_2) H_e R_0(r_1)R_0(r_2)r_1^2r_2^2dr_1dr_2 \\ \\ \iint R_e(r_1)R_e(r_2) H_e R_e(r_1)R_e(r_2)r_1^2r_2^2dr_1dr_2 \\ = \theta_e^4 \iint R_0(r_1)R_0(r_2) H_e R_0(r_1)R_0(r_2)r_1^2r_2^2dr_1dr_2 \end{aligned} \quad 5.9$$

From which it can be seen that

$$\tau = \theta_t \quad \epsilon = \theta_e \quad 5.10$$

Applying these definitions of θ_t and θ_e to the other integrals gives:

$$\begin{aligned} \iint R_t(r_1)R_t(r_2) H_e R_e(r_1)R_e(r_2)r_1^2r_2^2dr_1dr_2 \\ = \epsilon^2\tau^2 \iint R_0(r_1)R_0(r_2) H_e R_0(r_1)R_0(r_2)r_1^2r_2^2dr_1dr_2 \\ \\ \iint R_t(r_1)R_t(r_2) H_e R_e(r_1)R_e(r_2)r_1^2r_2^2dr_1dr_2 \\ = \epsilon^2\tau^2 \iint R_0(r_1)R_0(r_2) H_e R_0(r_1)R_0(r_2)r_1^2r_2^2dr_1dr_2 \\ \\ \iint R_t(r_1)R_t(r_2) H_e R_t(r_1)R_e(r_2)r_1^2r_2^2dr_1dr_2 \\ = \epsilon\tau^3 \iint R_0(r_1)R_0(r_2) H_e R_0(r_1)R_0(r_2)r_1^2r_2^2dr_1dr_2 \end{aligned} \quad 5.11$$

The equations 5.11 agree with those equations assumed to be correct in the $\epsilon\tau\Delta_p$ crystal field theory. Thus the theory is exact for the magnitude modification of the radial wavefunction at the impurity site.

Now the extension modification of the radial functions is considered, and temporarily no magnitude modification is assumed.

Again, comparing the definitions of eq.5.1 with the corresponding integrals in terms of Slater functions,

$$\begin{aligned} \iint R_t(r_1)R_t(r_2) H_e R_t(r_1)R_t(r_2)r_1^2r_2^2dr_1dr_2 \\ = \alpha_t \iint R_0(r_1)R_0(r_2) H_e R_0(r_1)R_0(r_2)r_1^2r_2^2dr_1dr_2 \\ \iint R_e(r_1)R_e(r_2) H_e R_e(r_1)R_e(r_2)r_1^2r_2^2dr_1dr_2 \\ = \alpha_e \iint R_0(r_1)R_0(r_2) H_e R_0(r_1)R_0(r_2)r_1^2r_2^2dr_1dr_2 \end{aligned} \quad 5.12$$

then the $\epsilon\tau\Delta_p$ theory would define

$$\tau = (\alpha_t)^{1/4} \quad \epsilon = (\alpha_e)^{1/4} \quad 5.13$$

The relative error, between the radial integrals evaluated using the definitions of eq.5.13 and evaluated using the modified Slater radial functions in eq.5.7, has been calculated numerically for a range of values of ϵ and τ for different radial integrals and can be found in table 5.1. These results show that the assumptions of the $\epsilon\tau\Delta_p$ theory are valid provided ϵ and τ are equal, but small errors occur when they differ.

In the last chapter, it was reported that ϵ and τ differ by up to 20% for the systems studied. In this section, it is suggested that this difference in ϵ and τ is made up from differences in θ_e and θ_t , and from differences in α_e and α_t . It has been seen that if the difference in extensions of the radial functions is negligible, then there is no error in the theory. However, if all of the difference between ϵ and τ is a consequence of the difference in extensions of the orbitals, errors of up to 8% in some matrix elements in the $\epsilon\tau\Delta_p$ theory occur, in the extreme case of a difference in ϵ and τ of 20% (see table 5.1).

Table 5.1

Relative error in the radial integrals constructed from the modified Slater radial functions.

$$1) \frac{\langle R_e R_e | H_e | R_t R_t \rangle - \epsilon^2 \tau^2 \langle R_0 R_0 | H_e | R_0 R_0 \rangle}{\langle R_e R_e | H_e | R_t R_t \rangle}$$

Ratio of extensions α_t/α_e | Relative error

1.0	0.000
0.95	0.004
0.9	0.018
0.85	0.042
0.8	0.078

$$2) \frac{\langle R_e R_t | H_e | R_t R_t \rangle - \epsilon \tau^3 \langle R_0 R_0 | H_e | R_0 R_0 \rangle}{\langle R_e R_t | H_e | R_t R_t \rangle}$$

Ratio of extensions α_t/α_e | Relative error

1.0	0.000
0.95	0.003
0.9	0.012
0.85	0.028
0.8	0.053

$$3) \frac{\langle R_e R_t | H_e | R_e R_t \rangle - \epsilon^2 \tau^2 \langle R_0 R_0 | H_e | R_0 R_0 \rangle}{\langle R_e R_t | H_e | R_e R_t \rangle}$$

Ratio of extensions α_t/α_e | Relative error

1.0	0.000
0.95	0.003
0.9	0.014
0.85	0.034
0.8	0.062

5.2.2 -first principles wavefunction-

In the previous section I imposed modifications on a free ion radial wavefunction, which were assumed to take account of the changes in the function when the ion is put into a II-VI tetrahedral semiconductor. This estimate of the radial functions which presupposes a knowledge of the nature of the modification is not entirely satisfactory. An alternative is to use radial functions found from first principles calculations.

Calculations using the $X\alpha$ scattered wave method seemed a promising approach. This method has been discussed briefly in chapter two. Unfortunately, a series of computational difficulties meant that these calculations had to be abandoned. A computer package program was obtained from the CPC library [86] with the intention of using the cluster $(\text{CoSe}_4\text{Zn}_{12})^{27-}$ to simulate ZnSe:Co, following Fazzio and Leite [17] who have performed cluster calculations for transition metal impurities in GaAs. The program was large, occupying some 488Kbytes of computer core memory. This might be compared with the maximum storage capacity of a typical laboratory microcomputer of 32Kbytes. An inadequate technical report accompanying the program meant that it could not be modified to run successfully on a Digital Vax-11/780 computer.

The quasiband crystal field (QBCF) Green's function method has been used by Lindefelt and Zunger to calculate radial functions for transition metal impurities in GaP. The results of these unpublished calculations have been used in this thesis to estimate errors in the construction of the $\epsilon\tau\Delta_p$ theory. The particular system studied was GaP:Mn.

It may be recalled from sec.2.5.2 that the impurity wavefunction

found from the QBCF method can be written as

$$\psi_i^{\alpha\lambda} = \sum_{l=0}^{l_{\max}} G_{il}^{\alpha}(|\underline{r}|) K_l^{\alpha\lambda}(\hat{\underline{r}}) \quad 5.14$$

where $G_{il}^{\alpha}(|\underline{r}|)$ are the radial functions of the α th irreducible representation. The localised d-orbital radial functions of interest here correspond to the $l=2$ component of $G_{il}^{\alpha}(|\underline{r}|)$ for $\alpha=e$ and t_2 . The choice of i is such that the radial functions belong to gap states.

To test the assumptions in the construction of the $\epsilon\tau\Delta_p$ theory the $G_{il}^{\alpha}(|\underline{r}|)$ were used to evaluate electrostatic radial integrals of the form

$$\begin{aligned} & \langle R_1(r_1)R_2(r_2) | H_e | R_3(r_1)R_4(r_2) \rangle \\ &= |e| \int_{r_1=0}^{\infty} \int_{r_2=0}^{\infty} R_1(r_1)R_2(r_2) \frac{r_2^k}{r_1^{k+1}} R_3(r_1)R_4(r_2) r_1^2 r_2^2 dr_1 dr_2 \quad 5.15 \end{aligned}$$

where each of the $R(r)$ may be an e radial function or a t_2 radial function. The radial functions $G_{il}^{\alpha}(|\underline{r}|)$ were provided in numerical form and may be trusted up to around 6 \AA . The radial integral, eq.5.15, was evaluated numerically in the form:

$$\begin{aligned} & |e| \int_{r_1=0}^6 \left[\int_{r_2=0}^{r_1} R_1(r_1)R_2(r_2) \frac{r_2^k}{r_1^{k+1}} R_3(r_1)R_4(r_2) r_1^2 r_2^2 dr_1 dr_2 \right. \\ & \quad \left. + \int_{r_2=r_1}^6 R_1(r_1)R_2(r_2) \frac{r_1^k}{r_2^{k+1}} R_3(r_1)R_4(r_2) r_1^2 r_2^2 dr_1 dr_2 \right] \quad 5.16 \end{aligned}$$

using the NAG subroutine D01GAF for one-dimensional integrals recursively [87].

Initially the calculation was performed for $k=2$ and $k=4$ for the radial integrals:

$$\begin{aligned} & \langle R_t(r_1)R_t(r_2) | H_e | R_t(r_1)R_t(r_2) \rangle \\ & \langle R_e(r_1)R_e(r_2) | H_e | R_e(r_1)R_e(r_2) \rangle. \quad 5.17 \end{aligned}$$

Using the results of these calculations, estimates for the other three possible radial integrals were determined by using the approximations of the $\epsilon\tau\Delta_p$ theory, eq.5.1. Finally the remaining three radial integrals

$$\begin{aligned} &\langle R_e(r_1)R_t(r_2)|H_e|R_e(r_1)R_t(r_2)\rangle \\ &\langle R_e(r_1)R_e(r_2)|H_e|R_t(r_1)R_t(r_2)\rangle \\ &\langle R_e(r_1)R_t(r_2)|H_e|R_t(r_1)R_t(r_2)\rangle \end{aligned} \quad 5.18$$

were evaluated numerically using the QBCF radial functions in eq.5.16. The radial integrals calculated from the QBCF radial functions, together with the values predicted by the $\epsilon\tau\Delta_p$ theory are given in table 5.2. The relative error between the calculated radial integrals and the estimated integrals is less than 0.5% in each case. This result means that the approximations made in the construction of the $\epsilon\tau\Delta_p$ theory are very accurate if the radial functions calculated from the QBCF method are reliable.

In eq.5.16 the upper limit of integration has been reduced from ∞ to 6 Å. This approximation is valid if it can be shown that the major contribution to the radial integral is between 0 Å and 6 Å. Numerical tests show that radial integrals evaluated using different upper limits of integration in eq.5.16 (between 2 Å and 6 Å) are identical to within three significant figures. This demonstrates that the main component of the radial integral is contained at small values of r . In addition to justifying the approximation made in eq.5.16, the result gives support to the approximation made in chapter three that only one-centre integrals on the impurity site are significant.

Using the impurity radial integrals presented in table 5.2, together with free ion values for the electrostatic radial integrals obtained from atomic data, it is possible to calculate ϵ and τ for GaP:Mn:

Table 5.2

Radial integrals calculated by the QBCF method.

1) k=2

radial integral	QBCF calculated value	$\epsilon\tau\Delta_p$ theory predicted value
$\langle R_e R_e H_e R_e R_e \rangle$	757.4	
$\langle R_t R_t H_e R_t R_t \rangle$	255.5	
$\langle R_e R_t H_e R_e R_t \rangle$	439.1	439.9
$\langle R_e R_e H_e R_t R_t \rangle$	435.4	439.9
$\langle R_e R_t H_e R_t R_t \rangle$	333.3	335.3

2) k=4

radial integral	QBCF calculated value	$\epsilon\tau\Delta_p$ theory predicted value
$\langle R_e R_e H_e R_e R_e \rangle$	52.41	
$\langle R_t R_t H_e R_t R_t \rangle$	17.85	
$\langle R_e R_t H_e R_e R_t \rangle$	30.52	30.59
$\langle R_e R_e H_e R_t R_t \rangle$	30.42	30.59
$\langle R_e R_t H_e R_t R_t \rangle$	23.28	23.34

all energies are measured in cm^{-1} .

In this table,

For k=2

$$\langle R_1 R_2 | H_e | R_3 R_4 \rangle = (1/49) |e| \iint R_1(r_1) R_2(r_2) H_e R_3(r_1) R_4(r_2) r_1^2 r_2^2 dr_1 dr_2$$

For k=4

$$\langle R_1 R_2 | H_e | R_3 R_4 \rangle = (1/441) |e| \iint R_1(r_1) R_2(r_2) H_e R_3(r_1) R_4(r_2) r_1^2 r_2^2 dr_1 dr_2$$

$$\epsilon = 0.85 \text{ to } 0.86 \quad \tau = 0.65 \text{ to } 0.56$$

This result for GaP:Mn may be compared with typical values for ϵ and τ found from the application of the $\epsilon\tau\Delta_p$ theory to transition metal impurities in III-V compounds which are presented in chapter seven. The theoretical value of ϵ is very similar to the experimentally determined values, whilst the theoretical value of τ is about 10% lower than the empirical values. A comparison between the theoretical and empirical estimates of ϵ and τ for the same system would be desirable, but this is not yet possible.

If the radial functions calculated by the QBCF method are used to calculate the electrostatic radial integrals then the relative error between these integrals and those estimated by the $\epsilon\tau\Delta_p$ theory is less than 0.5%. The values of ϵ and τ obtained from the QBCF calculations for GaP:Mn are similar to those values determined empirically for other III-V systems. These results suggest that the first principles wavefunctions are a good estimate of the true impurity wavefunctions, and that the $\epsilon\tau\Delta_p$ theory provides an accurate description of the excited states of a d^n configuration.

5.2.3 -relative error in the construction of the theory.

Table 5.1 lists the error in matrix elements constructed from the Slater functions as the ratio of α_t/α_e decreases from unity. The error in the matrix elements leads to errors in ϵ , τ and Δ_p . I decided to use the results of sec.5.2.1 rather than sec.5.2.2 because the errors were larger. The errors are estimated here by considering the example of ZnSe:Co. Each matrix element can be rewritten with a multiplicative "error constant":

$$\begin{aligned} \langle R_t R_t | H_e | R_t R_e \rangle &= \epsilon \tau^3 \langle R_0 R_0 | H_e | R_0 R_0 \rangle \text{ettt} \\ \langle R_t R_t | H_e | R_e R_e \rangle &= \epsilon^2 \tau^2 \langle R_0 R_0 | H_e | R_0 R_0 \rangle \text{eett} \end{aligned} \quad 5.19$$

and so on, where eett and ettt are the error constants. For those matrix elements which are exact, the error constant is unity. Thus

$$\text{tttt} = \text{eeee} = 1.0 \quad 5.20$$

For those matrix elements which are inaccurate then the error constant differs from unity by the relative error of that matrix element.

Thus:

$$\langle R_t R_t | H_e | R_e R_e \rangle = \epsilon^2 \tau^2 \langle R_0 R_0 | H_e | R_0 R_0 \rangle \text{eett} \quad 5.21$$

where $\text{eett} = 1.0 \pm (\text{relative error})$

and the relative error in $\langle R_t R_t | H_e | R_e R_e \rangle$ has been defined in eq.5.3.

A simple numerical procedure can be used to estimate the errors in the crystal field parameters. First, each of the error constants are set to unity and the crystal field parameters are calculated according to the flow chart in fig.4.2. In the next stage the effect of the error constants is introduced into the procedure. For ZnSe:Co the appropriate error constants are:

$$\begin{aligned} \text{tttt} &= 1.0 \\ \text{eeee} &= 1.0 \\ \text{eett} &= 1.0 \pm 0.078 \\ \text{ettt} &= 1.0 \pm 0.056 \end{aligned} \quad 5.22$$

Thus four different parameter assignments may be made by using different combinations of values for the error constants. The resulting sets of parameters are given in table 5.3. Finally, the sample standard deviation for each of the parameters was evaluated, and recorded in table 5.3. Twice the sample standard deviation is taken to be the error in ϵ , τ and Δ_p as a consequence of inaccuracies in the matrix elements. This corresponds to a 95% confidence interval for each parameter. These errors can be expressed in terms of the

Table 5.3

Relative error in the construction of the theory.

eeee	tttt	ettt	eett	ϵ	τ	Δ_p
1.0	1.0	1.0	1.0	0.813	0.945	5380cm ⁻¹
1.0	1.0	1.056	1.078	0.789	0.959	6080cm ⁻¹
1.0	1.0	0.944	1.078	0.779	0.986	6479cm ⁻¹
1.0	1.0	1.056	0.922	0.814	0.960	5495cm ⁻¹

results

standard deviation in ϵ = 0.017, mean = 0.963, relative error = 0.036

standard deviation in τ = 0.018, mean = 0.799, relative error = 0.046

standard deviation in Δ_p = 514cm⁻¹, mean = 5860cm⁻¹, relative error = 0.178

relative error:

$$\text{Relative error} = 2 \times \text{Standard deviation}/\text{Mean value}$$

thus

$$\text{relative error in } \epsilon = 0.036$$

$$\text{relative error in } \tau = 0.046$$

$$\text{relative error in } \Delta_p = 0.178 \quad 5.23$$

The error in ϵ and τ is approximately the same, but the error in Δ_p is larger. This might be expected since Δ_p is a disposable parameter containing both one electron and two electron contributions.

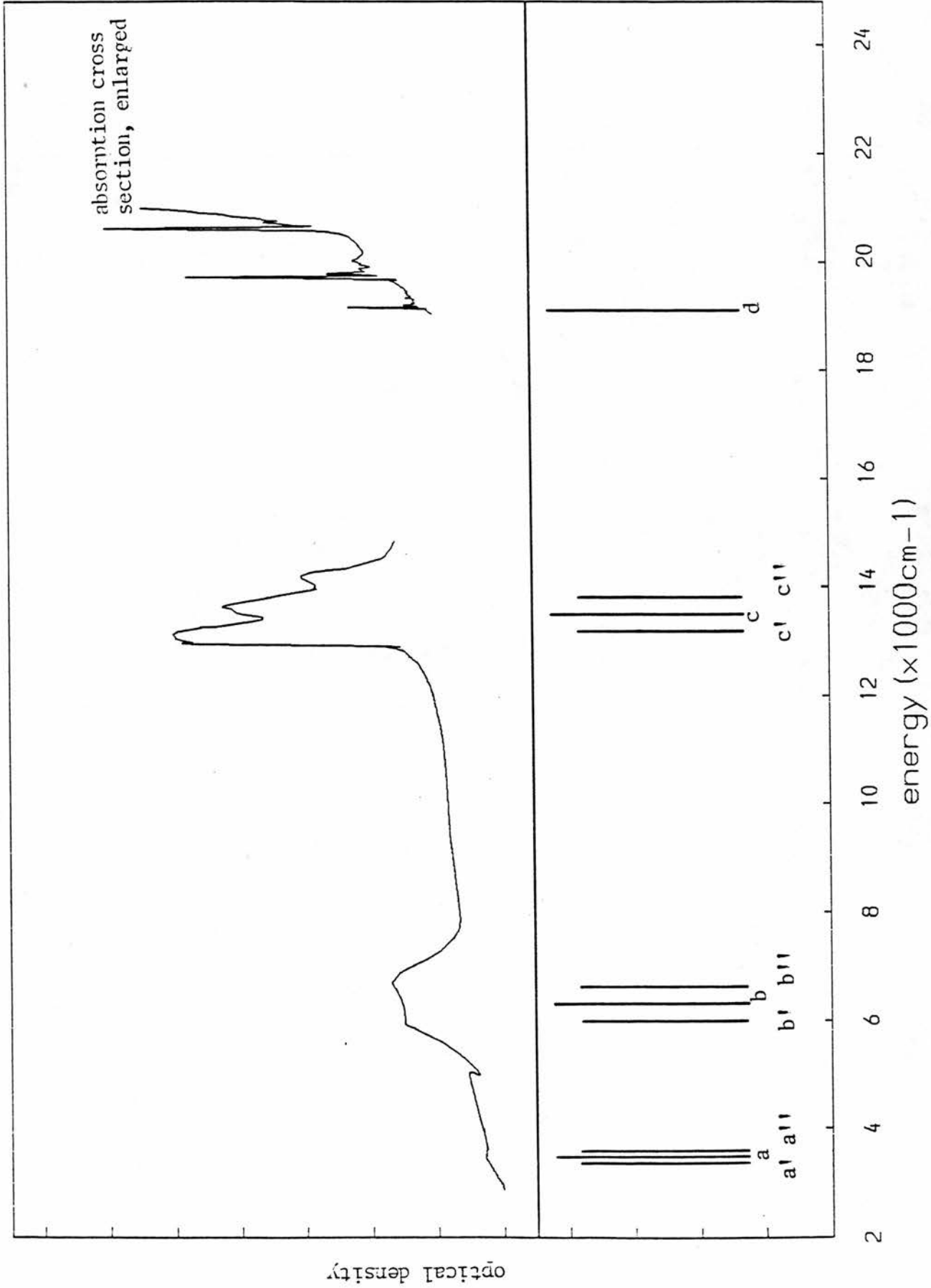
5.3 -Errors in the Analysis-

The $\epsilon\tau\Delta_p$ theory predicts a set of crystal field energy levels which have no bandwidth. The experimentally observed spectrum with which the theory is compared contains absorption bands which are broad and have fine structure. The theoretical levels correspond with the barycentres of these bands. In the application of the $\epsilon\tau\Delta_p$ theory, these barycentres are judged by eye. In the version of the theory used, Jahn-Teller coupling and fields of low symmetry were ignored and spin-orbit coupling was only included approximately. Consequently, a precise assignment of the barycentres was not possible and so errors in the analysis were necessarily introduced.

An estimate of the error introduced by the barycentre assignment can be gained by considering in some detail the spectrum of ZnSe:Co(d^7). The analysis of this spectrum involved a fit to four crystal field levels and so is typical of many of the spectra investigated. Fig.5.1 shows the absorption spectrum of ZnSe:Co. The parameters tabulated in table 4.6 were derived with the points a,b,c,d

ZnSe:Co

Fig 5.1
Possible absorption barycentres for ZnSe:Co



chosen as the experimental barycentres. The width of the absorption peaks means that a finite range of values for the barycentre could reasonably have been chosen, and these have been marked on fig.5.1. As an example, the barycentre of absorption band b could lie anywhere between b' and b''.

Eight new sets of parameters ϵ , τ , and Δ_p were generated by choosing the ${}^4T_1(F)$ absorption band barycentre to be b' or b'' instead of b, and similarly for the other absorption bands. The error introduced by the barycentre assignment was then judged to correspond with twice the sample standard deviation of each parameter, which is approximately a 95% confidence interval. The sets of parameters generated and the sample standard deviations are presented in table 5.4.

The errors resulting from the analysis can be compared with one another and with the errors as a result of the assumptions in the $\epsilon\tau\Delta_p$ theory by considering the relative error:

$$\text{Relative Error} = 2 \times \text{Standard Deviation} / \text{Magnitude of Parameter}$$

where the magnitude of each parameter is that value quoted for ZnSe:Co in table 4.2.

$$\text{Relative Error for } \epsilon = 0.030$$

$$\text{Relative Error for } \tau = 0.028$$

$$\text{Relative Error for } \Delta_p = 0.202 \qquad 5.24$$

The relative errors in ϵ and τ are approximately equal and are small. However, the error in Δ_p is large and consequently trends in Δ_p will be obscured to a greater extent than those in ϵ and τ .

Table 5.4
Relative error in the analysis.

Absorption Barycentres

$a = 3500\text{cm}^{-1}$	$b = 6300\text{cm}^{-1}$	$c = 13500\text{cm}^{-1}$	$d = 19100\text{cm}^{-1}$
$a' = 3400\text{cm}^{-1}$	$b' = 6000\text{cm}^{-1}$	$c' = 13200\text{cm}^{-1}$	
$a'' = 3600\text{cm}^{-1}$	$b'' = 6600\text{cm}^{-1}$	$c'' = 13800\text{cm}^{-1}$	

set of barycentres | parameters found

				ϵ	τ	Δ_p
a	b	c	d	0.813	0.945	8780 cm^{-1}
a'	b'	c'	d	0.811	0.954	9150 cm^{-1}
a''	b'	c'	d	0.802	0.964	9970 cm^{-1}
a'	b''	c'	d	0.807	0.941	8900 cm^{-1}
a''	b''	c'	d	0.800	0.948	9440 cm^{-1}
a'	b'	c''	d	0.831	0.935	7640 cm^{-1}
a''	b'	c''	d	0.813	0.959	9350 cm^{-1}
a'	b''	c''	d	0.828	0.922	7400 cm^{-1}
a''	b''	c''	d	0.822	0.927	7880 cm^{-1}

results

standard deviation in $\epsilon = 0.0142$, $\epsilon = 0.945$, relative error= 0.030
 standard deviation in $\tau = 0.0109$, $\tau = 0.813$, relative error= 0.028
 standard deviation in $\Delta_p = 888\text{cm}^{-1}$, $\Delta_p = 8780\text{cm}^{-1}$, relative error= 0.202

5.4 -The error bars-

Table 5.5 summarises the calculations of the relative errors as a result of errors in the construction and application of the theory. These two errors must now be combined to give the "total error" for the $\epsilon\tau\Delta_p$ method. The total relative error is taken to be

$$\text{Total error} = [(\delta a/a)^2 + (\delta b/b)^2]^{1/2} \quad 5.25$$

where $\delta a/a$ is the relative error in each parameter due to errors in the construction of the theory, as calculated in sec.5.2, and $\delta b/b$ is the relative error in each parameter due to errors in the application of the theory, as calculated in sec.5.3. Both of these quantities, calculated for ZnSe:Co, are given in table 5.5. Using the equation given above, the total error for each parameter can be calculated:

$$\text{Total relative error for } \epsilon = 0.046$$

$$\text{Total relative error for } \tau = 0.054$$

$$\text{Total relative error for } \Delta_p = 0.27 \quad 5.26$$

Having calculated this total relative error, the error bars for each parameter are taken to be $\pm(\text{total error})$. Thus, for ZnSe:Co

$$\epsilon = 0.94(5) \pm 0.04$$

$$\tau = 0.81(3) \pm 0.04$$

$$\Delta_p = 5370 \pm 1000 \text{ cm}^{-1}. \quad 5.27$$

In principle, this procedure should now be repeated for each of the sixteen systems which were studied in the previous chapter. However, this estimation of errors should be sufficient for the spectra of Ni(d^8) and Co(d^7), since an analysis of these spectra typically involves a fit to four crystal field levels, which was the case for ZnSe:Co.

Additional errors may need to be considered for some of the spectra of $3d^n$ ions in ZnS. In particular, the lack of data for

Table 5.5
Total relative error in the parameters.

relative error in the construction of the theory, $\delta a/a$

$$\epsilon = 0.036$$

$$\tau = 0.046$$

$$\Delta_p = 0.178$$

relative error in the application of the theory, $\delta b/b$

$$\epsilon = 0.030$$

$$\tau = 0.028$$

$$\Delta_p = 0.202$$

Total relative error, $[(\delta a/a)^2 + (\delta b/b)^2]^{1/2}$

$$\epsilon = 0.046$$

$$\tau = 0.054$$

$$\Delta_p = 0.27$$

similar systems with which to make a comparison, together with the complicated nature of some spectra means that the assignment of crystal field levels to the wrong absorption details is possible. An example is in the analysis of $\text{ZnS:Ti}(d^2)$ where two possible sets of parameters are quoted (see sec.4.4.1). No attempt has been made to quantify such errors, but their possible existence means that a thorough investigation of the trends in parameters of different impurities in the same host is difficult.

In the next chapter the total error quoted here for the parameters of ZnSe:Co is used as the error bar width associated with the calculated parameters of the spectra analysed in the last chapter. Because the error associated with each parameter is known, an investigation of the trends in parameters as a function of the host crystal is now possible.

5.5 -Summary-

In this chapter, the errors associated with the $\epsilon\tau\Delta_p$ method have been considered. Such an investigation was necessary to separate random fluctuations in the calculated crystal field parameters from genuine trends.

In section 5.2, errors in the construction of the theory were considered. In particular, the validity of the assumptions contained in eq.5.1 were tested by calculating the relative error (eq.5.3) for such matrix elements. This involved the construction of radial integrals. No reliable radial function calculations are known, but two attempts were made to calculate the integrals using approximate radial functions. In the first, modified free atom radial Slater

functions were used. Calculations showed that errors of up to 8% in some matrix elements could occur. Numerical calculations then showed that this led at worst to an error of around 4% in ϵ and τ , and an error of almost 18% in Δ_p . In the second method, radial functions calculated by the QBCF method are used to calculate the electrostatic radial integrals. The relative error between these integrals and those estimated by the $\epsilon\tau\Delta_p$ theory is less than 0.5%. The values of ϵ and τ obtained from the QBCF calculations for GaP:Mn are similar to those values determined empirically for other III-V systems. These results suggest that the first principles wavefunctions are a good estimate of the true impurity wavefunctions, and that the $\epsilon\tau\Delta_p$ theory provides an accurate description of the excited states of a d^n configuration.

In section 5.3, errors in the application of the theory were considered. The $\epsilon\tau\Delta_p$ theory predicts a set of crystal field energy levels with no bandwidth. The experimentally observed absorption bands with which these levels were compared are broad and have fine structure. The theoretical levels must be compared with the absorption barycentres, which were only found approximately. Errors are introduced because there is a small range of energies in each absorption band which could be chosen as the barycentre. The relative error as a result of this uncertainty in barycentre assignment was calculated numerically and found to be around 3% for ϵ and τ , and around 20% for Δ_p .

Having calculated the relative error in each parameter as a result of the two sources of error, the errors were combined to give a total error for each parameter. For ϵ and τ this total error is around 5%, whilst it is around 27% for Δ_p . The total error is to be used as the error bar width associated with each parameter in the

discussion of trends.

This account of errors carried out in detail for ZnSe:Co is believed to be sufficient for the spectra of Co(d^7) and Ni(d^8) studied in the last chapter. Additional errors should be considered for some of the spectra of the $3d^n$ ions in ZnS. The lack of similar data with which to make comparisons, and the complicated nature of some spectra, mean that errors in the assignment of crystal field levels to absorption data are possible. No attempt has been made to quantify such errors.

It is my hope that the $\epsilon\tau\Delta_p$ theory will replace the $BC\Delta$ theory as the method used by experimentalists to describe their absorption data. A four level fit to barycentres judged by eye is perhaps typical of the way in which the theory might be used by other workers. Thus the error analysis presented here, for the example of ZnSe:Co, should give a good estimate of the errors encountered in such an application.

In conclusion, the calculated error bar width of around 5% for ϵ and τ means that variations in these parameters caused by specific differences in the system must be greater than 5% if they are to be taken as trends. It is not possible to be sure whether smaller variations are real trends or random variations caused by errors in the $\epsilon\tau\Delta_p$ method.

CHAPTER SIX

TRENDS IN THE CRYSTAL FIELD PARAMETERS

6 TRENDS IN THE CRYSTAL FIELD PARAMETERS

6.1 -Introduction-

An investigation of trends, found in the parameters obtained from the application of the $\epsilon\tau\Delta_p$ theory in chapter 4, is presented in this chapter. The magnitude of the parameters ϵ and τ , from which the degree of delocalisation of the d-orbitals may be established, is of principal importance. But another objective here is to search for correlations between changes in the parameters (ϵ , τ and Δ_p) and some corresponding changes in the systems investigated. The interpretation of such correlations leads to a greater understanding of transition metal impurities in II-VI compounds. In addition, the explanation of deviations from expected trends, and of the non-correlation with complementary data, is instructive.

The work covered in this chapter is as follows. To begin, there are some general comments about the magnitude of the crystal field parameters. Next a correlation is found between the parameters ϵ and τ and the nearest neighbour covalent radius. Deviations from this trend are expected, because of the trigonal distortion in some of the host crystals studied, and these are discussed. Following this, there is an attempt to separate the one-electron and two-electron contributions to Δ_p for the $\text{Co}(d^7)$ systems and for the $\text{Ni}(d^8)$ systems.

When a trend is observed in the spectra of $\text{Co}(d^7)$ and the spectra of $\text{Ni}(d^8)$, it is reasonable to expect that such a trend should also be seen in the spectra of the other transition metal impurities

in II-VI compounds. This idea is used to explain the pinning of the absorption edge in $\text{Cd}_{1-x}\text{Mn}_x\text{Te}$ [88]. The pinning is discussed in terms of internal transitions within $\text{Mn}(d^5)$, which are estimated by a consideration of the $\text{ZnS:Mn}(d^5)$ spectrum, together with trends in ϵ , τ , and Δ_p which are seen in $\text{Co}(d^7)$ and $\text{Ni}(d^8)$ spectra, and therefore expected for $\text{Mn}(d^5)$ spectra.

Finally, a correlation between the crystal field covalency parameters ϵ and τ and the esr covalency parameter k is sought.

6.2 -General comments on the parameters-

The crystal field parameters obtained from the application of the $\epsilon\tau\Delta_p$ theory may be found in table 4.2 ($\text{Co}(d^7)$), table 4.12 ($\text{Ni}(d^8)$), and table 4.13 ($3d^n$ impurities in ZnS). The parameters ϵ and τ have been plotted as a function of the nearest neighbour Pauling tetrahedral covalent radius for the spectra of $\text{Co}(d^7)$ and $\text{Ni}(d^8)$, and as a function of n for the spectra of the $3d^n$ impurities in ZnS. These graphs are shown in fig.6.1.

An inspection of the tables and of the graphs shows that ϵ and τ both vary between 0.77 and 1.0 for the systems studied. In the construction of the $\epsilon\tau\Delta_p$ crystal field theory it was assumed that the d -orbitals of the transition metal impurity remain strongly localised when it is substitutional on a cation site in a tetrahedral crystal. Thus the theory is only valid provided ϵ and τ are close to unity. In the applications of the theory reported in this thesis, ϵ and τ are close to unity, and the predicted crystal field levels are in good agreement with experimental data.

Crystal field theory also suggests that for impurities in

crystals of T_d symmetry the t_2 -orbitals are allowed by symmetry to mix with the ligand orbitals, whilst mixing by the e-orbitals is forbidden. Thus the t_2 -orbitals delocalise to a greater extent giving the result that ϵ is greater than τ . This is found to be the case in most of the systems studied. Exceptions to this are found for the spectra of $\text{Co}(d^7)$ and $\text{Ni}(d^8)$ in ZnO , where the trigonal distortion allows the e-orbitals to mix with the ligand orbitals.

If it had been the case that the d-orbitals strongly delocalise and mix with the ligands then the parameters obtained in the application of the theory would not have been consistently physically reasonable, and the agreement with data should not have been so good. Thus the values of ϵ and τ obtained, which are close to unity, and where ϵ is greater than τ , give strong support to the crystal field model, where the d-orbitals are strongly localised for a transition metal impurity in a II-VI host.

The parameter Δ_p varies from around 3000cm^{-1} for ZnS:Ti to around 7000cm^{-1} for $\text{ZnS:Mn}(d^5)$. This difference of 4000cm^{-1} can be compared with a difference of 2000cm^{-1} in the values of Δ_p for the $\text{Co}(d^7)$ spectra (ignoring ZnO:Co) and less than 1000cm^{-1} for the $\text{Ni}(d^8)$ spectra. This shows that Δ_p is determined largely by the impurity, rather than by the host. A similar result was found for Δ in the application of the BCA theory [10].

6.3 -Covalent radius correlation-

In this section, the correlation between the anion covalent radius, and the parameters ϵ and τ , is established. A correlation with Δ_p has not been considered, because this parameter has contributions from several sources, and the correlation (if one exists) would not be particularly enlightening.

In fig.6.1 the parameters ϵ and τ are shown as a function of the anion Pauling tetrahedral covalent radius for the spectra of $\text{Co}(d^7)$ and $\text{Ni}(d^8)$. In each case straight lines can be drawn through the sets of points with their associated error bars. As the covalent radius of the nearest neighbours increases the parameters ϵ and τ are observed to decrease. This corresponds to a reduction of the electrostatic interaction within the impurity d-shell. The increase in the covalency effect is consistent with the increasing covalency of the host crystal, which is indicated by the larger covalent radius of the anion. A greater delocalisation of the ligand electrons accordingly increases the covalent radius.

The effect of the cation, Cd or Zn, on ϵ and τ is small. There is a large overlap of the error bars, associated with ϵ or τ , for those systems which differ only by the identity of their cation. Thus any changes in ϵ or τ brought about by the difference in cations Cd or Zn is too small to be "observed" by the present investigation.

The anion Pauling tetrahedral covalent radius for ZnO is 0.66 \AA , whilst the anion covalent radius in ZnTe is 1.32 \AA [89]. This is a difference of 0.7 \AA , and gives rise to a change in ϵ and τ of around 0.15. The parameters ϵ and τ found for the $3d^n$ impurities in ZnS vary by about the same amount for the range of systems investigated in chapter 4. For these systems the covalent radius of the anion, S, is

Fig.6.1

The covalency parameters ϵ and τ in tetrahedral crystals

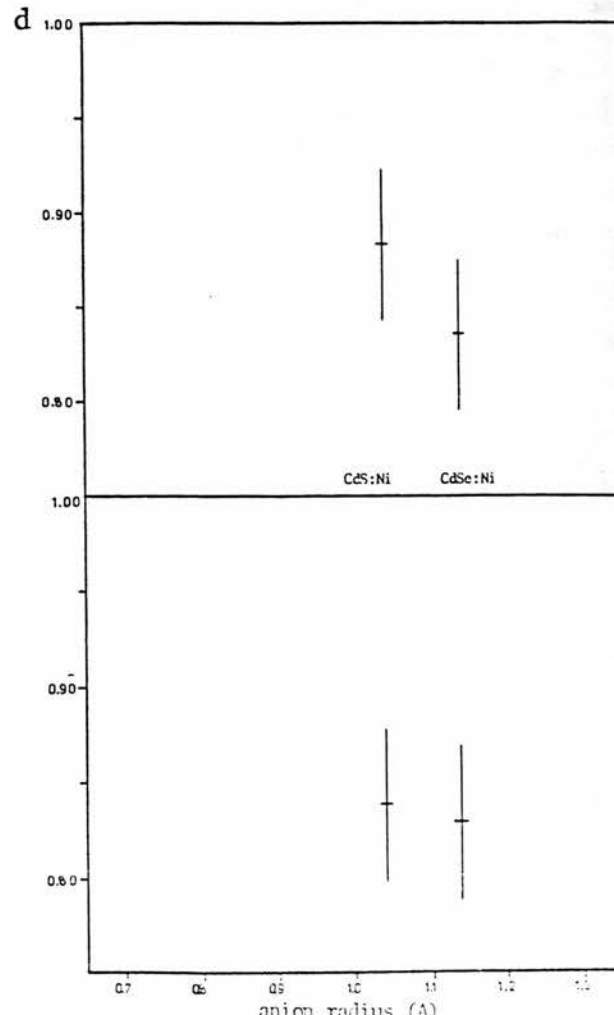
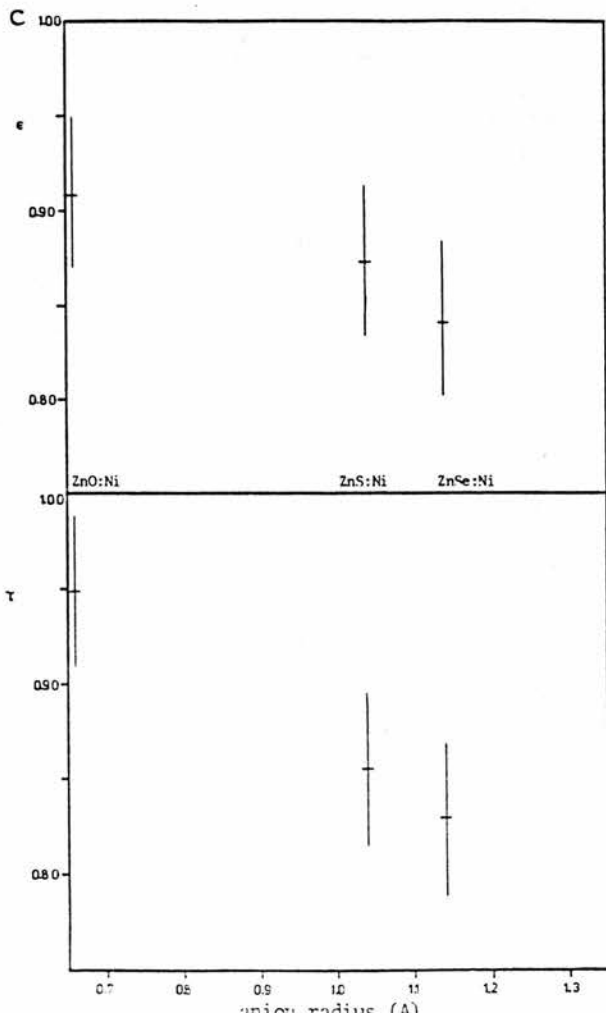
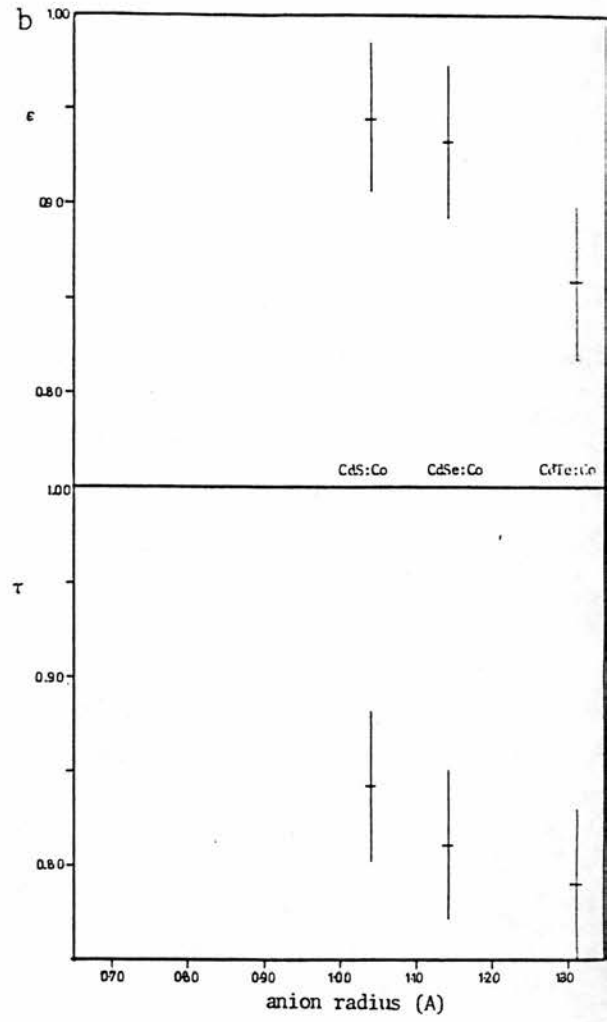
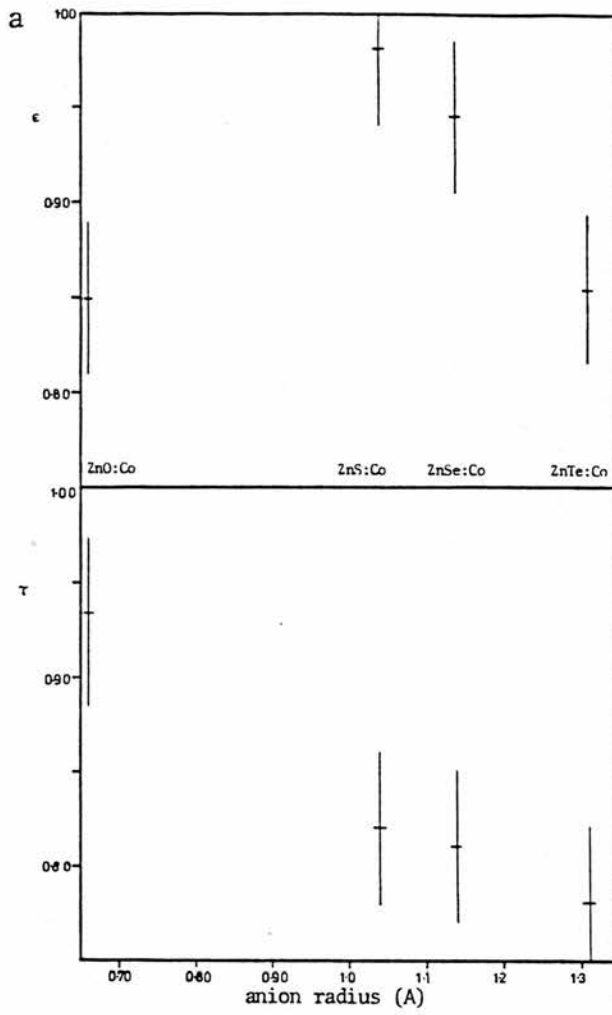
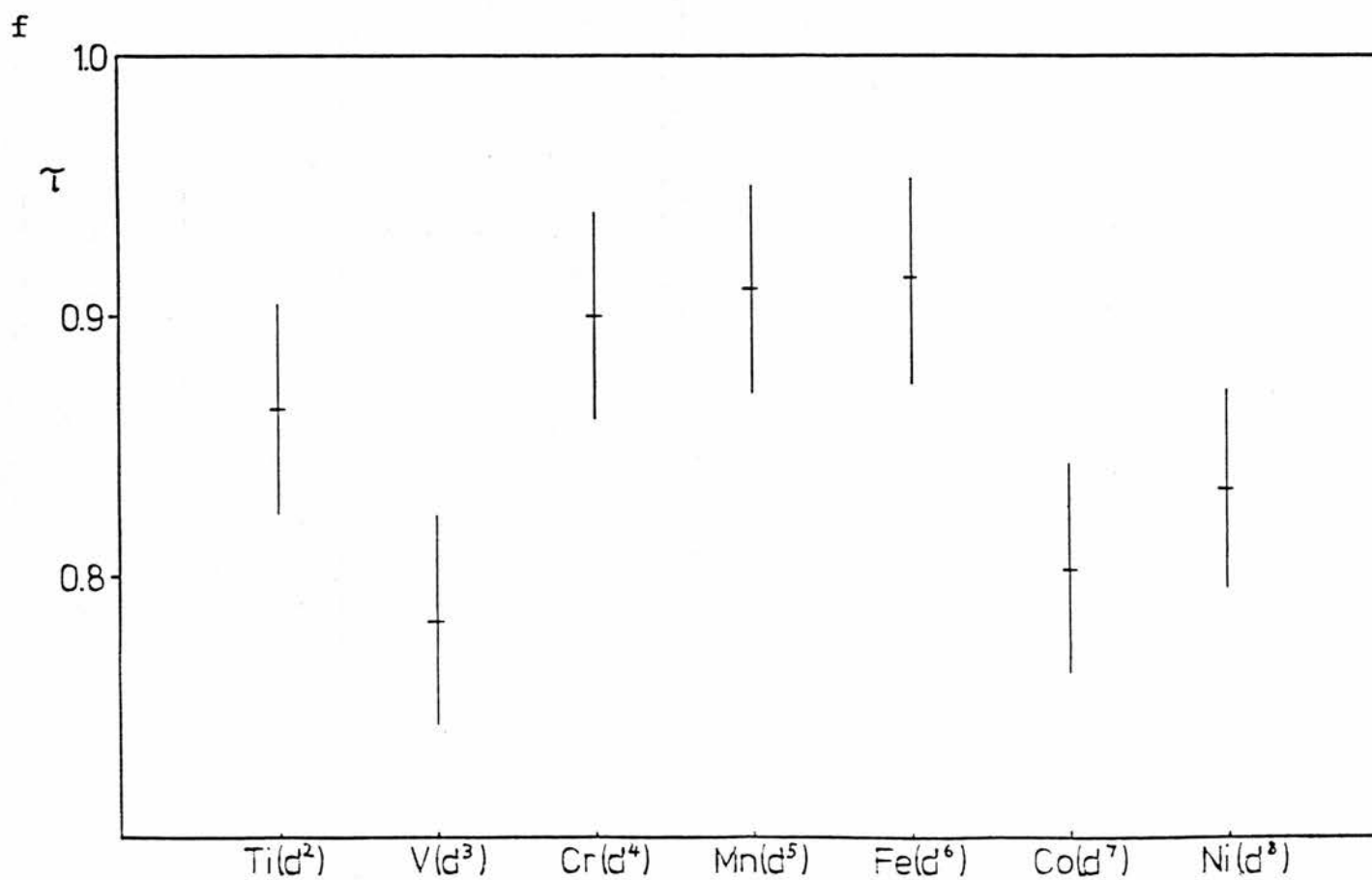
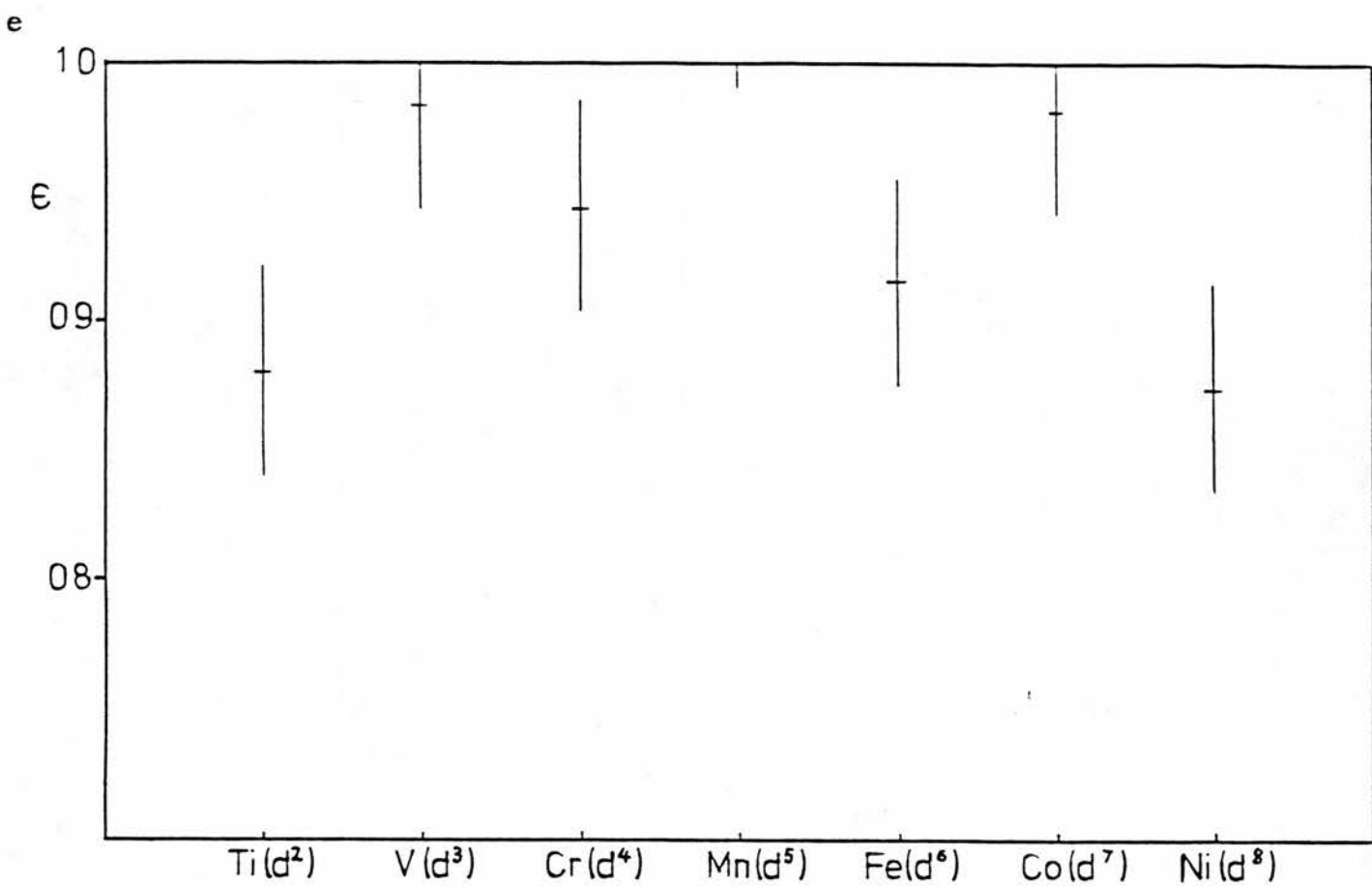


Fig.6.1
The covalency parameters ϵ and τ in tetrahedral crystals



fixed. But there is a variation of the covalent radius of the impurity ions (around 0.2 \AA) [90], although this is much smaller than the variation of the anion covalent radius from ZnO to ZnTe. A satisfactory interpretation of trends in the covalency parameters for the $3d^n$ impurities in ZnS has not been established.

A deviation from the linear variation of the parameter ϵ as a function of the anion covalent radius is found in the cases of $\text{Co}(d^7)$ and $\text{Ni}(d^8)$ in ZnO. It has previously been noted (section 4.2.2, section 4.3.1) that for these systems τ is greater than ϵ . This has been explained by the trigonal distortion in ZnO lowering the symmetry of the ligand t_2 -orbital to $a_1 + e$. Now mixing is allowed by symmetry between the ligand orbital and both the e - and t_2 -orbitals. For a cubic crystal the e -orbitals are forbidden by symmetry to mix with the ligand (t_2) orbitals leading to the usual result that ϵ is greater than τ (corresponding to a greater delocalisation of the t_2 -orbitals). Thus a trigonal distortion is expected to give rise to deviations from the linear trend between covalent radius and the covalency parameters ϵ and τ .

In addition to ZnO, small trigonal distortions are present in ZnS, CdS, and CdSe. The magnitude of this distortion, and so the extent to which it will cause deviations from the trend, can be quantified by comparing the two different bond lengths present in the pure trigonal crystals. These bond lengths are given in table 6.1 [91]. The table shows that the greatest difference in bond lengths is found in ZnO, and so a strong deviation from the trend in ϵ is expected. Some lesser departure from the trend should be expected for impurities in CdS, and an even smaller departure should exist in CdSe. The smallest departure from the trend in ϵ is expected in ZnS. Inspection of fig.6.1 shows that the degree of overlap of the error

Table 6.1
Bond lengths of crystals with trigonal distortion

III. COMPOUNDS RX

TABLE III,11. CRYSTALS WITH THE ZINCITE ARRANGEMENT

Crystal			Observed	Cor. ionic radii	Neutral
	a_0	c_0	R-X	R-X	R-X
NH ₄ F	4.39 A.	7.02 A.	2.63, 2.69 A.	2.64 A.	—
CuH	2.693	4.614	—	—	—
AgI	4.580	7.494	2.81, 2.80	3.18	2.81 A.
BeO	2.695	4.39	1.64, 1.65	1.59	1.72
MgTe	4.52	7.33	2.75, 2.76	2.65	2.72
MnS(pink)	3.976	6.432	2.41, 2.44	2.45	2.28
MnSe	4.12	6.72	2.52, 2.52	2.58	2.38
ZnO	3.2426	5.1948	1.95, 1.98	1.99	1.97
ZnS	3.811	6.234	2.33, 2.33	2.39	2.35
CdS	4.131	6.691	2.51, 2.53	2.61	2.52
CdSe	4.30	7.02	2.63, 2.64	2.74	2.62
AlN	3.104	4.965	1.86, 1.90	2.04	1.96
GaN	3.180	5.166	1.94, 1.94	2.16	1.96
InN	3.533	5.693	2.13, 2.16	2.34	2.14
TaN	3.05	4.94	1.85, 1.86	—	—
CbN ^a	3.017	5.580	—	—	—

^a If this hexagonal form of CbN really exists, it is the only known crystal with the ZnO arrangement having a value of c/a far from 1.63.

bars associated with the parameter ϵ for the spectra of ZnS:Co(d^7) and CdS:Co(d^7) is less than the corresponding overlap for either CdSe:Co/ZnSe:Co or CdTe:Co/ZnTe:Co. Clearly this could be just a statistical fluctuation, but it is tempting to suggest that it is a real deviation from the linear trend in ϵ , caused by the small trigonal distortion in CdS.

6.4 The crystal field parameter Δ_p

In the BC Δ theory, the physical interpretation of the parameter Δ is taken to be the separation in energy of the e- and t_2 -orbitals, when electrostatic interactions within the d-shell are ignored. Thus Δ is a one-electron parameter. In the $\epsilon\tau\Delta_p$ theory, the adjustable parameter corresponding to Δ is Δ_p . But Δ_p has both one-electron and two-electron contributions. In this section, the constituents of Δ_p are identified and separated.

Electrostatic interactions within the d-shell are described by terms involving the Racah parameters A, B, and C [4]. In the BC Δ theory, the terms involving the Racah parameter A appear identically on each diagonal matrix element, and so can be ignored in the calculation of excited states. Such terms can not be ignored in the $\epsilon\tau\Delta_p$ theory because they are no longer identical. However, since terms involving A only appear on diagonal matrix elements, they are included within Δ_p and constitute the two-electron contribution to this parameter. In the application of the theory this is an advantage, because only three adjustable parameters (ϵ, τ, Δ_p) rather than four ($\epsilon, \tau, \Delta, A$) are needed.

For those transition metals where the d-shell is more than half

filled, a hole formalism rather than electron formalism is used in the calculation of the multiplet structure. Thus the d^7 configuration becomes the d^{3h} (h=hole) configuration. This introduces additional electrostatic terms in the diagonal matrix elements, which have been included within Δ_p in the application of the theory. This additional contribution to Δ_p involves terms in A, B, and C. Those components involving B and C can be calculated, leaving an "adjusted" crystal field parameter Δ_p^0 . For those systems where the d-shell is less than half full, then Δ_p^0 is the same as Δ_p . Thus Δ_p^0 corresponds to the energy difference between the configurations $t^m e^l$ and $t^{m+1} e^{l-1}$ when terms involving B and C (i.e. the non-spherically symmetric electrostatic integrals) are ignored.

Similar to Δ in the BC Δ theory, Δ_p is an empirically determined parameter of the theory. It is constant for a particular system and so the difference in energy between the configurations $t^m e^l$ and $t^{m+1} e^{l-1}$ arising from terms in A should also be constant for all values of m and l. Unfortunately this is not the case, and so some error is introduced by making the approximation of including terms involving A within Δ_p . For Co(d^7), the contributions to the diagonal matrix elements associated with each $t^m e^l$ configuration arising from terms in A are:

$$\begin{aligned}
 t^3 & \dots\dots\dots 3A\tau^4 \\
 t^2 e & \dots\dots\dots A\tau^4 + 2A\epsilon^2 \tau^2 \\
 t e^2 & \dots\dots\dots 2A\epsilon^2 \tau^2 + A\epsilon^4
 \end{aligned}
 \tag{6.1}$$

where $3A\tau^4$ is the contribution to the diagonal matrix element between the two (hole) configurations t^3 , and so on. These terms, involving the Racah parameter A, appearing on the diagonal matrix elements, give a contribution to Δ_p^0 which is either:

$$t^2 e - t^3 \dots\dots\dots (A\tau^4 + 2A\epsilon^2 \tau^2) - 3A\tau^4$$

$$= 2A\tau^2(\epsilon^2 - \tau^2) \quad 6.2$$

or

$$\begin{aligned} 1/2(\tau\epsilon^2 - \tau^3) &\dots 1/2 ((2A\epsilon^2\tau^2 + A\epsilon^4) - 3A\tau^4) \\ &= 2A\tau^2(\epsilon^2 - \tau^2) \left(1 + \frac{(\epsilon^2 - \tau^2)}{4}\right) \end{aligned} \quad 6.3$$

Equations 6.2 and 6.3 represent, in analytical form, a two electron contribution to Δ_p^0 . The error introduced by overlooking the difference between eq.6.2 and eq.6.3 is estimated after the other two-electron contribution to Δ_p^0 has been established.

In the application of the $\epsilon\tau\Delta_p$ theory to the spectra of $\text{Co}(d^7)$ it is convenient to use a hole formalism instead of the electron formalism. This means that the d^3 energy matrices can be used in the calculation of excited states, where the sign of Δ_p is reversed for d^{3h} . This idea is also used in applications of the $BC\Delta$ theory. It has been shown by Sharma et al [92] that an additional contribution to the diagonal matrix elements, from electrostatic interactions within the d-shell, must be included in the d^{3h} or d^7 matrices. In terms of the parameters of the $\epsilon\tau\Delta_p$ theory the contribution is:

$$\begin{aligned} t^{6-m}e^{4-1} &= t^m e^1 + \tau^4(3-m)(5A - 10B + 5C) + \epsilon^2\tau^2(2m + 31 - 12) \\ &\quad \cdot (-2A + 2B - C) + \epsilon^4(2-1)(3A - 8B + 4C) \end{aligned} \quad 6.4$$

where $t^{6-m}e^{4-1}$ and $t^m e^1$ in this case are the diagonal matrix elements of the respective configurations. The terms involving B and C can be calculated so that the adjusted parameter Δ_p^0 is found:

$$\Delta_p^0 = \Delta_p + \tau^4(-10B + 5C) + \epsilon^2\tau^2(2B - C) - \epsilon^4(-8B + 4C) \quad 6.5$$

where Δ_p is the parameter found from the application of the theory to experimental data. The parameter Δ_p^0 contains two-electron contributions, involving A only, as well as the one-electron

Table 6.2
Parameters and results for graph of Δ_p^0 against $3(\tau^4 - \epsilon^4)$ for Co(d⁷).

System	ϵ	τ	Δ_p	Δ_p^0	$3(\tau^4 - \epsilon^4)$
ZnS:Co	0.981	0.823	5900cm ⁻¹	1500 ± 400cm ⁻¹	-1.4 ± 0.4
ZnSe:Co	0.945	0.813	5370cm ⁻¹	2000 ± 500cm ⁻¹	-1.1 ± 0.3
ZnTe:Co	0.854	0.770	4290cm ⁻¹	2500 ± 700cm ⁻¹	-0.54 ± 0.15
CdS:Co	0.947	0.842	5000cm ⁻¹	2100 ± 600cm ⁻¹	-0.9 ± 0.25
CdSe:Co	0.935	0.813	4700cm ⁻¹	1600 ± 400cm ⁻¹	-1.0 ± 0.3
CdTe:Co	0.859	0.780	4020cm ⁻¹	2400 ± 600cm ⁻¹	-0.52 ± 0.15

Results

Best straight line:

By method of least squares, gradient = 1000cm⁻¹

intercept = 3000cm⁻¹

contribution.

In table 6.2, the experimentally determined values Δ_p , together with the adjusted parameter Δ_p^0 , are given. The diagonal correction term introduced when changing from electron to hole formalism gives a contribution to Δ_p^0 :

$$5A\tau^4 - 2A\epsilon^2\tau^2 - 3A\epsilon^4 \quad 6.6$$

Thus the total two-electron contribution to Δ_p^0 is either

$$A\{2\tau^2(\epsilon^2 - \tau^2) + 5\tau^4 - 2\epsilon^2\tau^2 - 3A\epsilon^4\} \quad 6.7$$

or

$$A\{2\tau^2(\epsilon^2 - \tau^2)\left(1 + \frac{(\epsilon^2 - \tau^2)}{4}\right) + 5\tau^4 - 2\epsilon^2\tau^2 - 3\epsilon^4\} \quad 6.8$$

An error is introduced by assuming that eq.6.7 and eq.6.8 are the same, i.e. by assuming a constant difference in energy between configurations $t^m e^1$ and $t^{m+1} e^{1-1}$ arising from terms in A. Using values of ϵ and τ found for ZnS:Co(d⁷), the relative error between eq.6.7 and eq.6.8 is around 3%. The contribution to Δ_p^0 from terms involving A is taken as eq.6.7 rather than eq.6.8, because more transitions in the Co(d⁷) spectra are observed between the configurations t^3 (the ground state) and et^2 .

In addition to this two electron contribution to Δ_p^0 , there remains the one-electron component. But the one-electron contribution to Δ_p is the separation of the e and t_2 orbitals when electrostatic interactions within the d-shell (i.e. terms involving A, B, and C) are ignored, which is equivalent to Δ in the BC Δ theory, and so is called Δ here. Thus for Co(d⁷):

$$\Delta_p^0 = 3A(\tau^4 - \epsilon^4) + \Delta \quad 6.9$$

where the first term is a simplified form of eq.6.7, and Δ is the one-electron contribution to Δ_p^0 (and Δ_p). The parameter Δ_p^0 is related

to Δ_p , the latter being obtained from the application of the $\epsilon\tau\Delta_p$ theory to the $\text{Co}(d^7)$ spectra, by eq.6.5. Note that eq.6.9 is appropriate only for $\text{Co}(d^7)$: a new formula must be calculated to describe Δ_p^0 for each d^n configuration.

In chapter three it was seen that Δ has contributions from $U(r_i)$, the central part of the crystal field, and $V_c(r_i)$, the fourth order spherical harmonic component of the crystal field. It may be recalled from section 3.6 that the effect of the repulsive electrostatic interaction arising in terms of A is largely cancelled by the attractive central field component of Δ , called Δ_0 here. Both of these components are contained within Δ_p . An approximate analytic expression for Δ_0 can be determined. The strong field configuration orbitals are diagonal in the crystal field. If the orbital energy due to Δ_0 for a t_2 state is U_t and for an e state is U_e , then for the d^7 configuration

$$\Delta_0 = 7(U_t - U_e) \quad 6.10$$

The approximation is made that

$$\begin{aligned} U_e &= \langle \phi_e | U(r) | \phi_e \rangle = \epsilon^2 U \\ U_t &= \langle \phi_t | U(r) | \phi_t \rangle = \tau^2 U \end{aligned} \quad 6.11$$

where ϕ_e and ϕ_t are e and t_2 -orbitals respectively and U is the orbital energy of a free ion d -orbital due to $U(r_i)$. Thus

$$\Delta_0 = 7U(\tau^2 - \epsilon^2) \quad 6.12$$

For a d -shell which is more than half full, the hole formalism is used. In this case the sign of U is reversed (i.e. it is repulsive) and

$$\Delta_0 = 3U(\epsilon^2 - \tau^2)$$

$$= \frac{-U}{(\epsilon^2 + \tau^2)} \cdot 3(\tau^4 - \epsilon^4) \quad 6.13$$

What remains of Δ is the fourth order spherical harmonic component, which is called Δ_4 here. Thus

$$\Delta_p^0 = 3(\tau^4 - \epsilon^4) \left[A - \frac{U}{(\epsilon^2 + \tau^2)} \right] + \Delta_4 \quad 6.14$$

The two terms contained in the square brackets are both large compared with Δ_4 , but they cancel with one another to a great extent. It is assumed that the terms in the square brackets and Δ_4 remain roughly constant throughout the II-VI compounds [16]. Then eq.6.14 describes a straight line graph of Δ_p^0 against $3(\tau^4 - \epsilon^4)$, whose intercept on the Δ_p^0 axis is Δ_4 .

Six sets of coordinates $(\Delta_p^0, 3(\tau^4 - \epsilon^4))$ may be calculated from the results of the application of the theory in chapter 4. The relative error in ϵ , τ and Δ_p was calculated in chapter 5:

$$\text{relative error in } \epsilon = 0.046$$

$$\text{relative error in } \tau = 0.054$$

$$\text{relative error in } \Delta_p = 0.27$$

Thus the relative error in the coordinates of the graph is:

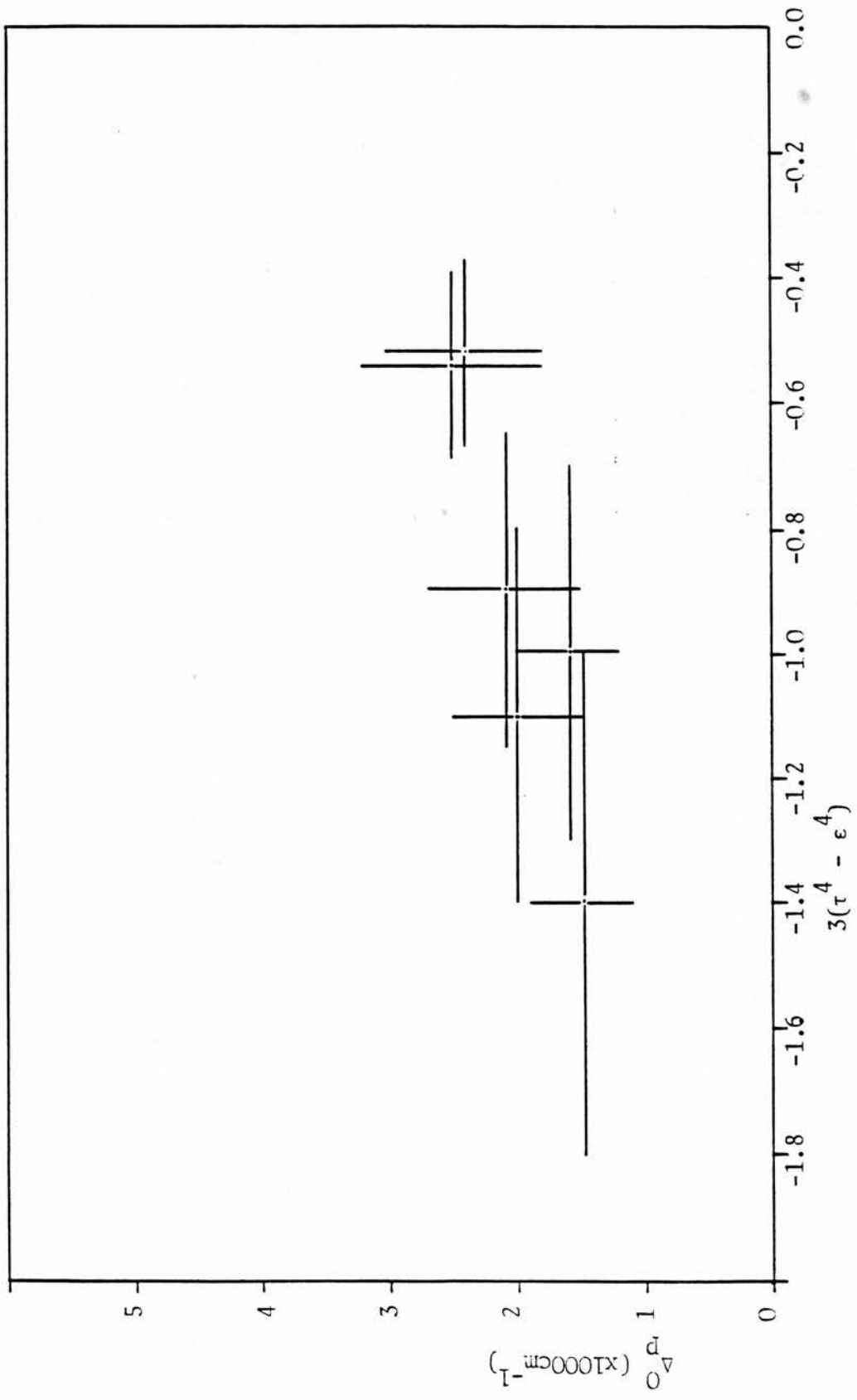
$$\text{relative error in } 3(\tau^4 - \epsilon^4) = 0.28$$

$$\text{relative error in } \Delta_p^0 = 0.27$$

The six sets of coordinates and their associated error bars are given in table 6.2.

The graph of Δ_p^0 against $3(\tau^4 - \epsilon^4)$ is given in fig.6.2. Within the limits of accuracy of the points, it is a straight line graph, with a positive gradient, and does not pass through the origin. There are several important conclusions to be drawn from the graph. First, the assumption that Δ_4 is approximately constant for the II-VI compounds is reasonable. This is borne out by the fact that the

Fig.6.2
Graph of Δ_p^0 against $3(\tau^4 - \epsilon^4)$ for $\text{Co}(d^7)$



points do fall on a good straight line. Second, the line does not pass through the origin, but intersects the Δ_p^0 axis around 3500cm^{-1} . This means that a large contribution to Δ_p comes from the term Δ_4 . Third, the gradient of the straight line is not large, compared with the calculated values of A [84]. The explanation of this is that contributions from A almost cancel with contributions from Δ_0 . This cancellation justifies the use of perturbation theory in the calculation of excited states (see sec.3.3, sec.3.6).

From the set of points plotted in fig.6.2, numerical estimates can be calculated for the gradient and Δ_4 . Using the method of least squares, the best values for the gradient and intercept are:

$$\text{gradient} = 1000\text{cm}^{-1} \quad \text{intercept} = 3000\text{cm}^{-1}$$

A similar calculation may be attempted for $\text{Ni}(d^8)$, where five experimental spectra have been analysed by the $\epsilon\tau\Delta_p$ theory. The diagonal correction, introduced because the hole formalism is used in the calculation of excited states, is still eq.6.5. The values of Δ_p and the adjusted parameter Δ_p^0 are given in table 6.3 for $\text{Ni}(d^8)$. The total two-electron contribution to Δ_p^0 is:

$$A[(\epsilon^4 - \epsilon^2\tau^2) + 5\tau^4 - 2\tau^2\epsilon^2 - 3\epsilon^4] \quad 6.15$$

where the first term in the square brackets arises from the energy difference between the configurations e^2 and $e\tau$, whilst the remainder comes from eq.6.6. This leads to an equation relating Δ_p^0 and Δ for $\text{Ni}(d^8)$:

$$\Delta_p^0 = A(5\tau^2 + 2\epsilon^2)(\tau^2 - \epsilon^2) + \Delta \quad 6.16$$

For $\text{Ni}(d^8)$ the contribution to Δ from Δ_0 is

$$\begin{aligned} \Delta_0 &= 2U(\epsilon^2 - \tau^2) \\ &= \frac{-2U}{5\tau^2 + 2\epsilon^2} \cdot (5\tau^2 + 2\epsilon^2)(\tau^2 - \epsilon^2) \end{aligned} \quad 6.17$$

Table 6.3
 Parameters and results for graph of Δ_p^0 against $(5\tau^2 + 2\epsilon^2)(\tau^2 - \epsilon^2)$
 for Ni(d⁸).

system	ϵ	τ	Δ_p^0	Δ_p^0	$(5\tau^2 + 2\epsilon^2)(\tau^2 - \epsilon^2)$
ZnS:Ni	0.874	0.855	5490 cm ⁻¹	4900 ± 1300 cm ⁻¹	-0.17 ± 0.05
ZnSe:Ni	0.844	0.828	4940 cm ⁻¹	4500 ± 1200 cm ⁻¹	-0.13 ± 0.04
CdS:Ni	0.873	0.838	5700 cm ⁻¹	4700 ± 1200 cm ⁻¹	-0.3 ± 0.1
CdSe:Ni	0.835	0.828	4950 cm ⁻¹	4800 ± 1300 cm ⁻¹	-0.056 ± 0.016

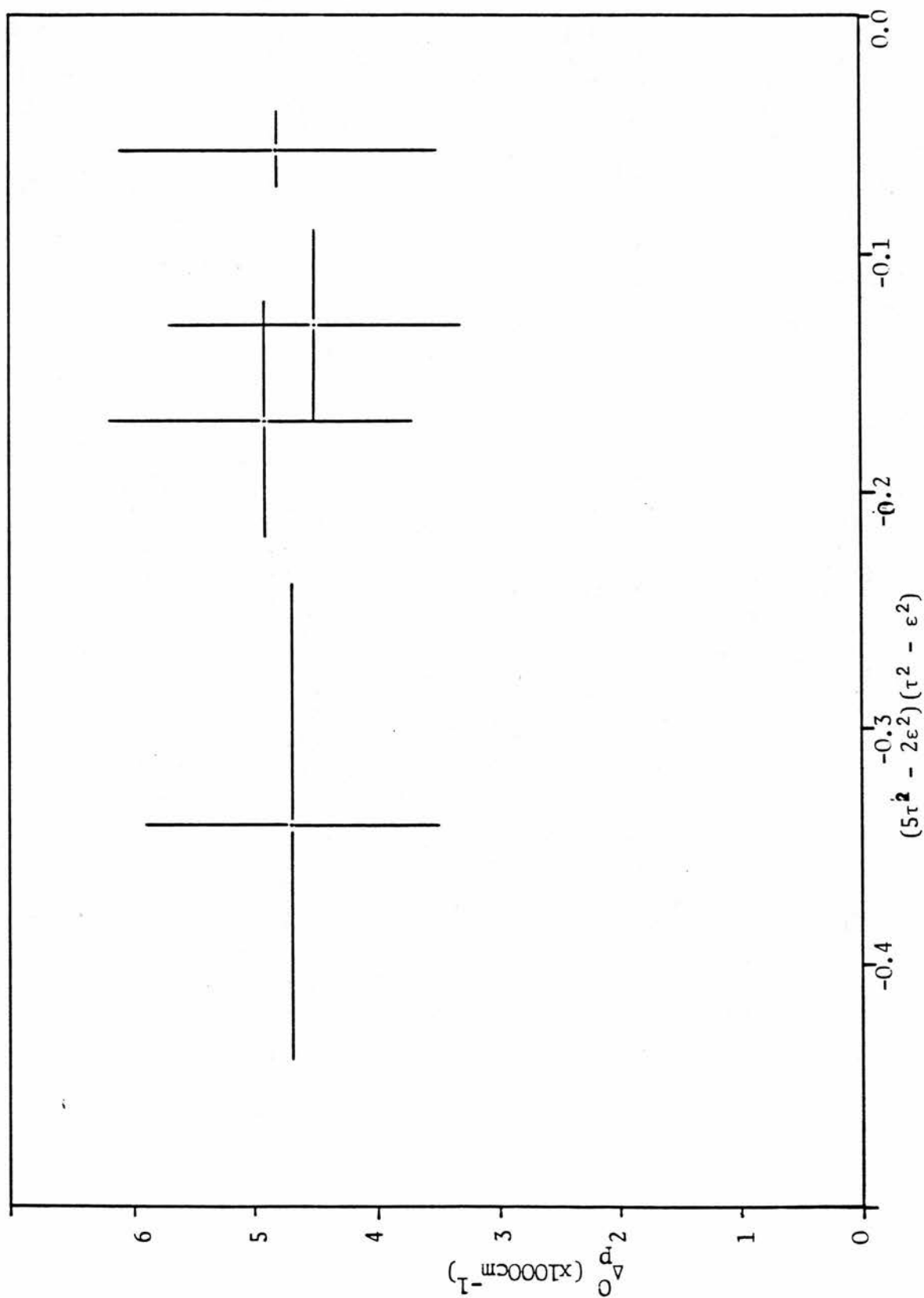
Results

Best straight line:

By method of least squares, gradient = 0 cm⁻¹

intercept = 4700 cm⁻¹

Fig.6.3
 Graph of Δ_p^0 against $(5\tau^2 + 2\epsilon^2)(\tau^2 - \epsilon^2)$ for Ni(d⁸)



which leads to the equation

$$\Delta_p^0 = (5\tau^2 + 2\varepsilon^2)(\tau^2 - \varepsilon^2) \left[A - \frac{2U}{5\tau^2 + 2\varepsilon^2} \right] + \Delta_4 \quad 6.18$$

If the approximation is made that the terms in the square brackets and Δ_4 are constant for the II-VI compounds, then the graph of Δ_p^0 against $(5\tau^2 + 2\varepsilon^2)(\tau^2 - \varepsilon^2)$ should be a straight line with Δ_4 for $\text{Ni}(d^8)$ in II-VI compounds as the intercept on the Δ_p^0 axis. The four sets of coordinates, taken from the results of the application of the $\varepsilon\tau\Delta_p$ theory to four $\text{Ni}(d^8)$ spectra in chapter 4, are given in table 6.3, and a graph has been plotted in fig.6.3. Once again, the graph is a straight line, and does not pass through the origin. The gradient is approximately zero, indicating a cancellation of terms in A with terms in Δ_0 . The component Δ_4 makes a major contribution to Δ_p for $\text{Ni}(d^8)$, as was found to be the case in $\text{Co}(d^7)$. The best values for gradient and intercept are:

$$\text{gradient} = 0.\text{cm}^{-1} \quad \text{intercept} = 4700\text{cm}^{-1}.$$

In table 6.4 the theoretical values of Δ obtained from two sources [16,93] are given. In both cases the values of Δ are of the same order of magnitude as Δ_4 . In these one-electron calculations of Δ , the central field part of the d-d interaction has been included and this almost completely cancels out Δ_0 . As a result the separation of the e and t_2 -orbitals is largely due to Δ_4 .

To summarise, Δ_p found in the application of the theory to experimental data has one-electron and two-electron components. The two-electron components involving B and C can be calculated and separated from Δ_p leaving the adjusted parameter Δ_p^0 . This parameter Δ_p^0 has two-electron components involving terms in A only, and a one-electron component called Δ . Then Δ may be reduced into its zeroth and fourth order spherical harmonic components called Δ_0 and

Table 6.4

Values of the one-electron parameter Δ in $\text{Co}(d^7)$ and $\text{Ni}(d^8)$.

Δ , $\text{Co}(d^7)$	Δ , $\text{Ni}(d^8)$	Host Crystal	reference
5700cm^{-1}	5000cm^{-1}	ZnS	Majewski [93]
4700cm^{-1}	5000cm^{-1}	ZnS	deSiqueira, Larsson [16]
3400cm^{-1}	4400cm^{-1}	CdS	deSiqueira, Larsson [16]
4400cm^{-1}	5600cm^{-1}	ZnO	deSiqueira, Larsson [16]

Δ_4 respectively. Assuming that Δ_4 is constant for a $3d^n$ impurity in any II-VI compound, a straight line graph may be plotted, using the parameters found from a comparison of theory with experiment. The graph shows that a significant contribution to Δ_p comes from Δ_4 and that Δ_0 cancels largely with terms involving A, which justifies the use of perturbation theory in the calculation of excited states.

6.5 The absorption edge in $Cd_{1-x}Mn_xTe$

In this section, the study of trends in the spectra of $Co(d^7)$ and $Ni(d^8)$ is used to predict the position of the first excited state of $Mn(d^5)$ in $Cd_{1-x}Mn_xTe$, given the best fit parameters for $ZnS:Mn$. This work is intended to illustrate a useful application of the study of trends in the parameters.

Optical absorption in $Cd_{1-x}Mn_xTe$ has been studied for a wide range of compositions ($0 < x < 0.7$) by Khoi and Gaj [88]. They found that the absorption curves can be divided into two groups, being $x < 0.4$ and $x > 0.4$. In the first region, $x < 0.4$, the absorption edge position increases linearly from around 12000cm^{-1} to 17600cm^{-1} (1.5eV - 2.2eV) with increasing x . In the second region, $x > 0.4$, the absorption edge is pinned at around 17600cm^{-1} . Khoi and Gaj [88] suggested that internal transitions within the d-shell of $Mn(d^5)$ were responsible for the pinning behaviour. Transitions from the ground state 6A_1 to the first excited state 4T_1 in $Mn(d^5)$ are observed at around 18600cm^{-1} in $ZnS:Mn(d^5)$ [77], which is close to the pinning energy in $Cd_{1-x}Mn_xTe$.

More recently, Grancharova et al [94] rejected this explanation of the pinning. Instead, they suggest that the transition is due to

some strongly localised defects. Their principal objection to the model involving the d^5 internal transitions is outlined here. It is observed that the crystal field parameter Δ decreases with increasing covalent radius of the ligand. The parameters Δ were obtained from the analysis of several absorption spectra of $3d^n$ impurities in II-VI hosts using the $BC\Delta$ theory. The same trend can be expected for the $Mn(d^5)$ impurities. But a decrease in Δ leads to an increase in the separation of the 6A_1 and 4T_1 levels, and so it is claimed that the ${}^6A_1 - {}^4T_1$ absorption in $CdTe:Mn(d^5)$ must be at a higher energy than that in, say, $ZnS:Mn(d^5)$. The ${}^6A_1 - {}^4T_1$ absorption in $ZnS:Mn(d^5)$ is at 18900cm^{-1} and so the corresponding absorption in $CdTe:Mn(d^5)$ must be at a higher energy. The pinning energy in $Cd_{1-x}Mn_xTe$ is at 17600cm^{-1} and so can not correspond to an internal transition within $Mn(d^5)$.

The $\epsilon\tau\Delta_p$ theory has been applied to the spectra of $Co(d^7)$ and $Ni(d^8)$ in several II-VI compounds, as well as to $ZnS:Mn(d^5)$, and from a study of trends in the parameters ϵ , τ and Δ_p , there would seem to be good grounds to suggest that the pinning is indeed a consequence of the transition ${}^6A_1 - {}^4T_1$. A summary of the parameters found in the application of the theory is presented in table 6.5, together with values for τ^4 and ϵ/τ . The quantity ϵ/τ governs the relative separation of the excited states as a consequence of electrostatic interactions within the d-shell, whilst τ^4 scales the overall separation of the levels.

As the covalent radius of the nearest neighbour ion increases then there is an observed decrease in Δ_p . This is analogous to the observed decrease in Δ , using the $BC\Delta$ theory. However, there is also an observed decrease in τ^4 and ϵ/τ . The trend in τ^4 is particularly strong for both $Ni(d^8)$ and $Co(d^7)$ spectra. The effect of each of

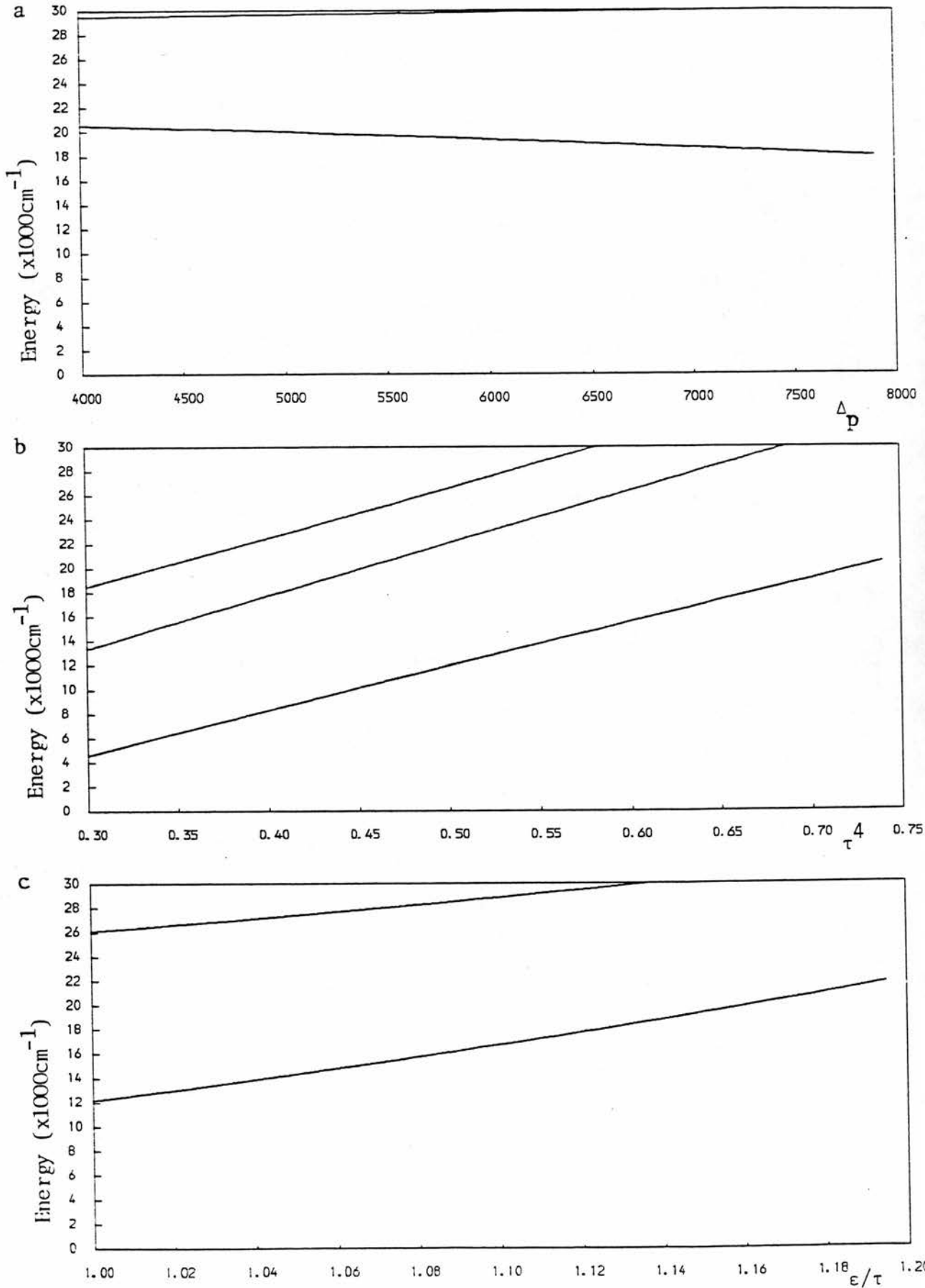
Table 6.5

Trends in the parameters Δ_p , τ^4 , and ϵ/τ .

system	ϵ	τ	Δ_p	τ^4	ϵ/τ	
ZnO:Co	0.849	0.934	2650 cm ⁻¹	0.761	0.909	(hex)
ZnS:Co	0.981	0.823	5900 cm ⁻¹	0.459	1.192	
ZnSe:Co	0.945	0.813	5370 cm ⁻¹	0.437	1.162	
ZnTe:Co	0.854	0.770	4260 cm ⁻¹	0.352	1.109	
CdS:Co	0.947	0.842	5000 cm ⁻¹	0.503	1.125	(hex)
CdSe:Co	0.935	0.813	4700 cm ⁻¹	0.437	1.150	
CdTe:Co	0.859	0.780	4020 cm ⁻¹	0.370	1.101	
ZnO:Ni	0.910	0.949	5735 cm ⁻¹	0.811	0.959	(hex)
ZnS:Ni	0.874	0.855	4910 cm ⁻¹	0.534	1.022	
ZnSe:Ni	0.844	0.828	4500 cm ⁻¹	0.470	1.019	
CdS:Ni	0.873	0.833	4650 cm ⁻¹	0.481	1.048	(hex)
CdSe:Ni	0.835	0.828	4760 cm ⁻¹	0.470	1.008	
ZnS:Ti	0.881	0.864	2960 cm ⁻¹	0.557	1.020	
ZnS:V	0.985	0.783	2220 cm ⁻¹	0.376	1.258	
ZnS:Cr	0.945	0.900	4790 cm ⁻¹	0.656	1.050	
ZnS:Fe	0.915	0.913	3310 cm ⁻¹	0.965	1.002	

Fig.6.4

4T_1 energy levels for Mn ion in a tetrahedral crystal.



these trends must be taken into account, rather than just considering the trend in Δ_p (or Δ).

In fig.6.4 the separation of the 4T_1 levels from the ground state 6A_1 is shown as a function of Δ_p , τ^4 , and finally ϵ/τ . For ZnS:Co(d^7), the best choice of Δ_p is 5900cm^{-1} , whilst for CdTe:Co(d^7), Δ_p is 4020cm^{-1} . The difference in the parameter Δ_p between these two systems is around 2000cm^{-1} . A similar decrease in the magnitude of Δ_p might be expected between ZnS:Mn(d^5) and CdTe:Mn(d^5). For ZnS:Mn(d^5) the best choice of parameters was

$$\epsilon = 1.034 \qquad \tau = 0.910 \qquad \Delta_p = 7140\text{cm}^{-1}.$$

In fig.6.4a, the ${}^6A_1 - {}^4T_1$ levels are shown as calculated using the values of ϵ and τ found for ZnS:Mn(d^5), but where Δ_p varies from 4000cm^{-1} to 8000cm^{-1} . As Δ_p decreases, the 4T_1 level moves higher in energy. This was also found to be the case when decreasing Δ in the BCA theory. In fig.6.4b, the 4T_1 levels are plotted, using the values of Δ_p and ϵ found for ZnS:Mn(d^5), but decreasing τ^4 from 0.75 ($\tau = 0.93$) to 0.3 ($\tau = 0.74$). The range of values of τ^4 cover a physically reasonable range of values, which was also true of the range of values of Δ_p in fig.6.4a. Here, the 4T_1 level moves lower in energy as τ^4 decreases, and it does so at a greater rate than the corresponding rise in energy as Δ_p is reduced.

For the example of Co(d^7), Δ_p is reduced by 2000cm^{-1} whilst τ^4 decreases by 0.089, between the spectra of ZnS:Co(d^7) and CdTe:Co(d^7). For Mn(d^5), the same decrease in Δ_p will increase the energy of the 4T_1 level by around 1400cm^{-1} . The same decrease in τ^4 will decrease the energy of the 4T_1 level by around 3200cm^{-1} . The decrease in energy of the 4T_1 level, caused by the decrease in τ^4 , is more than twice the magnitude of the increase in energy, caused by the decrease in Δ_p .

The trends in the parameters for $\text{Co}(d^7)$ also suggest that the ratio of ϵ/τ decreases towards unity. In fig.6.4c the 4T_1 level is shown as ϵ/τ decreases, with Δ_p and τ held at the values appropriate for $\text{ZnS:Mn}(d^5)$. The graph suggests that the trend in ϵ/τ observed in $\text{Co}(d^7)$ would further decrease the energy of the 4T_1 level if it occurs in the $\text{Mn}(d^5)$ spectra.

Summarising, the study of trends made by Grancharova et al [94] only deals with one of the adjustable parameters. In a fuller treatment, using the parameters found with the $\epsilon\tau\Delta_p$ theory, the increase in energy of the 4T_1 level, caused by the trend in Δ_p to decrease as the covalent radius of the ligand increases, is less than the decrease in energy of the level, caused by the trend in τ^4 to decrease as the covalent radius of the ligand increases. The neglect of the trends in the covalency parameters ϵ and τ by Grancharova et al led them to the unjustified conclusion that the 4T_1 level in $\text{CdTe:Mn}(d^5)$ must lie above the corresponding level in $\text{ZnS:Mn}(d^5)$. The work in this section shows how the study of trends in the parameters ϵ , τ and Δ_p can be used to resolve difficulties in the interpretation of other absorption data. In the present case, trends in $\text{Co}(d^7)$ and $\text{Ni}(d^8)$ have been used to predict the spectrum of $\text{CdTe:Mn}(d^5)$.

6.6 -Comparison with esr data-

Measurements from esr have been reported for many different examples of transition metal impurities in semiconductors [50,95,96,97,98]. From the position of the esr absorptions, a g-factor for that system can be determined. For $\text{Co}(d^7)$ impurities in tetrahedral semiconductors, the value of g is close to 2. The amount

by which it differs from two determines a covalency parameter k . In this section, the esr covalency parameter k is compared with the crystal field covalency parameters ϵ and τ found from optical absorption experiments.

For an impurity in the presence of a uniform magnetic field, B_z , the electron energy levels are split by an amount

$$\Delta E = g\beta B_z M_S \quad 6.19$$

where β is the Bohr magneton, and $M_S=3/2$ here. To first order, if $|G\rangle$ is the impurity ground state then

$$g = \langle G | (1_z + 2 s_z) | G \rangle. \quad 6.20$$

In tetrahedral coordination, the ground state of $\text{Co}(d^7)$ is 4A_2 , which is orbitally non-degenerate. This leaves just the spin g -factor [30]:

$$g = 2.0023 \quad 6.21$$

Because of the orbital non-degeneracy of the ground state, the orbital contribution to g is included by taking into account spin orbit coupling to the first excited state. To second order, then

$$\Delta E = 3\beta B_z - \frac{|\langle G | \sum_i \epsilon 1_i \cdot s_i + \beta B_z 1_z | \text{Ex} \rangle|^2}{E_{\text{ex}} - E_g} \quad 6.22$$

where $|\text{Ex}\rangle$ is the first excited state, 4T_2 , and $E_{\text{ex}} - E_g$ is the energy separation of the ground state and first excited state determined from experimental data, see chapter four.

Attention is now focussed on the second term in eq.6.22. The wavefunction for the ground state ${}^4A_2(\Gamma_8)$ is

$${}^4A_2 = |\xi^+ \eta^+ \zeta^+ \rangle \quad 6.23$$

and for the first excited state ${}^4T_2(\Gamma_8, M_J=3/2)$ is

$${}^4T_2 = |\xi^+ \eta^+ \epsilon^+ \rangle \quad 6.24$$

The wavefunctions (3x3 Slater determinants) are inserted into eq.6.22, giving

$$\Delta E = 3\beta B_z - \frac{|\langle \zeta^+ | \xi \underline{1} \cdot \underline{s} | \epsilon^+ \rangle + \langle \zeta^+ | \beta B_z \underline{1} \cdot \underline{z} | \epsilon^+ \rangle|^2}{E_{ex} - E_g} \quad 6.25$$

From eq.3.4 the strong field configuration one-electron functions can be written in terms of the weak field functions:

$$\begin{aligned} \zeta^+ &= (1/i\sqrt{2}) [2^+ - (-2^+)] \\ \epsilon^+ &= (i/\sqrt{2}) [2^+ + (-2^+)] \end{aligned} \quad 6.26$$

These expressions show that

$$\begin{aligned} \langle \zeta^+ | \xi \underline{1} \cdot \underline{s} | \epsilon^+ \rangle &= (1/2) [\langle 2^+ | \xi \underline{1} \cdot \underline{s} | 2^+ \rangle - \langle -2^+ | \xi \underline{1} \cdot \underline{s} | -2^+ \rangle] \\ &= (1/2) [2 \cdot (1/2) - (-2) \cdot (1/2)] \zeta' \\ &= \zeta' \end{aligned} \quad 6.27$$

where ζ' is defined in section 3.12.1, and

$$\begin{aligned} \langle \zeta^+ | \beta B_z \underline{1} \cdot \underline{z} | \epsilon^+ \rangle &= (1/2) [\langle 2^+ | \beta B_z \underline{1} \cdot \underline{z} | 2^+ \rangle - \langle -2^+ | \beta B_z \underline{1} \cdot \underline{z} | -2^+ \rangle] \\ &= (\beta B_z \underline{1} \cdot \underline{z} / 2) [2 - (-2)] \langle R_t | R_e \rangle \\ &= 2\beta B_z \langle R_t | R_e \rangle \end{aligned} \quad 6.28$$

This leads to the simplification:

$$\Delta E = 3\beta B_z - \frac{|\zeta' + 2\beta B_z \langle R_t | R_e \rangle|^2}{E_{ex} - E_g} \quad 6.29$$

Finally by retaining only terms linear in B_z

$$\Delta E = 3\beta B_z - \frac{4\zeta' \beta B_z \langle R_t | R_e \rangle}{E_{ex} - E_g} \quad 6.30$$

The product of $\langle R_t | R_e \rangle$ with the ratio between ζ' and the free ion spin orbit coupling constant, ζ , is conventionally referred to as k , and ζ is rewritten as $2\lambda S$ where $S = 3/2$ for $\text{Co}(d^7)$:

$$\begin{aligned} (3/2)g &= 3 - \frac{4\zeta' \langle R_t | R_e \rangle}{E_{ex} - E_g} \\ g &= 2 - \frac{8\lambda k}{E_{ex} - E_g} \end{aligned} \quad 6.31$$

Table 6.6
 Comparison of esr and crystal field covalency parameters.

System	g	$E_{ex} - E_g$	λ	k	ϵ_{τ}^2
ZnS:Co	2.248	3700cm^{-1}	-178cm^{-1}	0.638	0.651
ZnSe:Co	2.27	3500cm^{-1}	-178cm^{-1}	0.66	0.59
ZnTe:Co	2.297	3200cm^{-1}	-178cm^{-1}	0.663	0.433
CdS:Co	2.27	3100cm^{-1}	-178cm^{-1}	0.59	0.64
CdTe:Co	2.31	2900cm^{-1}	-178cm^{-1}	0.63	0.449

If it is now assumed that the reduction of the spin orbit coupling constant between the impurity orbitals e and t_2 is approximately given by

$$\zeta' = \epsilon\tau\zeta \quad 6.32$$

$$\text{and } \langle R_t | R_e \rangle = \epsilon\tau$$

then k corresponds with the product $\epsilon^2\tau^2$. In this way the spin orbit covalency factor can be compared with the crystal field covalency parameters ϵ and τ .

In table 6.6 the quantities k and $\epsilon^2\tau^2$ are given for those $\text{Co}(d^7)$ systems where both esr and optical absorption data are available. The table shows that there is some similarity between the magnitudes of the two quantities. However, no direct correlation in their variation is observed, for example $\epsilon^2\tau^2$ decreases between ZnS:Co and ZnTe:Co whereas k increases.

The covalency parameters ϵ and τ are defined by two-electron integrals, whilst the parameter k is defined by a one-electron integral. Because of this difference in the definition of the two types of covalency parameter, the absence of a close correlation is not surprising.

6.7 -Summary-

The crystal field parameters, ϵ and τ , have been found from the application of the $\epsilon\tau\Delta_p$ theory to a wide range of transition metal impurities in II-VI compounds. In each case, they are close to unity, suggesting only a small delocalisation of the impurity d-orbitals. Agreement between theory and experimental data is good, and in general the t_2 -orbitals delocalise more than the e -orbitals, i.e. ϵ is greater than τ . Thus the successful application of the $\epsilon\tau\Delta_p$ theory in

chapter 4 gives strong support to the crystal field model, where it is assumed that the d-orbitals of the transition metal impurity remain strongly localised when it is substitutional on a cation site in a tetrahedral crystal. This is the most important conclusion arising from the study of the crystal field parameters in this chapter.

As the covalent radius of the impurity nearest neighbours increases, both ϵ and τ decrease. This increase in the degree of delocalisation of the d-orbitals agrees with the known increase in covalency of the host materials. Departures from the trend in the parameter ϵ are expected for those crystals with a trigonal distortion, and are seen in ZnO:Co(d^7) and ZnO:Ni(d^8).

The parameter Δ_p found in the application of the theory to experimental data has one-electron and two-electron components. The two-electron components involving B and C can be calculated and separated from Δ_p leaving the adjusted parameter Δ_p^0 . This parameter Δ_p^0 has two-electron components involving terms in A only, and a one-electron component called Δ . Then Δ may be reduced into its zeroth and fourth order spherical harmonic components called Δ_0 and Δ_4 respectively. Assuming that Δ_4 is constant for a $3d^n$ impurity in any II-VI compound, a straight line graph may be plotted, using the parameters found from a comparison of theory with experiment. The graph shows that a significant contribution to Δ_p comes from Δ_4 and that Δ_0 cancels largely with terms involving A, which justifies the use of perturbation theory in the calculation of excited states.

Trends in the spectra of Co(d^7) and Ni(d^8) have been used to predict energy levels in Mn(d^5). Specifically, the trends for Δ_p , τ^4 , and ϵ/τ to decrease, if the host crystal is changed from ZnS to CdTe, have been seen for the spectra of Co(d^7) and Ni(d^8). The same trends are expected to occur for the spectra of Mn(d^5). Since the

spectrum of ZnS:Mn(d⁵) is known, predictions about the spectrum of CdTe:Mn(d⁵) can be made. A decrease in Δ_p increases the energy of the first excited state. But the decrease in τ^4 (and ϵ/τ) will decrease the energy of the first excited state by a much larger amount. It is the conclusion of this work that an overall decrease in the energy of the first excited state should occur between ZnS:Mn(d⁵) and CdTe:Mn(d⁵). Thus the pinning of the absorption edge in Cd_{1-x}Mn_xTe for $x > 0.4$ may be due to internal transitions within Mn(d⁵): the pinning energy is 17600cm^{-1} compared with the first excited state energy of 18600cm^{-1} in ZnS:Mn(d⁵).

No strong correlation has been found between the esr covalency parameter k and the product of crystal field parameters ϵ and τ , although there is a similarity in the magnitudes of the parameters being compared. The weak correlation suggests that there is not a simple relationship between covalency parameters for one-electron integrals (k) and two-electron integrals (ϵ and τ).

A survey of the empirical parameter B , found from the spectra Co(d⁷), using the BCA theory has been carried out by Hennel [99]. One conclusion of his work is that the reduction of the parameter B depends on the covalent radius of the anion, which can be compared to the dependence of the parameters ϵ and τ on the covalent radius in the $\epsilon\tau\Delta_p$ theory. Whilst this is a reasonable and useful conclusion to be drawn from the parameters, his discussion of trends concentrates on an analytic expression for B :

$$B = B_0 - a \frac{N+1}{\chi} \quad 6.33$$

Here B_0 is the free ion Racah parameter, χ is the Phillips electronegativity of the anion, N is the anion valency, and $a=275\text{cm}^{-1}$ is a constant determined from a graph of B against $1/\chi$. The accuracy of a , quoted to three significant figures, suggests that eq.6.33 is

quite precise. But, certain data have not been included in his survey [8,9], and no treatment of errors in the parameters B has been presented. The value of B_0 used was 1027cm^{-1} [100], which differs from the value quoted by Griffith by 10% [4]. Thus, in view of the spread of values for B and B_0 , the eq.6.33 can only be approximate, so that the quoted (high) accuracy of a is totally misleading.

The empirical parameters found from the application of crystal field theory to absorption data are only approximate. Therefore, there is a limit to the precision of any quantitative results which can be obtained from a study of the parameters.

CHAPTER SEVEN

APPLICATIONS OF CRYSTAL FIELD THEORY II:

IMPURITIES IN III-V COMPOUNDS

7 APPLICATIONS OF CRYSTAL FIELD THEORY II: IMPURITIES IN III-V COMPOUNDS

7.1 -Introduction-

In chapter four it was demonstrated that the $\epsilon\tau\Delta_p$ version of crystal field theory was capable of describing the optical absorption data arising from transition metal impurities in II-VI compounds. In this chapter I aim to show that the theory may also be applied successfully to interpret the optical absorption spectra of transition metal impurities in the III-V compounds.

It is important to know whether the approximations made in the $\epsilon\tau\Delta_p$ theory are satisfactory in the more covalent III-V materials. If these approximations are no longer valid, then the application of the theory should result in unreasonable values of the adjustable parameters and poor agreement between theory and experiment. However the work in this chapter shows that the range of systems, to which the crystal field theory can be applied meaningfully, may be extended to include the III-V compounds in addition to the II-VI compounds.

A further motivation for using the crystal field theory in the description of transition metal impurities in the III-V compounds is that first principles calculations of the one-electron d-orbitals have been made for these systems [2,3,20]. At present a comparison between first principles theory and experiment is only possible for these III-V systems. Although first principles calculations have also been made for transition metal impurities in the elemental semiconductors [101,9] the stronger covalency and small band gap in these materials mean that it is unlikely that the $\epsilon\tau\Delta_p$ theory could be applied

successfully.

Because the III-V compounds are more covalent than the II-VI materials, it is questionable whether the assumptions in the $\epsilon\tau\Delta_p$ theory concerning the localised nature of the d-orbitals are still valid. Evidence for the localised nature of d-orbitals for transition metal impurities in III-V semiconductors is found in their absorption spectra. For example, the broad features of the spectra of $\text{Co}(d^7)$ in II-VI compounds (see chapter four) are retained in the spectra of cobalt in the III-V compounds (see figs.7.1 and 7.2). The similarity between the spectra suggests that cobalt keeps something of its atomic identity. Thus substitutional cobalt in the III-V compounds may form a deep acceptor state with a localised d^7 configuration [102,103].

The $\epsilon\tau\Delta_p$ theory may be used to describe the excited states of a localised d^n configuration provided several crystal field levels can be observed experimentally. These levels are then used to determine the crystal field parameters. A small band gap in many of the III-V materials makes the application of the theory difficult. However, adequate data is available for GaAs:Co and GaP:Co and so these systems are used as a test of the validity of the $\epsilon\tau\Delta_p$ theory in the III-V systems.

The method of application of the $\epsilon\tau\Delta_p$ theory to the absorption spectra here is similar to the application of the theory to the II-VI systems. This method is described in sec.4.2 and is summarised in fig.4.2. In the next two sections, the application of the theory to $\text{Co}(d^7)$ in GaAs and GaP is described. Following these, there is a discussion of the results obtained from the application of the theory.

7.2 -GaAs:Co-

The optical absorption spectrum for GaAs:Co was first reported by Baranowski, Allen and Pearson [51]. Hennel and Uba [104] have also studied the system and described the absorption data in terms of internal transitions within $\text{Co}(d^7)$ using the $BC\Delta$ theory. They also attempted to describe the observed fine structure of the levels by using the spin orbit and Jahn-Teller interactions. The absorption peak around 8500cm^{-1} observed by Baranowski et al is not shown in the more detailed spectra of Hennel and Uba, suggesting that it may be due to some stray impurity. Ennen, Kaufmann and Schneider [103] reported a weak transition around 4200cm^{-1} which they claim to be the ${}^4A_2 - {}^4T_2$ crystal field transition. The crystal field parameters were calculated as [102]

$$B = 380\text{cm}^{-1} \qquad \Delta = 4250\text{cm}^{-1}$$

Using the absorption data reported previously, the $\epsilon\tau\Delta_p$ theory has been used to describe the spectra in terms of internal transitions within $\text{Co}(d^7)$. The absorption data, together with the predicted levels, are shown in fig.7.1. The intensity of the levels is estimated by the fraction of 4T_1 character in each crystal field level. Spin orbit coupling was included approximately by setting $\zeta = \zeta' = -400\text{cm}^{-1}$, and the crystal field parameters used were:

$$\epsilon = 0.842 \qquad \tau = 0.736 \qquad \Delta_p = 5470\text{cm}^{-1}$$

Satisfactory agreement between theory and experiment is found using the $\epsilon\tau\Delta_p$ theory, although a relatively strong absorption is predicted around 8800cm^{-1} which is not observed by Hennel and Uba.

Fig. 7.1
Absorption spectrum of GaAs:Co compared with levels
calculated by the $\epsilon\tau\Delta_p$ theory.

GaAs:Co

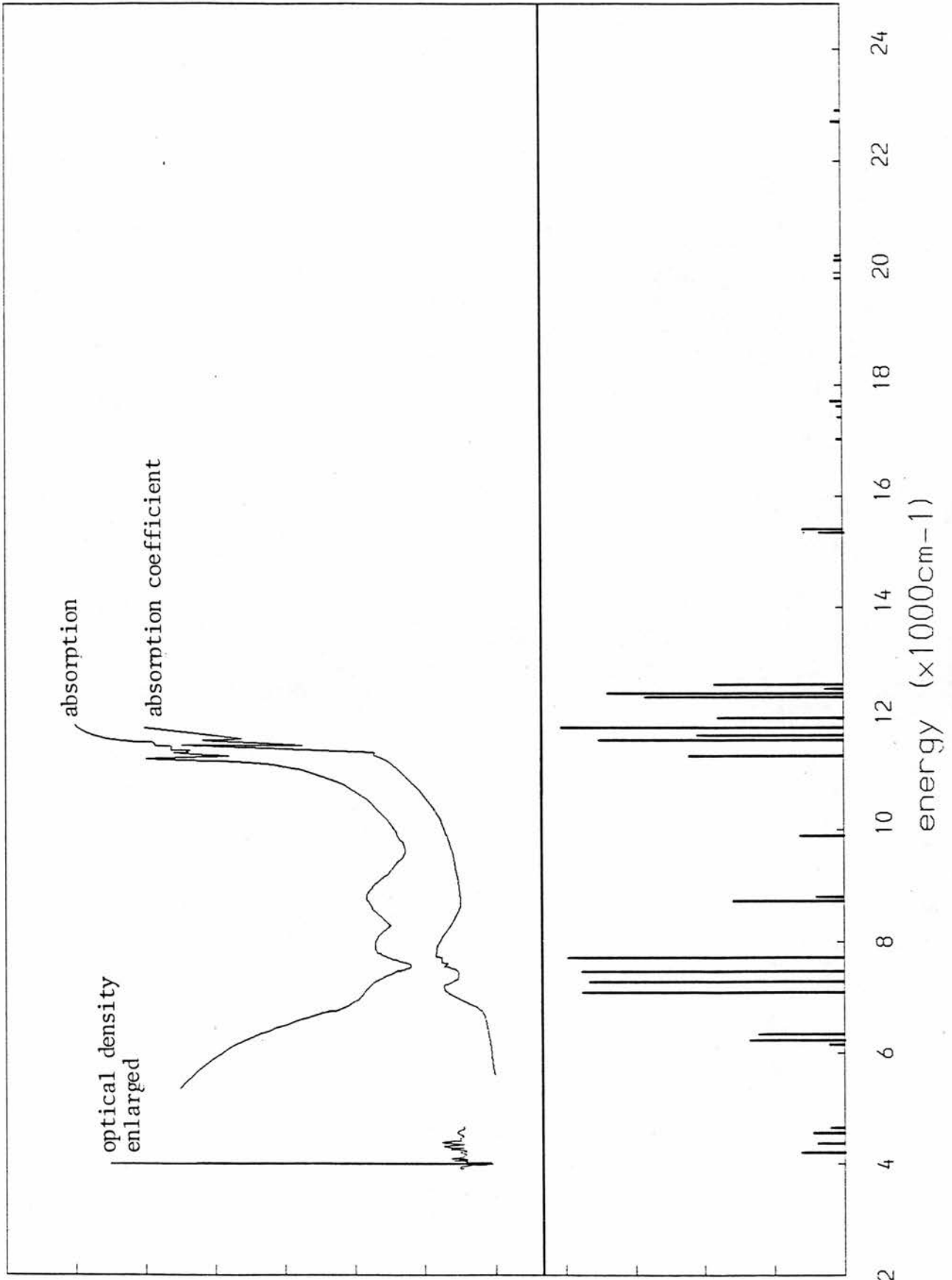


Table 7.1
Comparison of energy levels for GaAs:Co

a) $\epsilon\tau\Delta_p$ theory		b) $BC\Delta$ theory	
$\epsilon = 0.842$		$B = 570 \text{ cm}^{-1}$	
$\tau = 0.736$		$C = 1670 \text{ cm}^{-1}$	
$\Delta_p = 5470 \text{ cm}^{-1}$		$\Delta = 4250 \text{ cm}^{-1}$	
4200	Γ_8	4060	Γ_8
4370	Γ_6	4120	Γ_6
4560	Γ_8	4370	Γ_8
4690	Γ_7	4480	Γ_7
6110	Γ_8	6530	Γ_6
6230	Γ_6	6780	Γ_8
6370	Γ_8	7140	Γ_7
7080	Γ_6	7250	Γ_8
7450	Γ_8	7640	Γ_8
7520	Γ_7	7900	Γ_6
7740	Γ_8	8170	Γ_8
8700	Γ_7	10400	Γ_7
8800	Γ_8	10400	Γ_8
10000	Γ_6	10900	Γ_6
11300	Γ_8	11400	Γ_8
11600	Γ_8	11500	Γ_8
11700	Γ_6	11500	Γ_7
11800	Γ_7	11800	Γ_6
12000	Γ_8	12000	Γ_8
12400	Γ_8	12000	Γ_7
12400	Γ_6	12400	Γ_8
12500	Γ_7	12700	Γ_6

all energies are measured in cm^{-1} .

7.3 -GaP:Co-

The absorption spectrum for GaP:Co was first taken at liquid-helium temperatures by Baranowski et al [51]. They used the B Δ theory to describe their results. Weber et al [102] measured the spectrum in more detail and also reported the weak ${}^4A_2 - {}^4T_2$ transition. Using the B Δ theory they found

$$B = 395\text{cm}^{-1} \qquad \Delta = 4750\text{cm}^{-1}$$

The $\epsilon\tau\Delta_p$ theory is used to describe the spectrum by fitting to the three high spin states. This leads to the following assignment of the crystal field parameters:

$$\epsilon = 0.859 \qquad \tau = 0.726 \qquad \Delta_p = 6150\text{cm}^{-1}.$$

Agreement between theory and experiment for the high spin states is good, and in addition low spin states now account for some of the weaker absorptions which were not described by the B Δ theory. The experimental data are shown in fig.7.2 together with the theoretically predicted levels calculated using the crystal field parameters given above and with the spin orbit coupling constants $\zeta = \zeta' = -400\text{cm}^{-1}$.

7.4 -Discussion-

The work presented in the previous sections shows that the $\epsilon\tau\Delta_p$ theory can adequately describe the broad details of the optical absorption spectra arising from transition metal impurities in III-V compounds in terms of internal transitions within a localised d^n configuration. Agreement between theory and experiment is good for the two systems studied, and for GaP:Co the $\epsilon\tau\Delta_p$ theory assigns doublet levels to some of the weaker absorptions which are not

Fig.7.2
Absorption spectrum of GaP:Co compared with levels
calculated by the $\epsilon\tau\Delta_p$ theory.

GaP:Co

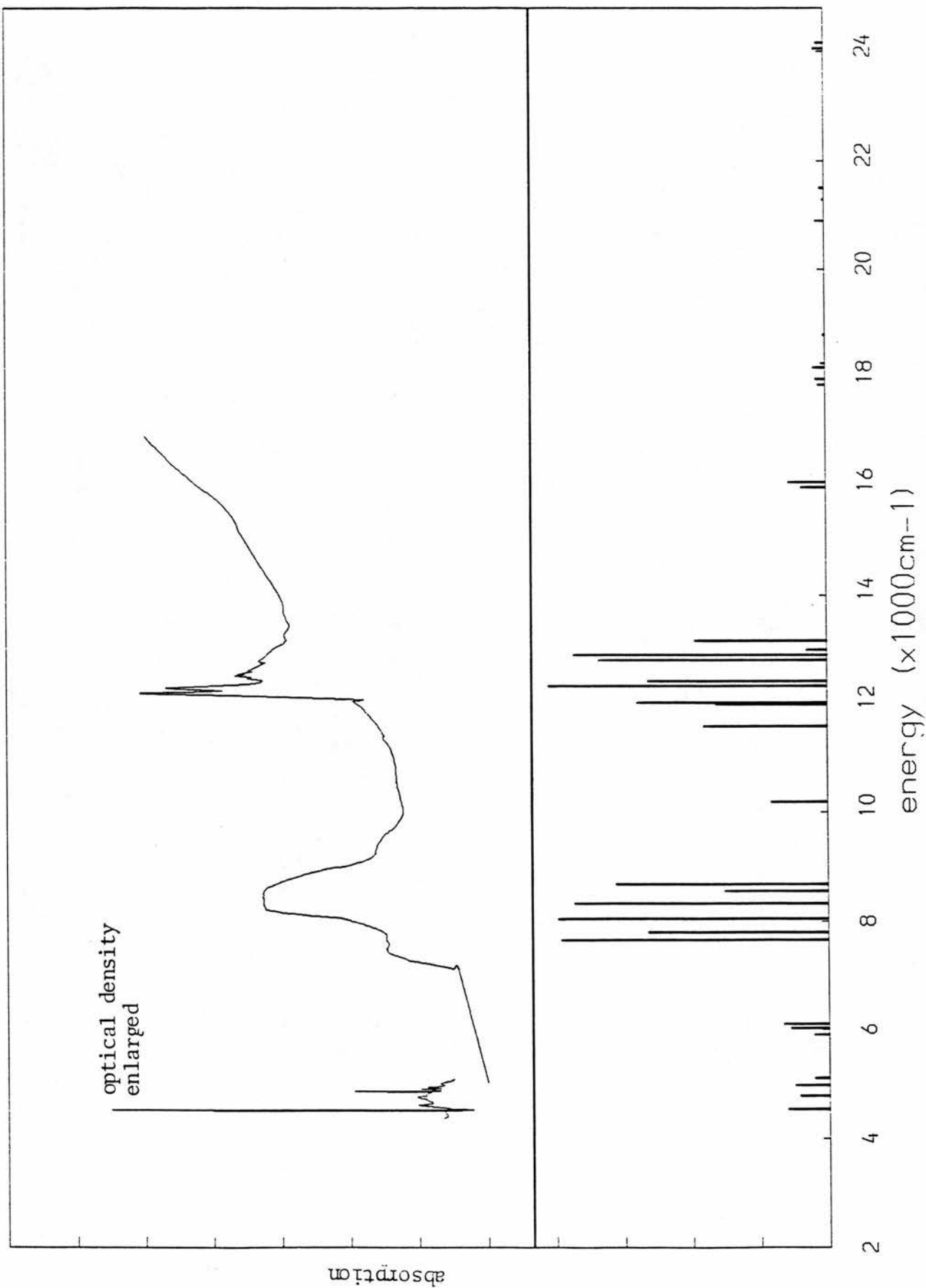


Table 7.2
 Comparison of energy levels calculated for GaP:Co

a) $\epsilon\tau\Delta_p$ theory		b) $BC\Delta$ theory	
$\epsilon=0.859$		$B=395\text{cm}^{-1}$	
$\tau=0.726$		$C=1660\text{cm}^{-1}$	
$\Delta_p=6150\text{cm}^{-1}$		$\Delta=4750\text{cm}^{-1}$	
4570	Γ_8	4550	Γ_8
4800	Γ_6	4680	Γ_6
5000	Γ_8	4860	Γ_8
5140	Γ_7	4970	Γ_7
5940	Γ_8	7220	Γ_6
6050	Γ_6	7410	Γ_8
6140	Γ_8	7750	Γ_8
7700	Γ_6	7850	Γ_7
7860	Γ_7	7960	Γ_8
8070	Γ_8	8060	Γ_6
8380	Γ_8	8348	Γ_8
8590	Γ_8	10700	Γ_7
8730	Γ_7	10800	Γ_8
10300	Γ_6	11444	Γ_6
11700	Γ_8	12300	Γ_8
12000	Γ_6	12300	Γ_8
12100	Γ_8	12500	Γ_7
12400	Γ_7	12600	Γ_8
12500	Γ_8	12600	Γ_7
12900	Γ_8	12600	Γ_6
12900	Γ_6	13100	Γ_8
13100	Γ_7	13300	Γ_6
13200	Γ_8		

all energies are measured in cm^{-1}

explained by the $BC\Delta$ theory.

The covalency parameters are close to unity, which means there is only a small delocalisation of the d-orbitals. The parameters ϵ and τ are smaller than the corresponding parameters obtained in the application of the theory to the II-VI systems. This corresponds to a stronger delocalisation of the d-orbitals which is to be expected because the III-V compounds are more covalent than the II-VI compounds. The value of ϵ is greater than τ in both cases corresponding to a greater delocalisation of the t_2 -orbitals, which was also found to be the case in applications of the theory to II-VI systems. Thus the values of ϵ and τ found from the application of the $\epsilon\tau\Delta_p$ theory to the III-V systems are physically reasonable, because they are close to unity but are smaller than the parameters found for the II-VI systems.

The parameter Δ_p for $Co(d^7)$ contains contributions in terms of the Racah parameters B and C. This component can be evaluated leaving the adjusted parameter Δ_p^0 . For GaP:Co Δ_p^0 is 3670cm^{-1} , and for GaAs:Co Δ_p^0 is 3520cm^{-1} . It was seen in chapter six that typical values for Δ_p^0 calculated for $Co(d^7)$ in the II-VI compounds were around 2000cm^{-1} . Thus for the III-V systems the magnitude of Δ_p^0 is larger than for the II-VI systems.

7.5 -Summary-

The $\epsilon\tau\Delta_p$ theory can be used successfully to interpret the optical absorption spectra arising from the transition metal impurities in III-V compound semiconductors. Agreement between theory and experiment is good. The values of ϵ and τ are close to unity, corresponding to a small delocalisation of the d-orbitals. But they are smaller in the III-V systems than in the II-VI systems, which is a consequence of the more covalent nature of the III-V hosts. The parameter Δ_p^0 , which is the energy difference between the configurations $t^m e^1$ and $t^{m+1} e^{1-1}$ when terms involving B and C are ignored, is larger in the III-V systems than in the II-VI systems.

CHAPTER EIGHT
THE CRYSTAL FIELD STRENGTH

8 THE CRYSTAL FIELD STRENGTH

8.1 -Introduction-

In this thesis crystal field theory has been used with considerable success to interpret optical absorption data on transition metal impurities in tetrahedral semiconductors. This success has been achieved by determining the parameters ϵ , τ , and Δ_p empirically. The physical origin of ϵ and τ has been discussed previously. The impurity one-electron d-orbitals are modified because of the crystalline environment which leads to a reduction of the electrostatic interactions within the d-shell. The parameters ϵ and τ define this reduction. The impurity d-orbitals are affected for example by mixing with the ligand orbitals and by partial screening of the impurity core by the host electrons.

The physical origin of the crystal field has not been considered previously in this thesis because it is only the point symmetry of the crystal field which is important in the interpretation of data. Therefore in this chapter, an attempt is made to calculate the components of Δ_p , or more specifically components of the one-electron part Δ , so as to understand better the physical origin of the crystal field splittings.

Several estimates of the crystal field splitting have been made previously. The first calculations were made by Van Vleck [105] and Polder [106] who used a point charge approximation for the ligands. Kleiner [107] moved away from the point ion model and used extended ligands described by Slater orbitals. Although the point ion

calculations gave quite good agreement with experiment, the improved model of Kleiner predicted the wrong sign for Δ . A series of molecular orbital calculations followed [1,108,109,110] which became successively more complex. An alternative view of the crystal field, in terms of a bond charge model of covalent semiconductors [111,112], was used by Wray and Allen [10] and by Hennel [113]. More recent work on the crystal field splitting has been carried out by Biernacki and Schulz [36].

The crystal field at the impurity site has contributions from the lattice of ion cores, which are approximated to point charges here, and from the valence electrons. The valence electron charge density is determined by the pseudopotential method. The charge density is related to the valence electron electrostatic potential, which contributes to the crystal field, by Poisson's equation.

A brief summary of the pseudopotential method is given in the next section. All of this material may be found elsewhere [114,115,116,89], and in particular volume 24 of the series "Solid State Physics, advances in research and applications", Academic Press (1970), is devoted to the pseudopotential method. The purpose of my survey is to indicate the method of approach, and to establish the notation and terminology used. Atomic units are used, and a useful summary of these units is given in the appendix of ref [23].

The two impurity systems investigated in this chapter are GaAs:Co(d^7) and ZnSe:Co(d^7). Crystal field theory has been used to interpret absorption data from both of these systems, and a comparison between calculations for a III-V system and a II-VI system should be interesting. In section 6.3 the valence electron pseudocharge density is calculated and in section 6.4 the calculations for the crystal field splitting in the two systems are presented. The crystal

potential derived from the pseudocharge density has not been used previously in calculations of the crystal field splitting. To simplify some of the equations given in this chapter, the arguments of functions have been omitted occasionally.

8.2 -Pseudopotential method-

The empirical pseudopotential method [114,115] is used to calculate the eigenvalues and eigenfunctions of the valence electrons for the perfect crystals GaAs and ZnSe. From the results of these calculations the valence electron charge density can be found.

The fundamental concept involved in a pseudopotential calculation is that the ion core can be omitted. Computationally this is crucial because it means that the deep core potential has been removed and a rapidly converging plane wave basis set may be used to describe the crystal eigenfunctions. My calculations were based on those originally made by Chelikowsky and Cohen [115], but with some modifications.

In the pseudopotential method, the one-electron Hamiltonian is rewritten as

$$H = -(1/2) \nabla^2 + V_p(\mathbf{r}) \quad 8.1$$

where $V_p(\mathbf{r})$ is the true crystal potential $V(\mathbf{r})$ outside the core regions of the crystal, but is much weaker than the true potential within the core regions [117]. If it is assumed that the pseudopotential $V_p(\mathbf{r})$ is a simple function of position then

$$V_p(\mathbf{r}) = \sum_{\underline{G}-\underline{G}'} V(\underline{G}-\underline{G}') e^{i(\underline{G}-\underline{G}') \cdot \mathbf{r}} \quad 8.2$$

where \underline{G} and \underline{G}' are reciprocal lattice vectors. The term $V(\underline{G}-\underline{G}')$ may be broken down further:

$$V(\underline{G}-\underline{G}') = \sum_{\alpha} v_{\alpha}(\underline{G}-\underline{G}') S_{\alpha}(\underline{G}-\underline{G}') \quad 8.3$$

where $v_{\alpha}(\underline{G}-\underline{G}')$ are the atomic form factors, $S_{\alpha}(\underline{G}-\underline{G}')$ are the structure factors, and the sum is over the atomic species α . In my calculations the sum is:

$$V(\underline{G}) = 1/2 \{v_c(\underline{G}) + v_a(\underline{G})[\cos(h+k+1)\pi/2 + i \sin(h+k+1)\pi/2]\} \quad 8.4$$

where $(\underline{G}-\underline{G}')$ has been replaced by \underline{G} for simplicity. Here $v_c(\underline{G})$ and $v_a(\underline{G})$ are the atomic form factors of the cation and anion respectively, and the reciprocal lattice vector \underline{G} is

$$\underline{G} = (h,k,l) 2\pi/a, \quad 8.5$$

where a is the lattice constant. This potential term $V(\underline{G})$ differs from the one used by Chelikowsky and Cohen. Their coordinate origin was taken at the mid-point of a bond, whereas here the coordinate origin is taken at the cation site. The impurity is substitutional at a cation site and it will be useful later to have the coordinate origin at the impurity site.

The sum of reciprocal lattice vectors in eq.8.2 is only over a few terms because $V_p(\underline{r})$ is smooth. In these calculations, following Chelikowsky and Cohen, the sum is truncated beyond $|\underline{G} - \underline{G}'| = \sqrt{12}$, so that the only non-zero form factors are $v(\sqrt{3})$, $v(\sqrt{4})$, $v(\sqrt{8})$, and $v(\sqrt{11})$. The pseudopotentials are taken to be spherical so that $v_{\alpha}(\underline{r}) = v_{\alpha}(|\underline{r}|)$. Thus the form factors depend just on the magnitude of $(\underline{G} - \underline{G}')$. The form factors are determined empirically from reflectivity and photoemission data [115]. These parameters, based on those found by Chelikowsky and Cohen, are given in table 8.1 for GaAs and ZnSe.

The form for the pseudopotential $V_p(\underline{r})$ given in eq.8.2 is not exact and may be improved by adding a correction term to the atomic potential term of the form [114,115]:

Table 8.1

Pseudopotential parameters for GaAs and ZnSe.

	Cation				Form Factors		Anion	
	$v(\sqrt{3})$	$v(\sqrt{4})$	$v(\sqrt{8})$	$v(\sqrt{11})$	$v(\sqrt{3})$	$v(\sqrt{4})$	$v(\sqrt{8})$	$v(\sqrt{11})$
GaAs	-0.040	0.010	0.004	0.017	-0.067	-0.010	0.004	0.017
ZnSe	-0.040	0.031	0.015	0.040	-0.179	-0.031	0.015	0.024

Other Parameters

	Cation		Anion		Lattice Constant
	$A_2(E)$	r_c	$A_2(E)$	r_c	
GaAs	0.063	2.38	0.313	2.48	10.68
ZnSe	-0.063	2.23	0.463	2.16	10.68

All parameters are measured in atomic units.

$$V_{NL}^{\alpha}(\underline{r}, E) = \sum_{l=0}^{\infty} A_l(E) f_l(\underline{r}) P_l \quad 8.6$$

where P_l is a projection operator for the l th angular momentum component, $A_l(E)$ is an energy dependent well depth, $f_l(\underline{r})$ is a Gaussian well [118]

$$f_l(\underline{r}) = \exp(-r/r_c^{\alpha})^2 \quad 8.7$$

and r_c^{α} is the core radius of the atom. The correction arises because a different potential term is necessary for each value of $l = 0, 1, \text{ or } 2$ in order to satisfy the boundary conditions at the ion core boundary [114]. In the first approximation, eq.8.2, it is assumed that the same potential term is satisfactory for all values of l . For a plane wave basis set the required correction matrix elements have the form:

$$V_{NL}(\underline{K}, \underline{K}') = \sum_{\alpha} [(2\pi/\Omega_c)^{\alpha} A_2^{\alpha}(E) 5 P_2(\cos\theta_{\underline{K}\underline{K}'}) F_2^{\alpha}(\underline{K}\underline{K}') S_{\alpha}(\underline{K}-\underline{K}')] \quad 8.8$$

where Ω_c is the unit cell volume ($= a^3/8$), $A_2^{\alpha}(E)$ are constants given in table 8.1, and $\underline{K} = \underline{k} + \underline{G}$, $\underline{K}' = \underline{k} + \underline{G}'$. The term $P_2(\cos\theta_{\underline{K}\underline{K}'})$ is a second order Legendre polynomial and

$$F_2^{\alpha}(\underline{K}\underline{K}') = \int_0^{\infty} j_2(\underline{K} \cdot \underline{r}) \exp(-r/r_c^{\alpha})^2 j_2(\underline{K}' \cdot \underline{r}) r^2 dr \quad 8.9$$

where $j_2(\underline{K} \cdot \underline{r})$ are second order spherical Bessel functions. The structure factor $S_{\alpha}(\underline{K}-\underline{K}')$ is the same as that given in eq.8.4. The notation here, as elsewhere, follows that used by Chelikowsky and Cohen and eq.8.8 in this thesis corresponds to eq.9 in ref [115]. The core radii, r_c^{α} , used in my calculations are the Pauling tetrahedral covalent radii. The other parameters are taken from ref [115].

Once the potential is determined, it is a straightforward calculation to find the eigenvalues and eigenfunctions. The plane wave representation of the Schrodinger equation is:

$$\{ [(1/2) (\underline{k} + \underline{G})^2 - E(\underline{k})] \delta_{\underline{G}\underline{G}'} + V(\underline{G}-\underline{G}') + V_{NL}(\underline{K}, \underline{K}') \} = 0 \quad 8.10$$

where $E(\underline{k})$ are the eigenvalues. In my calculation 113 plane waves were

Table 8.2
Eigenvalues for GaAs and ZnSe at the Γ point.

GaAs	ZnSe
-12.41	-12.04
0.00	0.00
0.00	0.00
0.00	0.00
1.65	2.97
4.70	7.22
4.70	7.22
4.70	7.22
6.92	9.54
9.87	11.04

All energies are measured in eV.

used in the wavefunction expansion. The secular determinant was evaluated using a Digital Vax-11/780 computer. The NAG subroutine F02AXF was used for the diagonalisation of eq.8.10 whilst the subroutine D01AHF was used to solve eq.8.9 [87].

The calculation of the eigenvalues at the Γ point are in good agreement with the results of Chelikowsky and Cohen who used only 50 plane waves in the wavefunction expansion, see table 8.2. The wavefunction obtained from the pseudopotential calculations at some point \underline{k} in the Brillouin zone for the n th electron is of the form:

$$\psi_n(\underline{k}, \underline{r}) = \sum_{\underline{G}} (a_{\underline{G}, \underline{k}} + ib_{\underline{G}, \underline{k}}) e^{i(\underline{k} + \underline{G}) \cdot \underline{r}} \quad 8.11$$

where the sum is over 113 reciprocal lattice vectors.

8.3 -The pseudocharge density-

The valence electron charge density at any point \underline{r} can be evaluated using the wavefunctions calculated by the pseudopotential method discussed in the previous section. The pseudocharge density is

$$\rho(\underline{r}) = -|e| \sum_{\underline{k}} \sum_n \psi_n(\underline{k}, \underline{r}) \psi_n^*(\underline{k}, \underline{r}) \quad 8.12$$

where \sum_n is a sum over the four valence electrons and $\sum_{\underline{k}}$ is a sum over points in the Brillouin zone. In principle such a calculation is very long and complicated because a knowledge of the charge density at each \underline{k} point in the Brillouin zone is required. However, only a few representative points need to be considered [119]. The choice of these special points needs some discussion.

The valence electron charge density can be written as [119]

$$\rho(\underline{r}) = \sum_{\underline{T}} \rho_{\underline{T}\underline{k}}(\underline{r}) + \sum_{\underline{R}_j = |\underline{c}_m|} S(\underline{r}) \exp(i\underline{k} \cdot \underline{R}_j) \quad 8.13$$

where $\rho_{\underline{T}\underline{k}}(\underline{r})$ is the valence electron charge density at some point \underline{k} in the Brillouin zone and $\sum_{\underline{T}}$ is a sum over all of the equivalent points

T_k . R_j are the lattice point vectors, and $|c_m|$ is the m th nearest neighbour distance so that $\sum_{R_j=|c_m|}$ is a sum of the shells of ions around the coordinate origin. The function $S(\underline{r})$ is constant for each $R_j=|c_m|$. The notation here is that used by Chadi and Cohen [119].

If a value of \underline{k} can be found such that

$$\sum_{R_j=|c_m|} \exp(i\underline{k} \cdot R_j) = 0 \quad 8.14$$

for all values of m then the charge density is just

$$\rho(\underline{r}) = \sum_T \rho_{T\underline{k}}(\underline{r}) \quad 8.15$$

Such a value for \underline{k} has not been found, but a special point found by Baldereschi [120]:

$$\underline{k} = (0.622, 0.295, 0) 2\pi/a \quad 8.16$$

satisfies eq.8.14 for $m = 1, 2, 3$. By using two special points:

$$\underline{k}_1 = (3/4, 1/4, 1/4) 2\pi/a \quad \underline{k}_2 = (1/4, 1/4, 1/4) 2\pi/a \quad 8.17$$

Chadi and Cohen found that eq.8.14 is satisfied for all m up to $m = 8$. Thus within the first eight shells surrounding the coordinate origin:

$$\rho(\underline{r}) = (1/N) (\sum_T \rho_{T\underline{k}_1}(\underline{r}) + \sum_{T'} \rho_{T'\underline{k}_2}(\underline{r})) \quad 8.18$$

where N is a normalising constant. There are 24 equivalent points to \underline{k}_1 and 8 equivalent points to \underline{k}_2 . Therefore the valence electron charge density is approximately

$$\rho(\underline{r}) = (1/4) (3\bar{\rho}_{\underline{k}_1}(\underline{r}) + \bar{\rho}_{\underline{k}_2}(\underline{r})) \quad 8.19$$

where $\bar{\rho}_{\underline{k}}(\underline{r})$ is the mean value of charge density over the equivalent points $T\underline{k}$.

The eigenfunctions for the valence electrons are calculated by solving eq.8.10 at the two special points \underline{k}_1 and \underline{k}_2 . These eigenfunctions are then used to find the pseudocharge density at the two special points. At each \underline{k} point the charge density is written as a sum over reciprocal lattice vectors:

$$\rho_{\underline{k}}(\underline{r}) = -|e| \sum_{\underline{G}} \sum_{\underline{G}'} (a_{\underline{k}, \underline{G}} + ib_{\underline{k}, \underline{G}}) (a_{\underline{k}, \underline{G}'} - ib_{\underline{k}, \underline{G}'}) e^{i(\underline{G}-\underline{G}') \cdot \underline{r}}$$

$$= -|e| \sum_{\underline{G}} (R_{\underline{k},\underline{G}} + iI_{\underline{k},\underline{G}}) e^{i\underline{G}\cdot\underline{r}} \quad 8.20$$

The mean value of the charge density $\bar{\rho}_{\underline{k}}(\underline{r})$ is found by taking the mean of the Fourier coefficients $R_{\underline{k},\underline{G}}$ and $I_{\underline{k},\underline{G}}$ for each set of equivalent reciprocal lattice vectors \underline{G} :

$$\begin{aligned} \bar{\rho}_{\underline{k}}(\underline{r}) &= (1/N_{\underline{k}}) \sum_{\underline{T}} \rho_{\underline{T}\underline{k}}(\underline{r}) \\ &= -|e| \sum_{\underline{G}} [(1/N_{\underline{G}}) \sum_{\underline{T}'} (R_{\underline{k},\underline{T}'\underline{G}} + iI_{\underline{k},\underline{T}'\underline{G}}) e^{i\underline{G}\cdot\underline{r}}]. \end{aligned} \quad 8.21$$

Finally the valence electron charge density is found by summing the two mean charge densities at the special points according to eq.8.19.

The total charge density is written

$$\rho(\underline{r}) = \sum_{\underline{G}} (R_{\underline{G}} + iI_{\underline{G}}) e^{i\underline{G}\cdot\underline{r}} \quad 8.22$$

where $R_{\underline{G}}$ and $I_{\underline{G}}$ are the real and imaginary Fourier coefficients of the charge density.

The valence electron charge density has been calculated by the pseudopotential method for GaAs and ZnSe. The Fourier coefficients of charge density are given in table 8.3 for GaAs and in table 8.4 for ZnSe. It is interesting to note that the imaginary Fourier coefficients are zero for $\underline{G} = (h,k,0) 2\pi/a$ and its equivalent points. This arises because of the two-fold rotation axes perpendicular to the set of equivalent planes $[h,k,0]$. The valence electron charge density must have the symmetry of the crystal and so for these planes the charge density

$$\rho(\underline{r}) = \rho(-\underline{r}). \quad 8.23$$

The charge density is written as

$$\begin{aligned} \rho(\underline{r}) &= \sum_{\underline{G}} (R_{\underline{G}} + iI_{\underline{G}}) e^{i\underline{G}\cdot\underline{r}} \\ &= \sum_{\underline{G}} (R_{\underline{G}} \cos\underline{G}\cdot\underline{r} - I_{\underline{G}} \sin\underline{G}\cdot\underline{r}) \end{aligned} \quad 8.24$$

$$\text{and } \rho(-\underline{r}) = \sum_{\underline{G}} (R_{\underline{G}} \cos\underline{G}\cdot\underline{r} + I_{\underline{G}} \sin\underline{G}\cdot\underline{r}) \quad 8.25$$

If the condition eq.8.23 is to be satisfied then $-I_{\underline{G}} = I_{\underline{G}} = 0$. Thus the imaginary Fourier coefficient of charge density must be zero for $\underline{G} = (h,k,0) 2\pi/a$ and its equivalent points.

Table 8.3

Fourier coefficients of the valence electron charge density in GaAs.

$\underline{G}(a/2\pi)$	$R_{\underline{G}}$	$I_{\underline{G}}$
0,0,0	4.000	0.000
1,1,1	0.415	0.873
2,0,0	-0.324	0.000
2,2,0	-0.042	0.000
3,1,1	-0.130	0.136
2,2,2	0.030	0.227
4,0,0	-0.134	0.000
3,1,1	0.027	0.014
4,2,0	0.026	0.000
4,2,2	-0.013	0.011
3,3,3	-0.009	0.005
5,1,1	0.001	0.011
4,4,2	0.000	0.002
4,4,0	0.008	0.000
5,3,1	0.002	0.002
6,0,0	0.002	0.000
6,2,0	0.002	0.000

Fourier coefficients have the units $(2|e|/\Omega_c)$

Table 8.4

Fourier coefficients of the valence electron charge density in ZnSe.

$\underline{G}(a/2\pi)$	$R_{\underline{G}}$	$I_{\underline{G}}$
0,0,0	4.000	0.000
1,1,1	0.216	1.109
2,0,0	-0.611	0.000
2,2,0	-0.001	0.000
3,1,1	-0.107	0.109
2,2,2	0.043	0.185
4,0,0	-0.115	0.000
3,3,1	0.037	0.042
4,2,0	0.049	0.000
4,2,2	-0.021	0.022
3,3,3	-0.013	0.008
5,1,1	0.648	0.018
4,4,2	0.001	0.000
4,4,0	0.001	0.000
5,3,1	0.000	0.000
6,0,0	0.004	0.000
6,2,0	0.000	0.000

Fourier coefficients have the units $(2|e|/\Omega_c)$

8.4 -Calculation of the crystal field contributions-

In the previous section, the valence electron charge density in GaAs and in ZnSe was calculated using the pseudopotential method. The valence electrons produce an electrostatic field at the cation site which has the symmetry of the crystal. The field splits the d-orbital energy levels of a substitutional transition metal impurity. The energy level splitting caused by the tetrahedral field has been discussed previously in section 3.3. The separation in energy of the e and t_2 -orbitals defines the parameter Δ :

$$\Delta = E(t_2) - E(e) \quad 8.26$$

for tetrahedral symmetry.

A second contribution to the level splitting must come from the lattice of ion cores, which also produce a tetrahedral electrostatic field at the impurity site. These two contributions to Δ are the subject of this section. In the following two sub-sections the perturbing potentials, caused by the valence electrons and the ion cores, are established. In the final sub-section the contributions to Δ from the fourth order spherical harmonic component of the crystal field are determined. Another contribution to Δ comes from the spherically symmetric part of the crystal field, but the effect of this component is largely masked by a spherically symmetric repulsive d-d electrostatic interaction. This matter has been discussed in chapter three. The valence electron contribution to the electrostatic potential calculated by the pseudopotential method has not been used previously in calculations of the crystal field splitting.

8.4.1 -valence electron perturbing potential-

In the previous section, the valence electron charge density was calculated as a sum over reciprocal lattice vectors \underline{G} :

$$\rho(\underline{r}) = (-2|e|/\Omega_c) \sum_{\underline{G}} (R_{\underline{G}} + iI_{\underline{G}}) e^{i\underline{G}\cdot\underline{r}} \quad 8.27$$

where $R_{\underline{G}}$ and $I_{\underline{G}}$ are the real and imaginary Fourier coefficients of the charge density given in tables 8.3 and 8.4, and $(-2|e|/\Omega_c)$ are the appropriate units.

The charge density is related to the electrostatic potential $V(\underline{r})$ by Poissons equation:

$$\nabla^2 V(\underline{r}) = -4\pi \rho(\underline{r}). \quad 8.28$$

Combining the equations 8.27 and 8.28 leads to

$$\nabla^2 V(\underline{r}) = -4\pi [(-2|e|/\Omega_c) \sum_{\underline{G}} (R_{\underline{G}} + iI_{\underline{G}}) e^{i\underline{G}\cdot\underline{r}}]. \quad 8.29$$

Taking the reciprocal lattice vector as $\underline{G} = (h,k,l) 2\pi/a$ then

$$V(\underline{r}) = \frac{-32|e|}{4\pi a} \sum_{\underline{G}} \frac{(R_{\underline{G}} + iI_{\underline{G}})}{(h^2+k^2+l^2)} e^{i\underline{G}\cdot\underline{r}} \quad 8.30$$

The potential can be written as an expansion in spherical harmonics using [121]:

$$e^{i\underline{G}\cdot\underline{r}} = 4\pi \sum_{l=0}^{\infty} \sum_{m=-l}^l i^l j_l(\underline{G}\cdot\underline{r}) Y_{l,m}^*(\hat{\underline{G}}) Y_{l,m}(\theta,\phi) \quad 8.31$$

where $j_l(\underline{G}\cdot\underline{r})$ is a spherical Bessel function and $Y_{l,m}(\theta,\phi)$ is a spherical harmonic. The potential is:

$$V(\underline{r}) = \sum_{l=0}^{\infty} \sum_{m=-l}^{+l} \left[\frac{-32}{a} \sum_{\underline{G}} \frac{(R_{\underline{G}} + iI_{\underline{G}})}{(h^2+k^2+l^2)} i^l j_l(\underline{G}\cdot\underline{r}) Y_{l,m}^*(\hat{\underline{G}}) \right] Y_{l,m}(\theta,\phi) \quad 8.32$$

The crystal potential must have T_d point symmetry. Consequently certain terms in the potential expansion, eq.8.32, cancel with one another [122]. For example the coefficients of $Y_{2,0}(\theta,\phi)$, $Y_{2,2}(\theta,\phi)$ and $Y_{2,-2}(\theta,\phi)$ cancel each other out, and so do the coefficients of $Y_{4,2}(\theta,\phi)$ and $Y_{4,-2}(\theta,\phi)$. The perturbing potential due to the valence

electrons simplifies to:

$$V(\underline{r}) = f_0 Y_{0,0} + f_4 [Y_{4,0} + \sqrt{(5/14)} (Y_{4,4} + Y_{4,-4})] \quad 8.33$$

where the arguments have been omitted for simplicity and

$$f_1(r) = \frac{-32}{a} \sum_{\underline{G}} \frac{(R_{\underline{G}} + iI_{\underline{G}})}{(h^2 + k^2 + l^2)} j_1(\underline{G} \cdot \underline{r}) Y_{10}^*(\hat{\underline{G}}) \quad 8.34$$

Higher terms in the expansion of the potential do not perturb the d-orbitals [24].

Using the Fourier coefficients of charge density calculated in the previous section, it can be verified that the contribution to the potential from the imaginary parts is zero. Thus the term $f_1(r)$ can be rewritten as

$$f_1(r) = \frac{-32}{a} \sum_{\underline{G}} \frac{R_{\underline{G}}}{(h^2 + k^2 + l^2)} j_1(\underline{G} \cdot \underline{r}) Y_{10}^*(\hat{\underline{G}}) \quad 8.35$$

The perturbing potential due to the valence electrons is given by eq.8.33 where f_1 is given by eq.8.35.

8.4.2 -ion core perturbing potential-

In addition to the electrostatic potential due to the valence electrons, there remains the core contribution. The cores are assumed to be point charges. Then the electrostatic field at the impurity site due to the four nearest neighbours is [122]:

$$V(\underline{r}) = D_0 Y_{0,0} + D_4 [Y_{4,0} + \sqrt{(5/14)} (Y_{4,4} + Y_{4,-4})] \quad 8.36$$

where

$$D_4(r) = \frac{4\sqrt{\pi}}{5} r^2 \left[\frac{-35 Z e}{9(\sqrt{3}a/4)^5} \right] \quad 8.37$$

Here Z is the charge on the anion cores, and a is the lattice constant. The contribution from the second nearest neighbours is small

compared with the nearest neighbour contribution and it is therefore ignored here.

8.4.3 -crystal field splitting-

In this section the orbital energies of the e and t_2 -orbitals, as a consequence of the fourth order spherical harmonic contribution to the perturbing potential arising from the valence electrons and the ion cores, are determined. The difference between these orbital energies, called Δ_4 , can be compared with those values for Δ_p^0 found from experiment. It will be recalled from section 6.4 that the main contribution to Δ_p^0 was from Δ_4 . The contribution from the spherically symmetric part of the central field, Δ_0 , can not be compared with any experimental value and so it is not evaluated here. The systems studied in this section are GaAs:Co(d^7) and ZnSe:Co(d^7). Values for Δ_p^0 have been determined for these two systems empirically in previous chapters.

The one-electron d-orbitals may be written as a product of the radial and angular parts. The angular part is a linear combination of second order spherical harmonics. If the radial part is $R_t(r)$ for the t_2 -orbitals and $R_e(r)$ for the e-orbitals, then the t_2 -orbitals are:

$$\begin{aligned} & (i/\sqrt{2}) R_t [Y_{2,1} + Y_{2,-1}] \\ & (-i/\sqrt{2}) R_t [Y_{2,1} - Y_{2,-1}] \\ & (1/i\sqrt{2}) R_t [Y_{2,2} - Y_{2,-2}] \end{aligned} \quad 8.38$$

where the arguments have been omitted for simplicity, and the e-orbitals are

$$\begin{aligned} & R_e [Y_{2,0}] \\ & (i/\sqrt{2}) R_e [Y_{2,2} + Y_{2,-2}]. \end{aligned} \quad 8.39$$

The crystal field interaction matrix elements are of the form:

$$\langle \phi_d | V(\underline{r}) | \phi_d \rangle \quad 8.40$$

where $|\phi_d\rangle$ is a one-electron d-orbital. The contribution to Δ_p^0 in terms of these matrix elements is:

$$\Delta_4 = \langle \phi_t | V(\underline{r}) | \phi_t \rangle - \langle \phi_e | V(\underline{r}) | \phi_e \rangle \quad 8.41$$

The angular parts of these matrix elements are the same for the valence electron contributions and the ion core contributions. These may be evaluated analytically. For an e-orbital matrix element, the simplest angular integral is:

$$14\sqrt{\pi} \int \int \{ [Y_{2,0}]^2 [Y_{4,0} + \sqrt{(5/14)}(Y_{4,4} + Y_{4,-4})] \sin\theta \} d\theta d\phi = 6. \quad 8.42$$

For a t_2 -orbital matrix element, an angular integral is

$$\begin{aligned} -14\sqrt{\pi} \int \int \{ (1/2)[Y_{2,1} + Y_{2,-1}]^2 [Y_{4,0} + \sqrt{(5/14)}(Y_{4,4} + Y_{4,-4})] \sin\theta \} d\theta d\phi \\ = -4. \end{aligned} \quad 8.43$$

For the valence electrons, the remaining radial integral in the matrix element is

$$(1/14\sqrt{\pi}) \int [R_d]^2 f_4 r^2 dr \quad 8.44$$

where $R_d(\underline{r})$ is the radial function. For the ion cores, the radial integral is

$$(1/14\sqrt{\pi}) \int [R_d]^2 D_4 r^2 dr \quad 8.45$$

Thus the contribution to Δ_p^0 from the crystal field interaction is:

$$\begin{aligned} \Delta_4 = (1/14\sqrt{\pi}) \{ -4[\int [R_t]^2 f_4 r^2 dr + \int [R_t]^2 D_4 r^2 dr] \\ -6[\int [R_e]^2 f_4 r^2 dr + \int [R_e]^2 D_4 r^2 dr] \} \end{aligned} \quad 8.46$$

The solutions of equations 8.44 and 8.45 depend on the one-electron radial function R_d . Calculations from first principles are not yet at a stage where accurate one-electron radial wavefunctions for transition metal impurities can be determined. In section 5.2.1 the simple analytic radial function proposed by Slater [83] for a free atom was modified and used as an impurity radial wavefunction. The modifications imposed were a reduction in magnitude

at the central ion site, governed by a parameter θ_d , and a radial extension of the function, governed by a parameter α_d . Thus the impurity radial functions are

$$\begin{aligned} R_t(r) &= \theta_t [(2\alpha_t)^7 / 6!]^{1/2} r^2 \exp(-\alpha_t r) \\ R_e(r) &= \theta_e [(2\alpha_e)^7 / 6!]^{1/2} r^2 \exp(-\alpha_e r) \end{aligned} \quad 8.47$$

where $\alpha = 2.3$ for $\text{Co}(d^7)$ [83]. The approximation is simple, but crude; there is clearly a need for a more reliable one-electron radial function. These modified radial Slater functions are used here in the calculation of the radial integrals in equations 8.44 and 8.45. However, the approximate nature of these functions means that exact agreement between theory and experiment can not be expected.

It can be seen from equations 5.10 and 5.13 that the parameters θ_d and α_d are related to the crystal field covalency parameters by

$$\varepsilon = \theta_e (\alpha_e)^{1/4} \qquad \tau = \theta_t (\alpha_t)^{1/4} \quad 8.48$$

Values for ε and τ for $\text{Co}(d^7)$ in GaAs and ZnSe have already been determined empirically from absorption data. In this model, the magnitude of the parameters ε and τ may be governed purely by the reduced magnitude of the d-orbitals at the impurity site, θ_d , or purely by the extension of the d-orbitals, α_d . A more accurate picture would probably be somewhere between these two extremes. Two possible modifications are considered in this section. First, the magnitude modification reduces the covalency parameters by the same amount, and the difference between parameters is caused by the different extensions. In this case

$$\begin{aligned} \theta_e &= \theta_t = \varepsilon \\ (\alpha_e)^{1/4} &= 1 \\ (\alpha_t)^{1/4} &= \tau/\varepsilon \end{aligned} \quad 8.49$$

The second possibility is that the extension coefficient α_d reduces

the covalency parameters by the same amount, and the difference between parameters is caused by the magnitude modification parameter. In this second case

$$\begin{aligned}(\alpha_e)^{1/4} + (\alpha_t)^{1/4} &= \epsilon \\ \theta_e &= 1 \\ \theta_t &= \tau/\epsilon\end{aligned}$$

8.50

Many other possible cases may be envisaged, but these two are used for the calculations in this section. The results of the calculation for GaAs:Co(d^7) are given in table 8.5 and the results for ZnSe:Co(d^7) are given in table 8.6.

An inspection of tables 8.5 and 8.6 shows that agreement between theory and experiment is not satisfactory and the calculations overestimate the crystal field strength. The principle cause of the discrepancy is the one-electron radial function. This is illustrated by the large variation in the values of the matrix elements obtained as a result of the two interpretations of the crystal field covalency parameters (equations 8.49 and 8.50) in terms of θ_d and α_d .

In particular, the magnitude of the radial integrals depends critically on the degree of extension of the radial functions. Thus for small decreases in α_t and α_e the magnitude of the radial integrals significantly increases. Agreement between theory and experiment is best for small extensions of the radial functions. The conclusion to be drawn from this result is that a radial function containing only a small extension more accurately describes the real impurity in this approximation.

It should also be remembered that Hartree Fock calculations by Watson [84] have demonstrated that a single Slater orbital overestimates the degree of extension of a free atomic orbital. It is

Table 3.5
Calculation of the crystal field splitting in GaAs:Co(d⁷).

Crystal field parameters

$$\epsilon = 0.842$$

$$\tau = 0.736$$

$$\Delta_p = 5470 \text{cm}^{-1}$$

$$\Delta_p^0 = 3500 \text{cm}^{-1}$$

Case 1

$$\theta_t = \theta_e = \epsilon$$

$$(\alpha_e)^{1/4} = 1.0$$

$$(\alpha_t)^{1/4} = \tau/\epsilon$$

$$\text{Contribution from valence electrons} = -4030 \text{cm}^{-1}$$

$$\text{Contribution from ion cores} = 9080 \text{cm}^{-1}$$

$$\text{Total contribution, } \Delta_u = 5050 \text{cm}^{-1}$$

Case 2

$$(\alpha_t)^{1/4} = (\alpha_e)^{1/4} = \epsilon$$

$$\theta_e = 1.0$$

$$\theta_t = \tau/\epsilon$$

$$\text{Contribution from valence electrons} = -10100 \text{cm}^{-1}$$

$$\text{Contribution from ion cores} = 30400 \text{cm}^{-1}$$

$$\text{Total contribution, } \Delta_u = 20000 \text{cm}^{-1}$$

Table 3.6

Calculation of the crystal field splitting in ZnSe:Co(d^7).Crystal field parameters

$$\epsilon = 0.945$$

$$\tau = 0.813$$

$$\Delta_p = 5370 \text{ cm}^{-1}$$

$$\Delta_p^0 = 2000 \text{ cm}^{-1}$$

Case 1

$$\theta_t = \theta_e = \epsilon$$

$$(\alpha_e)^{1/4} = 1.0$$

$$(\alpha_t)^{1/4} = \tau/\epsilon$$

$$\text{Contribution from valence electrons} = -6090 \text{ cm}^{-1}$$

$$\text{Contribution from ion cores} = 15300 \text{ cm}^{-1}$$

$$\text{Total contribution, } \Delta_4 = 9210 \text{ cm}^{-1}$$

Case 2

$$(\alpha_t)^{1/4} = (\alpha_e)^{1/4} = \epsilon$$

$$\theta_e = 1.0$$

$$\theta_t = \tau/\epsilon$$

$$\text{Contribution from valence electrons} = -5510 \text{ cm}^{-1}$$

$$\text{Contribution from ion cores} = 10900 \text{ cm}^{-1}$$

$$\text{Total contribution, } \Delta_4 = 5390 \text{ cm}^{-1}.$$

therefore likely that the single Slater orbitals used in this section overestimate the degree of extension of the impurity orbitals. The results in tables 8.5 and 8.6 show that the interaction integrals significantly increase for small increases in the spatial extension of the orbitals. Therefore any overestimation in the impurity orbital extensions will result in calculated values for the crystal field strength which are larger than those observed experimentally. Such an overestimation of the crystal field strength has been found in the results presented in this section.

Another source of error is that the charge density used in the calculations is that of a pure crystal. The substitutional impurity will create some distortion of the charge density [123], which may add significant contributions to the fourth order spherical harmonic component of the crystal potential.

A consistent feature in all of the results is that the contribution to Δ_4 from the valence electrons is negative, whilst the contribution from the point ions is positive. Further, the point ion component is the larger contribution so that overall the term Δ_4 is positive.

Empirically it has been observed that the crystal field strength in the III-V systems is larger than in the II-VI systems. Unfortunately it is not possible to say directly from the results in tables 8.5 and 8.6 whether this is the case theoretically. However the stronger covalency in the III-V systems indicates that the orbitals in these systems should be more spatially extended than those in the II-VI systems. This suggests that the crystal field strength in the III-V systems may well be larger than in the II-VI systems, since the crystal field interaction matrix elements increase significantly with increases in the spatial extension.

CHAPTER NINE

SUMMARY

9 SUMMARY

It is the aim of this final chapter to consider the results contained in this thesis in a more general context: to show what the present research has added to the field of transition metal impurities in semiconductors and to consider those areas in which further research would be useful. More detailed summaries of important results are provided at the end of each chapter.

It will be recalled from chapter three that the new version of crystal field theory relies on certain assumptions concerning the localised nature of the deep levels produced by a transition metal impurity. The work presented in subsequent chapters has shown that these approximations are justified. In chapter four the $\epsilon\tau\Delta_p$ theory was used successfully to describe the absorption data arising from transition metal impurities in II-VI compounds. The values for the disposable parameters ϵ and τ are close to unity corresponding to a small modification of the electrostatic interaction within the impurity d-shell and thus only a small delocalisation. Good agreement with experimental data is obtained using these physically reasonable values for the covalency parameters. In chapter seven the approximations in the crystal field theory were seen to be valid for transition metals in the more covalent III-V hosts.

The method of application of the new theory is similar to the $BC\Delta$ version of the crystal field theory used previously by experimentalists in the interpretation of data. It involves the use of just three adjustable parameters. However the $\epsilon\tau\Delta_p$ theory has been shown here to be preferable to the $BC\Delta$ theory. For example it predicts low spin crystal field energy levels which are in better agreement with experimental data. The physical interpretation of the

adjustable parameters is more meaningful, and several previously unexplained experimental data can be understood with the new interpretation.

The $\epsilon\tau\Delta_p$ theory and the BCA theory predict different sets of crystal field energy levels. In some systems, such as ZnSe:Co [32] or ZnSe:Ni [61], the levels predicted by the $\epsilon\tau\Delta_p$ theory give better agreement with experimental data. For other systems no relevant experimental data are available. A useful test of the new version of crystal field theory would be an experimental search for those levels predicted by the theory but previously unobserved. Another useful area of work will be in the interpretation of spectra not included in this thesis. It has been demonstrated in chapter six that the study of trends in the parameters has many useful applications and may reveal information on systems which at first sight appear unrelated to the systems studied.

The $\epsilon\tau\Delta_p$ theory represents a practical crystal field fitting scheme in which covalency has been included in a very general way. In previous versions of the crystal field theory where covalency effects have been introduced [34,37,35,39], the adjustable parameters contained in the energy matrices define a particular choice of modification imposed on the one-electron wavefunctions. In the $\epsilon\tau\Delta_p$ model it is recognised that the wavefunctions are modified by the crystalline environment and that this will affect the electrostatic matrix elements. The adjustable parameters are then defined in terms of these modified electrostatic interaction integrals. The more restricted parameters found in previous versions of crystal field theory can be related to the general parameters of the $\epsilon\tau\Delta_p$ theory. Thus the previous theories represent particular limits of the new theory.

The necessary link between experimental observations and first principles theory is provided by the $\epsilon\tau\Delta_p$ theory. The experimentalist can describe large quantities of data in terms of three adjustable parameters. First principles theory may be used to calculate the same parameters. Thus theory and experiment may be compared through estimates for the parameters ϵ , τ and Δ_p . Some cross-link is vital between first principles theory and experiment for progress in the field of deep levels. Unfortunately those systems which are simplest to treat theoretically, transition metal impurities in the elemental semiconductors silicon and germanium [124,101], have a narrow band gap which makes the experimental observation of the impurity excited states difficult. Much more experimental data on the excited states are available for transition metal impurities in the II-VI compounds, see chapter four. Only a few theoretical studies have been published on these systems [93,16] and it is not possible to calculate ϵ and τ from the results provided.

There is clearly a need for more work on the calculation of d-orbital wavefunctions. Results presented in the literature [2,3] indicate that many current calculations overestimate the degree of delocalisation of impurity d-orbitals, particularly for the heavier transition metals. In this thesis the description of errors in the construction of the $\epsilon\tau\Delta_p$ theory, presented in chapter five, and the estimation of the crystal field splitting in chapter eight were both complicated by the lack of a reliable wavefunction.

The semiempirical theory presented in this thesis should have a significant impact on the understanding of deep levels. The success of the $\epsilon\tau\Delta_p$ theory in the interpretation of data is evidence that the d-orbitals of a substitutional transition metal impurity in a tetrahedral semiconductor remain localised. Previously, the results

of experimental investigations on the excited states of deep impurities in semiconductors have been described in terms of the adjustable parameters B , C and Δ . At the same time theoretical studies generally have calculated Δ_d and the degree of localisation of the d-orbitals. It has therefore not been possible to make a direct comparison between first principles theory and experiment. By using the $\epsilon\tau\Delta_p$ theory both experimentalists and theorists may present their results in terms of the same parameters, which must necessarily lead to a better communication between experiment and first principles theory and therefore to a better understanding of the deep level problem.

APPENDIX

Energy matrices for the d^2 configuration in tetrahedral symmetry

1A_1		
t^2	$\tau^4(10B + 5C)$	$\epsilon^2 \tau^2(\sqrt{6}(2B + C))$
e^2	$+ (4/5)\Delta_p$	$\epsilon^4(8B + 4C)$
		$- (6/5)\Delta_p$

3A_2		
e^2	$\epsilon^4(-8B) - (6/5)\Delta_p$	

1E		
t^2	$\tau^4(B + 2C)$	$\epsilon^2 \tau^2(2\sqrt{3}B)$
e^2	$+ (4/5)\Delta_p$	$\epsilon^4(2C)$
		$- (6/5)\Delta_p$

1T_1		
et	$\epsilon^2 \tau^2(4B + 2C) - (1/5)\Delta_p$	

Energy matrices for the d^2 configuration in tetrahedral symmetry

3T_1		
t^2	$\tau^4(-5B)$	$\epsilon\tau^3(-6B)$
	$+ (4/5)\Delta_P$	
et		$\epsilon^2\tau^2(4B)$
		$- (1/5)\Delta_P$

1T_2		
t^2	$\tau^4(B + 2C)$	$\epsilon\tau^3(-2\sqrt{3}B)$
	$+ (4/5)\Delta_P$	
et		$\epsilon^2\tau^2(2C)$
		$- (1/5)\Delta_P$

3T_2	
et	$\epsilon^2\tau^2(-8B) - (1/5)\Delta_P$

Energy matrices for the d^3 configuration in tetrahedral symmetry

4A_2		
t^3	$\tau^4(-15B) + (6/5)\Delta_p$	
2A_2		
$t^2({}^1E)e$	$\tau^4(B + 2C) + \epsilon^2\tau^2(8B + C) + (1/5)\Delta_p$	
2A_1		
$t^2({}^1E)e$	$\tau^4(B + 2C) + \epsilon^2\tau^2(-12B + C) + (1/5)\Delta_p$	
4T_2		
$t^2({}^3T_1)e$	$\tau^4(-5B) + \epsilon^2\tau^2(-10B) + (1/5)\Delta_p$	
4T_1		
$t^2({}^3T_1)e$	$\tau^4(-5B)$	$\epsilon\tau^3(6B)$
	$\epsilon^2\tau^2(2B)$	
	+ $(1/5)\Delta_p$	
$te^2({}^3A_2)$		$\epsilon^2\tau^2(-4B)$
		$\epsilon^4(-8B)$
		- $(4/5)\Delta_p$

Energy matrices for the d^3 configuration in tetrahedral symmetry

$2E$					
t^3	$\tau^4(-6B + 3C)$ + $(6/5)\Delta_p$	$\epsilon\tau^3(-6\sqrt{2}B)$	$\epsilon\tau^3(-3\sqrt{2}B)$	0	
$t^2({}^1A_1)e$	$\tau^4(10B + 5C)$ + $\epsilon\tau^2(-2B + C)$ + $(1/5)\Delta_p$	$\epsilon\tau^2(10B)$	$\epsilon\tau^2(10B)$	$\epsilon\tau^2(\sqrt{3}(2B + C))$	
$t^2({}^1E)e$			$\tau^4(B + 2C)$ + $\epsilon\tau^2(-2B + C)$ + $(1/5)\Delta_p$	$\epsilon\tau^2(2\sqrt{3}B)$	
e^3				$\epsilon^4(-8B + 4C)$ - $(9/5)\Delta_p$	

Energy matrices for the d^3 configuration in tetrahedral symmetry

$2T_1$						
t^3	$\tau^4(-6B + 3C)$ + $(6/5)\Delta_p$	$\epsilon\tau^3(-3B)$	$\epsilon\tau^3(3B)$	0	$\epsilon^2\tau^2(-2\sqrt{3}B)$	
$t^2({}^3T_1)e$	$\tau^4(-5B)$ + $\epsilon\tau^2(5B + 3C)$ + $(1/5)\Delta_p$	$\epsilon\tau^2(-3B)$	$\epsilon\tau^3(3B)$	$\epsilon\tau^3(3B)$	$\epsilon\tau^3(3\sqrt{3}B)$	
$t^2({}^1T_2)e$		$\tau^4(B + 2C)$ + $\epsilon\tau^2(-7B + C)$ + $(1/5)\Delta_p$	$\epsilon\tau^3(-3B)$	$\epsilon\tau^3(-3B)$	$\epsilon\tau^3(-\sqrt{3}B)$	
$te^2({}^3A_2)$			$\epsilon\tau^2(2B + 3C)$ + $\epsilon^4(-8B)$ - $(4/5)\Delta_p$	$\epsilon\tau^2(2B + 3C)$ + $\epsilon^4(-8B)$ - $(4/5)\Delta_p$	$\epsilon^2\tau^2(2\sqrt{3}B)$	
$te^2({}^1E)$					$\epsilon^2\tau^2(-2B + C)$ + $\epsilon^4(2C)$ - $(4/5)\Delta_p$	

Energy matrices for the d^3 configuration in tetrahedral symmetry

$2T_2$						
t^3	$\tau^4(5C)$ $+ (6/5)\Delta_p$	$\epsilon\tau^3(-3\sqrt{3}B)$	$\epsilon\tau^3(-5\sqrt{3}B)$	$\epsilon^2\tau^2(4B + 2C)$	$\epsilon^2\tau^2(2B)$	
$t^2({}^3T_1)e$	$\tau^4(-5B)$ $+ \epsilon\tau^2(-B + 3C)$ $+ (1/5)\Delta_p$	$\epsilon^2\tau^2(3B)$	$\epsilon\tau^3(-3\sqrt{3}B)$	$\epsilon\tau^3(-3\sqrt{3}B)$	$\epsilon\tau^3(-3\sqrt{3}B)$	
$t^2({}^1T_2)e$		$\tau^4(B + 2C)$ $+ \epsilon\tau^2(3B + C)$ $+ (1/5)\Delta_p$		$\epsilon\tau^3(-\sqrt{3}B)$	$\epsilon\tau^3(\sqrt{3}B)$	
$te^2({}^1A_1)$				$\epsilon^2\tau^2(-2B + C)$ $+ \epsilon^4(8B + 4C)$ $- (4/5)\Delta_p$	$\epsilon^2\tau^2(10B)$	
$te^2({}^1E)$					$\epsilon^2\tau^2(-7B + C)$ $+ \epsilon^4(2C)$ $- (4/5)\Delta_p$	

Energy matrices for the d^4 configuration in tetrahedral symmetry

1A_2	
$t^3({}^2E)e$	$\tau^4(-6B + 3C) + \epsilon^2 \tau^2(-6B + 3C) + (3/5)\Delta_P$ $\epsilon \tau^3(6B)$ $\tau^4(B + 2C) + \epsilon^2 \tau^2(-4B + 2C) + \epsilon^4(2C) - (2/5)\Delta_P$
3A_1	
$t^3({}^2E)e$	$\tau^4(-6B + 3C) + \epsilon^2 \tau^2(-6B + 3C) + (3/5)\Delta_P$
5E	
$t^3({}^4A_2)e$	$\tau^4(-15B) + \epsilon^2 \tau^2(-6B) + (3/5)\Delta_P$
5T_2	
$t^2({}^3T_1)e^2({}^3A_2)$	$\tau^4(-5B) + \epsilon^2 \tau^2(-8B) + \epsilon^4(-8B) - (2/5)\Delta_P$

Energy matrices for the d^4 configuration in tetrahedral symmetry

3A_2			
$t^3({}^2E)e$	$\tau^2(-6B + 3C)$ $+ \epsilon^2\tau^2(-2B + C)$ $+ (3/5)\Delta_p$	$\epsilon\tau^3(-12B)$	
$t^2({}^1A_1)e^2({}^3A_2)$		$\tau^4(10B + 5C)$ $+ \tau^2\epsilon^2(-4B + 2C)$ $+ \epsilon^4(-8B)$ $- (2/5)\Delta_p$	
3E			
$t^3({}^4A_2)e$	$+ \tau^4(-15B)$ $+ \tau^2\epsilon^2(2B + 4C)$ $+ (3/5)\Delta_p$	$\tau^2\epsilon^2(-4B)$	0
$t^3({}^2E)e$		$\tau^4(-6B + 3C)$ $+ \tau^2\epsilon^2(-4B + C)$ $+ (3/5)\Delta_p$	$\epsilon\tau^3(-3\sqrt{2}B)$
$t^2({}^1E)e^2({}^3A_2)$			$\tau^4(B + 2C)$ $+ \tau^2\epsilon^2(-4B + 2C)$ $+ \epsilon^4(-8B)$ $- (2/5)\Delta_p$

Energy matrices for the d^4 configuration in tetrahedral symmetry

3T_1									
t^4	$\tau^4(-15B + 5C)$ $+ (8/5)\Delta_p$	$\epsilon\tau^3(-1/6B)$	$\epsilon\tau^3(-3/2B)$	$\epsilon^2\tau^2(\sqrt{2}(2B + C))$	$\epsilon^2\tau^2(-2/2B)$	0	0	0	0
$t^3({}^2T_1)e$	$\tau^4(-6B + 3C)$ $+ \epsilon^2\tau^2(-5B + C)$ $+ (3/5)\Delta_p$	$\epsilon^2\tau^2(5/3B)$	$\epsilon\tau^3(\sqrt{3B})$	$\epsilon\tau^3(\sqrt{3B})$	$\epsilon\tau^3(-\sqrt{3B})$	$\epsilon\tau^3(3B)$	$\epsilon^2\tau^2(\sqrt{6B})$		
$t^3({}^1T_2)e$	$\tau^4(5C)$ $+ \epsilon^2\tau^2(-3B + C)$ $+ (3/5)\Delta_p$	$\epsilon\tau^3(-3B)$	$\epsilon\tau^3(-3B)$	$\epsilon\tau^3(-3B)$	$\epsilon\tau^3(-3B)$	$\epsilon\tau^3(5/3B)$	$\epsilon^2\tau^2(\sqrt{2}(B + C))$		
$t^2({}^3T_1)e^2({}^3A_2)$	$\tau^4(-5B)$ $+ \epsilon^2\tau^2(-4B + 2C)$ $+ \epsilon^4(8B + 4C)$ $- (2/5)\Delta_p$	$\tau^4(-5B)$	$\epsilon^2\tau^2(-10B)$	$\epsilon^2\tau^2(-10B)$	0	0	$\epsilon\tau^3(3/2B)$		
$t^2({}^1T_2)e^2({}^1E)$	$\tau^4(-5B)$ $+ \epsilon^2\tau^2(-4B + 2C)$ $+ \epsilon^4(2C)$ $- (2/5)\Delta_p$	$\tau^4(-5B)$	$\tau^4(-5B)$ $+ \epsilon^2\tau^2(-4B + 2C)$ $+ \epsilon^4(2C)$	$\tau^4(-5B)$ $+ \epsilon^2\tau^2(-4B + 2C)$ $+ \epsilon^4(2C)$	$\tau^4(-5B)$ $+ \epsilon^2\tau^2(-4B + 2C)$ $+ \epsilon^4(2C)$	$\epsilon^2\tau^2(-2/3B)$	$\epsilon\tau^3(-3/2B)$		
$t^2({}^1E)e^2({}^1E)$						$\tau^4(B + 2C)$ $+ \epsilon^2\tau^2(-4B + 2C)$ $+ \epsilon^4(-8B)$ $- (2/5)\Delta_p$	$\epsilon\tau^3(\sqrt{6B})$		
te^3							$\epsilon^2\tau^2(-8B + C)$ $+ \epsilon^4(-8B + 4C)$ $- (7/5)\Delta_p$		

Energy matrices for the d^4 configuration in tetrahedral symmetry

3T_2								
$t^3({}^2T_1)e$	$\tau^4(-6B + 3C)$ $+ \epsilon^2 \tau^2(-3B + C)$ $+ (3/5)\Delta_p$	$\epsilon^2 \tau^2(-5\sqrt{3}B)$	$\epsilon \tau^3(\sqrt{6}B)$	$\epsilon^2 \tau^2(\sqrt{3}B)$	$\epsilon^2 \tau^2(-\sqrt{6}B)$			
$t^3({}^2T_2)e$	$\tau^4(5C)$ $+ \epsilon^2 \tau^2(-5B + C)$ $+ (3/5)\Delta_p$	$\epsilon \tau^3(-3\sqrt{2}B)$		$\epsilon \tau^3(3B)$	$\epsilon^2 \tau^2 \sqrt{2}(3B + C)$			
$t^2({}^3T_1)e^2({}^3A_2)$			$\tau^4(-5B)$ $+ \epsilon^2 \tau^2(4C)$ $+ \epsilon^4(-8B)$ $- (2/5)\Delta_p$	$\epsilon^2 \tau^2(-2\sqrt{2}B)$	$\epsilon \tau^3(-6B)$			
$t^2({}^3T_1)e^2({}^1E)$				$\tau^4(-5B)$ $+ \epsilon^2 \tau^2(-4B + 2C)$ $+ \epsilon^4(2C)$ $- (2/5)\Delta_p$	$\epsilon \tau^3(3\sqrt{2}B)$			
te^3					$\epsilon^2 \tau^2(C)$ $+ \epsilon^4(-8B + 4C)$ $- (7/5)\Delta_p$			

Energy matrices for the d^4 configuration in tetrahedral symmetry

1A_1					
t^4	$\tau^4(10C)$ $+ (3/5)\Delta_p$	$\epsilon\tau^3(-12\sqrt{2}B)$	$\epsilon^2\tau^2(\sqrt{2}(4B + C))$	$\epsilon^2\tau^2(2\sqrt{2}B)$	0
$t^3({}^2E)e$	$\tau^4(-6B + 3C)$ $+ \epsilon^2\tau^2(6B + 3C)$ $+ (3/5)\Delta_p$	$\epsilon\tau^3(-12B)$		$\epsilon\tau^3(-6B)$	0
$t^2({}^1A_1)e^2({}^1A_1)$			$\tau^4(10B + 5C)$ $+ \epsilon^2\tau^2(-4B + 2C)$ $+ \epsilon^4(8B + 4C)$ $- (2/5)\Delta_p$	$\epsilon^2\tau^2(20B)$	$\epsilon^2\tau^2(\sqrt{6}(2B + C))$
$t^2({}^1E)e^2({}^1E)$				$\tau^4(B + 2C)$ $+ \epsilon^2\tau^2(-4B + 2C)$ $+ \epsilon^4(2C)$ $- (2/5)\Delta_p$	$\epsilon^2\tau^2(2\sqrt{6}B)$
e^4					$\epsilon^4(-16B + 8C)$ $- (12/5)\Delta_p$

Energy matrices for the d^4 configuration in tetrahedral symmetry

1E						
t^4	${}^4\tau(-9B + 7C)$ $+ (8/5)\Delta_p$	${}^3\epsilon\tau(6B)$	${}^2\epsilon\tau(\sqrt{2}(2B + C))$	${}^2\epsilon\tau(-2B)$	${}^2\epsilon\tau(-4B)$	
$t^3({}^2E)e$	${}^4\tau(-6B + 3C)$ $+ \epsilon {}^2\tau^2(3C)$ $+ (3/5)\Delta_p$	${}^3\epsilon\tau(-3\sqrt{2}B)$		${}^3\epsilon\tau(-12B)$	0	
$t^2({}^1E)e^2({}^1A_1)$		${}^4\tau(B + 2C)$ $+ \epsilon {}^2\tau(-4B + 2C)$ $+ \epsilon {}^4(8B + 4C)$ $- (2/5)\Delta_p$		${}^2\epsilon\tau(10\sqrt{2}B)$	${}^2\epsilon\tau(-10\sqrt{2}B)$	
$t^2({}^1A_1)e^2({}^1E)$			${}^4\tau(10B + 5C)$ $+ \epsilon {}^2\tau(-4B + 2C)$ $+ \epsilon {}^4(2C)$ $- (2/5)\Delta_p$		0	
$t^2({}^1E)e^2({}^1E)$					${}^4\tau(B + 2C)$ $+ \epsilon {}^2\tau(-4B + 2C)$ $+ \epsilon {}^4(2C)$ $- (2/5)\Delta_p$	

Energy matrices for the d^4 configuration in tetrahedral symmetry

1T_1					
$t^3({}^2T_1)e$	$\tau^4(-6B + 3C)$ $+ \epsilon \tau^2(3B + 3C)$ $+ (3/5)\Delta_p$	$\epsilon \tau^2(5\sqrt{3}B)$	$\epsilon \tau^3(3B)$	$\epsilon \tau^3(\sqrt{6}B)$	
$t^3({}^2T_2)e$	$\tau^4(5C)$ $+ \epsilon \tau^2(-3B + 3C)$ $+ (3/5)\Delta_p$	$\epsilon \tau^3(-5\sqrt{3}B)$		$\epsilon \tau^2(\sqrt{2}(B + C))$	
$t^2({}^1T_2)e^2({}^1E)$			$\tau^4(B + 2C)$ $+ \epsilon \tau^2(-4B + 2C)$ $+ \epsilon^4(2C)$ $- (2/5)\Delta_p$	$\epsilon \tau^3(-\sqrt{6}B)$	
te^3				$\epsilon \tau^2(-8B + 3C)$ $+ \tau^4(-8B + 4C)$ $- (7/5)\Delta_p$	

Energy matrices for the d^5 configuration in tetrahedral symmetry

6A_1	
$t^3({}^4A_2)e^2({}^3A_2)$	$\tau^4(-15B) + \epsilon^2\tau^2(-12B) + \epsilon^4(-8B)$
4A_2	
$t^3({}^4A_2)e^2({}^1A_1)$	$\tau^4(-15B) + \epsilon^2\tau^2(-6B + 3C) + \epsilon^4(8B + 4C)$
4E	
$t^3({}^2E)e^2({}^3A_2)$	$\tau^4(-6B + 3C) \quad \epsilon^2\tau^2(-2\sqrt{3}B)$ $+ \epsilon^2\tau^2(-8B + 2C)$ $+ \epsilon^4(-8B)$
$t^3({}^4A_2)e^2({}^1E)$	$\tau^4(-15B)$ $+ \epsilon^2\tau^2(-6B + 3C)$ $+ \epsilon^4(2C)$
4A_1	
$t^3({}^4A_2)e^2({}^3A_2)$	$\tau^4(-15B) + \epsilon^2\tau^2(-2B + 5C) + \epsilon^4(-8B)$

Energy matrices for the d^5 configuration in tetrahedral symmetry

4T_1			
$t^4({}^3T_1)e$	$\tau^4(-15B + 5C)$ $+ \epsilon^2\tau^2(-10B + C)$	$\epsilon\tau^3(3\sqrt{2}B)$	$\epsilon^2\tau^2(-C)$
$t^3({}^2T_2)e^2({}^3A_2)$	$+ \Delta_p$	$\tau^4(5C)$ $+ \epsilon^2\tau^2(-8B + 2C)$ $+ \epsilon^4(-8B)$	$\epsilon\tau^3(-3\sqrt{2}B)$
$t^2({}^3T_1)e^3$			$\tau^4(-5B)$ $+ \epsilon^2\tau^2(-12B + 2C)$ $+ \epsilon^4(-8B + 4C)$ $- \Delta_p$
4T_2			
$t^4({}^3T_1)e$	$\tau^4(-15B + 5C)$ $+ \epsilon^2\tau^2(-2B + C)$	$\epsilon\tau^3(-\sqrt{6}B)$	$\epsilon^2\tau^2(-4B - C)$
$t^3({}^2T_1)e^2({}^3A_2)$	$+ \Delta_p$	$\tau^4(-6B + 3C)$ $+ \epsilon^2\tau^2(-8B + 2C)$ $+ \epsilon^4(-8B)$	$\epsilon\tau^3(-\sqrt{6}B)$
$t^2({}^3T_1)e^3$			$\tau^4(-5B)$ $+ \epsilon^2\tau^2(-4B + 2C)$ $+ \epsilon^4(-8B + 4C)$ $- \Delta_p$

Energy matrices for the d^5 configuration in tetrahedral symmetry

2A_1				
$t^4({}^1E)e$	$\tau^4(-9B + 7C)$ $+ \epsilon \tau^2(6B + 2C)$ $+ \Delta_p$	$\epsilon \tau^3(-3\sqrt{2}B)$	0	$\epsilon \tau^2(6B + C)$
$t^3({}^2E)e^2({}^1E)$	$\tau^4(-6B + 3C)$ $+ \epsilon \tau^2(-6B + 3C)$ $+ \epsilon^4(2C)$	$\epsilon \tau^2(-4\sqrt{3}B)$		$\epsilon \tau^3(3\sqrt{2}B)$
$t^3({}^4A_2)e^2({}^3A_2)$			$\tau^4(-15B)$ $+ \epsilon \tau^2(4B + 8C)$ $+ \epsilon^4(-8B)$	0
$t^2({}^1E)e^3$			$\tau^4(B + 2C)$ $+ \epsilon \tau^2(4B + 2C)$ $+ \epsilon^4(-8B + 4C)$ $- \Delta_p$	

Energy matrices for the d^5 configuration in tetrahedral symmetry

2A_2			
$t^4({}^1E)e$	$\tau^4(-9B + 7C)$ $+ \epsilon^2 \tau^2(-14B + 2C)$	$\epsilon \tau^3(3\sqrt{2}B)$	$\epsilon^2 \tau^2(-2B + C)$
$t^3({}^2E)e^2({}^1E)$	$+ \Delta_P$	$\tau^4(-6B + 3C)$ $+ \epsilon^2 \tau^2(-6B + 3C)$ $+ \epsilon^4(2C)$	$\epsilon \tau^3(-3\sqrt{2}B)$
$t^2({}^1E)e^3$			$\tau^4(B + 2C)$ $+ \epsilon^2 \tau^2(-16B + 3C)$ $+ \epsilon^4(-8B + 4C)$ $- \Delta_P$

Atomic spectral parameters

The parameters listed below are derived from experiment for the doubly charged free ion.

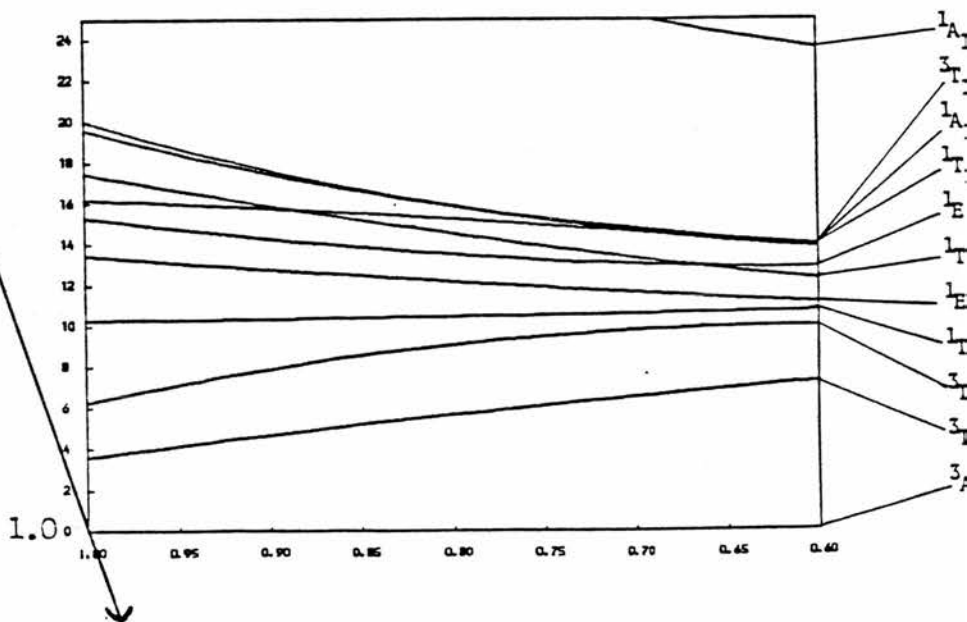
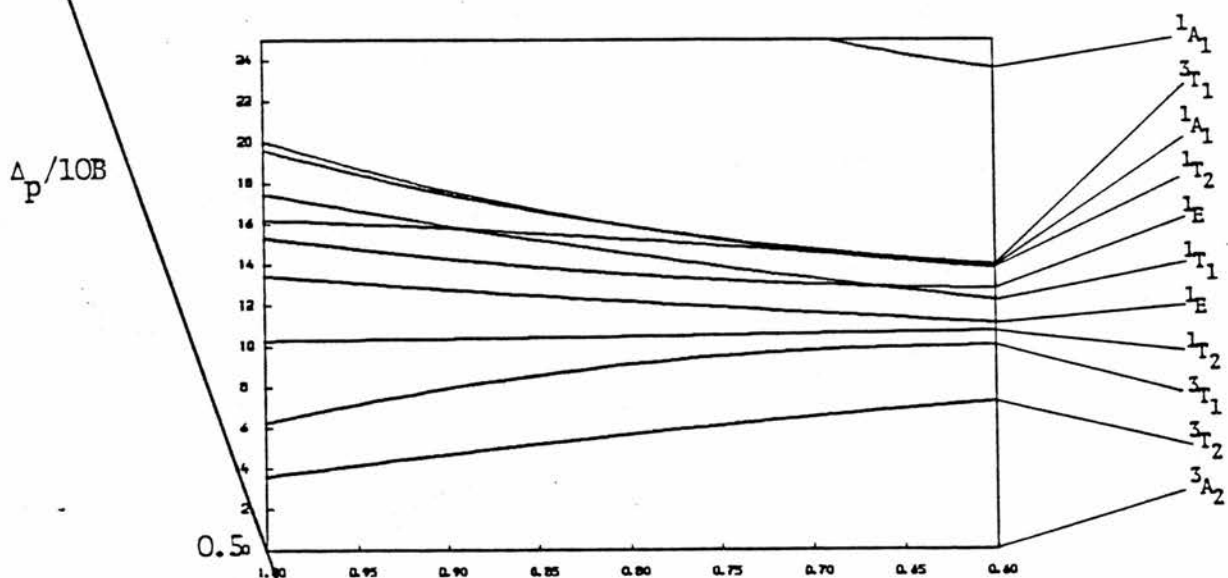
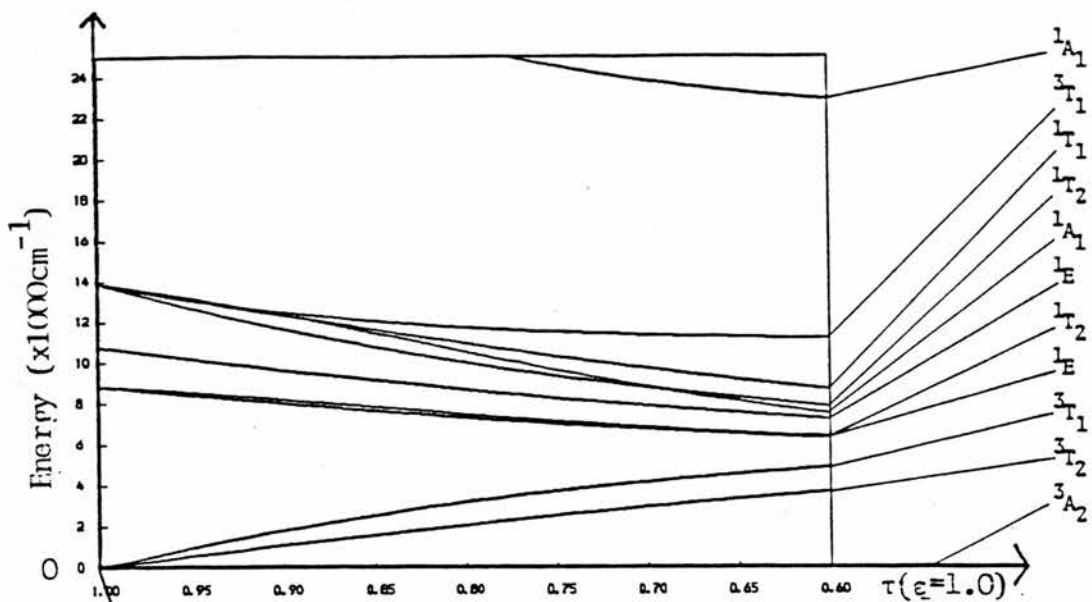
	B	C	ζ
Ti(d ²)	718	2629	121
V(d ³)	766	2855	167
Cr(d ⁴)	830	3430	230
Mn(d ⁵)	960	3325	347
Fe(d ⁶)	1058	3901	410
Co(d ⁷)	1115	4366	533
Ni(d ⁸)	1048	4831	649

All energies are measured in cm⁻¹.

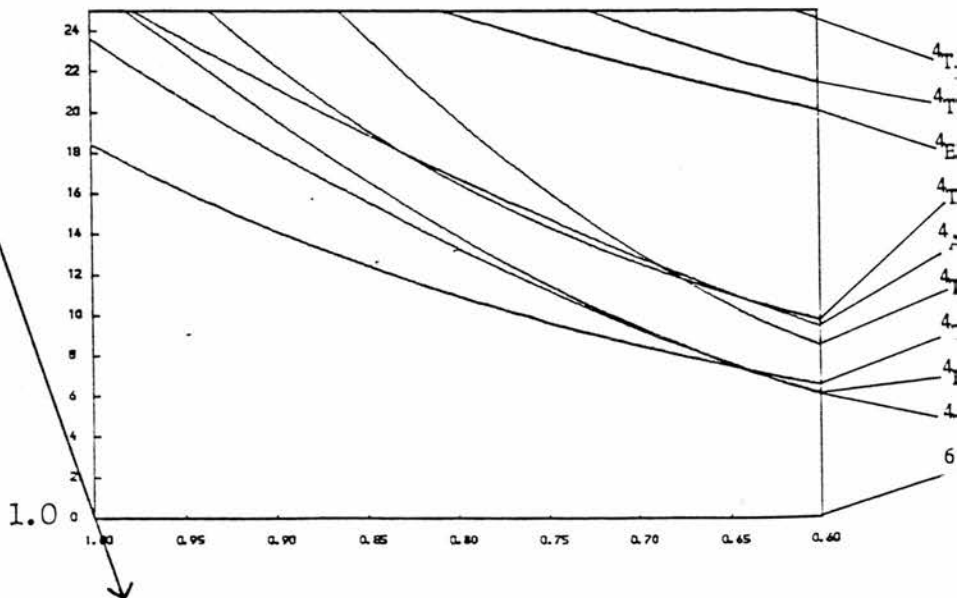
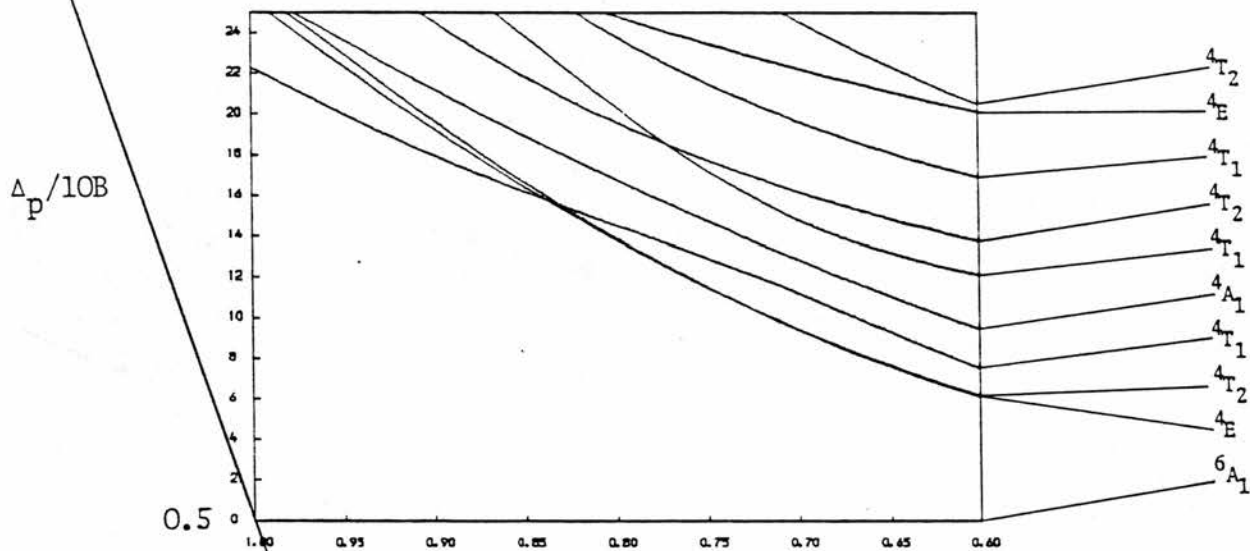
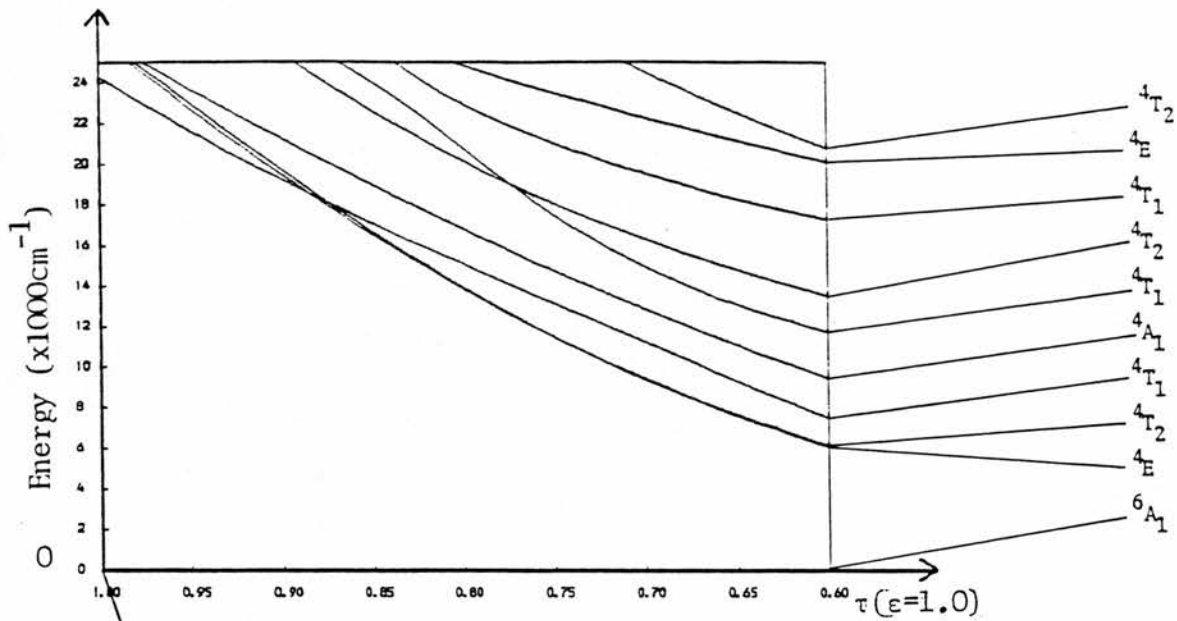
	B	C	ζ
Ti(d ²)	89.0	325.9	15.0
V(d ³)	95.0	354.0	20.7
Cr(d ⁴)	103	425.3	28.5
Mn(d ⁵)	119	412.2	43.0
Fe(d ⁶)	131.2	483.6	50.8
Co(d ⁷)	138.2	541.3	66.1
Ni(d ⁸)	134.4	598.9	80.5

All energies are measured in meV.

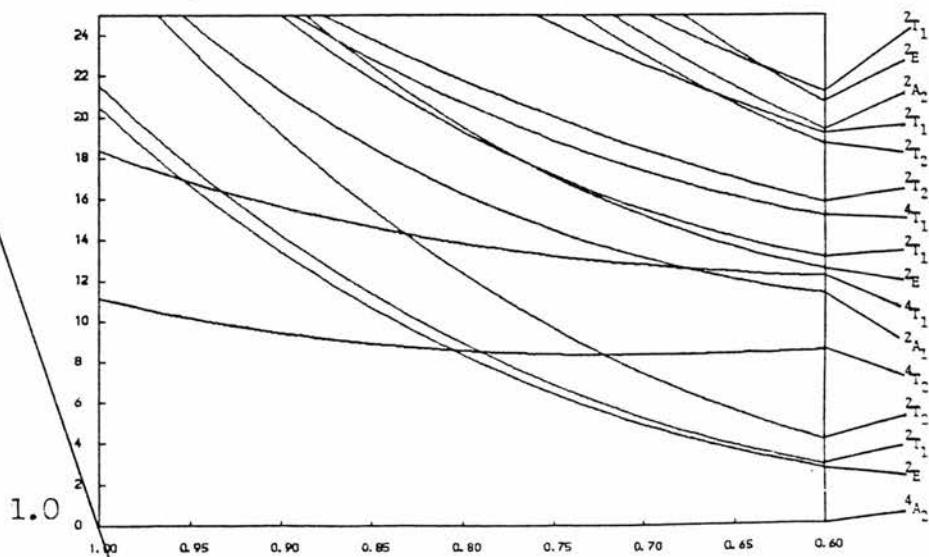
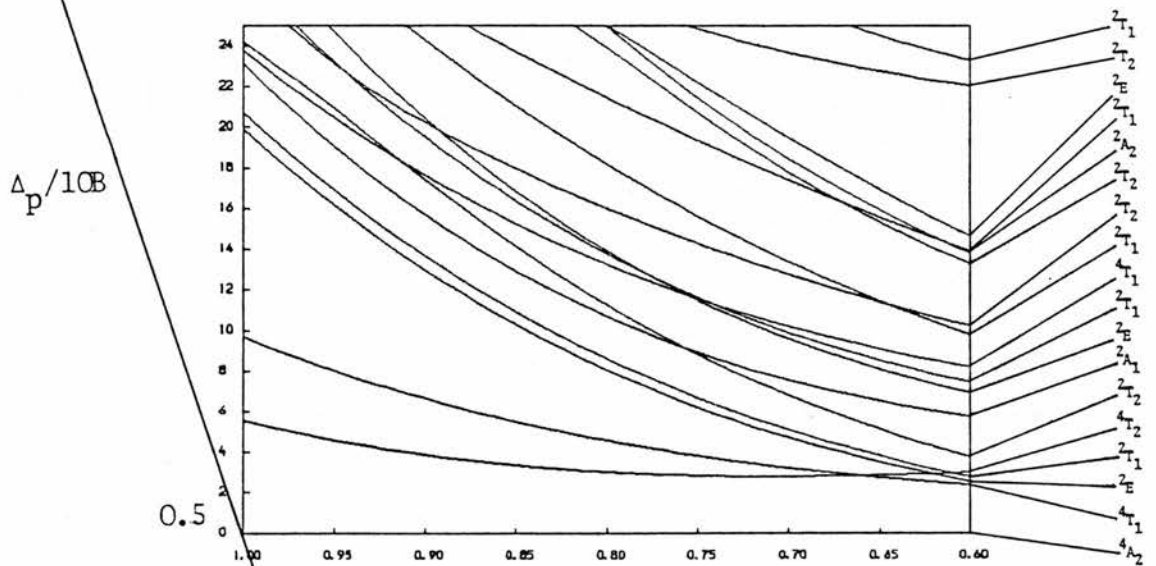
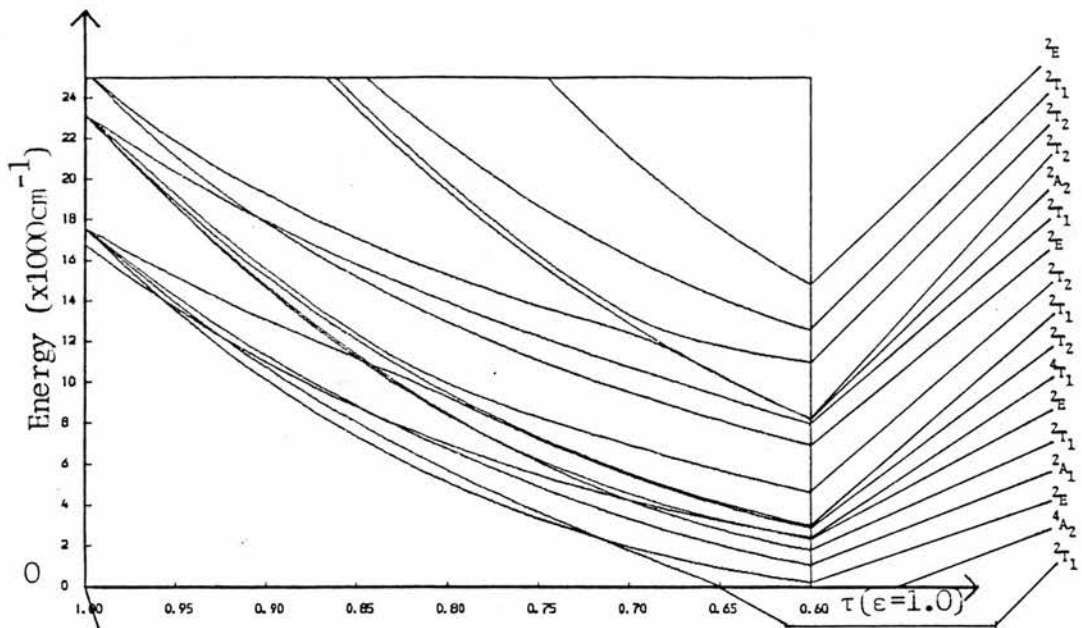
Energy level diagram for the d^2 configuration



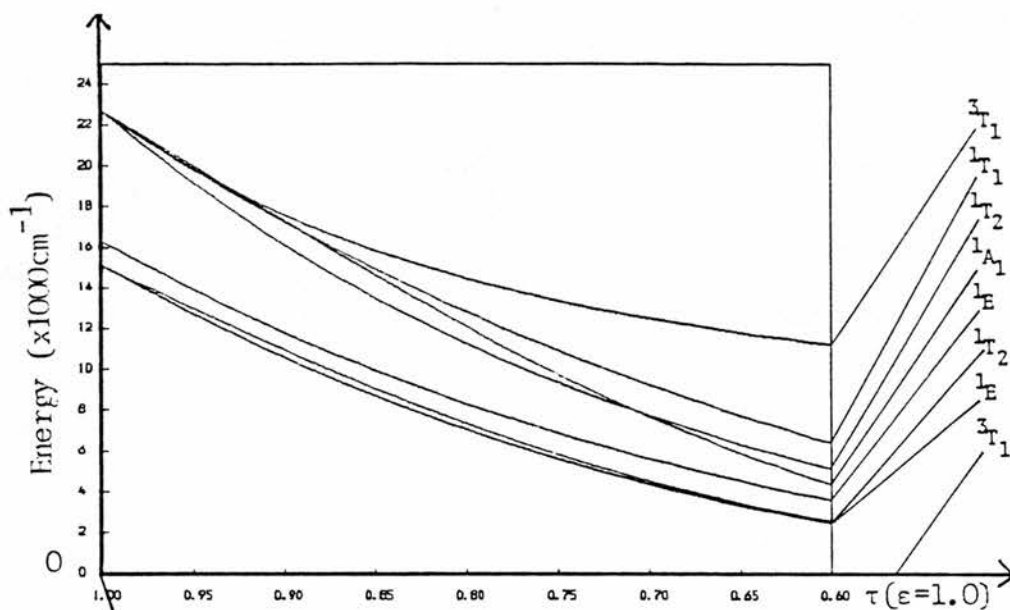
Energy level diagram for the d^5 configuration



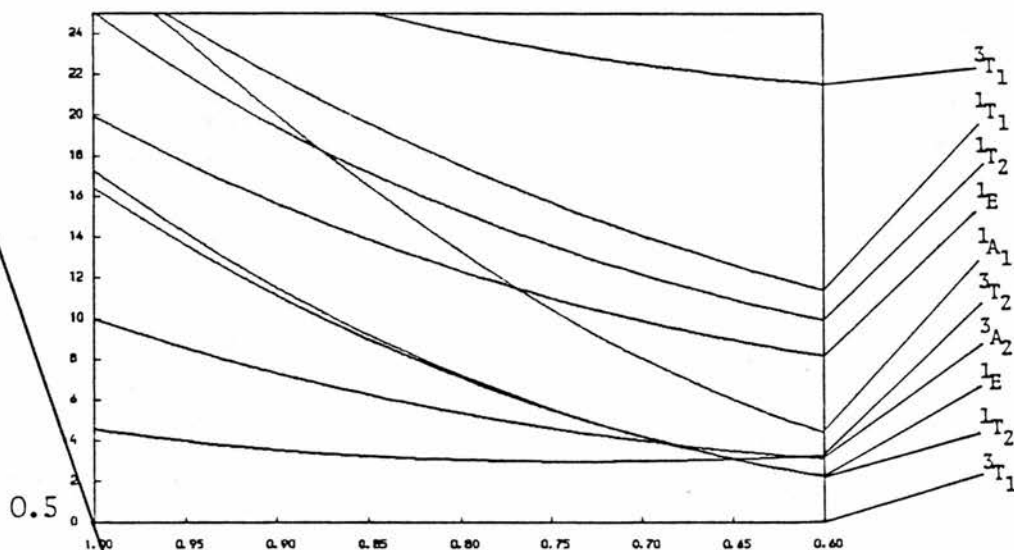
Energy level diagram for the d^7 configuration



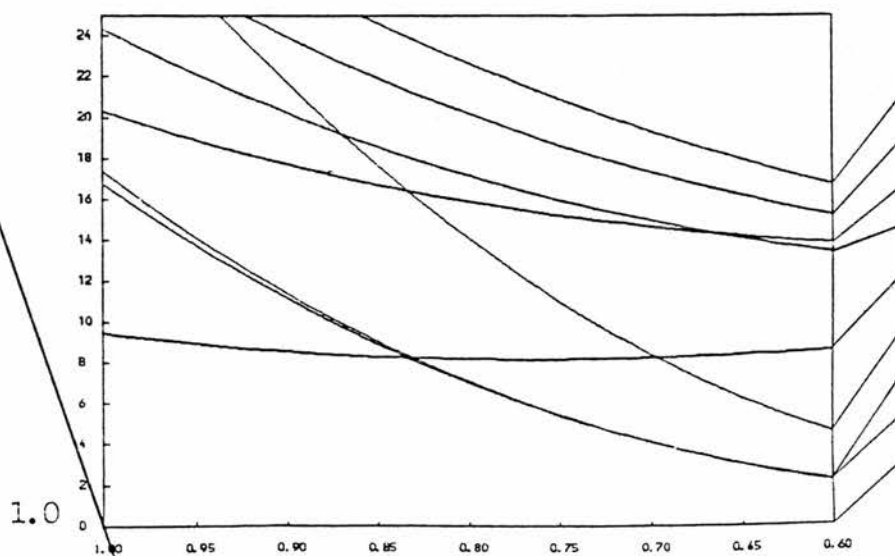
Energy level diagram for the d^8 configuration



$\Delta_p/10B$



0.5



1.0

REFERENCES

REFERENCES

- 1) Y. Tanabe and S. Sugano, J. Phys. Soc. Jpn. 9, 753 (1954)
- 2) L.A. Hemstreet, Phys. Rev. B 22, 4590 (1980)
- 3) N.P. Il'in and V.P. Masterov, Sov. Phys. Semicond. 11, 864 (1977)
- 4) J.S. Griffith, "The Theory of Transition Metal Ions", Cambridge University Press, Cambridge (1964)
- 5) C.J. Ballhausen, "Introduction to Ligand Field Theory", McGraw Hill Book Company, New York (1962)
- 6) H.H. Theissing and P.J. Caplan, "Spectroscopic Calculations for a Multielectron Ion", Interscience Publishers, New York (1966)
- 7) J.W. Allen and G.L. Pearson, "Transition Metal Impurities in Semiconductors", Stanford Electronics Laboratories: Technical Report No. 5115-1, (1967)
- 8) H.A. Weakliem, J. Chem. Phys. 36, 2117 (1962)
- 9) J.M. Langer and J.M. Baranowski, Phys. Stat. Sol. (b) 44, 155 (1971)
- 10) E.M. Wray and J.W. Allen, J. Phys. C 4, 512 (1971)
- 11) M.G. Clark and P.J. Dean, Inst. Phys. Conf. Ser. No. 43, p291 (1979)
- 12) K.H. Johnson, Adv. Quantum Chem. 7, 143 (1973)
- 13) U. Lindefelt and A. Zunger, Phys. Rev. B 26, 846 (1982)
- 14) R.E. Watson, Phys. Rev. 111, 1108 (1958)
- 15) L.A. Hemstreet and J.O. Dimmock, Phys. Rev. B 20, 1527 (1979)
- 16) M.L. deSiqueira and S.Larsson, Chem. Phys. Lett. 32, 359 (1975)
- 17) A. Fazzio and J.R. Leite, Phys. Rev. B 21, 4710 (1980)
- 18) G.A. Baraff and M. Schluter, Festkorperprobleme 19, 303 (1979)
- 19) A. Zunger and U. Lindefelt, Phys. Rev. B 26, 5989 (1982)
- 20) V. Singh, A. Zunger and U. Lindefelt, (unpublished)
- 21) J.M. Noras, Ph.D. thesis, St. Andrews University (unpublished)
- 22) G.Grebe and H.-J. Schulz, Phys. Stat. Sol. (b) 54, K69 (1972)
- 23) E.U. Condon and G.H. Shortley, "Theory of Atomic Spectra", Cambridge University Press, Cambridge (1951)
- 24) J.W. Leech and D.J. Newman, "How to use Groups", Methuen & Co. Ltd. (1969)

- 25) D.E. McCumber, Phys. Rev. 135 A1676 (1964)
- 26) H.A. Bethe, Ann. Physik 3, 133 (1929)
- 27) J.H. Van Vleck, J. Chem. Phys. 8, 787 (1940)
- 28) L.E. Orgel, J. Chem. Phys. 23 1004 (1955)
- 29) D.S. McClure, Solid State Physics 9, 399 (1959)
- 30) R. Eisberg and R. Resnick, "Quantum Physics of atoms, molecules, solids, nuclei and particles", John Wiley, New York (1974)
- 31) G. Racah, Phys. Rev. 62, 438 (1942)
- 32) J.M. Noras, H.R. Szawelska and J.W. Allen, J. Phys. C 14, 3255 (1981)
- 33) W. Busse, H.-E. Gumlich and U. Pohl, Fourth "Lund" International Conference on Deep Level Impurities in Semiconductors, p148 (1983)
- 34) S. Koide and M.H.L. Pryce, Phil. Mag. 3, 607 (1958)
- 35) L.L. Lohr, J. Chem. Phys. 45, 3611 (1966)
- 36) S.W. Biernacki and H.-J. Schulz, Phys. Stat. Sol. (b) 103, K163 (1981)
- 37) D. Curie, C.Barthou and B. Canny, J. Chem. Phys. 61, 3048 (1974)
- 38) L.L. Lohr, J. Chem. Phys. 55, 27 (1971)
- 39) S.W. Biernacki, Phys. Stat. Sol. (b) 118, (1983)
- 40) J.C. Eisenstein, J. Chem. Phys. 34, 1628 (1961)
- 41) H.A. Jahn and E. Teller, Proc. Roy. Soc. A 161, 220 (1937)
- 42) M.D. Sturge, Solid State Physics 20, 91 (1967)
- 43) U.G. Kaufmann and P. Koidl, J. Phys. C 7, 791 (1974)
- 44) G. Racah, Phys. Rev. 85, 381 (1952)
- 45) R.E. Trees, Phys. Rev. 85, 382 (1952)
- 46) R.M. Macfarlane, Phys. Rev. B 1, 989 (1970)
- 47) P. Koidl, Phys. Rev. B 15, 2493 (1977)
- 48) J.W. Allen, Proc. 7th International Conf. Physics of Semiconductors, p781, Dunod, Paris (1964)
- 49) J.W. Allen, Proc. Semi-insulating III-V Materials, Nottingham 1980, p261, Shiva Publishing Ltd.
- 50) G.W. Ludwig and H.H. Woodbury, Solid State Physics 13, 223 (1962)
- 51) J.M. Baranowski, J.W. Allen and G.L. Pearson, Phys. Rev. 160, 627 (1967)

- 52) R. Pappalardo and R.E. Dietz, Phys. Rev. 123, 1188 (1961)
- 53) D. Buhman, H.-J Schulz and M. Thiede, Phys. Rev. B 24, 6221 (1981)
- 54) D.J. Robbins, P.J. Dean, J.C. Glasper and S.G. Bishop, Sol. St. Commun. 36,
61 (1980)
- 55) D.J. Robbins, P.J. Dean, C.C. West and W. Hayes, Phil. Trans. R. Soc. Lond.
A 304, 499 (1982)
- 56) R.S Anderson, Phys. Rev. 164, 398 (1967)
- 57) A.P. Radlinski, J. Lumin 18/19, 147 (1979)
- 58) U.G. Kaufmann, P. Koidl and O.F. Schirmer, J. Phys. C 6, 310 (1973)
- 59) R. Pappalardo, D.L. Wood and R.C. Linares, J. Chem. Phys. 35, 1460 (1961)
- 60) G. Roussos and H.-J. Schulz, Phys. Stat. Sol. (b) 100, 577 (1980)
- 61) A. Karipidou, H. Nelkowski and G. Roussos, J. Cryst. Growth (Netherlands)
59, 301 (1982)
- 62) S.G. Bishop, P.J. Dean, P. Porteous and D.J. Robbins, J. Phys. C 13, 1331
(1980)
- 63) U.G. Kaufmann, W.H. Koschel, J. Schneider and J. Weber, Phys. Rev. B 19,
3343 (1979)
- 64) J.M. Noras and J.W. Allen, J. Phys. C 12, L133 (1979)
- 65) J. Schneider and A. Rauber, Phys. Lett. 27 A, 469 (1968)
- 66) L.M. Hoang and J.M. Baranowski, Phys. Stat. Sol. (b) 84, 361 (1977)
- 67) W.C. Holten, J. Schneider and T.L. Estle, Phys. Rev. 133, A1638 (1964)
- 68) J.W. Allen, Physica 29, 764 (1963)
- 69) G. Meijer and M. Avinor, Philips Res. Repts. 15, 225 (1960)
- 70) M. Avinor and G. Meijer, J. Phys. Chem. Sol. 12, 211 (1960)
- 71) W.E. Hagston, J. Phys. C 1, 818 (1968)
- 72) C.S. Kelley and F. Williams, Phys. Rev. B 2, 3 (1970)
- 73) J.T. Vallin, G.A. Slack, S. Roberts and A.E. Hughes, Phys. Rev. B 2, 4313
(1970)
- 74) H. Nelkowski, G. Grebe, J. Lumin 1/2, 88 (1970)
- 75) G. Grebe, G. Roussos and H.-J. Schulz, J. Phys. C 9, 4511 (1976)
- 76) D.S. McClure, J. Chem. Phys. 39, 2850 (1963)

- 77) D. Langer and S. Ibuki, Phys. Rev. 138 A809 (1965)
- 78) A. Mehra, J. Electrochem. Soc. 118, 136 (1971)
- 79) J.W. Stout, J. Chem. Phys. 31, 709 (1959)
- 80) G.A. Slack, F.S. Ham and R.M. Chrenko, Phys. Rev. 152, 376 (1966)
- 81) A.S. Marfunin, A.N. Platonov and V.E. Fedorov, Sov. Phys. Solid State 9, 2847 (1968)
- 82) M. Skowronski and Z. Liro, J. Phys. C 15, 137 (1982)
- 83) J.C. Slater, Phys. Rev. 36, 57 (1930)
- 84) R.E. Watson, Phys. Rev. 119, 1934 (1960)
- 85) D.A. Brown and N.J. Fitzpatrick, J. Chem. Soc. (A) 1966, 941
- 86) S. Katsuki, M. Klobukowski and P. Palting, Comp. Phys. Commun. 25, 39 (1982)
- 87) NAG Fortran Library Manual Mark 9, Numerical Algorithms Group (1982)
- 88) N.T. Khoi and J.A. Gaj, Phys. Stat. Sol. (b) 83, K133 (1977)
- 89) J.C. Philips, "Bonds and Bands in Semiconductors", Academic Press, New York (1973)
- 90) G.A. Slack and S. Galginaitis, Phys. Rev. 133, A253 (1964)
- 91) R.W.G. Wyckoff, "Crystal Structures", Interscience Publishers, New York (1948)
- 92) R.R. Sharma, M.H.deA. Viccaro and S. Sundaram, Phys. Rev. B 23, 738 (1981)
- 93) J.A. Majewski, Phys. Stat. Sol. (b) 108, 663 (1981)
- 94) E.I. Grancharova, J.P. Lascarais, J. Diouri and J. Allegre, Phys. Stat. Sol (b) 113, 503 (1982)
- 95) F.S. Ham, G.W. Ludwig, G.D. Watkins and H.H. Woodbury, Phys. Rev. Lett. 5, 468 (1960)
- 96) J.C.M. Henning, H. Van den Boom and J. Dielman, Philips Res. Repts. 21, 16 (1966)
- 97) K. Morigaki, J. Phys. Soc. Jpn. 19, 2064 (1964)
- 98) A. Hausmann, Phys. Stat. Sol. 31, K131 (1969)
- 99) A.M. Hennel, J. Phys. C 11, L389 (1978)
- 100) Y. Shadmi, Bull. Res. Conc. Israel 10, F109 (1962)
- 101) L.A. Hemstreet, Phys. Rev. B 15, 834 (1977)

- 102) J. Weber, H. Ennen, U. Kaufmann and J. Schneider, Phys. Rev. B 21, 2394 (1980)
- 103) H. Ennen, U. Kaufmann and Schneider, Sol. St. Commun. 34, 603 (1980)
- 104) A.M. Hennel and S.M. Uba, J. Phys. C 11, 4565 (1978)
- 105) J.H. Van Vleck, J. Chem. Phys. 7, 72 (1939)
- 106) D. Polder, Physica 9, 702 (1942)
- 107) W.H. Kleiner, J. Chem. Phys. 20, 1784 (1952)
- 108) J.C. Phillips, J. Phys. Chem. Solids 11, 266 (1959)
- 109) S. Sugano and R.G. Shulman, Phys. Rev. 130, 517 (1963)
- 110) R.E. Watson and A.J. Freeman, Phys. Rev. 134, A1526 (1964)
- 111) J.C. Phillips, Phys. Rev. 166, 832 (1968)
- 112) H.-G. Bruhl and U. Pietsch, Phys. Stat. Sol. (a) 68, 689 (1981)
- 113) A.M. Hennel, Phys. Stat. Sol (b) 72, K9 (1978)
- 114) M.L. Cohen and V. Heine, Solid State Physics 24, 37 (1970)
- 115) J.R. Chelikowsky and M.L. Cohen, Phys. Rev. B 14, 556 (1976)
- 116) J. Callaway, "Quantum Theory of the Solid State", Academic Press, New York (1974)
- 117) J.C. Phillips and L. Kleinman, Phys. Rev. 116, 287 (1959)
- 118) J.R. Chelikowsky and M.L. Cohen, Phys. Rev. Lett. 32, 674 (1974)
- 119) D.J. Chadi and M.L. Cohen, Phys. Rev. B 8, 5747 (1973)
- 120) A. Baldereschi, Phys. Rev. B 7, 5212 (1973)
- 121) A. Messiah "Quantum Mechanics" Vol. 1, North Holland Publishing Co, Amsterdam (1961)
- 122) M.T. Hutchings, Solid State Physics 16, 227 (1964)
- 123) U. Lindefelt, Fourth "Lund" International Conference on Deep Level Impurities in Semiconductors, p6 (1983)
- 124) G.D. Watkins, Physica 117 and 118 B + C, 9 (1983)